STRUCTURES OF SOME MERCURY COMPOUNDS IN LOW OXIDATION STATES

By

Zin Tun, B.Sc.

A Thesis

Submitted to the School of Graduate Studies

in Partial Fulfilment of the Requirements

for the Degree

Doctor of Philosophy

McMaster University

SOME MERCURY COMPOUNDS

IN

LOW OXIDATION STATES

To my parents

DOCTOR OF PHILOSOPHY (1984)

McMASTER UNIVERSITY
Hamilton, Ontario

TITLE: Structures of Some Mercury Compounds in Low Oxidation States.

AUTHOR: Zin Tun, B.Sc. (Arts and Science University, Rangoon, Burma)

SUPERVISOR: Professor I.D. Brown

NUMBER OF PAGES: xiv, 154

ABSTRACT

Structures of Hg compounds in fractional oxidation states lower than +1, $Hg_{3-\delta}MF_6$ (M = Sb, Nb, Ta), Hg_3MF_6 (M = Nb, Ta), $Hg_4(Ta_2F_{11})_2$ and $Hg_3(NbF_5)_2SO_4$, were determined at room temperature and at lower temperatures using X ray and neutron diffraction. The $Hg_{3-\delta}MF_6$ compounds, isostructural with $Hg_{3-\delta}AsF_6$, contain infinite chains of Hg which are incommensurate and thus disorder with the MF_6 host lattice. A comparison between the structures showed that the differences observed in the parameters of the chain compounds are completely accounted for by the difference in anion size. The chain-host lattice incommensurability also results in disorder among the chains at room temperature but an ordering develops at lower temperatures. As in $Hg_{3-\delta}AsF_6$, short and long range order phases were observed in experiments with $Hg_{3-\delta}SbF_6$ and $Hg_{3-\delta}TaF_6$. The characteristics of the short range order phase are different in each compound indicating that the details of chain-chain interactions are not the same. Emery-Axe order parameter theory which predicts the development of long range order phase was tested for M = As, Sb, Ta but agreement was obtained only for $Hg_{3-\delta}SbF_6$.

A structure consisting of hexagonal closed-packed layers of Hg atoms was proposed for the Hg_3MF_6 compounds. The unusual 2-dimensional Hg-Hg bonding of these compounds represents an intermediate stage between the elemental solid Hg and the $Hg_{3-\delta}MF_6$ compounds which

form 3- and 1-dimensional Hg-Hg bonds respectively.

The $Hg_4(Ta_2F_{11})_2$ and $Hg_3(NbF_5)_2SO_4$ consists of finite polyatomic Hg ions. The former shows a tendency of cations to link into infinite zigzag chains, a feature also seen in $Hg_4(AsF_6)_2$, while the latter does not show such a tendency.

ACKNOWLEDGEMENTS

I would like to thank my supervisor, Dr. I.D. Brown, for his encouragement, friendship and guidance throughout my graduate study. I am also grateful to Doctors W.R. Datars and R.J. Gillespie for their helpful advice and criticism on my research project and this thesis.

Thanks are due to Mr. R. Faggiani for his invaluable technical assistance in X ray crystallography and Doctors K. Morgan and P. Unmat for supplying as many crystals I needed for both X ray and neutron diffraction experiments. I also would like to thank Kerstin Stockman for her fast and reliable typing of this work.

Financial assistance in the form of a departmental scholarship and a teaching assistantship from McMaster University is gratefully acknowledged.

TABLE OF CONTENTS

LIST OF TABLES

LIST OF FIGURES

CHAPTER I

HISTORICAL REVIEW

1.1 Introduction

Among metals which are characterized by high electrical and thermal conductivity, mercury (Hg) is the only metal which exists in the liquid state at room temperature. High electrical conductivity of the metals including mercury is the result of the conduction (or free) electrons which are not localized within a region of the material but can drift from one part to another encountering little resistance.

When metals react with other materials to form compounds the metallic atoms usually either transfer their electrons completely to other atoms and become ions without any free electrons (ionic compounds) or use them to form bonds with nearby atoms (covalent compounds). Since free electrons become localized in either case, electronic conduction is not observed even though the compounds contain a metal atom.

One of the few ionic compounds which shows high electrical conductivity is $Hg_{3-\delta}AsF_6$. It has infinite chains of metallically bonded mercury atoms (Brown, Cutforth, Davies, Gillespie, Ireland, Vekris, 1974) and grows as large crystals with a golden metallic luster. Pure mercury solidifies below 234 K (-39°C) and behaves like a normal 3-dimensional metal. $Hg_{3-\delta}AsF_6$ differs in that the electrical conductivity

is mostly in the direction of the chains and, hence, the material is classified as an 1-dimensional conductor (Cutforth, Datars, van Schyndel, Gillespie, 1977).

Since solids with high anisotropy in their properties (known as low dimensional solids) are of considerable interest to physicists the discovery of this compound has inspired a search for new mercury compounds with unusual properties. A number have been successfully prepared over the last few years and the common feature among them is that the mercury is in oxidation states which are lower than +1, the lowest oxidation state of mercury known to chemists before 1970.

1.2 Discovery of new oxidation states of mercury

It has been known for a very long time that Hg exists in two oxidation states, 1 and 2, which can be seen in the well-known mercurous and mercuric compounds. The evidence for lower oxidation states of Hg appeared for the first time in 1970 when Torsi and Mamantov (1970) reported the preparation of $Hg_3(AlCl_4)_2$. The Hg_3^{2+} cation indicates that Hg can exist in an oxidation state of +2/3. The X ray structure determination of this material showed the Hg_3^{2+} ion to be essentially linear with Hg-Hg bonds of about 2.56 Å as depicted in the following diagram (Ellison, Levy, Fung, 1972).

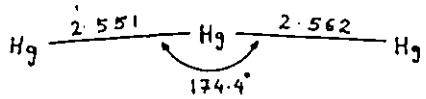

About the same time preparation of a different material but with the same ion was reported by Davies, Dean, Gillespie, Ummat (1971)

(also see Cutforth, Davies, Dean, Gillespie, Ireland, Ummat, 1973). The material was prepared by oxidizing elemental Hg at room temperature with an equimolar amount of AsF_5 dissolved in liquid SO_2. Immediately after the reaction was started a crystalline solid with golden luster was observed on the surface of Hg while the initially colorless solution became deep-red in color. The color of the solution then gradually changed to orange as the golden crystals slowly disappeared. Orange crystals obtained from this solution by slowly vaporizing the SO_2 were characterized as $Hg_3(AsF_6)_2$ so that the reaction that took place in the solution was

$$3Hg + 3AsF_5 \xrightarrow{SO_2} Hg_3(AsF_6)_2 + AsF_3$$

Gillespie et al. reasoned that the deep-red solution which appeared before the orange solution might contain Hg ions in lower oxidation state than +2/3. By using a smaller amount of oxidant the reaction could be stopped at the stage where the deep-red solution and the golden crystals coexisted in an equilibrium and the crystallization of this solution gave red-black needles. An X ray structure determination of this product showed that the material indeed contained Hg ions in lower oxidation state (Cutforth, Gillespie, Ireland (1973) and Cutforth, Gillespie, Ireland, Sawyer, Ummat (1983)) the chemical composition being $Hg_4(AsF_6)_2$, the oxidation state of Hg in this material is $+\frac{1}{2}$. The reaction may be represented by the following equation.

$$4Hg + 3AsF_5 \xrightarrow{SO_2} Hg_4(AsF_6)_2 + AsF_3$$

The geometry of Hg_4^{2+} ion is shown below.

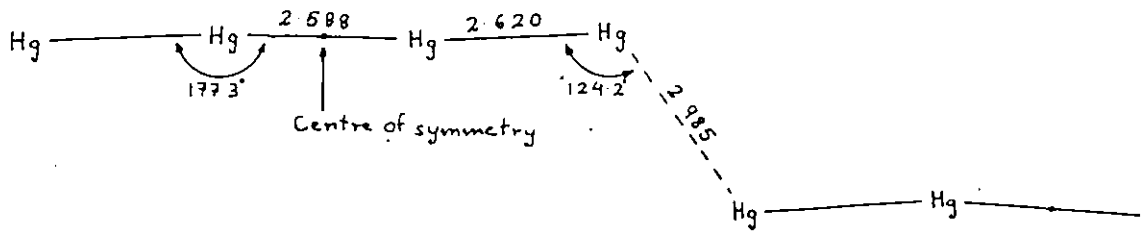

The Hg_4^{2+} ion, like the Hg_3^{2+} ion, is almost linear but with the difference that the Hg_4^{2+} ions are linked by the relatively short distance of 2.985 Å between the terminal Hg atoms. Since this distance is comparable to the shortest distances in solid Hg, 2.99 Å for α-Hg (Barrett, 1957) and 2.83 Å for β-Hg (Atoji, Schirber, Swenson, 1959), it may indicate a significant interaction linking the Hg_4^{2+} ions together to form infinite zigzag chains.

By using even a smaller amount of oxidant Gillespie et al. were able to stop the reaction at the stage of the golden crystals. When these crystals were subjected to a chemical analysis yet another oxidation state of Hg, namely +1/3, was discovered since the composition turned out to be Hg_3AsF_6. In the brief report of the preparation of this new material Gillespie and Ummat (1971) expressed the reaction as

$$6Hg + 3AsF_5 \xrightarrow{SO_2} 2Hg_3AsF_6 + AsF_3$$

A subsequent X ray investigation (Brown et al., 1974), however, revealed that the composition of this material is more appropriately written as $Hg_{3-\delta}AsF_6 (\delta \geq 0)$. Moreover, the study shows that the Hg atoms link into uniform infinite chains with a Hg-Hg bond length of 2.64 Å. Since the structure of $Hg_{3-\delta}AsF_6$ is rather unusual it will be

discussed in detail in the following section.

1.3 The structure of $Hg_{3-\delta}AsF_6$.

The structure of $Hg_{3-\delta}AsF_6$ was first determined by Brown et al. (1974) using X ray diffraction. Precession photographs of this material showed two distinct features.* One is a lattice of well-defined Bragg reflections consistent with the symmetry and systematic absences of the tetragonal space group $I4_1/amd$ and the other is a series of sheets of diffuse scattering perpendicular to $\underline{a}^*$ and $\underline{b}^*$ axes. The lattice parameters of the tetragonal unit cell were found to be $\underline{a}$ = 7.538(4), $\underline{c}$ = 12.339(5) Å. The separation of diffuse sheets, however, corresponds to a distance of 2.64 Å which is incommensurate with the tetragonal lattice parameters and led to the conclusion that the structure consists of two incommensurate components.

To explain the observed diffraction pattern Brown et al. proposed a model in which infinite chains of Hg atoms occupy straight non-intersecting tunnels in the $\underline{a}$ and $\underline{b}$ direction of an AsF_6 tetragonal lattice (see Fig. 1.1). The AsF_6 ions are ordered on a lattice with a space group $I4_1/amd$ and give well-defined Bragg peaks. To explain the diffuse scattering sheets the Hg atoms within the chains are assumed to be separated by 2.64 Å. The incommensurability of the two components results in the chains being disordered with respect to the AsF_6 host lattice which, in turn, leads to disorder among the chains themselves since, due to their large separation and heavy screening by the host

* An hk0 precession photograph of $Hg_{3-\delta}SbF_6$, an isostructural compound with $Hg_{3-\delta}AsF_6$ is shown in fig. 3.1.

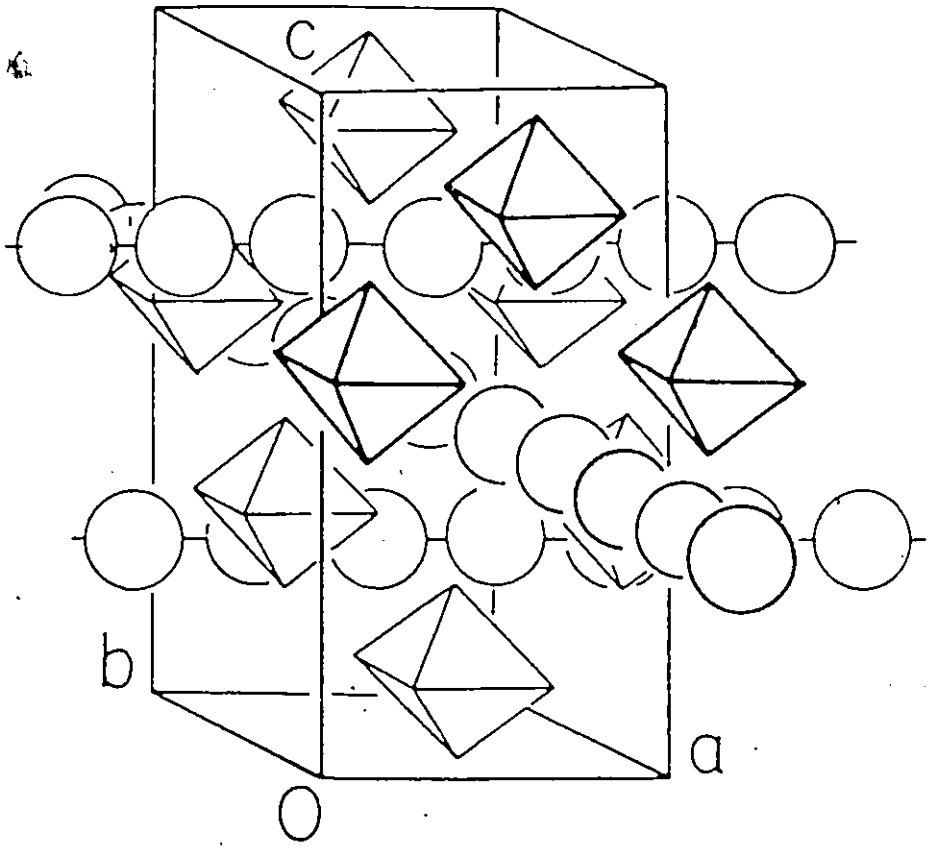

Figure 1.1

Structure of $Hg_{3-\delta}AsF_6$ proposed by Brown et al. (1974). Taken from Brown et al., 1982. The structure consists of infinite chains of Hg atoms (circles) occupying straight non-intersecting tunnels formed by a lattice of AsF_6 ions (octahedra) ordered in space group $I4_1/amd$.

lattice, the direct interaction between the chains is weak. As a result the X rays scattered from the chains are in the form of diffuse sheets rather than well-defined Bragg peaks.

Another consequence of incommensurability between the two components is that the ratio of Hg atoms to the AsF_6 ions in the formula is non-integral. Since there are slightly less than three Hg atoms for each AsF_6 ion the composition of the material should be expressed as $Hg_{3-\delta}AsF_6$ where $\delta = 0.14$.

The model of $Hg_{3-\delta}AsF_6$ was later confirmed by Schultz, Williams, Miro MacDiarmid, Heeger (1978) using neutron diffraction. In their structure refinement an additional degree of freedom was incorporated into the model by allowing the chains to be displaced in the c direction since the symmetry of the space group does not fix the z coordinate of the atoms in the chains. Their refined model revealed a small undulation of the chains caused by the repulsion of the mutually perpendicular chains at the crossing points. The maximum displacement of the chains from the mean position (i.e., z = 1/4) is only 0.071 Å.

Schultz et al. also measured the density which indicated that in spite of the apparent composition of $Hg_{3-\delta}AsF_6$ implied by the crystallographic structure, the actual composition is closer to Hg_3AsF_6 due to a degree of anion deficiency.

1.4 Attempts to prepare isostructural compounds

Shortly after the preparation of $Hg_{3-\delta}AsF_6$ similar golden crystals were obtained by oxidizing Hg with SbF_5 dissolved in liquid SO_2. As in the case of AsF_5, the reaction could be stopped at the stage of the

golden crystals by using the appropriate amount of oxidant. A preliminary X ray examination showed that this compound was isostructural with $Hg_{3-\delta}AsF_6$ (Cutforth, 1976).

Attempts to prepare other infinite Hg chain compounds (e.g. with PF_6 and BiF_6) were not successful. When the experiments for this thesis were initiated in 1980, $Hg_{3-\delta}AsF_6$ and $Hg_{3-\delta}SbF_6$ were the only two compounds known with the general formula $Hg_{3-\delta}MF_6$.

1.5 Experiments and Theories on the inifinte chain compounds

Because of their unusual structure the infinite chain compounds (with M = As, Sb) have been studied extensively over the last decade. The metallic character of the compounds was established by Cutforth et al., (1977) who measured the variation of low temperature conductivity. The conductivity was high in the a and b directions because of the conduction along the chains. A lower conductivity observed in the c direction was attributed to the conduction through the crossing points between the mutually perpendicular chains which are 3.24 Å apart. A temperature independent anisotropy ρ_a/ρ_c (ratio between conductivities in a and c directions) was reported to be 100 for $Hg_{3-\delta}AsF_6$ and 40 for $Hg_{3-\delta}SbF_6$.

The Fermi surface of $Hg_{3-\delta}AsF_6$ has been determined by Razavi, Datars, Chartier, Gillespie (1979) using de Haas - van Alphen effect (Fermi surface of $Hg_{3-\delta}SbF_6$ has also been reported by Batalla, Razavi, Datars, 1982). It consists of rectangular cylinders with axes parallel to the c axis which are formed by two sets of flat 1-dimensional Fermi surfaces normal to the a and b axes. The rectangular shape confirms that the materials have been correctly classified as 1-dimensional conductors although high conductivity is observed in two (a and b)

directions. (For a truly 2-dimensional conductor the Fermi surface would be a circular cylinder). From the positions of the flat Fermi surfaces the authors inferred that each Hg atom contributes two free electrons, but one electron for every (3-δ) Hg atoms is transferred to the AsF_6^{1-} ions of the host lattice and the rest are responsible for the electronic conduction.

Other properties such as optical reflectivity and thermoelectric power have also been studied (Koteles, Datars, Cutforth, Gillespie, 1976; Scholz, Datars, Chartier, Gillespie, 1977). When the materials were examined by a low temperature DTA experiment, extrusion of Hg from the host lattice was observed indicating that the thermal contraction of the chains is smaller than that of the host lattice (Datars, van Schyndel, Lass, Chartier, Gillespie, 1978). In a neutron diffraction experiment Pouget, Shirane, Hastings, Heeger, Miro, MacDiarmid (1978) noted that the contraction of the chains is so small that it is unobservable.

Only the diffraction experiments will be described in the rest of this chapter since they are related to this thesis. For the other experiments the reader should consult the review article by Brown, Datars and Gillespie (1982).

The first low temperature neutron scattering experiment on $Hg_{3-\delta}AsF_6$ was carried out by Hastings, Pouget, Shirane, Heeger, Miro, MacDiarmid in 1977. They observed phonon-like excitations in the Hg chains with a high velocity of sound ($c = 4.4 \times 10^5$ cm/sec)* indicating a strong intrachain bonding between the Hg atoms. A room temperature scan along the first order diffuse scattering sheet in the $\underline{a}^*\underline{b}^*$ plane

* More recent measurements give $c = 3.6 \times 10^5$ cm/sec (Heilmann et al., 1979).

gave a uniform distribution of elastically scattered neutrons from the chains. This observation confirms the conclusion of Brown et al. (1974) that there is no coherence between parallel chains at room temperature. Similar scans at lower temperatures showed intensity modulation of the sheets signalling the development of ordering between the chains. For T > 120 K broad peaks were observed but as T → 120 K new narrow peaks suddenly appeared at different locations from the broad peaks. As T was lowered below T_c (120 K) the narrow peaks grew very quickly while the original broad peaks disappeared. Hastings et al. associated the broad peaks with partial ordering between the parallel chains and the narrow peaks with a long-range three dimensional ordering of the two perpendicular sets of chains.

The nature of this order-disorder phase transition was studied thoroughly by the same workers and reported in a subsequent publication (Pouget et al., 1978).

About the same time Emery and Axe (1978) published a theory of the disordered chains in which they argued that the chains must be in a 1-dimensional liquid state at temperatures above T_c, i.e., before they freeze into a 3-dimensional lattice, since a 1-dimensional system cannot sustain long range order at any finite temperature. Their theory made a number of predictions which can be tested by experiment. One of these was that the thickness of the diffuse scattering sheets is finite and should vary as n^2T where n is the order of the sheet. This prediction was verified by Spal, Chen, Egami, Nigrey, Heeger (1980) using X ray scattering.

Emery and Axe also proposed a theory dealing with the evolution of the long-range order phase at temperatures below T_c. In this theory an order parameter is defined so that it is proportional to the square-root of the intensity of the narrow peaks which appear on the

first order diffuse scattering sheet. By using mean field theory the order parameter was calculated as a function of T.

1.6 Discovery of more mercury compounds and further experiments

After the experimental work for this thesis was started with a structure determination of $Hg_{3-\delta}SbF_6$, two more Hg chain compounds $Hg_{3-\delta}NbF_6$ and $Hg_{3-\delta}TaF_6$ were discovered. During attempts to prepare them other new materials were also produced and some have been successfully isolated. This thesis reports X ray and neutron diffraction studies on these materials.

Basic diffraction theory underlining the experiments is described in Chapter II. Diffraction from infinite disordered chains (Emery and Axe, 1978) is also discussed in that chapter (sec. 2.5). Techniques used for X ray structure determination are given towards the end of the chapter (sec. 2.6 and on).

Chapter III reports the structures of the chain compounds at room temperature as well as at lower temperatures.

Chapter IV also deals with the chain compounds but lays emphasis on the ordering of the chains at low temperatures. Emery-Axe theory for the evolution of long-range order is described (sec. 4.6) before presenting the experiments to verify the theory (sec. 4.7).

Chapter V reports the structure of two new materials, Hg_3NbF_6 and Hg_3TaF_6 in which Hg exists in the form of infinite sheets rather than chains. Like the chain compounds they are also metallic but have silver luster instead of gold.

Structures of two new compounds with Hg_4^{2+} and Hg_3^{2+} ions are

described in Chapter VI.

The last chapter of this thesis, Chapter VII, provides conclusions and makes predictions about the possible existence of new oxidation state(s) of Hg and new Hg compounds.

CHAPTER II

INTRODUCTION TO DIFFRACTION THEORY AND EXPERIMENTAL TECHNIQUES

2.1 General introduction to X ray and neutron scattering; dynamic, static and geometrical structure factors

In the first Born approximation the cross section of a scattering process involving an unpolarized incident beam and a scattered beam into a solid angle $d\Omega$ is given by (Marshall and Lovesey, 1971)

$$\frac{d^2\sigma}{d\Omega dE'} = \frac{k'}{k}\left(\frac{m}{2\pi\hbar^2}\right)^2 \sum_{\lambda\lambda'} p_\lambda \left|\langle \vec{k}'\lambda' | \hat{V}_T(\vec{r}) | \vec{k}\lambda \rangle\right|^2 \delta(\hbar\omega + E_\lambda - E_{\lambda'}) \quad (2.1)$$

where E' = energy of scattered particle

$\vec{k},\vec{k}'$ = incident and scattered wave vectors

m = mass of the scattered particle

λ,λ' = initial and final states of the target

p_λ = probability of having the target in state λ

$\hat{V}_T(\vec{r})$ = interaction potential between the target and the radiation

$E_\lambda, E_{\lambda'}$ = initial and final energies of the target.

Since this quantity represents the proportion of the intensity of the incident beam scattered with coordinates E' and $\vec{k}'$, it is also proportional to the intensity of the scattered beam.

To keep the analysis simple one can first consider a target consisting of N identical scattering centers for which the interaction

potential is represented by

$$\hat{V}_T(\vec{r}) = \sum_{j=1}^{N} \hat{V}(\vec{r}-\vec{R}_j) \tag{2.2}$$

The lack of subscript j on $V(\vec{r}-\vec{R}_j)$ emphasizes that the scattering centers are identical. In this case eq. (2.1) reduces to the scattering law (Marshall and Lovesey, 1971)

$$\frac{d^2\sigma}{d\Omega dE'} = N\frac{k'}{k}\left(\frac{m}{2\pi\hbar^2}\right)^2 |\hat{V}(\vec{q})|^2 S(\vec{q},\omega) \tag{2.3}$$

where $\vec{q} \equiv \vec{k}' - \vec{k}$ (2.4)

$$\hat{V}(q) \equiv \int d\vec{r}\, \exp(i\vec{q}\cdot\vec{r})V(\vec{r}) \tag{2.5}$$

and $$S(\vec{q},\omega) \equiv \frac{1}{2\pi\hbar N}\int_{-\infty}^{\infty} dt\, e^{-i\omega t} \sum_{jj'} \langle \exp\{-i\vec{q}\cdot\vec{R}_j(0)\}\exp\{i\vec{q}\cdot\vec{R}_{j'}(t)\}\rangle \tag{2.6}$$

where $\langle\ \rangle$ denotes the ensemble average which is also the time average of the system (Ergodic Theorem; Reichl, 1980).

The quantity $S(\vec{q},\omega)$ is called the dynamic structure factor which describes elastic and inelastic scattering from a sample. It is therefore used in the analysis of inelastic neutron scattering experiments and scattering from liquids. This is, however, by no means to imply that the above equations hold only for neutron scattering. They are indeed good for scattering of any kind of radiation in the limit of the first Born approximation.

In an X ray scattering experiment one usually does not analyse the scattered radiation in energy as the resolution is very poor. The cross-section or, equivalently, the observed scattered intensity is therefore proportional to the dynamic structure factor integrated over all energies.

$$S(\vec{q}) \equiv \int_{-\infty}^{\infty} d(\hbar\omega) S(\vec{q},\omega) \tag{2.7}$$

$$= \frac{1}{N} \sum_{jj'} \langle \exp\{-i\vec{q}\cdot\vec{R}_j(0)\} \exp\{i\vec{q}\cdot\vec{R}_{j'}(0)\} \rangle \tag{2.8}$$

The quantity $S(\vec{q})$ is called static structure factor.

It is now convenient to define a quantity $F(\vec{q})$ so that $|F(\vec{q})|$ is equal to the time averaged total amplitude of the scattered radiation from the target. By considering the interference of wavelets scattered by a system of identical scattering centers at $\vec{R}_j$ (j = 1,N) one gets (Woolfson, 1979)

$$F(\vec{q}) \equiv \langle \sum_j \exp\{i\vec{q}\cdot\vec{R}_j\} \rangle \tag{2.9}$$

$F(\vec{q})$ is called geometrical structure factor and is widely used in X ray and elastic neutron diffraction experiments. From (2.8) and (2.9) the relation between the two structure factors is seen to be

$$S(\vec{q}) = \frac{1}{N} F^*(\vec{q}) F(\vec{q}) \tag{2.10}$$

The lack of a factor representing the relative scattering amplitude of each scattering center on the R.H.S. of eq. (2.9) is again a consequence of having only one type of scattering centers in the target. For the targets with more than one type of scattering centers such a factor is essential and is called form factor or scattering factor. In general, it is a complex number and a function of $\vec{q}$, hence is denoted by $f(\vec{q})$. The phase of $f(\vec{q})$ represents the phase shift suffered by the radiation when it is scattered from the scattering center. If the scattering centers are spherically symmetric, which is a normal assumption in practice, $f(\vec{q})$ reduces to $f(q)$. In this case

eq. (2.9) becomes

$$F(\vec{q}) = \langle \sum_j f_j(q) \exp\{i\vec{q}\cdot\vec{R}_j\} \rangle \qquad (2.11)$$

An alternative way of writing eq. (2.11) can be found if one recognises that X rays are scattered by electrons and the electronic distribution in a crystal is continuous. Each point inside the crystal can therefore be viewed as a scattering center with scattering amplitude $\langle \rho(\vec{r}) \rangle$ where the latter is the time averaged electron density at that point. Therefore, (2.11) can also be written as (Woolfson, 1979)

$$F(\vec{q}) = \int_{\text{crystal}} d^3r \langle \rho(\vec{r}) \rangle \exp\{i\vec{q}\cdot\vec{r}\} \qquad (2.12)$$

2.2 X ray diffraction from a 3-dimensional crystal

In the previous section the geometrical structure factor $F(\vec{q})$ was defined without giving the physical concept behind the definition eq. (2.11). The jnsight into this equation can be gained by considering the following elastic scattering problem.

Consider two stationary scattering centers which are different and are separated by a vector $\vec{r}$ as shown in fig. (2.1). For collimated incident radiation the indicent beams are parallel. The scattered beams are also shown parallel because the detector is usually at a distance much larger than $|\vec{r}|$ (Fraunhofer diffraction).

From the diagram;

path difference = $r(\sin\mu_1 + \sin\mu_2) = \vec{r}\cdot\hat{S}' - \vec{r}\cdot\hat{S}$

where $\hat{S}$ and $\hat{S}'$ are the unit vectors in the direction of incident beam and the diffracted beam.

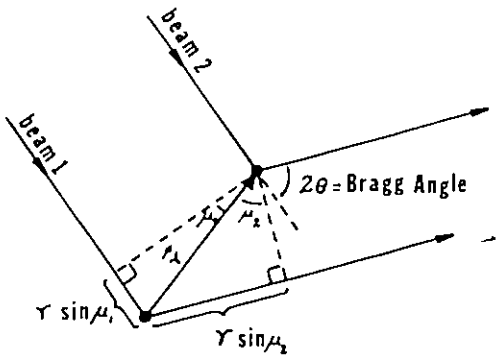

Fig. 2.1. Two scattering centers exposed to a well-collimated incident radiation. Scattering center 2 is located at vector $\vec{r}$ from 1:

A vector $\vec{s}$ which is called "scattering vector" is defined as

$$\vec{s} \equiv \frac{\hat{S}' - \hat{S}}{\lambda} = \frac{1}{2\pi}\vec{q} \tag{2.13}$$

$$\therefore \text{ phase difference} = \frac{\text{path difference}}{\lambda}$$

$$= \vec{r}\cdot\vec{s} \tag{2.14}$$

The following simple relation between $|\vec{s}|$ and the Bragg angle, 2θ, should also be noted.

$$|\vec{s}|^2 = (2 - 2\hat{S}'\cdot\hat{S})/\lambda^2 = \frac{2}{\lambda^2}(1-\cos 2\theta) = \frac{4\sin^2\theta}{\lambda^2}$$

$$\therefore \quad |\vec{s}| = 2\sin\theta/\lambda \tag{2.15}$$

By using the phase relation given in eq. (2.14) the amplitude of the resultant radiation can be calculated.

$$\text{resultant amplitude} = f_1(s) + f_2(s)e^{2\pi i\vec{r}\cdot\vec{s}} \tag{2.16}$$

where $f_1(s)$ and $f_2(s)$ are the form factors of scattering center 1 and 2.

If there are N scattering centers at $\vec{r}_1, \vec{r}_2, \ldots, \vec{r}_N$ in a crystal

$$\text{resultant amplitude} \quad F(\vec{s}) = \sum_{j=1}^{N} f_j(s) e^{2\pi i \vec{r}_j \cdot \vec{s}} \tag{2.17}$$

A number of approximations have been employed in generalizing eq. (2.16) into (2.17). For a real crystal, N is a very large number ($\sim 10^{23}$). The probability of multiple scattering is enhanced by having many scattering centers (Primary extinction). Moreover, scattering centers further from the source of radiation experience weaker incident radiation because some part of it has already been scattered by the centers closer to the source (Secondary extinction). As an approximation both extinction effects may be ignored when the interaction between radiation and matter is weak. The diffraction theory based on this assumption is known as the kinematic diffraction theory. The approximation is reasonably good for X rays and neutrons but the effects are not entirely negligible. (See sec. 2.11 for a discussion on methods of correcting for extinction).

One should also note that radiation absorption by the sample has been ignored in deriving eq. (2.17). This is an approximation in the theory but the effect is often too strong to be ignored in practice. (See sec. 2.10 for discussion on methods of correcting for absorption).

For a real crystal in which the atoms are oscillating about their equilibrium positions because of thermal vibrations

$$F(\vec{s}) = \left\langle \sum_j f_j(s)\, e^{2\pi i \vec{R}_j \cdot \vec{s}} \right\rangle \tag{2.18}$$

which is the same as eq. (2.11). Note that the upper case letter $\vec{R}_j$ is

used to denote the instantaneous position of the j^{th} atom. The lower case letter $\vec{r}_j$ denotes the equilibrium position of the same atom or, in the special case of static crystal, the position. $\vec{R}_j$ and $\vec{r}_j$ are related by

$$\vec{R}_j(t) = \vec{r}_j + \vec{u}_j(t) \tag{2.19}$$

where $\vec{u}_j(t)$ is the instantaneous displacement of the atom.

Similarly, for a continuous distribution of electron density $\bar{\rho}(\vec{r}) = \langle \rho(\vec{r}) \rangle$

$$F(\vec{s}) = \int_{\text{crystal}} d^3r \bar{\rho}(\vec{r}) \exp\{2\pi i \vec{r}\cdot\vec{s}\} \tag{2.20}$$

Eq. (2.18) and (2.20) are extensively used in X ray determination of the structures of the crystals. To take the full advantage of these equations one must study the two basic properties of $\bar{\rho}(\vec{r})$; the periodicity and the spatial extension throughout the crystal.

2.3 Unit cell and reciprocal lattice

To a very good approximation the time-averaged electron density inside a crystal is a 3-dimensional periodic function provided the crystal does not suffer from any kind of serious disorder. As a consequence one can define a small parallelepiped with edges $\vec{a}$, $\vec{b}$ and $\vec{c}$ so that the whole crystal can be generated by translations of this unit by vectors $n_1\vec{a} + n_2\vec{b} + n_3\vec{c}$ for all possible integers n_1, n_2, n_3. This is called a unit cell and $\vec{a}$, $\vec{b}$, $\vec{c}$ and the angles between them are called the lattice parameters. The unit cell is not unique but it is normally chosen to minimize the cell volume V while maintaining as high internal symmetry as possible.

A reciprocal unit cell is defined as follows.

$$\vec{a}^* \equiv \vec{b}\times\vec{c}/V$$
$$\vec{b}^* \equiv \vec{c}\times\vec{a}/V \qquad (2.21)$$
$$\vec{c}^* \equiv \vec{a}\times\vec{b}/V$$

The following linear combination of the above vectors is known as a reciprocal lattice vector and will be denoted by $\vec{K}$.

$$\vec{K} \equiv n_1\vec{a}^* + n_2\vec{b}^* + n_3\vec{c}^* \qquad (2.22)$$
$$(n_1, n_2, n_3 \text{ are integers})$$

Note that the orientations of $\vec{a}$, $\vec{b}$, $\vec{c}$ and $\vec{a}^*$, $\vec{b}^*$, $\vec{c}^*$ depend on the orientation of the crystal.

The equilibrium position of an atom in the crystal is usually specified by

$$\vec{r} = X\hat{a} + Y\hat{b} + Z\hat{c} = x\vec{a} + y\vec{b} + z\vec{c} \qquad (2.23)$$

where $\hat{a} = \vec{a}/|\vec{a}|$, etc. are the unit vectors.

The coordinates $x = X/|\vec{a}|$, $y = Y/|\vec{b}|$, $z = Z/|\vec{c}|$ are the fractional coordinates in the units of $|\vec{a}|, |\vec{b}|, |\vec{c}|$.

If the scattering vector $\vec{s}$ is expressed in terms of $\vec{a}^*$, $\vec{b}^*$, $\vec{c}^*$,

$$\vec{s} = h\vec{a}^* + k\vec{b}^* + \ell\vec{c}^*, \qquad (2.24)$$

it is easy to prove that the phase difference $\vec{r}\cdot\vec{s}$ is,

$$\vec{r}\cdot\vec{s} = hx + ky + \ell z \qquad (2.25)$$

Similarly,

$$\vec{r}\cdot\vec{K} = n_1x + n_2y + n_3z \qquad (2.26)$$

The space spanned by vector $\vec{s}$ is known as the reciprocal space.

2.4 The "infinite" crystal

One more approximation is introduced at this point for the sake of mathematical convenience; the periodic function $\bar{\rho}(\vec{r})$ is assumed to entend from $-\infty$ to $+\infty$ in all three directions. Obviously, no real crystal even if it is a perfect single crystal free from defects, meets this condition. Most of the real crystals are divided into perfectly ordered mosaic crystallites of smaller dimension ($\sim$ a few microns), but as long as the mosaic size is large enough to accommodate many ordered unit cells the approximation is justified.

Eq. (2.20) now becomes,

$$F(\vec{s}) = \int_{\text{infinite}} d^3r \bar{\rho}(\vec{r}) \exp\{2\pi i \vec{r}\cdot\vec{s}\} \tag{2.27}$$

The above relation between $\bar{\rho}(\vec{r})$ and $F(\vec{s})$ is a Fourier transform. The inverse relation is given by the Fourier theorem.

$$\bar{\rho}(\vec{r}) = \int_{\text{infinite}} d^3s F(\vec{s}) \exp\{-2\pi i \vec{r}\cdot\vec{s}\} \tag{2.28}$$

Another very important benefit of having $\bar{\rho}(\vec{r})$ as an infinite periodic function is that it can be expressed as a Fourier series.

$$\begin{aligned}
\bar{\rho}(\vec{r}) &= \sum_{n_1=-\infty}^{\infty} \sum_{n_2=-\infty}^{\infty} \sum_{n_3=-\infty}^{\infty} C_{n_1 n_2 n_3} \exp\{-2\pi i (n_1 \tfrac{X}{a} + n_2 \tfrac{Y}{b} + n_3 \tfrac{Z}{a})\} \\
&= \sum_{n_1=-\infty}^{\infty} \sum_{n_2=-\infty}^{\infty} \sum_{n_3=-\infty}^{\infty} C_{n_1 n_2 n_3} \exp\{-2\pi i (n_1 x + n_2 y + n_3 z)\} \\
&= \sum_{n_1=-\infty}^{\infty} \sum_{n_2=-\infty}^{\infty} \sum_{n_3=-\infty}^{\infty} C_{n_1 n_2 n_3} \exp\{-2\pi i \vec{r}\cdot\vec{K}\},
\end{aligned} \tag{2.29}$$

the last step using eq. (2.26).

Eq. (2.29) implies that $\bar{\rho}(\vec{r})$ is the summation of exponential

waves with wave vector $-2\pi\vec{K}$, amplitude $|C_{n_1n_2n_3}|$ and the initial phase $\alpha_{n_1n_2n_3}$. These waves are the Fourier components of $\bar{\rho}(\vec{r})$.

The Fourier transform of one of the components can be written as

$$\Gamma(\vec{s}) = \int dr C_{n_1n_2n_3} \exp\{-2\pi i\vec{r}\cdot\vec{K}\}\exp\{2\pi i\vec{r}\cdot\vec{s}\}$$

$$= C_{n_1n_2n_3}\int d\vec{r}\ \exp\{2\pi i\vec{r}\cdot(\vec{s}-\vec{K})\}$$

In the above integral, exponential terms will sum up constructively only if $\vec{s} = \vec{K}$.

$$\therefore\ \Gamma(\vec{s}) = C_{n_1n_2n_3}\delta(\vec{s}-\vec{K}) \qquad (2.30)$$

Note that $\Gamma(\vec{s})$ is a δ-function at $\vec{s} = \vec{K}$ and is weighted by the magnitude of the corresponding Fourier component, $|C_{n_1n_2n_3}|$. Combining eq. (2.27), (2.29) and (2.30) gives,

$$F(\vec{s}) = \sum_{n_1=-\infty}^{\infty}\sum_{n_2=-\infty}^{\infty}\sum_{n_3=-\infty}^{\infty} C_{n_1n_2n_3}\delta(\vec{s}-\vec{K}) \qquad (2.31)$$

The above equation shows that $F(\vec{s})$ is a set of δ-functions located at the reciprocal lattice points and weighted by the amplitude of the corresponding Fourier component. $F(\vec{s} \neq \vec{K}) = 0$ which implies that the amplitude (or intensity) of diffracted X rays is zero unless the scattering vector $\vec{s}$ happens to be equal to one of the reciprocal lattice vectors $\vec{K}$. This is the well-known Bragg condition for X ray diffraction.

What happens to the δ functions if the infinite crystal approximation breaks down? A complete analysis of this problem is provided by James (1958) in The Optical Principle of the Diffraction of X Rays.

He considered that there were $N_1 << \infty$ ordered unit cells along the crystal axis $\vec{a}$. The calculations suggested that the δ-peaks would become broader in the direction of $\vec{a}^*$ with small diffraction ripples around and the first diffraction minima at $(h \pm \frac{1}{N_1})a^*$. (See the dotted curve of Fig. 2.2)*. Broad diffraction peaks are indeed taken as the sign of poor or short range ordering of the crystal.

Since $F(\vec{s})$ is a set of δ-functions for an ordered crystal eq. (2.28) is reduced to

$$\bar{\rho}(\vec{r}) = \sum_{h=-\infty}^{\infty} \sum_{k=-\infty}^{\infty} \sum_{\ell=-\infty}^{\infty} F(\vec{s}) \exp\{-2\pi i(hx + ky + \ell z)\} \qquad (2.32)$$

In crystal structure determination the crystallographer's task is to calculate $\bar{\rho}(\vec{r})$ in order to find the position of the atoms. According to eq. (2.32) this can be done once the magnitude and the phase of $F(\vec{s})$ are known.

2.5 Diffraction from one-dimensional disordered chains

The diffraction from 1-dimensional disordered chains of the $Hg_{3-\delta}MF_6$ compounds was first systematically studied by Emery and Axe (1978). In their model the chains are assumed to be isolated chains with harmonic interaction only between nearest neighbours. All other interactions such as those between chains or between the chains and the host lattice are completely ignored. The physical picture is extremely simple, the chain consists of identical masses connected by identical harmonic springs. The strong Hg-Hg bond suggests that springs should

* The same broadening will occur to all the peaks regardless of their coordinates in $\vec{b}^*$ and $\vec{c}^*$ directions.

be very stiff. The classical Hamiltonian for each chain can be expressed as follows.

$$H = \text{kinetic energy} + \text{potential energy in the bonds} \qquad (2.33)$$

$$H = \tfrac{1}{2}\sum_{\alpha}\left[\frac{p_\alpha^2}{m} + mc^2\frac{(x_{\alpha+1} - x_\alpha - d)^2}{d^2}\right] \qquad (2.34)$$

where α = α^{th} atom in a particular chain

d = equilibrium Hg-Hg distance = $d_{Hg\text{-}Hg}$

m = mass of Hg atom

c = speed of sound along the chain (longitudinal)

x_α = instantaneous position of α^{th} atom (origin at 0^{th} atom)

p_α = instantaneous momentum of the α^{th} atom,

and the summation is over the whole chain. All vector quantities are written as scalars in the equation since the system is 1-dimensional. The instantaneous position of the α^{th} atom at time t, $x_\alpha(t)$, is related to its ground state position (ignoring the zero point motion of the atoms) αd by

$$x_\alpha(t) = \alpha d + u_\alpha(t) \qquad (2.35)$$

where $u_\alpha(t)$ is the instantaneous displacement of the atom.

To comprehend the Emery-Axe model it is essential to consider the nature of $u_\alpha(t)$ or its r.m.s. value σ_α. Although the Hg-Hg bonds are strong they are not perfectly rigid and the bond length is associated with a small uncertainty σ which is defined as the r.m.s. value of $(x_1(t) - d)$, or equivalently, σ_1. The mean square value σ^2 is directly proportional to the temperature of the sample since it measures the

(amplitude)^2 of the harmonic motion of an atom with respect to its neighbours.

$$\sigma^2/d^2 = \sigma_1^2/d^2 = \frac{k_B T}{mc^2} \qquad (2.36)$$

$m = 3.35 \times 10^{-25}$ kg, $c = 3.6 \times 10^3$ ms^{-1} (Heilmann et al., 1979)

At 300 K, $\frac{\sigma}{d} = 3.1 \times 10^{-2}$

The uncertainty in the bonds adds up in a statistical manner so that for a string of α bonds

$$\sigma_\alpha^2 = |\alpha|\sigma^2 \qquad (2.37)$$

Since $\alpha \to \infty$ in a real crystal the last equation implies that there is no long range ordering within a chain; a well-known characteristic of 1-dimensional systems with finite interaction. The lack of long range order, however, does not prevent one from using harmonic approximation and considering phonon-like excitations and the dispersion relation, because there is very good short range ordering due to the stiff Hg-Hg bonds. In fact, the dispersion curve of the chains have been measured by Hastings et al. (1977) who found a large velocity for the longitudinal acoustic waves.

The lack of long range ordering has important consequences on the scattering of neutrons and X rays from the chains. The Debye-Waller factors along the chains are infinite due to the infinite value of $\langle u_\alpha^2 \rangle$ and no truly elastic scattering (Bragg scattering) is possible. The sheets of the diffuse scattering must therefore be the result of inelastic scattering.

For this 1-dimensional case the dynamic structure factor defined by eq. (2.6) reduces to*

$$S(Q,\omega) = \frac{1}{2\pi N}\int_{-\infty}^{\infty} dt\, e^{-i\omega t} \sum_{\alpha\alpha'} \langle \exp\{-iQx_{\alpha}(0)\}\exp\{iQx_{\alpha'}(t)\}\rangle \qquad (2.38)$$

where Q is the x-component of $\vec{q}$.**

Emery and Axe calculated both the static and the dynamic structure factors and obtained the former as,†

$$S(Q) = \frac{\sinh(Q^2\sigma^2/2)}{\cosh(Q^2\sigma^2/2) - \cos Qd} \qquad (2.39)$$

Fig. 2.2 illustrates a plot of S(Q) vs. Q with σ = 0.1. The broadening of the high order peaks is more characteristic of the scattering from liquids rather than solids. The peaks are Lorentzian centered upon

$$Q_n = \frac{2\pi}{d}\cdot n \qquad (2.40)$$

with the width (HWHM) of

$$K_n = \frac{Q_n^2\sigma^2}{2d} \propto n^2 T \qquad (2.41)$$

The predicted proportionality of eq. (2.41) has been verified by using X ray scattering (Spal et al., 1980). The n^2T variation basically confirms the Emery-Axe model of the chains but the measured peak widths are consistantly smaller than the predicted values by ~ 20%.

---

* For a classical calculation the $\hbar$ in the denominator has been dropped.

** For simplicity, we are considering only a-chains and this will be the case throughout the thesis unless otherwise stated.

† In the original paper only the major results were presented without any intermediate steps. The calculation has been repeated independently by Talbot (1979) and presented in detail in his thesis.

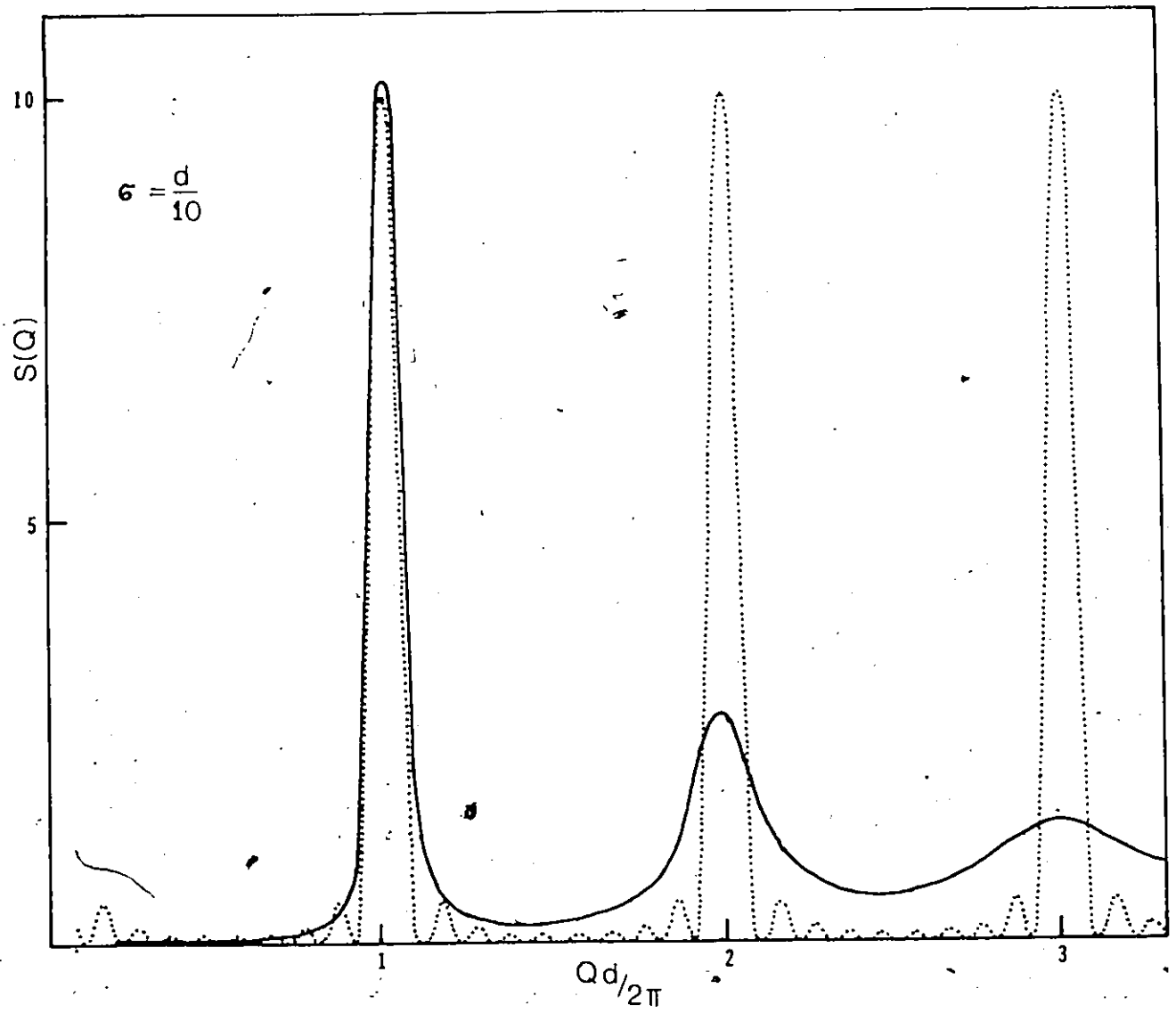

Figure 2.2

Intensity of scattered radiation from 1-dimensional harmonic liquid (solid curve) predicted by eq. (2.39). After Axe (1980). To make the broadening of the peaks visible in the plot the uncertainty in the Hg-Hg bond length is exaggerated as if $\sigma/d = 0.1$ but the actual value is only 0.031 at room temperature. This is so small that the broadening of the diffuse scattering sheets is not noticeable in the precession photograph fig. 3.1 . For comparison the dotted curve representing the diffracted intensity (scaled down by a factor of 10) resulted from a finite chain of 10 atoms but with no uncertainty in the bond length is shown.

The dynamic structure factor obtained by Emery and Axe is rather complicated but can be simplified for small $\Delta Q = Q - Q_n$ to

$$S(Q,\omega) \sim \frac{K_n}{[(\Delta Q - \omega/c)^2 + K_n^2]} \frac{K_n}{[(\Delta Q + \omega/c)^2 + K_n^2]} \tag{2.42}$$

Note that there is no term proportional to $\delta(\omega)$ since no true elastic scattering is possible. In particular, when $\Delta Q = 0$,

$$S(Q,\omega) \sim \frac{K_1^2}{[(\omega/c)^2 + K_1^2]^2} \tag{2.43}$$

Since K_1 is very small, $S(Q,\omega)$ is very large only when ω is extremely close to zero. For larger values of ω, $S(Q,\omega) \to 0$. This implies that the diffuse scattering sheets arise from inelastic scattering with extremely small energy transfer.

The disordered Hg chains of the $Hg_{3-\delta}MF_6$ compounds are often referred to as "1-dimensional liquid" because the chains do not have any long range ordering and their scattering is very much like that of liquid samples.

2.6 Crystal structure determination; practical considerations

Since the intensity of radiation is proportional to the square of the amplitude the magnitude of $F(\vec{s})$ can easily be measured on an arbitrary scale.

$$I(\vec{s}) \propto F^*(\vec{s})F(\vec{s})$$

$$\therefore \quad |F(\vec{s})| \propto \sqrt{I(\vec{s})} \tag{2.44}$$

where $I(\vec{s})$ is the observed diffracted intensity in the direction

corresponding to the scattering vector $\vec{s}$.*

Note that eq. (2.44) alone is not enough to determine $F(\vec{s})$ since it does not contain any phase information. Crystallographers, therefore, have to use some indirect methods to deduce the phase of $F(\vec{s})$. The standard technique is to propose a model for $\rho(\vec{r})$, at least approximately, and then verify and improve the model by a least-squares refinement. The aim of the refinement is to improve the agreement between $|F(\vec{s})|_{\text{observed}}$ and $|F(\vec{s})|_{\text{calculated}}$ usually denoted by F_o and F_c respectively.

The model most commonly used by crystallographers is the "Independent Atom Model" (IAM). The model consists of spherical atoms (or ions) which are allowed to undergo harmonic oscillations, independently and anisotropically about their equilibrium positions.

In the IAM the electron density is not continuous but localized at the atomic sites. Eq. (2.18) is therefore more suitable than (2.20) for calculating $F(\vec{s})$. Since the time-averaged unit cells are identical to each other the summation needs only be done for one unit cell rather than the whole crystal. This scales down all the $F(\vec{s})$ by a common factor, i.e., 1/number of unit cells, and hence the proportionality (2.44) is not affected. Evaluating the thermal average in Eq. (1.18) is also easy for the independent harmonic oscillators. In the IAM, eq. (2.18) combined with (2.19) becomes (Woolfson, 1979)

$$F(\vec{s}) = \sum_{n=1}^{N} f_n(s) \langle \exp(2\pi i \vec{u}_n \cdot \vec{s}) \rangle \exp(2\pi i \vec{r}_n \cdot \vec{s})$$

---

* A number of corrections have to be applied to the measured diffracted intensities before using them in eq. (2.44) to get $|F(\vec{s})|$. These corrections are discussed in the following sections.

$$F(hk\ell) = \sum_{n=1}^{N} f_n(s)\exp\{-2\pi^2(\vec{u}_n\cdot\vec{s})^2\}\exp(2\pi i\vec{r}_n\cdot\vec{s})$$

where N = number of atoms inside a unit cell and h, k, ℓ are the components of $\vec{s}$ in unit of $\vec{a}^*$, $\vec{b}^*$, $\vec{c}^*$ axes.

In the last equation the first exponential factor is called temperature factor or Debye-Waller factor. For the independent harmonic oscillators of IAM

$$(\vec{u}_n\cdot\vec{s})^2 = \vec{s}^T\hat{U}_n\vec{s}$$

$$= \langle h^2a^{*2}u_x^2 + k^2b^{*2}u_y^2 + \ell^2c^{*2}u_z^2 + 2hka^*b^*u_xu_y + 2h\ell a^*c^*u_xu_z + 2k\ell b^*c^*u_yu_z\rangle$$

where $\vec{s}^T$ = $\vec{s}$(transposed) and $\hat{U}_n$ is a 3x3 matrix with the elements $U_{ij} = \langle u_iu_j\rangle$.

Therefore U_{11}, for example, gives the mean square displacement of the corresponding n^{th} atom in the direction of $\vec{a}$ axis. Note that $\hat{U}_n$ is symmetric and contains only six independent elements. In general, the thermal motion of the atom is anisotropic, i.e., $U_{11} \neq U_{22} \neq U_{33}$ and $\hat{U}_n$ is called anisotropic temperature factor. But it is sometimes desirable to assume an isotropic motion of the atom (in order to reduce the number of adjustable parameters in the model, for example). For such an atom $\hat{U}_n$ becomes an isotropic temperature factor $U_n\hat{I}_3$ for which U_n, a scalar, is the single adjustable thermal parameter and $\hat{I}_3$ is a 3x3 unit matrix.

The equation for $F(hk\ell)$ finally becomes,

$$F(hk\ell) = \sum_{n=1}^{N} f_n(s)\exp\{-2\pi^2\vec{s}^T\hat{U}_n\vec{s}\}\exp\{2\pi i\vec{r}_n\cdot\vec{s}\} \qquad (2.45)$$

Standard crystallographic programs use eq. (2.45) to compute the calculated structure factor F_c. The form factors are given in the International Tables for X ray crystallography (1974), Vol. IV, p. 72 for all atoms and most of the known ions. The agreement between F_o and F_c is then improved by a least-squares refinement of $\vec{r}_n$ (positional parameters) and U_n (thermal parameters) which, in combination, are referred to as atomic parameters.

Success of a structure determination therefore depends on the following factors.

(i) Accurate intensity measurements followed by a series of corrections to remove the systematic errors.

(ii) An IAM which represents $\rho(\vec{r})$ to a good approximation so that it can be used as the initial model for the least-squares refinement.

The rest of this chapter is devoted to the discussion of the instruments, corrections and techniques used to meet the requirements of these factors.

2.7 Instruments to survey the reciprocal space

(i) Photographic methods; the precession camera

Photographic methods are particularly useful to survey the reciprocal space of crystal with serious disorder whose diffraction pattern consists of unusual features such as diffuse scattering regions or deformed Bragg peaks. These features can most conveniently be studied when they are mapped out on a photographic plate, a two-dimensional detector of low accuracy but very large sensitive area.

Although many different kinds of camera are available to

X ray crystallographers precession camera is perhaps the most convenient one to use since it gives a non-distorted view of a plane of reciprocal space. Construction and diffraction geometry of this camera are given in many crystallographic text books.

(ii) Four-circle X ray diffractometer

More accurate intensity measurements can be obtained from a diffractometer than from a camera at the expense of longer experimental time since, unlike the camera, the diffractometer examines only one point of reciprocal space at a time.

A four-circle diffractometer is shown schematically in fig. 2.3. The angle 2θ is the usual Bragg angle while ω, χ and ϕ are the three Euler angles determining the orientation of the crystal on the instrument. Any point of reciprocal space can be examined by setting these four angles to the appropriate positions.

The incident X ray beam is monochromatized by using a high quality pyrolytic graphite crystal. The diffracted beam from the sample is directly measured by a scintillation counter without an energy analyzer. The diffracted intensity at a point of reciprocal space is usually measured by performing a 2θ-ω scan across the point. The scan is immediately preceded and followed by a pair of background intensity measurements.*

The diffractometer can also be used for low temperature diffraction experiments. The low temperature apparatus used consists

* Consult operating manual of Nicolet $P2_1$ diffractometer and LT1 low temperature apparatus for more details.

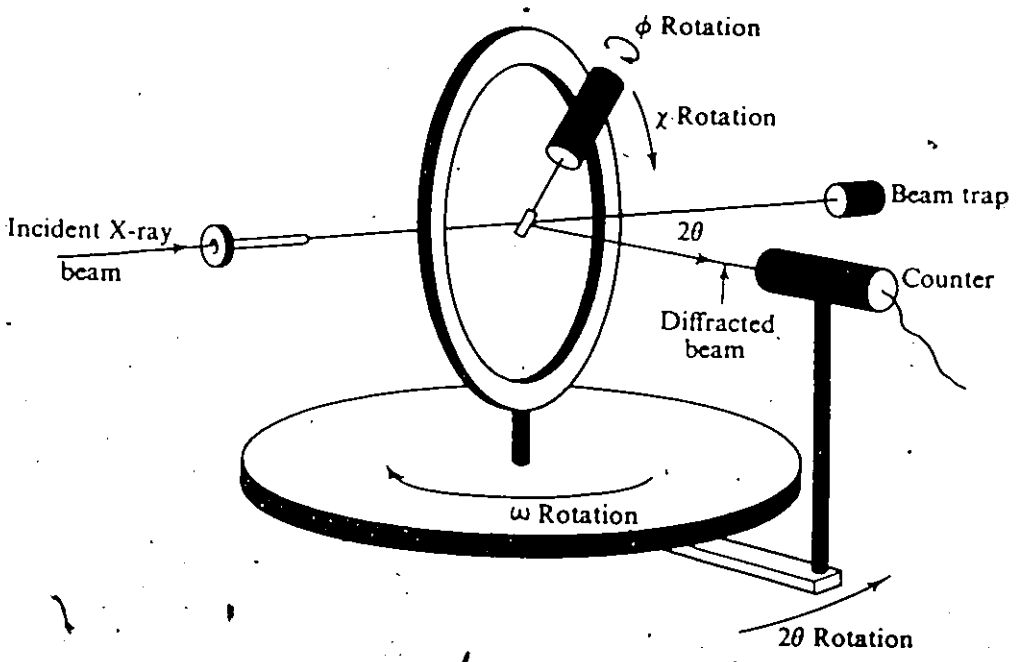

Figure 2.3

A four-circle X ray diffractometer. The angle 2θ is the usual Bragg angle while ω, φ and χ are the Euler angles determining the orientation of the crystal. (From Woolfson, 1979)

of a gas nozzle which blows regulated cold N_2 gas directly onto the crystal. Since the nozzle is firmly attached to the χ-circle its relative orientation to the crystal does not change throughout the experiment. The lowest temperature attainable by this apparatus is about 145 K but higher temperatures can be obtained by warming up the cold gas using a stream heater. The temperature cannot be monitored during the experiments but calibration of temperature against stream heater setting before the experiments indicated that the stability and reproducibility is within ± 3 K.*

(iii) Triple-axes neutron diffractometer

Fig. 2.4 shows a triple-axes diffractometer schematically. Both the monochromator for the incident beam and the energy analyzer for the diffracted beam are pyrolytic graphite crystals mounted on axes perpendicular to the plane of the instrument so that scattering angles at these crystals can be set to any desired values. The sample enclosed in an air-tight Al sample holder (see fig. 2.4) is mounted on a third axis which is parallel to the first two. Since the crystal can be rotated only about this axis (no χ circle) the diffraction is confined in the plane of the instrument and no region of reciprocal space outside this plane can be studied without remounting the sample with a different orientation.

For the low temperature experiments the sample holder is cooled by a close-cycle He refrigerator capable of stabilizing the

---

* Consult operating manual of Nicolet P2$_1$ diffractometer and LTI low temperature apparatus for more details.

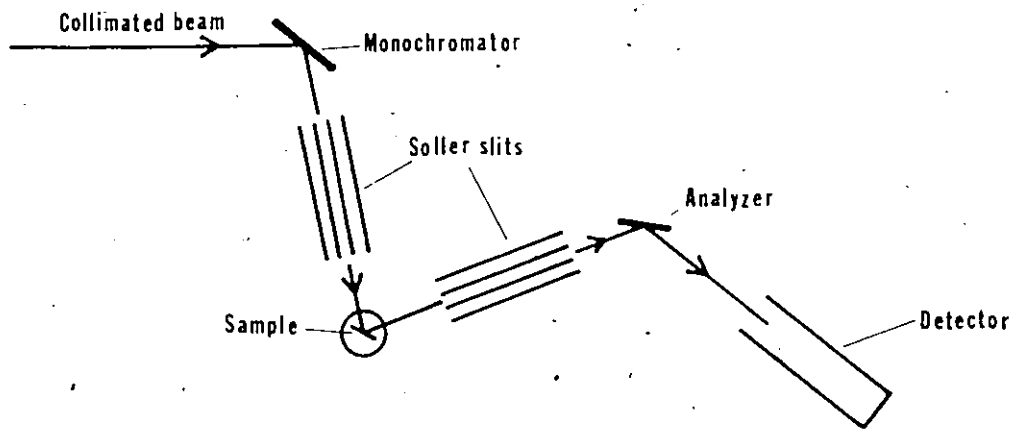

Figure 2.4(a)
Top view of a triple-axes neutron diffractometer.

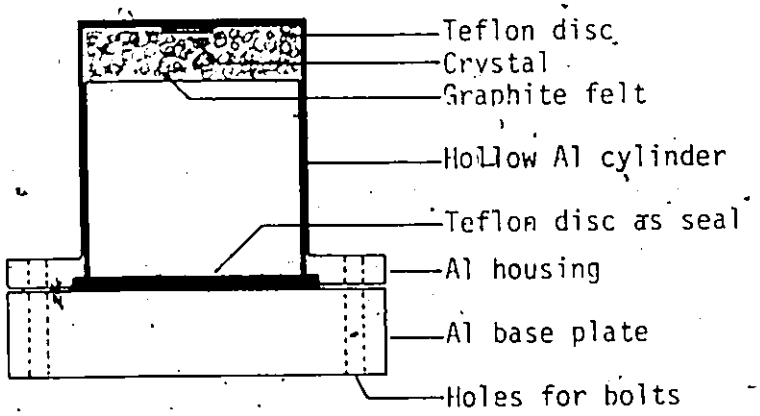

Figure 2.4(b)
Sample holder

temperature within ± 0.1 K in the range of 10 to 300 K. The temperature of the sample holder is continuously monitored throughout the experiment.*

2.8 Scaling the diffractometer-measured intensities

Because output power of the X ray source fluctuates over a period of ~ 1 hour the Bragg intensities measured by a diffractometer over a period of days should be scaled based on the systematic variations observed in a number of selected standard reflections. These reflections are measured periodically, say, every hour throughout the experiment.

Another reason to measure the standard reflections is to monitor the crystal alignment on the diffractometer. Any mechanical movement of the crystal inside the sample holder, for example, will result in a sudden decrease in the intensities of all the standard reflections.

2.9 The Lp correction

The Lorentz correction (L) is required since the time spent by the crystal in reflecting position differs from one Bragg reflection from another depending on the position in the reciprocal space. For a 4-circle diffractometer this correction is a function of 2θ alone. (Nicolet $P2_1$ and P3 reference manuals).

$$L = \frac{1}{\sin 2\theta}$$

The polarization correction (p) is required for the following reason. A certain fraction of incident beam cannot take part in

---

* A triple-axes diffractometer and He refrigerator at Brookhaven National Laboratory were used for the neutron diffraction experiments. Reference manuals may be consulted for details.

scattering if its polarization vector $\vec{E}$ happens to be in the direction of the diffracted beam. The effective incident beam intensity is thus reduced and hence the diffracted beam intensity decreases. Since this effect varies from one Bragg reflection to another the following correction is required (Nicolet reference manuals).

$$p = \left[f\frac{1 + \cos^2 2\theta_m \cdot \cos^2 2\theta_c}{1 + \cos^2 2\theta_m} + (1-f)\frac{1 + \cos 2\theta_m \cdot \cos^2 2\theta_c}{1 + \cos 2\theta_m}\right]$$

where f = 0.5 (depends on the mosaic size of monochromator)

$2\theta_m$ = monochromator angle = 12.160

$2\theta_c$ = usual 2θ angle at the sample crystal

2.10 Absorption correction

A correction to remove the systematic errors in the measured intensities caused by radiation absorption of the sample is necessary if it contains highly radiation absorbing elements such as Hg. The following techniques were used for the structure determinations reported in this thesis.

(i) Numerical integration method

For a crystal with linear absorption coefficient μ the fraction by which the diffracted intensity is reduced by absorption is (Woolfson, 1979)

$$A = \frac{1}{V}\int_{crystal} \exp\{-\mu(\tau+\tau')\}dv \qquad (2.46)$$

where V = volume of the crystal

$\tau(\tau')$ = length of incident (diffracted) beam inside the crystal, where the scattering takes place at volume element dv.

The correction factor applied to the measured intensity is $A^* = A^{-1}$.

For a crystal of regular shape, e.g., a sphere with known radius R, the factor A^* becomes a function of 2θ and its values are tabulated in the International Tables for X ray Crystallography (1959). Vol. II, p. 302. But if the crystal has an arbitrary shape A^* depends also on the other diffractometer angles and it has to be calculated for each reflection by evaluating the integral (2.46) numerically. In this case the volume of the crystal is a polyhedron defined by a set of crystal planes whose orientations and distances from an arbitrarily chosen origin inside the crystal are specified.

(ii) DIFABS correction:

This method developed by Walker and Stuart (1983a) assumes that the absorption correction factor can be factorized into two factors, one representing an isotropic absorption as if the crystal were a perfect sphere and the other a slowing varying function in the reciprocal space representing the anisotropic absorption due to the irregular shape of the crystal. The method is particularly useful if the crystal does not have well-defined faces and cannot be represented by a polyhedron. The absorption correction is applied as follows.

The measured intensities which have been scaled (sec. 2.8) and corrected by an Lp-correction (sec. 2.9) are subjected to the standard spherical absorption correction. The radius of the crystal R assumed

for this correction is the average radius. The resultant intensities are used to refine a model (IAM) in which the atoms are represented by isotropic temperature factors so that the yet uncorrected anisotropic absorption errors are not incorporated into the structure. Since the structure factors calculated from this model $|F_{iso}|$ are not greatly affected by the anisotropic errors they can be treated as the best estimates of absorption-free structure factors. The program DIFABS (Walker and Stuart,1983b) is run at this stage to construct a slowly varying correction function (a Fourier series) and apply it to the all measured structure factors.

2.11 Primary and secondary extinction

Primary extinction is the weakening of the diffracted X ray intensity caused by destructive interference between the original diffracted beam and the diffracted radiation arising from multiple scattering. Its effect is therefore serious for a large crystal with small mosaic spread where a large volume of crystalline material can be brought into a Bragg scattering condition enhancing the probability of multiple scattering. Darwin (1914) has shown that for a perfect crystal the diffracted beam intensity is greatly reduced and is equal to $\sqrt{F^*F}$ rather than F*F where F is given by eq. (2.20). Since the crystals used for X ray structure determination are small and usually have considerable mosaic spread primary extinction is negligible.

Secondary extinction is the weakening of the diffracted beam due to the weaker incident radiation experienced by the layers of the crystal further from the source since part of the radiation has already

been scattered by the layers closer to the source. Its effect is usually seen if the crystal is in a strong scattering position. Instead of applying a correction to the measured structure factors an additional parameter g (Larson, 1967) representing this effect is introduced in the least-squares refinement and refined along with the parameters of the IAM.

2.12 Averaging equivalent reflections

Because of the Fourier transform relationship between $\rho(\vec{r})$ and $F(\vec{s})$ most of the crystal symmetry elements are reflected in the diffraction pattern. For a tetragonal crystal, for instance, any $hk\ell$ reflection is symmetry-related (or equivalent) to the $kh\ell$ reflection due to the symmetry between a and b axes.

In practice, the observed intensities of equivalent reflections are not equal to each other because of the anisotropic absorption effects. The agreement between absorption-corrected equivalent reflections is used as an indicator of the accuracy of absorption correction.

Equivalent reflections are averaged after the absorption correction (if necessary). The program used for this purpose is AVER (Ng, 1978) which computes weighted average of equivalent reflections using σ_c^{-2} as the weights where σ_c is the statistical counting error of $|F_o|$ directly related to the counting error in intensity calculated and recorded by the diffractometer. New σ_c for the averaged $|F_o|$ and its e.s.d. σ_A based on the spread of the equivalent reflections are also calculated. Generally $\sigma_A > \sigma_c$ since it reflects errors from all sources of error while the other represents only the counting statistical error.

Variation of σ_C vs. $|F_o|$ and σ_A vs. $|F_o|$ are shown in fig. 2.5 and 2.6.

As an overall agreement index the following function, the internal agreement factor between equivalent reflections, is also calculated.

$$R_{int} = \frac{\sum_h \sum_i \left| |\bar{F}_h| - |F_{h,i}| \right|}{\sum_h \sum_i |F_{h,i}|}$$

where $\sum_h$ and $\sum_i$ represent summations over independent (non-equivalent) and equivalent reflections respectively. Note that a low value of R_{int} implies good agreement between the equivalent reflections.

2.13 Methods to deduce initial IAM from the measured intensities

(i) Patterson function

Patterson (1934) pointed out that the information on the relative positions of the atoms is contained in the observed Bragg intensities. He proved that the Fourier transform of the intensities (corrected for various systematic errors), $P(\vec{r})$, has peaks corresponding to all interatomic vectors of the structure. As an example, if a structure consists of two atoms, say, X and Y at $\vec{r}_X$ and $\vec{r}_Y$ of the unit cell the Patterson function will have peaks at $\vec{r}_x - \vec{r}_x$, $\vec{r}_x - \vec{r}_y$, $\vec{r}_y - \vec{r}_x$ and $\vec{r}_y - \vec{r}_y$. Since the first and the last vectors are null-vectors these two peaks will appear superimposed at the origin but the other peaks will remain resolved indicating the orientation of X-Y bond, a useful hint in postulating the initial model.

The Patterson function can always be calculated once the intensities are measured since the phase of I = F*F is always zero.

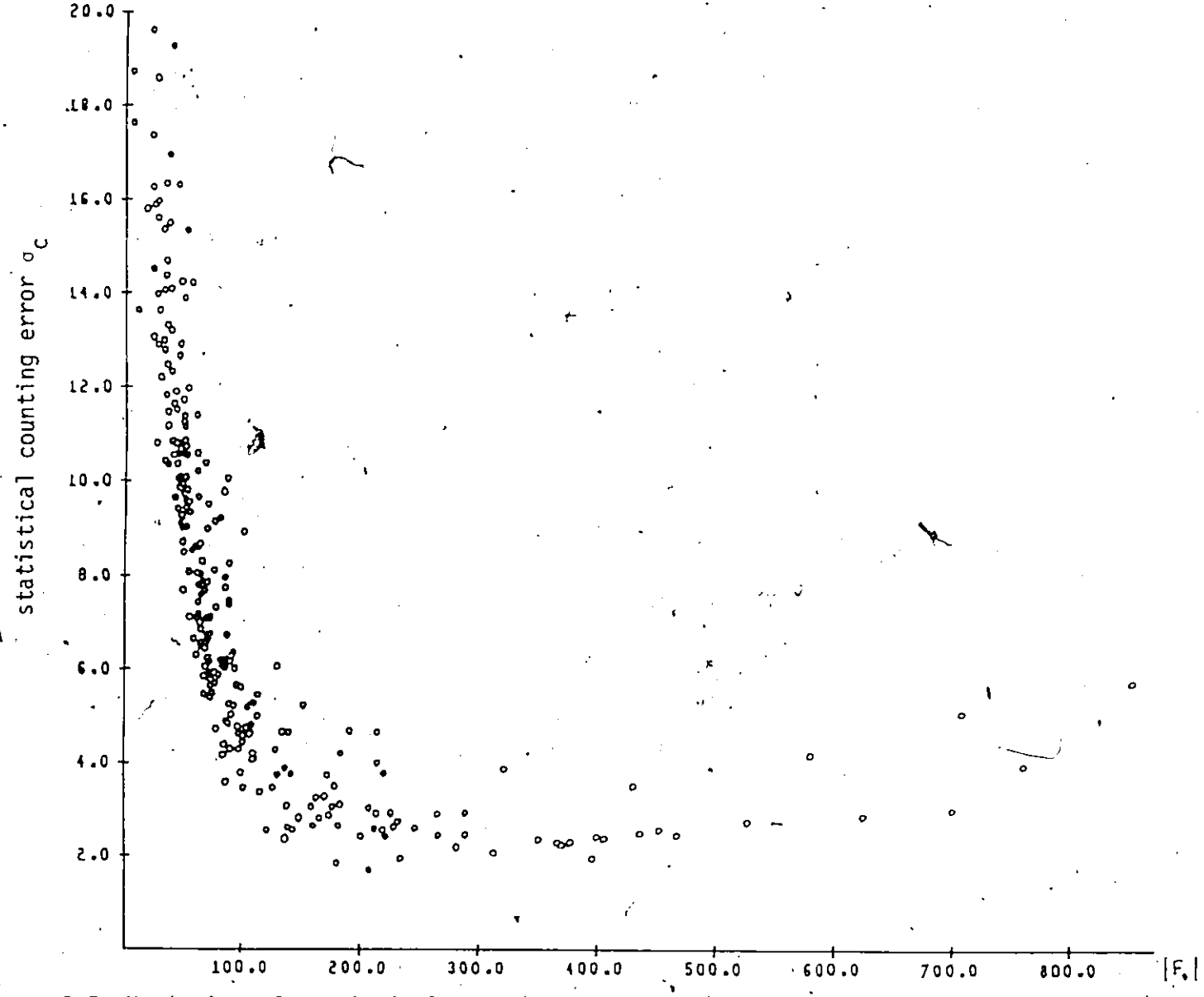

Figure 2.5 Variation of statistical counting error σ_C with the magnitude of observed structure factor $|F_o|$.

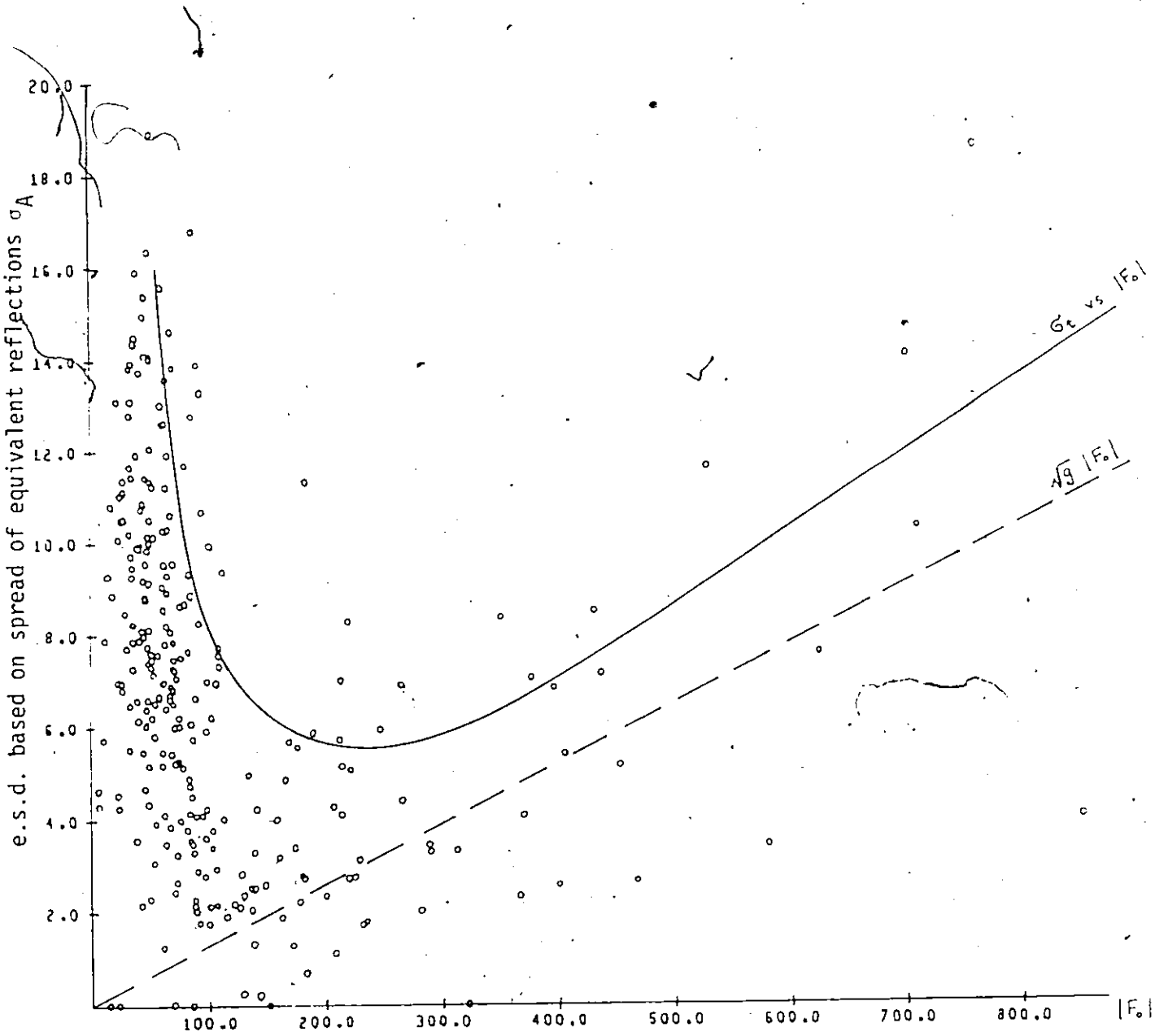

Figure 2.6 Variation of σ_A vs. $|F_o|$ (the points). The solid curve and the dashed line of slope $\sqrt{g}$ are used to establish a weighting scheme required for least-squares refinement described in sec. 2.14.

However, for a complicated structure with many atoms one might find it difficult (sometimes impossible) to interpret the Patterson function since it contains too many peaks. The aim is therefore to locate only the heaviest atoms of the structure which produce the strong Patterson peaks and then use other suitable methods to locate the lighter atoms.

(ii) Direct methods

One of the properties of the electron density distribution of the crystal $\rho(\vec{r})$ is that it is a positive quantity at every point of the unit cell. By using this property as a constraint it is possible to assign trial phases to a small number of accurately measured Bragg reflections based on the inequality relationships between the magnitudes of the structure factors (Woolfson, 1963). The phase assignment is not unique and a number of trial solutions are usually obtained by this method.

The solutions are displayed as E-maps which are the Fourier transforms of the normalized structure factors $E(hk\ell)$, a quantity directly proportional to $F(hk\ell)$ but without the reduction in magnitude produced by the small form factor values at large 2θ angles.

$$E(hk\ell) = \frac{F(hk\ell)}{\{\sum_{i=1}^{N} f_i^2(2\theta)\}^{\frac{1}{2}}}$$

The crystallographer has then to decide which of the E-maps shows the most chemically plausible arrangement of the atoms. As with the Patterson function, only the heaviest atoms of the structure are usually visible on the E-maps.

(iii) Difference synthesis

This technique is used to search for the lighter atoms once the heavy atoms of the structure have been located. The difference map is obtained by Fourier transforming the quantity $(|F_o| - |F'_c|)e^{i\phi'}$ where ϕ' is the phase of the structure factor F'_c calculated by using the already found heavy atoms. Since the missing atoms are responsible for the difference between $|F_o|$ and $|F'_c|$, the map shows peaks approximately at those atomic sites.

The reliability of the map progressively improves as more and more atoms are located and added into the partial model used to calculate F'_c. When all the atoms have been included the difference map should ideally show no peaks. Any significant features seen on the map at this stage usually indicate that the model is incapable of representing the actual electron density of the crystal. For example, significant residual electron density is often seen in the bonding regions of the completed model (an IAM) since the model does not have any adjustable parameter to represent the bonding electron density.

2.14 Least-squares refinement

Since F_c of eq. (2.45) does not relate linearly to the parameters of the IAM a non-linear least-squares refinement is required to refine the model. Detail theory is given in many crystallographic text books (e.g., Woolfson, 1979) and highly efficient computer programs are available for this purpose. The programs used to refine the structures reported in this thesis are CUDLS (Stephens, 1964) and SHELX (Sheldrick, 1976).

The program CUDLS minimizes the following function using full-matrix refinement.*

$$\delta_{min} = \sum_{\substack{\text{all} \\ \text{reflections}}} w(|F_o| - k|F_c|)^2$$

where w is the weight given to a reflection depending on its reliability. If σ_t represents the total standard deviation of $|F_o|$ due to all sources of error

$$w = \sigma_t^{-2}$$

is a suitable weighting scheme (Stout and Jensen, 1968). In CUDLS, σ_t is calculated as

$$\sigma_t = (\sigma_c^2 + g|F_o|^2)^{\frac{1}{2}}$$

where σ_c is the statistical counting error of averaged $|F_o|$ calculated by the program AVER (see sec. 2:7). The second term represents the errors from other sources such as slight crystal misalignment which can be shown to be approximately linear with $|F_o|$ (Grant et al., 1969). Fig. 2.6 shows a typical variation of σ_t vs. $|F_o|$. For large $|F_o|$ values, $\sigma_c \to 0$ and

$$\sigma_t \simeq \sqrt{g}|F_o|$$

where $\sqrt{g}$ is the slope of the straight line shown in the figure.

A number of methods have been suggested to estimate the slope (e.g. see Stout and Jensen, 1968). In this thesis the parameter is chosen so that a best fit is obtained between the straight line $\sqrt{g}|F_o|$

* The coefficient k of $|F_c|$ is called the overall scale factor. It is required as an adjustable parameter since the diffractometer-measured $|F_o|$ are still on an arbitrary scale.

and the variation of σ_A (e.s.d. of $|F_o|$ based on the spread of equivalent reflections) against $|F_o|$ as shown in fig. 2.6.

As the indicators of agreement between $|F_o|$ and $|F_c|$ of the refined IAM the program computes the following functions. (All reflections are included in the summations)

$$R_w = \left[\frac{\sum w(|F_o| - |F_c|)^2}{\sum wF_o^2}\right]^{\frac{1}{2}}$$

$$R = \frac{\sum \big||F_o| - |F_c|\big|}{\sum |F_o|}$$

e.s.d. of observations of unit weight $\sigma_1 = \left[\frac{\sum w(|F_o| - |F_c|)^2}{N_R - N_V}\right]^{\frac{1}{2}}$

where N_R = number of reflections

and N_V = number of parameters varied during the refinement.

Obviously, the lower the R_w and R the better the agreement. The expectation value of σ_1 is 1 since $(|F_o| - |F_c|)^2$ should approximately be $\sigma_t^2 = w^{-1}$. The value of $\sigma_1 >> 1$ suggests that the model is incapable of representing actual electron density. When $\sigma_1 << 1$ it usually implies that the weighting parameter $\sqrt{g}$ has been over-estimated.

The program SHELX is similar to CUDLS except in the weighting scheme which has the form

$$w = k/(\sigma_c^2 + gF^2)$$

where k is a parameter to be determined after each cycle of refinement. (g is estimated as in CUDLS). When the new set of structure factors has been calculated after the refinement k is determined by fitting

$(|F_o| - |F_c|)^2$ to $(\sigma_c^2 + gF^2)$. Since the two quantities should be approximately equal, the expectation value of k is 1; i.e., the parameter k plays the role of σ_1 of CUDLS. For this reason σ_1 is not calculated by SHELX.

CHAPTER III

STRUCTURES OF $Hg_{3-\delta}MF_6$ (M = As, Sb, Nb, Ta) COMPOUNDS

3.1 The independent atom model for structure determination of $Hg_{3-\delta}MF_6$ Compounds

As described in sec. 1.3 the diffraction pattern of $Hg_{3-\delta}MF_6$ compounds consists of two incommensurate components, one being series of sheets of diffuse scattering in the tetragonal $\underline{a}^*$ and $\underline{b}^*$ directions and the other a lattice of Bragg reflections with the symmetry and systematic absences of the space group $I4_1/amd$ (see fig. 3.1). The sheets arise entirely from the Hg chains running along the two equivalent tetragonal axes while the Bragg reflections are mostly from the MF_6 host lattice. Since the sheets do not coincide with the Bragg peaks their intensity is not included in the measured Bragg reflections. However, there are certain Bragg reflections which contain contributions from the chains for the following reason. The position of the chains with respect to the host lattice is determined and commensurate with the host lattice spacing because the chains occupy the tunnels formed by the lattice. The $\underline{a}$ chains, for instance, have y and z coordinates determined by the lattice and give a Bragg scattering contribution to the $0k\ell$ peaks. As the result, the measured intensities in this plane are proportional to $|F_{host} + F_{chain}|^2$. Note that the infinite U_{11}

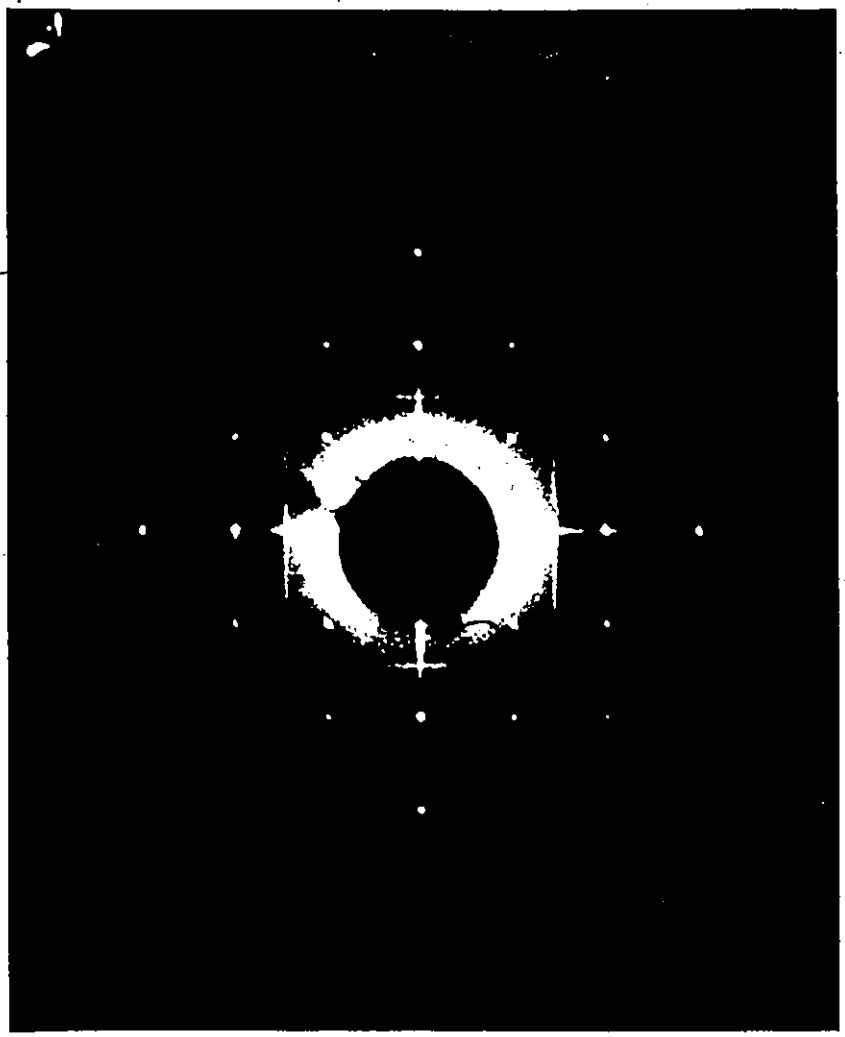

Figure 3.1

The hk0 precession photograph of $Hg_{3-\delta}SbF_6$ showing well-defined Bragg reflections from the ordered host lattice and diffuse scattering sheets perpendicular to a* and b* axes (can be seen as lines) from the disordered mercury chains.

term of the Debye-Waller factor does not quench the chain contribution to the plane with h=0, since h^2U_{11} is finite (see eq. 2.45).

It is obvious that one needs a special (and rather unusual) model to represent the electron density of the crystal $\bar{\rho}(\vec{r})$ in computing F_c. All standard crystallographic computer programs assume that the unit cells are identical. One must model the chains in a way so that they contribute only to the 0kℓ reflections and no other.

Brown, et al. (1974) modelled the chains by a closely spaced array of partial Hg atoms (16 per cell length)*. From such a chain the first non-zero contribution after the h=0 layer is on the h=16 layer ($2\theta > 95°$ for MoKα radiation). Since the reflections with $h > 10$ have never been included in the refinements the chain contribution is effectively restricted only to the 0kℓ plane. The partial occupancy of the atoms was held fixed throughout the refinement at the value corresponding to the actual linear density, i.e., $3\text{-}\delta/|\vec{a}|$.

With $h \lesssim 10$ it is possible to detect any periodic structure of the chains commensurate with the host lattice that have wavelengths $\gtrsim \vec{a}/10$. The undulation of the chains described in sec. 1.3 is such a structure reported by Schultz et al. (1978).

3.2 General procedure for structure determination

For X ray structure determination $Hg_{3-\delta}MF_6$ crystals were selected inside an ultra-dry dry-box equipped with a microscope. It was desirable to use spherical crystals in order to simplify the

---

* The rest of the model representing the host lattice is a standard independent atom model.

absorption correction but attempts to grind the crystals failed. Either the atmosphere of the dry-box or the crystal grinder was not completely moisture-free so that the crystals decomposed during grinding. Crystals with well-defined faces were therefore selected wherever possible and were inserted into glass capillaries of diameter 0.2 or 0.3 mm. Before sealing off the capillaries the crystals were pushed by using a glass fibre in order to wedge them against the tapering inside wall. This was the only means to achieve mechanical stability as the crystals were highly hygroscopic and no glue could be used.

The crystals were first examined on a precession camera to confirm that they were of good quality and isostructural with $Hg_{3-\delta}AsF_6$. The spacing between the diffuse scattering sheets on the photographs was measured to calculate the Hg-Hg distance within a chain.

Bragg intensity measurements were performed on a Nicolet $P2_1$ four-circle diffractometer, either at room temperature or at a lower temperature* using the standard LT1 unit supplied by the manufacturer. More information about the diffractometer and the low temperature apparatus is provided in sec. 2.7. The intensities were measured in two groups, data set (I) and (II). The former was used as usual in the least-squares refinement while the latter, chosen to include 14 complete sets of equivalent (symmetry-related) reflections, was used to improve the accuracy of absorption correction as follows.

---

* The temperature was low enough so that the chains were in the long range order phase described in sec. 1.5. The order-disorder phase transition temperature is 120K for $Hg_{3-\delta}AsF_6$ (Hasting et al., 1977) but it is 186K and 193K respectively for $Hg_{3-\delta}SbF_6$ and $Hg_{3-\delta}TaF_6$.

To apply an absorption correction by using numerical integration method described in sec. 2.10 it was necessary to know the orientations and distances of the crystal faces from an arbitrarily chosen origin inside the crystal. These measurements were made on a STOE two-circle optical goniometer. Because of the low magnification of the microscope attached to the goniometer the distance measurements were not very accurate. Any error in the distance measurements will result in poorer agreement between the absorption-corrected equivalent reflections. This effect is dramatic especially for data set II since it contains only strong low-2θ reflections for which absorption is the major source of error. The distances were therefore varied within the range of their experimental uncertainties to minimize the internal agreement factor R_{int} of data set II after application of the absorption correction.* (Definition of R_{int} is given in sec. 2.12. A lower R_{int} represents better agreement between equivalent reflections).

The absorption correction thus obtained was applied to both data sets I and II. Other corrections applied at this stage were scaling of the measured intensities based on the fluctuations of the standard reflections (sec. 2.8) and the Lp-correction (sec. 2.9). The two data sets were then combined and the intensities were converted into magnitudes of observed structure factors $|F_o|$.

The $|F_o|$ of equivalent reflections were averaged as described in sec. 2.12 and both data sets I and II were included in the averaging.

---

* Orientation of crystal faces and distances used for the absorption correction in each structure determination are given in Appendix I.

It was possible to calculate the estimated standard deviation σ_A of each average based on the agreement between the equivalent reflections. Since up to four equivalent reflections were included in the averaging for most of the reflections, σ_A could be assumed to be an estimate of total uncertainty in the average $|F_o|$. The parameter g of the weighting scheme used in the least-squares structure refinement was then chosen so that $\sigma_t = [\sigma_c^2 + g|F_o|^2]^{\frac{1}{2}}$ was approximately equal to σ_A. (Also see sec. 2.14)

The model to be refined by a least-squares refinement has been described in sec. 3.1. During refinement the partial Hg atoms representing the chains were allowed to move in the z-direction so that the small undulations of the chains could be determined. The initial parameters used in the refinements were those reported by Brown et al. (1974) for $Hg_{3-\delta}AsF_6$. A new feature of the present refinement was that in the final rounds U_{22} of Hg atoms (temperature factor along the chain since the chain refined is a b chain) was held fixed but U_{11} and U_{33} were allowed to vary separately.

The secondary extinction parameter g (Larson, 1967) was also refined in the final rounds. During the last cycle of refinement all parameters were refined and a difference map was calculated.

The magnitudes of the observed and calculated structure factors have been tabulated and deposited with McMaster University (Tun, 1984).

Table 3.1 summarizes details of the general procedure described above. Each of the next three sections discusses structure determination of the individual chain compounds with M = Sb, Nb and Ta. In each case the general procedure was followed unless otherwise stated.

Table 3.1

Summary of general procedure for structure determination of $Hg_{3-\delta}MF_6$ compounds

The following parameters were common to all structure determinations.

Bragg intensity measurements:

Diffractometer: Nicolet $P2_1$

Graphite monochromated MoKα radiation, λ = 0.71069 Å

Lattice constants determined from 15 well-centered reflections

Scan procedure: 2θ-ω scan

Scan angle: 2° + angle between $K\alpha_1$ and $K\alpha_2$ peaks

Background measuring time/scan time = 1

Data set (I)

Maximum 2θ = 55°

$0 \leq h, k \leq 10, -16 \leq \ell \leq 16$

Data set (II)

$-3 \leq h, k, \ell \leq 3$

Number of reflections measured: 144

Number of unique reflections: 14

Absorption correction (numerical integration method)

Program: ABSORB

Number of grid points for integration: 10 x 10 x 10

Averaging:

Program: AVER

Laue group: 4/mmm

Table 3.1 (continued)

Least-squares refinement:

Program: CUDLS

Initial parameters: refined parameter of $Hg_{3-\delta}AsF_6$

Scattering factors: neutral atoms from International Tables for X ray Crystallography (1974)

Weighting scheme: $w = [\sigma^2(\text{counting}) + gF_o^2]^{-1}$

3.3 Structure of $Hg_{3-\delta}SbF_6$ at 293K and 173K

The samples were produced at McMaster University by Dr. K. Morgan. A crystal with well-defined faces (sample 1) was used for the room temperature (293K) structure determination. Data set II was used to establish the absorption correction but not included in the averaging. The least-squares refinement was therefore entirely based on data set I. Since the absorption affects were corrected accurately a reliable room temperature structure was obtained. Details of the structure determination are summarized in Table 3.2 while the refined atomic parameters are given in Table 3.3. The bond lengths and the important distances depicted in Fig. 3.2 and Fig. 3.3 are listed in Table 3.4.

Sample 1 was lost during an attempt to measure the Bragg intensities at low temperature. Hence, a different crystal (sample 2) was used for this experiment. It was concave on one side but the other sides had well-defined faces and the absorption correction obtained for this crystal was not very accurate. Structure refinement was based only on data set I. To permit comparisons between the low temperature and room temperature structures sample 2 was also used for a room temperature refinement but, because of the poorer absorption correction, the structure was not as accurate as that from sample 1. However, since the two structures from sample 2 suffer from the same absorption errors it is better to compare these rather than compare the sample 1 room temperature structure with the sample 2 low temperature structure. Because of the limited accuracy of the structure factors only isotropic temperature factors were used on the Hg atoms in the least-squares refinement. Details of these structure determinations, the refined

Table 3.2

Summary of structure determination of $Hg_{3-\delta}MF_6$ compounds

	$Hg_{3-\delta}SbF_6$; 293K Sample 1	$Hg_{3-\delta}SbF_6$; 293K Sample 2	$Hg_{3-\delta}SbF_6$; 173K Sample 2	$Hg_{3-\delta}NbF_6$; 293K	$Hg_{3-\delta}TaF_6$; 293K	$Hg_{3-\delta}TaF_6$; 150K
Crystallographic composition parameter δ	0.10(2)		0.134(1)	0.119(3)	0.116(4)	0.142(1)
Lattice parameter a (Å)	7.711(2)	7.709(2)	7.655(1)	7.692(1)	7.711(1)	7.634(1)
c	12.641(2)	12.639(3)	12.558(1)	12.679(2)	12.714(2)	12.610(2)
Volume ($Å^3$)	751.6(5)		735.9(2)	750.2(2)	756.0(2)	734.9(2)
Calculated density* (Mgm^{-3})	7.22(4)		7.34(4)	6.95(1)	7.68(1)	7.847(3)
Reflections used to determine a and c	10°<2θ<29°	10°<2θ<26°	10°<2θ<52°	10°<2θ<28°	6°<2θ<26°	9°<2θ<27°
Variable scan speed (deg min^{-1})	4.0 - 29.3	2.0 - 29.3	4.0 - 29.3	2.0 - 29.3	3.0 - 29.3	3.0 - 20.0
Standard reflections	015, 024	015, 024	015, 024	015, 024	$4\bar{2}0$, 008	$4\bar{2}0$, 008
e.s.d. of standard reflections (%)	1.9, 2.1	2.3, 1.8	2.1, 2.3	1.1, 1.5	1.7, 1.7	2.0, 1.2
No. of standard reflection measurements	21	25	34	25	25	21
Data set (I): No. of reflections measured	925	933	907	933	935	912
No. of unique reflections	252	253	245	252	254	246
No. of unobserved^{SS} reflections measured	504	455	296	358	221	142
Linear absorption coefficient μ (mm^{-1})	63.9	63.9	64.8	61	64.9	76.4
Maximum absorption correction; reflection	30.31; 011	430.11; 002	300.90; $10\bar{1}$	37.78††	141.13; 011	182.76; 011
Minimum absorption correction; reflection	11.67; 097	16.63; 4,1,15	16.68; 5,1,14	20.88††	2.175; 200	2.175; 200
Internal agreement factor R_{int}^{**}; data set	0.146; I	not computed	not computed	0.056; I+II	0.181; I+II	(see $)
before absorption correction	0.096; II	0.173; II	0.187; II		0.189; II	
Internal agreement factor	0.119; I	0.166; I+II	0.190; I	(See ††)	0.052; I+II	0.079; I
after absorption correction	0.037; II	0.101; II	0.119; II		0.023; II	
Weighting parameter g	0.0135	0.0560	0.1100	0.0109	0.0180	0.0425

..... continued

Table 3.2 (continued)

	$Hg_{3-\delta}SbF_6$; 293K Sample 1	$Hg_{3-\delta}SbF_6$; 293K Sample 2	$Hg_{3-\delta}SbF_6$; 173K Sample 2	$Hg_{3-\delta}NbF_6$; 293K	$Hg_{3-\delta}TaF_6$; 293K	$Hg_{3-\delta}TaF_6$; 150K
Final R_w† (all reflections)	0.033	0.063	0.071	0.033	0.029	0.045
Final R† (all reflections)	0.040	0.057	0.058	0.031	0.025	0.039
s.d. of an observation of unit weight†	1.24	0.89	0.62	1.83	1.24	1.03
Maximum shift/error in final cycle	0.34	0.36	0.54	0.29	0.13	0.11
Average shift/error in final cycle	0.09	0.03	0.14	0.04	0.04	0.02
Secondary extinction correction g ($\times 10^7$)	1.2(2)	1.0(5)	2.4(7)	0.3(2)	1.4(2)	3.8(6)
Number of variables refined	25	21	21	25	25	25
Residual electron density: maximum ($eÅ^{-3}$)	+1.7	+1.5	+2.8	+0.7	+2.0	+6.3
-: minimum	-1.5	-1.6	-3.0	-1.1	-1.0	-1.9

* Ignoring anion deficiency reported by Schultz et al. (1978).

** See definition in Sec. 2.12.

† See definition in Sec. 2.14.

†† Standard spherical absorption correction. It is a function of 2θ only and R_{int} is not affected by the correction.

$ The crystal orientation remained unchanged during the room temperature and low temperature experiments so that it was not necessary to check the validity of absorption correction by computing R_{int} before the correction. Data set II was not needed since the same absorption correction was used.

$$ Reflections with $I < 3\sigma_I$.

Table 3.3

Refined atomic parameters of $Hg_{3-\delta}MF_6$ compounds

		$Hg_{3-\delta}AsF_6$* room temperature	$Hg_{3-\delta}SbF_6$; 293K sample 1	$Hg_{3-\delta}SbF_6$; 293K sample 2	$Hg_{3-\delta}SbF_6$; 173K sample 2	$Hg_{3-\delta}NbF_6$; 293K	$Hg_{3-\delta}TaF_6$; 293K	$Hg_{3-\delta}TaF_6$; 150K
Positional parameters:								
Hg(1)†	x	(See **)	0	0	0	0	0	0
	y		1/32	1/32	1/32	1/32	1/32	1/32
	z		0.0000(10)	-0.0010(10)	-0.0013(5)	-0.0011(6)	-0.0007(5)	-0.0016(4)
Hg(2)†	x		0	0	0	0	0	0
	y		3/32	3/32	3/32	3/32	3/32	3/32
	z		-0.0003(8)	-0.0006(8)	-0.0003(4)	-0.0008(5)	-0.0009(4)	-0.0010(4)
Hg(3)†	x		0	0	0	0	0	0
	y		5/32	5/32	5/32	5/32	5/32	5/32
	z		0.0013(6)	0.0019(6)	0.0015(4)	0.0009(4)	0.0014(4)	0.0010(3)
Hg(4)†	x		0	0	0	0	0	0
	y		7/32	7/32	7/32	7/32	7/32	7/32
	z		0.0029(3)	0.0025(4)	0.0028(3)	0.0020(2)	0.0023(2)	0.0024(2)
M	x	0	0	0	0	0	0	0
	y	1/4	1/4	1/4	1/4	1/4	1/4	1/4
	z	3/8	3/8	3/8	3/8	3/8	3/8	3/8

..... continued

Table 3.3 (continued)

		$Hg_{3-\delta}AsF_6$* room temperature	$Hg_{3-\delta}SbF_6$; 293K sample 1	$Hg_{3-\delta}SbF_6$; 293K sample 2	$Hg_{3-\delta}SbF_6$; 173K sample 2	$Hg_{3-\delta}NbF_6$; 293K	$Hg_{3-\delta}TaF_6$; 293K	$Hg_{3-\delta}TaF_6$; 150K
F(1)	x	0	0	0	0	0	0	0
	y	1/4	1/4	1/4	1/4	1/4	1/4	1/4
	z	0.2377(2)	0.2291(9)	0.2302(13)	0.2267(12)	0.2272(6)	0.2268(9)	0.2253(11)
F(2)	x	0.6611(3)	0.672(2)	0.672(2)	0.673(2)	0.673(1)	0.673(1)	0.675(1)
	y	x+½	x+½	x+½	x+½	x+½	x+½	x+½
	z	7/8	7/8	7/8	7/8	7/8	7/8	7/8
Thermal Parameters ($Å^2 \times 10^3$)								
Hg(1)	U_{11}	(See **)	49(3)	57(1)	29(1)	66(2)	57(1)	23(1)
	U_{22}		51			61	56	24
	U_{33}		54(3)			57(2)	57(2)	25(2)
	U_{12}		0			0	0	0
	U_{13}		0			0	0	0
	U_{23}		0			0	0	0
Hg(2)	U_{11}		57(5)	55(1)	28(1)	60(3)	56(2)	24(2)
	U_{22}		50			59	55	24
	U_{33}		47(4)			57(3)	55(2)	24(2)
	U_{12}		0			0	0	0
	U_{13}		0			0	0	0
	U_{23}		0			0	0	0

..... continued

Table 3.3 (continued)

		$Hg_{3-\delta}AsF_6$* room temperature	$Hg_{3-\delta}SbF_6$; 293K sample 1	$Hg_{3-\delta}SbF_6$; 293K sample 2	$Hg_{3-\delta}SbF_6$; 173K sample 2	$Hg_{3-\delta}NbF_6$; 293K	$Hg_{3-\delta}TaF_6$; 293K	$Hg_{3-\delta}TaF_6$; 150K
Hg(3)	U_{11}^S		47(4)	51(1)	26(1)	62(3)	57(2)	23(2)
	U_{22}		48			56	53	23
	U_{33}		45(4)			53(2)	49(2)	23(2)
	U_{12}		0			0	0	0
	U_{13}		0			0	0	0
	U_{23}		0			0	0	0
Hg(4)	U_{11}^S		52(3)	50(1)	26(1)	64(2)	57(1)	25(1)
	U_{22}		47			56	52	22
	U_{33}		43(2)			49(1)	47(1)	19(1)
	U_{12}		0			0	0	0
	U_{13}		0			0	0	0
	U_{23}		0			0	0	0
M	U_{11}	32(1)	31(2)	33(2)	16(2)	45(1)	34(1)	13(1)
	U_{22}	U_{11}	U_{11}	U_{11}	U_{11}	U_{11}	U_{11}	U_{11}
	U_{33}	22(1)	21(1)	25(1)	11(1)	29(1)	25(1)	12(1)
	U_{12}	0	0	0	0	0	0	0
	U_{13}	0	0	0	0	0	0	0
	U_{23}	0	0	0	0	0	0	0

..... continued

Table 3.3 (continued)

		$Hg_{3-\delta}AsF_6$* room temperature	$Hg_{3-\delta}SbF_6$; 293K sample 1	$Hg_{3-\delta}SbF_6$; 293K sample 2	$Hg_{3-\delta}SbF_6$; 173K sample 2	$Hg_{3-\delta}NbF_6$; 293K	$Hg_{3-\delta}TaF_6$; 293K	$Hg_{3-\delta}TaF_6$; 150K
F(1)	U_{11}	72(2)	58(1)	45(11)	43(11)	86(9)	56(7)	16(7)
	U_{22}	121(3)	150(18)	108(18)	36(10)	153(13)	154(14)	74(13)
	U_{33}	24(1)	15(6)	36(8)	19(7)	27(4)	30(6)	15(6)
	U_{12}	0	0	0	0	0	0	0
	U_{13}	0	0	0	0	0	0	0
	U_{23}	0	0	0	0	0	0	0
F(2)	U_{11}	48(1)	45(8)	46(7)	27(6)	58(5)	50(4)	19(4)
	U_{22}	U_{11}	U_{11}	U_{11}	U_{11}	U_{11}	U_{11}	U_{11}
	U_{33}	79(2)	80(7)	78(9)	35(6)	89(5)	89(6)	29(4)
	U_{12}	-13(1)	-14(5)	-7(5)	-4(4)	-13(3)	-11(3)	-5(3)
	U_{13}	$-U_{23}$	$-U_{23}$	$-U_{23}$	$-U_{23}$	$-U_{23}$	$-U_{23}$	$-U_{23}$
	U_{23}	7(1)	-3(9)	-4(10)	7(8)	2(6)	5(7)	3(6)

* Structure refined by Schultz et al. (1978) by using neutron diffraction.

† The incommensurate chains are represented by 4 closely spaced Hg atoms with a partial occupancy corresponding to the actual linear density.

§ U_{iso} if isotropic temperature factor was used.

** 5 independent Hg atoms instead of 4 were used by Schultz et al. (1978).

Table 3.4

Bond lengths and important distances (Å) in $Hg_{3-\delta}MF_6$ compounds

	$Hg_{3-\delta}AsF_6$* room temperature	$Hg_{3-\delta}SbF_6$; 293K sample 1	$Hg_{3-\delta}SbF_6$; 293K sample 2	$Hg_{3-\delta}SbF_6$; 173K sample 2	$Hg_{3-\delta}NbF_6$; 293K	$Hg_{3-\delta}TaF_6$; 293K	$Hg_{3-\delta}TaF_6$; 150K
	δ = 0.178(6)	δ = 0.10 (2)		δ = 0.134(1)	δ = 0.119(3)	δ = 0.116(4)	δ = 0.142(1)
a	7.534(7)	7.711(2)		7.655(1)	7.692(1)	7.711(1)	7.634(1)
c	12.395(8)	12.641(2)		12.558(1)	12.679(2)	12.714(2)	12.610(2)
d_{Hg-Hg}**	2.670(5)	2.66 (2)		2.671(1)	2.670(3)	2.674(4)	2.671(1)
$3-\delta = a/d_{Hg-Hg}$	2.822(6)	2.90 (2)		2.866(1)	2.881(3)	2.884(4)	2.858(1)
u_o†	0.07 (1)	0.037(4)	0.032(5)	0.035(4)	0.026(3)	0.030(3)	0.030(3)
M-F(1) (x2)	1.702(2)	1.84 (1)	1.83 (2)	1.86 (2)	1.874(8)	1.88 (1)	1.89 (1)
M-F(2) (x4)	1.720(2)	1.88 (1)	1.88 (2)	1.87 (1)	1.885(6)	1.884(6)	1.893(8)
chain-chain††	3.24 (2)	3.23 (1)	3.22 (1)	3.210(8)	3.222(7)	3.239(6)	3.213(6)
F(1)-chain§ (x1)	2.87 (1)	2.86 (1)	2.88 (1)	2.81 (1)	2.86 (1)	2.86 (1)	2.81 (1)
F(2)-chain§ (x2)	2.981(5)	2.98 (1)	2.98 (1)	2.958(6)	2.971(4)	2.983(4)	2.937(5)

* From Schultz et al. (1978) except a, c and d_{Hg-Hg} from Pouget et al. (1978).

** Room temperature values were calculated from the spacing between the diffuse scattering sheets on precession photographs. Low temperature values were determined by the diffractometer using atleast 4 well-centered narrow diffraction peaks arising from the ordered Hg chains.

† Maximum displacement of the chain from its mean position. For the chain with z=0 (see fig. 3.2) u_o is the z coordinate of the chain at y=½

†† The closest contact distance between the two neighbouring perpendicular chains which is greater than c/4 by $2u_o$. (see fig. 3.2)

§ Shortest distance to the neighbouring chain. (see fig. 3.2 and 3.3)

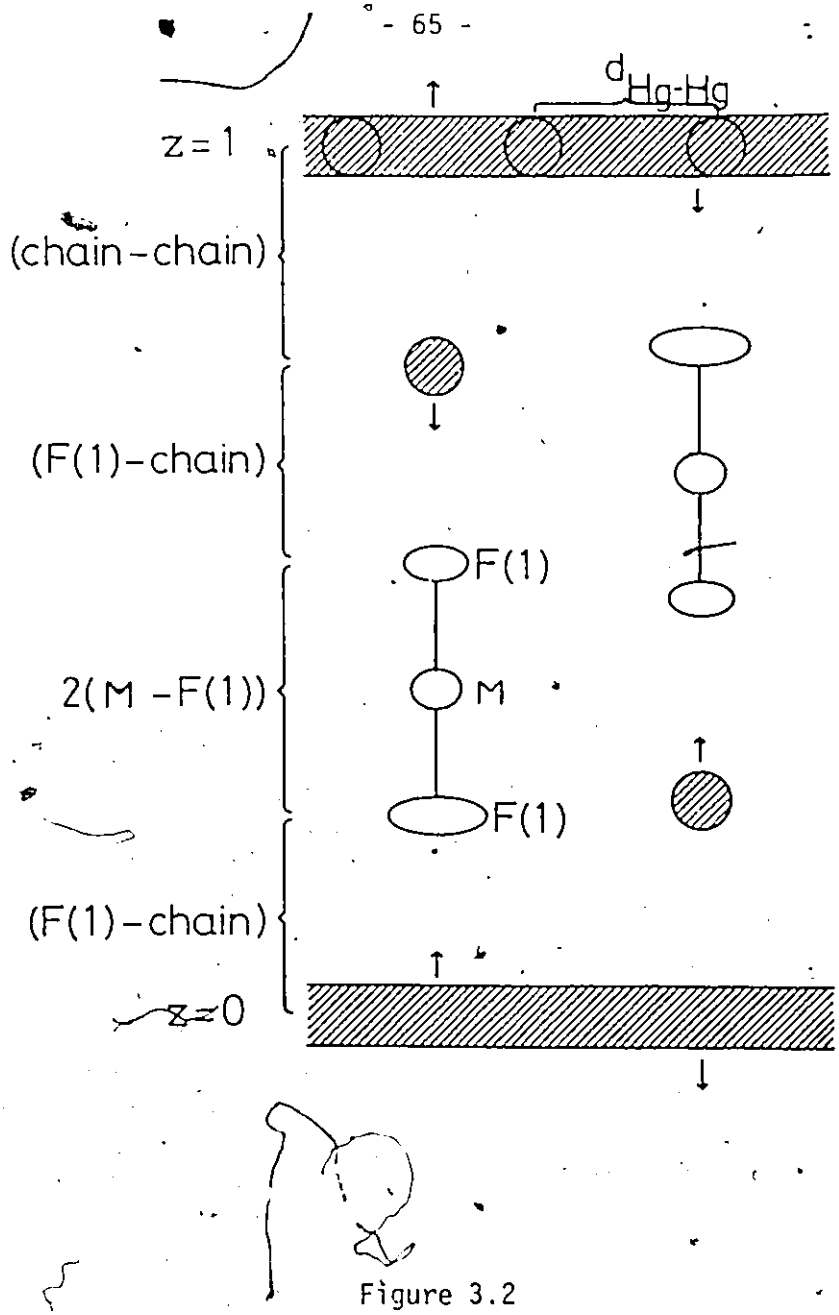

Figure 3.2

Arrangement of atoms in the x=0 plane. The shaded sections represent Hg chains seen end on (circles) or side on (bars). The undulation of the chains is too small to show on this scale but the maximum displacement, u_o, takes place in the directions indicated by the arrows.

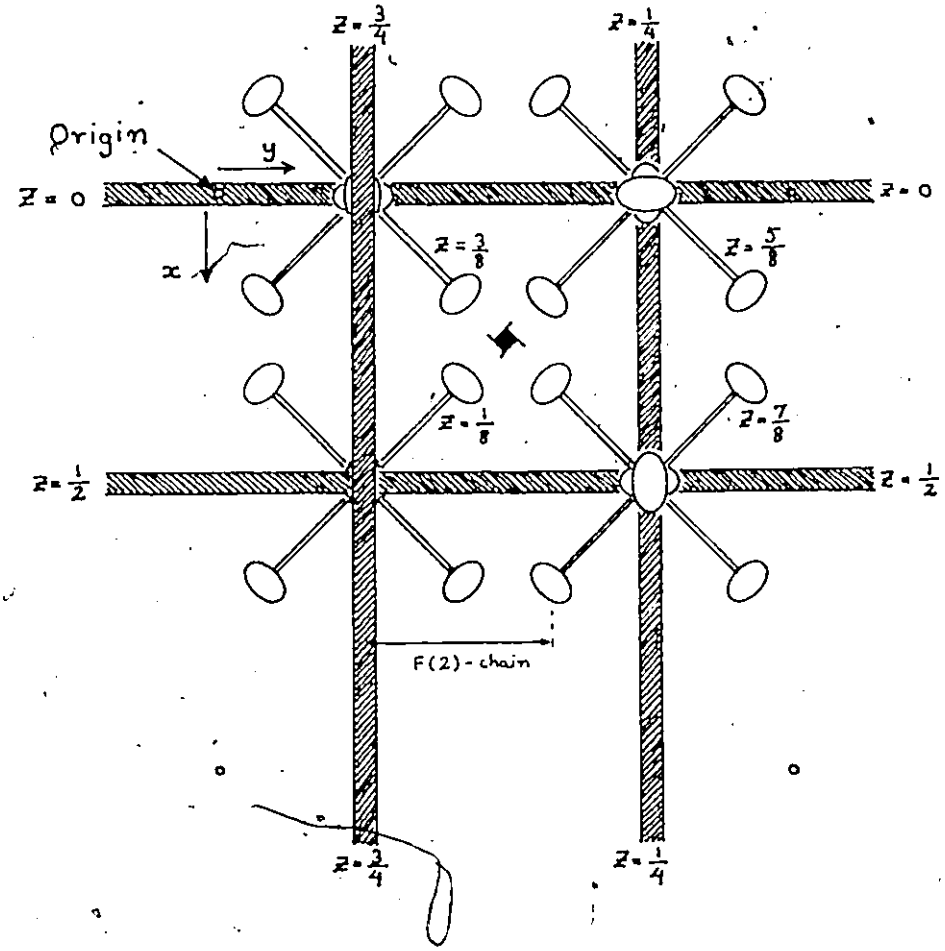

Figure 3.3

The a-b projection of the $Hg_{3-\delta}MF_6$ structure. The shaded regions represent the Hg chains.

atomic parameters and the bond lengths are listed respectively in Tables 3.2, 3.3 and 3.4.

3.4 Structure of $Hg_{3-\delta}NbF_6$ at 293K

Crystals prepared at McMaster University by Dr. P. Ummat were used for the X ray investigation. Since the crystals were small (about 0.1 - 0.2 mm) they could not be wedged securely inside the capillaries causing sample movement during the intensity measurements. This problem was extremely serious at low temperatures and no low temperature measurements could be made for this reason.

The small size of the crystals made the numerical integration absorption correction unsuitable since it was impossible to make sufficiently accurate measurements of the crystal size. An approximately spherical crystal with diameter of 0.1 mm was therefore used to measure the Bragg intensities which were then corrected by using the standard spherical absorption correction described in sec. 2.10. Since the internal agreement factor R_{int} of data set II was only 0.056 the spherical absorption was all that was needed. See table 3.2, 3.3 and 3.4 for details of structure determination and the resultant structure.

3.5 Structure of $Hg_{3-\delta}TaF_6$ at 293K and 150K

A crystal with well-defined faces produced by Dr. P. Ummat was used for the intensity measurements both at 293K and 153K. Data set II was only measured at 293K as it was only necessary to establish the absorption correction at one temperature. Details of structure determination, refined atomic parameters and bond lengths and other distances are given in Tables 3.2, 3.3 and 3.4 respectively.

3.6 Discussion

In Table 3.4 the chain compounds are arranged in the order of increasing size of MF_6 ions. The ionic size variation can be seen in both M-F(1) and M-F(2) bond lengths. For the AsF_6 and SbF_6 (293K) ions M-F(1) is slightly shorter than M-F(2) but the difference is insignificant in the other cases. Brown et al.(1982) attributed this difference to the different environments of the F atoms, F(1) has a single neighbouring chain at 2.87 Å while F(2) has two such chains at 2.98 Å.

The table also shows that the other interatomic distances which do not involve the M atom (i.e., d_{Hg-Hg}, chain-chain, F(1)-chain, F(2)-chain) are constant in all the compounds at room temperature.

The undulation of the chains is observed in every compound. It is largest in the case of smallest AsF_6 ion but decreases for the larger ions. Fig. 3.4 shows the chain undulation observed in the room temperature structures.

None of the room temperature d_{Hg-Hg} distances differ significantly from 2.671 Å, the value found at lower temperatures in both $Hg_{3-\delta}SbF_6$ and $Hg_{3-\delta}TaF_6$ indicating no observable thermal expansion of the chains.* Since zero expansion is a characteristic of a harmonic potential (Kittel, 1976), the ordered lattice formed by the chains below the phase transition temperature T_c must be harmonic.† The temperature-independent bond length is in accordance with the inverse relation known to exist between the bond valence and the thermal

---

* Lack of thermal expansion of the chains in $Hg_{3-\delta}AsF_6$ was noted by Pouget et al. (1978) who measured d_{Hg-Hg} = 2.670(5) Å over the temperature range of 300 - 10 K.

† Emery-Axe theory (1978) discussed in sec. 2.5 treats the chains above T_c as 1-dimensional harmonic liquid.

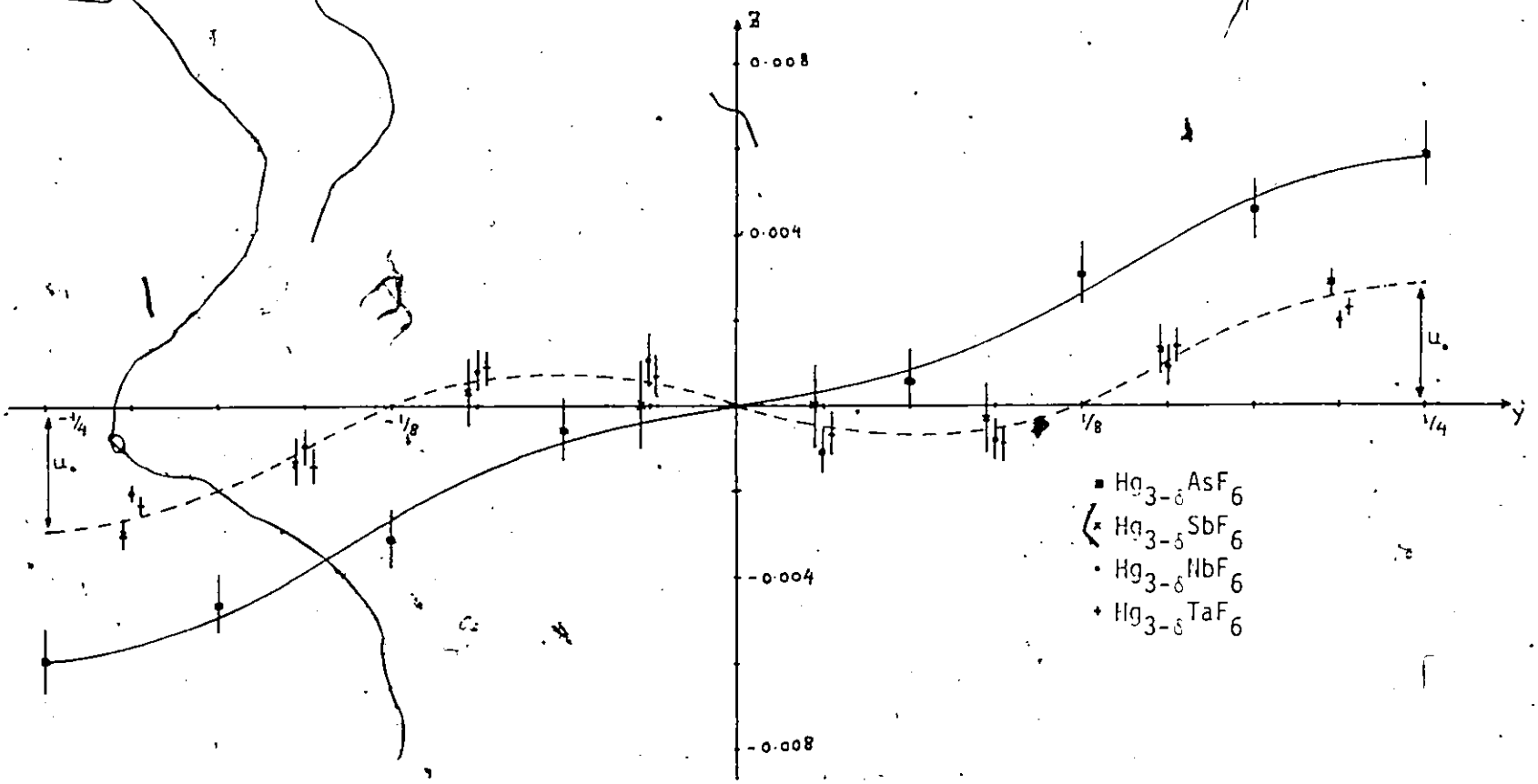

Figure 3.4

Undulation of Hg chains in room temperature structures of $Hg_{3-\delta}MF_6$. Atomic coordinates for $Hg_{3-\delta}AsF_6$ were taken from Schultz et al. (1978).

expansion coefficient of a bond (Khan, 1976). The Hg-Hg bonds are strong bonds with a high bond valence of 0.77 (Brown, Gillespie, Morgan, Tun, Ummat, submitted to Inorg. Chem.) and are expected to have very small thermal expansion.

The host lattice whose ions are linked by bonds of relatively low valence contracts significantly with temperature. The effect can be seen in low temperature structures of $Hg_{3-\delta}SbF_6$ and $Hg_{3-\delta}TaF_6$ listed in Table 3.4. Among the interatomic distances the contraction is most noticeable in the F-chain distances and chain-chain distance which are the weakest interactions of the structure. The M-F bond lengths (bond valence = $\frac{5}{6}$ = 0.83) do not change significantly. No stress is exerted on the chains by the host lattice contraction because, as argued by Sacco and Sokoloff (1978), the two components are completely decoupled and the chains are rigid enough to flow almost freely along the tunnels of the host lattice. This leads to the phenomenon of Hg extrusion from the lattice at low temperatures (Datars et al., 1978).

The anisotropic temperature factors U_{11} and U_{33} of the Hg atoms listed in Table 3.3 measure the extent of the lateral vibrations of the chains directed along the b axis. None of the compounds show significant variation of U_{11} along the chain indicating that the lateral vibration in the a-b plane is uniform. However, U_{33} which measures the chain vibration in the c direction does vary and becomes a minimum at the points where the chain is clamped by the neighbouring perpendicular chain and F(1) atom (see Fig. 3.2).

The thermal parameters of the M atoms show a small anisotropy with $U_{11} > U_{33}$ (see Table 3.3). The anisotropy is the largest in the case of $Hg_{3-\delta}NbF_6$ but this is probably an artifact of the simple

spherical absorption correction which leads to larger than usual U_{11} values for all the atoms.

A much larger anisotropy is observed in F(1) and F(2). The U_{22} of F(1), i.e., the mean-square thermal motion of F(1) parallel to the nearest chain is $\sim$ 3 times larger than U_{11} (see fig. 3.2) while U_{33} of F(2) is $\sim$ 2 times larger than the corresponding U_{11}. Tun and Brown (1982) explained this unusually large anisotropy as follows. Since the chains are incommensurate with the host lattice each F(1) atom has a different arrangement of nearest Hg atoms which in general are not symmetrical about the M-F(1) bond. This asymmetric arrangement induces a static disorder of F(1) in the direction of the chain leading to a static librational disorder of the rigid MF_6 ion and also the apparently large U_{33} of equatorial F(2) atoms. The argument, however, is not supported by the low temperature thermal parameters of Table 3.3. Since the chains remain incommensurate with the host lattice even at low temperatures, according to this argument only a small decrease is expected in U_{22} of F(1). Its dramatic decrease which is approximately proportional to k_BT suggests that the large anisotropy is due to a real thermal motion of the atoms rather than a static disorder.

CHAPTER IV

DENSITY FLUCTUATIONS OF THE CHAINS OF $Hg_{3-\delta}MF_6$ COMPOUNDS AND THE FREEZING OF THE 1-DIMENSIONAL LIQUID

4.1 Introduction

In sec. 2.5, it was pointed out that the room temperature behaviour of the chains of $Hg_{3-\delta}MF_6$ compounds can be explained by a model in which each chain is assumed to be an isolated harmonic chain, i.e., the neighbouring atoms of a chain interact with a harmonic potential but do not interact with the nearby chains, either parallel or perpendicular, or with the host lattice. The chains are completely (or almost completely) disordered with respect to each other and hence the room temperature phase is called the disorder phase or D-phase.

In the D-phase each chain is an independent 1-dimensional system. As in the other 1-dimensional systems, the chains do not have a long range internal order in spite of a good short range order resulting from the stiff Hg-Hg bonds. The X ray or neutron diffraction from the 1-dimensional chains is typical of that from a liquid sample and each chain behaves like a 1-dimensional liquid (Spal et al., 1980; also see fig. 2.2).

4.2 Prediction of low temperature phase(s)

What happens to the chains when the sample is cooled to lower temperatures? One might expect a Peierls transition because of the

large flat Fermi surfaces at $\pm k_F$. The transition will occur if the energy gained by introducing a new periodicity with the wavevector $2k_F$ is larger than the energy required to distort the Hg-Hg bonds of the chains. Since these bonds are very stiff it is unlikely that the chains will undergo a Peierls transition even at a very low temperature.

For a disordered system one generally expects to observe an increase in ordering at lower temperatures because of the lower entropy. Development of an infinite long range order within a single chain can be precluded since, as shown in sec. 2.5, the chains will never have a long range order as long as their dimensionality is not higher than one. In order to increase the dimensionality each chain must order with its surroundings, either with the host lattice or the nearby chains, and become a part of an ordered lattice of higher dimension.

Sacco and Sokoloff (1978) have demonstrated that the chains in $Hg_{3-\delta}MF_6$ crystals can flow almost freely through the host lattice. The most possible ordering process is therefore the one which involves displacement of the chains in their channels. Since the Hg-Hg bonds are associated with a high bond valence the bond length is expected to be (almost) temperature-independent (Khan, 1976). There are three possibilities of ordering between a chain and its surroundings.

(i) chain-host lattice ordering

(ii) ordering between parallel chains

(iii) ordering between perpendicular chains

The rest of this section is devoted to examining the above possibilities. A theorem which will prove useful for the discussion is Axe's Theorem (Axe, 1980).

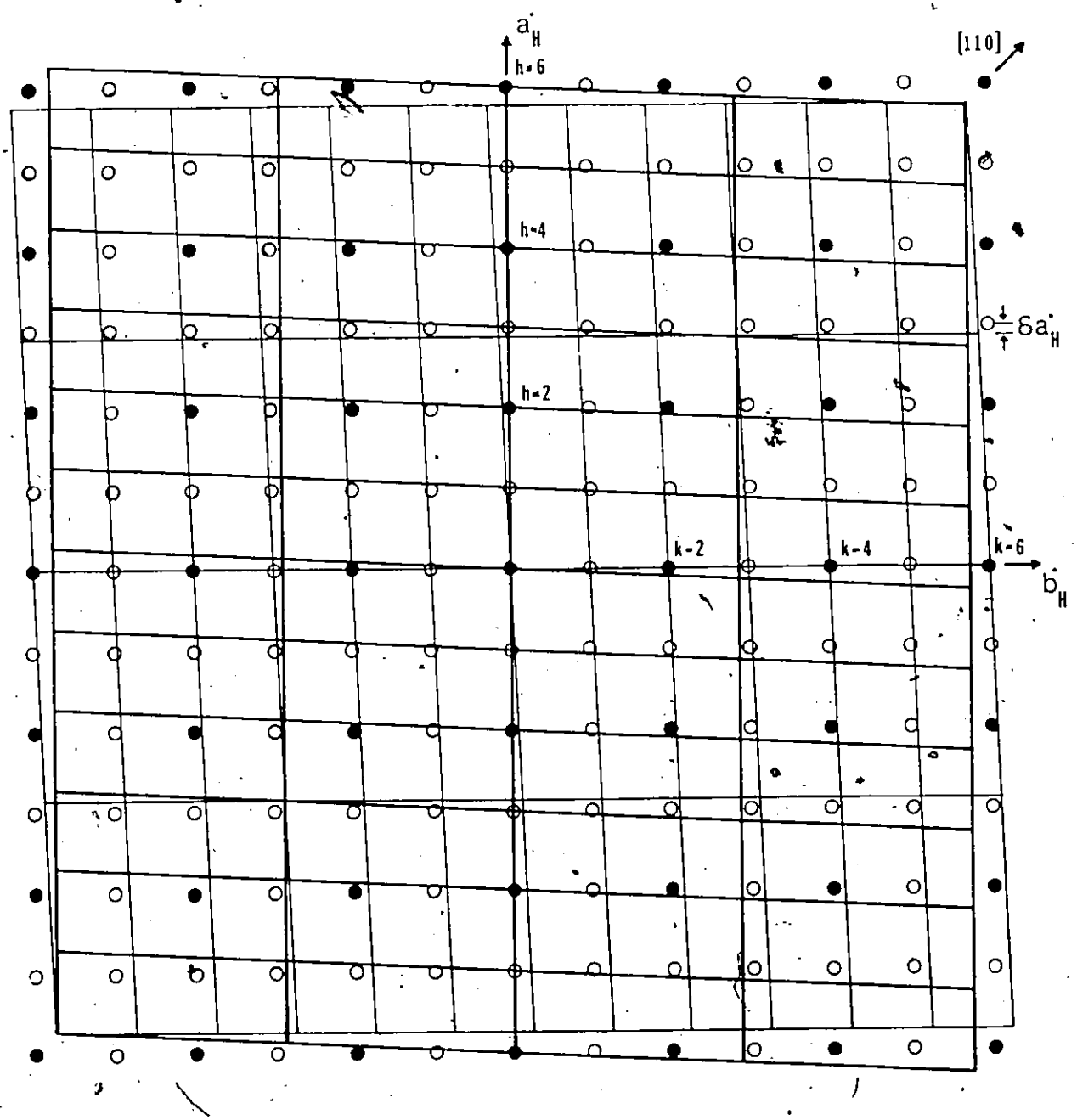

Figure 4.1

The a*-b* plane of the reciprocal space of $Hg_{3-\delta}MF_6$ structure. The circles represent well-defined reciprocal lattice points (black = observed, white = systematically absent) while the lattices shown by the lines arise from two sets of ordered Hg chains coupled coherently according to Axe's Theorem (light lattice from a chains and dark lattice from b chains).

Axe's Theorem: Two (or more) interpenetrating sublattices are coupled coherently only when they share at least one set of reciprocal lattice points.*

This theorem is the "Fourier transform" of the principle which states that two sublattices can couple coherently only if they are commensurate at least in one common direction.

(i) chain-host lattice ordering

Fig. 4.1 depicts the hk0 plane of the reciprocal space. It is similar to the precession photograph shown in Fig. 3.1, but the systematically absent reflections are also included. The closest host reciprocal lattice points to the first order Hg sheet (n=1) are the 3k0 reflections. If these reflections could be moved onto the sheet the required ordering would be achieved since the chains could then arrange themselves to form an Hg unit cell of $\vec{a} = \vec{d}_{Hg-Hg} = \frac{1}{3}\vec{a}_H$, $\vec{b} = \vec{b}_H$ and $\vec{c} = \vec{c}_H$. This however does not happen because the 3k0 reflections move further from the sheet when the sample is cooled. Is it possible to achieve ordering by warming up the crystal? The required expansion of the host lattice is $\frac{\delta}{3}$x100% or $\sim$ 5%. Because of the size of this

---

* "Ordering" and "coherent coupling" are not the same and are used in this chapter with the following meanings.

Two (or more) lattices are said to be ordered if they share all reciprocal lattice points, i.e., they combine into a one single lattice which is described by a single unit cell.

Two (or more) lattices are said to be coupled coherently if they share only some of the reciprocal lattice points.

Both ordering and coherent coupling are associated wtih a lowering of the total energy but the former is a special case of the latter.

expansion one may safely ignore the possibility of ordering between the host lattice and the chains at any temperature.

(ii) Ordering between parallel chains

According to Axe's Theorem the parallel ordering is possible since it will produce reciprocal lattice points in the planes of the diffuse scattering sheets which are common to all the parallel chains. This ordering would be favoured if the temperature is low enough so that the parallel chain interaction is $\sim k_B T$. Each chain has four nearest parallel chains ($\sim$ 7.4 Å apart) and two second-nearest parallel chains ($\sim$ 7.6 Å apart). Separations of $>$ 7 Å are too large for any kind of direct interaction except a pure Coulomb interaction which would be heavily screened by the host lattice. However, an indirect interaction through small local distortions of the host lattice is a possibility.

Any parallel chain ordering will result in replacing the diffuse scattering sheets by Bragg peaks. It is not possible to predict the exact position of the peaks without knowing details of the interaction but they must appear in the planes of the corresponding sheets since $d_{Hg\text{-}Hg}$ remains unchanged on cooling. For example, an orthorhombic unit cell with $\vec{a} = \vec{d}_{Hg\text{-}Hg}$, $\vec{b} = \vec{b}_H$, $\vec{c} = \vec{c}_H$ will produce peaks at $n(3-\delta)\vec{a}_H^*$, $k\vec{b}_H^*$, $\ell\vec{c}_H^*$. A change in the unit cell angles will be reflected by a displacement of the peaks in the $\vec{b}_H^*$ or $\vec{c}_H^*$ direction but they will remain on the $n(3-\delta)\vec{a}_H^*$ planes.

(iii) Ordering between perpendicular chains

The interaction between perpendicular chains at their points of closest approach is probably strong because of the short contact

distance (3.2 Å) which is comparable to the distances found in metallic mercury. As in the case of parallel chains, indirect interactions through small local distortions of the host lattice are also possible.

However, the positions of the crossings of the chains have the host lattice spacings and will always be incommensurate with the Hg-Hg distance in the chain. A full perpendicular chain ordering is therefore prevented by the same factor which prevents the chain-host lattice ordering.

This obstruction to the ordering does not necessarily rule out the possibility of establishing coherent coupling between the perpendicular chains. According to Axe's Theorem the a chains and b chains can couple coherently if they arrange themselves to produce reciprocal lattice points at the intersections of the sheets. The resulting lattices are indicated by the light and the dark lines shown in Fig. 4.1. The ordered a chains and b chains are coupled by sharing reciprocal lattice points at $n(3-\delta)\vec{a}_H^*$, $n(3-\delta)\vec{b}_H^*$, $\ell\vec{c}_H^*$. The crystal may have another domain in which the chains are coupled by sharing $n(3-\delta)\vec{a}_H^*$, $-n(3-\delta)\vec{b}_H^*$, c_H^* reciprocal lattice points.

Although Axe's Theorem predicts that both the parallel ordering and the perpendicular coherent coupling are possible it does not provide any clue to which ordering mechanism would be dominant at a given temperature since the details of the chain interactions are unknown. For this matter, one would have to resort to experimental investigations.

4.3 Early low temperature neutron scattering experiments on $Hg_{3-\delta}AsF_6$

The low temperature ordering of the Hg chains was first studied by Hastings et al., (1977). They observed both parallel ordering and perpendicular coupling between the chains. More detailed results and interpretation are provided by the same authors in a later publication (Pouget et al., 1978). Fig. 4.2(a) and (b) are the reproduction of two diagrams reported in that paper.

The first diagram shows the intensity distribution along the line $(3-\delta, \eta, 0)$, i.e., the intersection between the first diffuse scattering sheet and the a*b*-plane. The room temperature scan gave almost a uniform intensity distribution.* When the temperature was lowered broad peaks gradually appeared at $\eta = \pm 0.4$. Since they appeared at a general position rather than at the intersection of the sheets Pouget et al. identified them as arising from parallel chain ordering. The peaks grew in intensity as the temperature was decreased but remained broad. They reached a maximum intensity at T = 125 K and then suddenly dropped (see Fig. 4.2(b)). At 120 K they had dropped by more than a factor of 2.

Over this same temperature range a new set of peaks appeared at $\eta = 1 \pm \delta$. The position of the peaks at the sheet intersections shows that they resulted from the perpendicular chain coupling predicted by the Axe's Theorem. The peaks were narrow even at T = 125 K and no critical scattering could be observed meaning that the ordered regions

---

* The scan in fact shows a small intensity modulation which presumably will disappear at higher temperatures. For convenience in this thesis, the room temperature phase will be treated as if it is completely disordered.

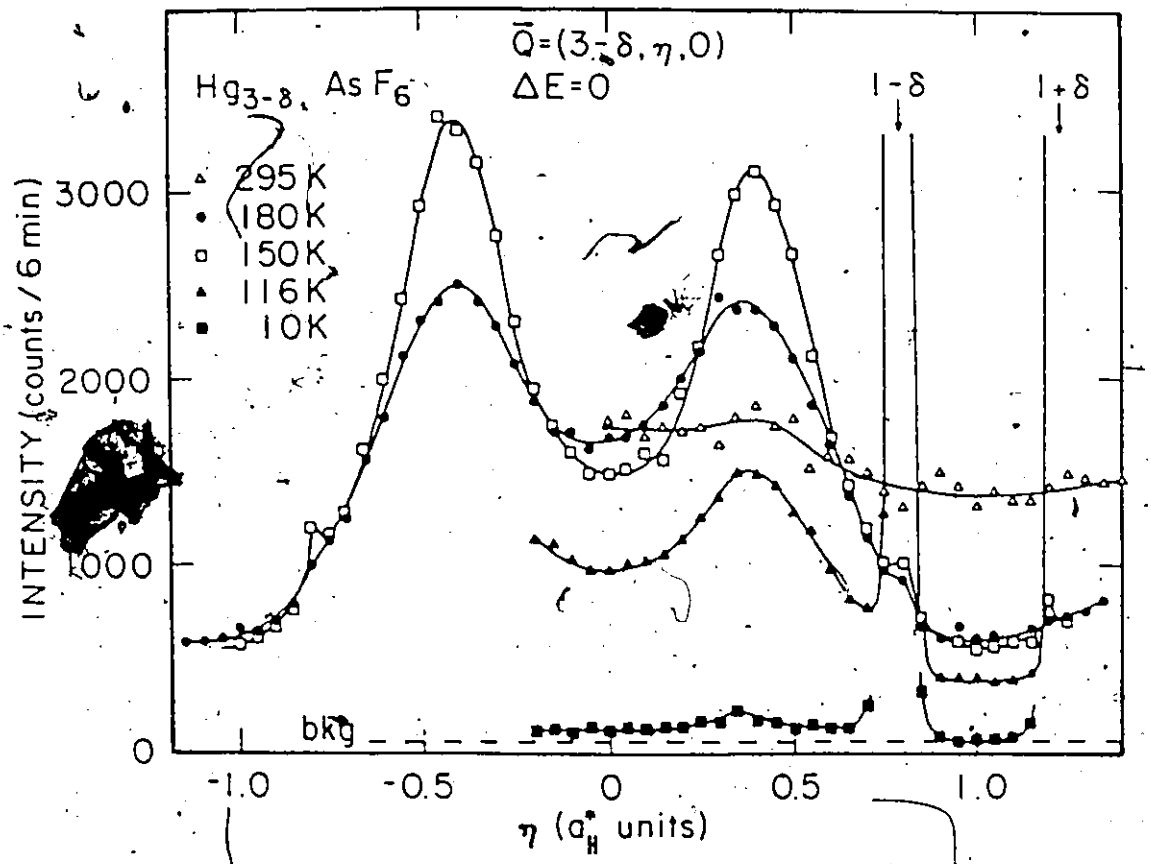

Figure 4.2(a)

The (3-δ, η, 0) scan of $Hg_{3-\delta}AsF_6$ at various temperatures. (After Pouget et al., 1978). The broad peaks observed at T > 120K signal development of a short range order between parallel chains (S-phase) while the narrow peaks at T < 120K represent a long range ordered phase (L-phase).

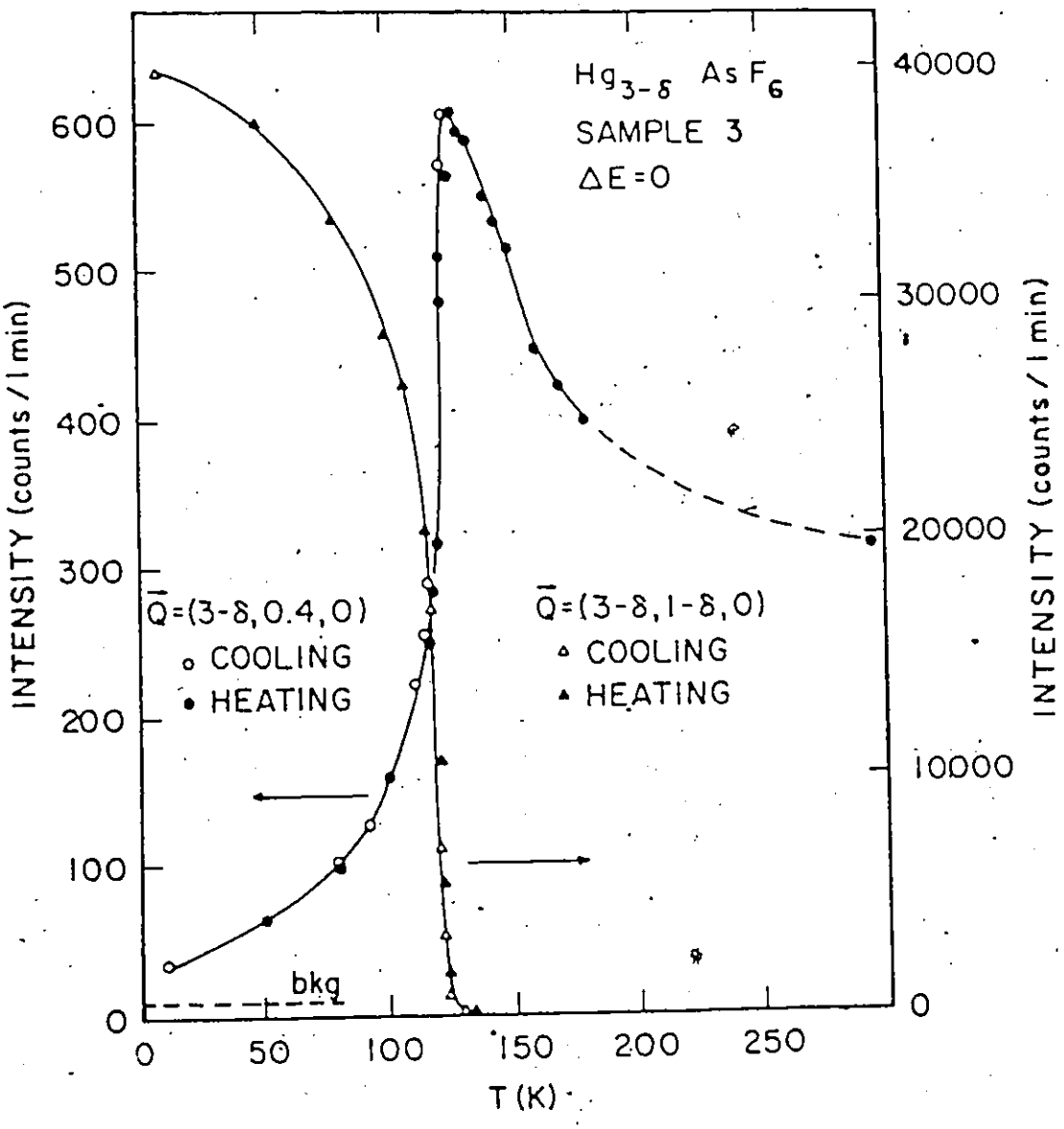

Figure 4.2(b)

Intensity variation of the broad peaks (circles) and the narrow peaks (triangles) with temperature (Pouget et al., 1978). The phase transition temperature T_c for $Hg_{3-\delta}AsF_6$ is taken to be ~120K.

must have grown very quickly to macroscopic sizes. At 120 K the intensity of the narrow peaks is already higher than that of the broad peaks and this temperature is taken as the phase transition temperature, T_c.

The broadness of the peaks observed at $T > 120$ K indicates that the ordering between the parallel chains is poor and extends only over short distances. For this reason this phase of $Hg_{3-\delta}AsF_6$ is called the short range order phase or S-phase. The D-phase and S-phase are not separated by a phase boundary. The former is merely the extreme case of the latter with a vanishingly small ordering between the parallel chains.

The narrowness of the peaks at $T < 120$ K is characteristic of ordering over very large distances. The corresponding phase is therefore called the long range order phase or L-phase.

This thesis describes work on the S-phase (sec. 4.4) and the L-phase (sec. 4.5) of $Hg_{3-\delta}SbF_6$ and $Hg_{3-\delta}TaF_6$. To make the discussion complete the corresponding phase of $Hg_{3-\delta}AsF_6$ studied by Pouget et al. (1978) is reviewed at the beginning of each section before describing the work on the new compounds. No study has been made for $Hg_{3-\delta}NbF_6$ because the crystals were too small and could not be fixed inside the capillaries especially at low temperatures.

4.4 The S-phase

(i) Studies on $Hg_{3-\delta}AsF_6$

Pouget et al. observed broad S-phase peaks of $Hg_{3-\delta}AsF_6$ at $3-\delta$, ± 0.4, 0 (Fig. 4.2(a)). On the $\ell=1$ layer similarly broad peaks were observed but at $3-\delta$, ± 0.6, 1. Although these peaks attain a

maximum intensity at T = 125 K no intensity modulation was observed on the second order diffuse scattering sheets even at that temperature. The authors explained this diffraction pattern by assuming two domains of partially ordered parallel chains. One such domain is shown in Fig. 4.3. The chains at y = 0 (z = 0 and 1) and y = ½ (z = ½) are ordered so that the unit cell defined by the Hg atoms is body-centered monoclinic while the chains at y = 1 (z = 0 and 1) are shifted with respect to these at y = 0 by about 0.6 d_{Hg} giving the diffraction peak at (3-δ, +0.4, 0). The peak at (3-δ, -0.6, 0) is systematically absent because of body-centering. In order to explain the broadening of the peaks on the first diffuse scattering sheet Pouget et al. could not simply assume that the ordered regions are small since this would give broad peaks with similar width on all the higher order sheets (see sec. 2.4). The absence of the peaks on the second order sheet was explained by introducing an uncertainty ε in the displacement of the chains at y = 1. This uncertainty which is associated with an uncertainty in the unit cell angle γ broadens the diffraction peaks and, as shown in Fig. 4.3, the higher the order of the reflection the broader the peak ($|\vec{q}|$-dependent broadening). If the uncertainty in γ is in the right range all the peaks on the second order sheet will be sufficiently broad as to be unresolved while those on the first order sheet are still narrow enough to be resolved. The S-phase peaks shown in Fig. 4.2(a) have a width (FWHM; full-width at half-maximum) of about $0.4\vec{a}^*_H$ corresponding to an uncertainty in the relative position of the chains ε of about ± 0.2 $d_{Hg\text{-}Hg}$.

In the other domain the shift of the y = 1 chains is about

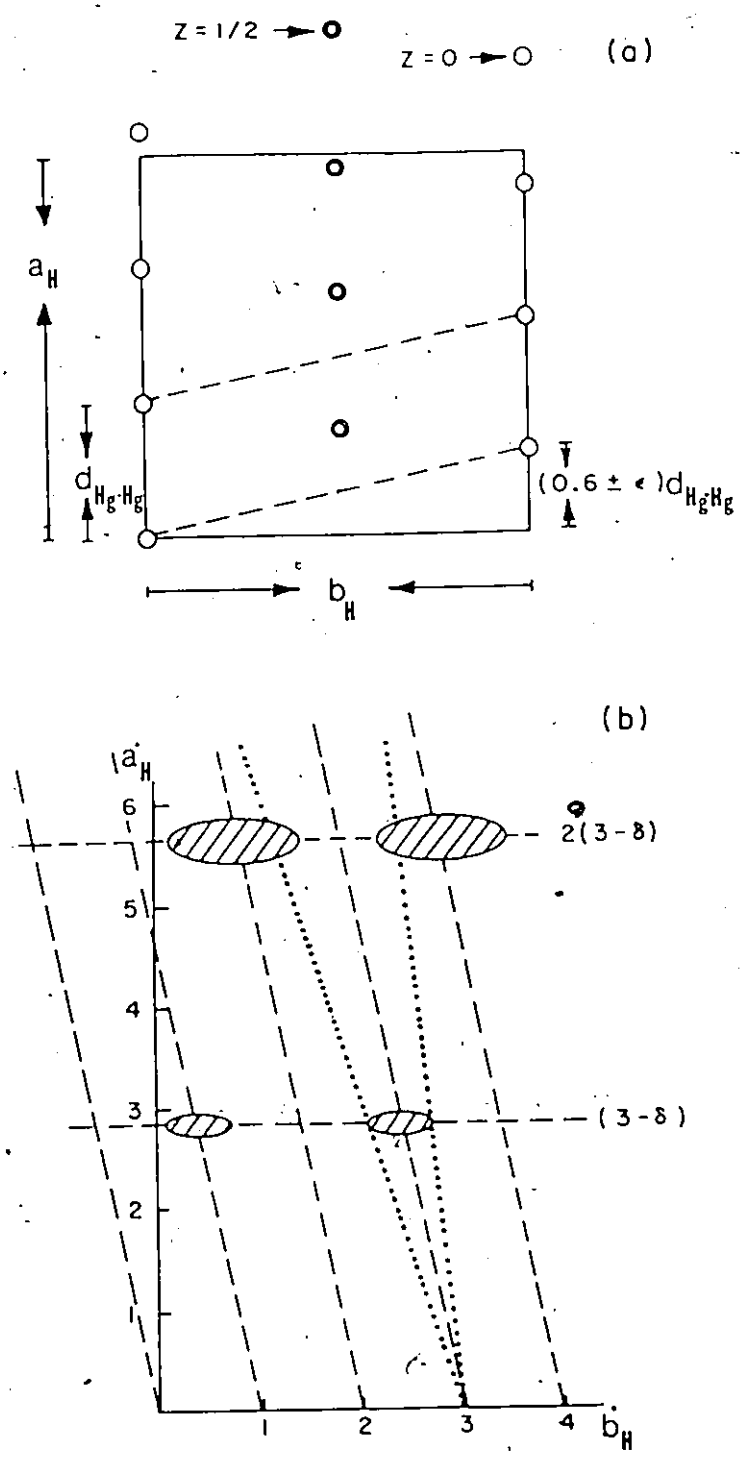

Figure 4.3

Arrangement of the chains in the S-phase of $Hg_{3-\delta}AsF_6$ (a) and the corresponding diffraction pattern (b). The S-phase peaks broadened by the $|\vec{q}|$ dependent broadening are represented by the shaded areas.

$-0.6\ a_H^*$ producing the diffraction peak at $(3-\delta, -0.4, 0)$. The peak at $(3-\delta, 0.6, 0)$ is again systematically absent due to the body-centering of the cell. Fig. 4.2(a) shows approximately equal S-phase peaks from the two domains over the whole range of temperature indicating that the relative volumes of the domains remain approximately equal. The growth of the peaks as the temperature is lowered must be interpreted as the result of more of the crystal being in the S-phase but the value of ε does not decrease with temperature as indicated by the constant width of the peaks.

(ii) Studies on $Hg_{3-\delta}SbF_6$ and $Hg_{3-\delta}TaF_6$

The S-phase of $Hg_{3-\delta}SbF_6$ was initially studied by using neutron diffraction but no intensity modulation that could be interpreted as an S-phase was found (Axe, Brown, Shirane and Tun, unpublished). The L-phase transition temperature T_c was measured to be 186 ± 1 K during this experiment. However, when the intensity distribution of the first order diffuse scattering sheet above T_c was re-examined in an X ray diffraction experiment using a very low scan speed, a weak S-phase was found* (see Fig. 4.4). Like the case of $Hg_{3-\delta}AsF_6$, the broad peaks are centered at $(3-\delta, \pm 0.4, 0)$ but have a much weaker amplitude and larger width while no peak is visible on the second order sheet. The arrangement of the parallel chains of $Hg_{3-\delta}SbF_6$ must therefore also be as shown in Fig. 4.3 but with a larger uncertainty ε in the relative positions of the chains. The value of ε corresponding to the observed

---

* Diffractometers and low temperature apparatus used for both X ray and neutron diffraction experiments are described in sec. 2.7.

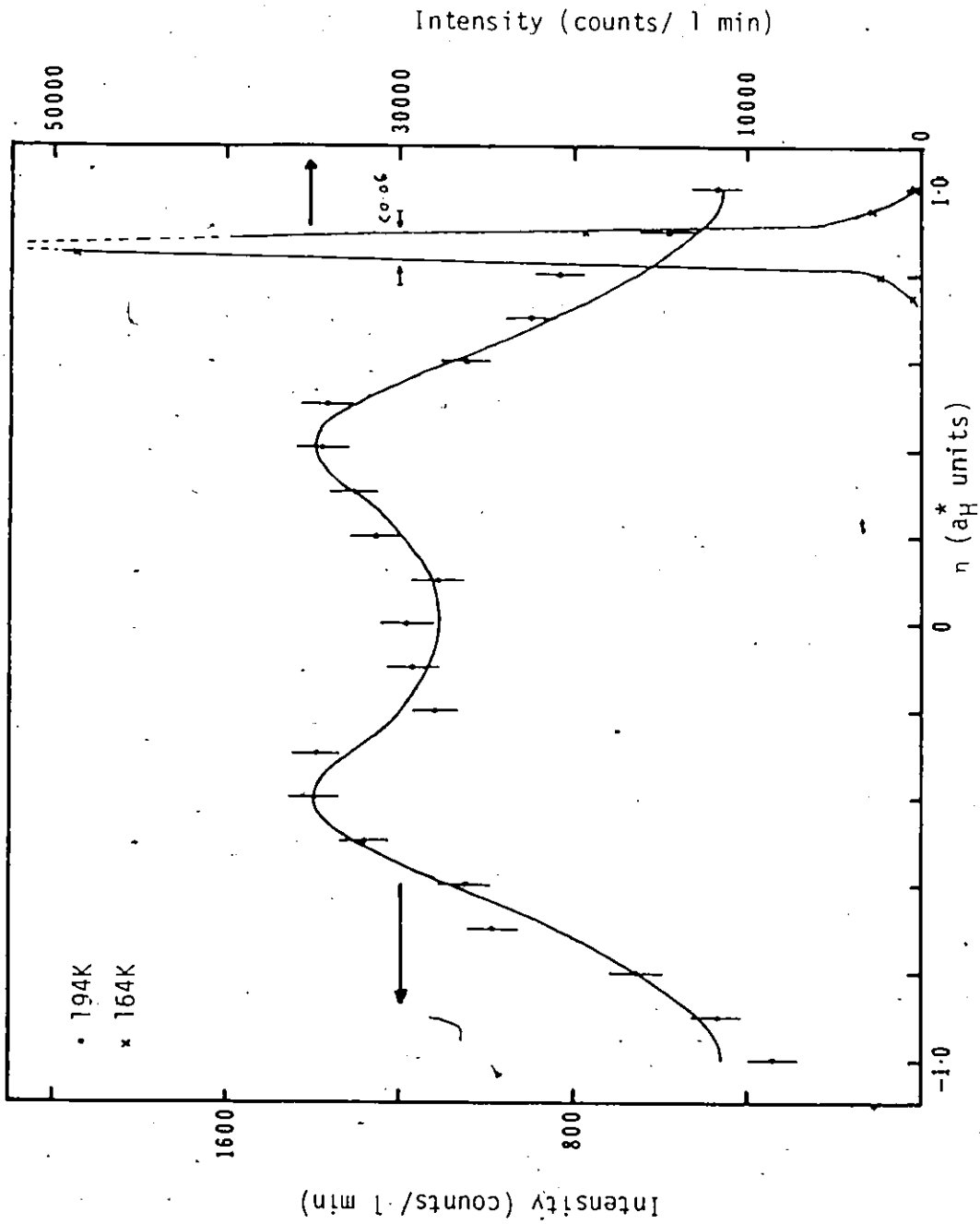

Figure 4.4 The (3-δ, η, 0) scan of $Hg_{3-\delta}SbF_6$.

width (FWHM $\simeq$ 0.6 a_H^*) is about $\pm$ 0.3 d_{Hg-Hg}.

No neutron diffraction experiment can be done on $Hg_{3-\delta}TaF_6$ since the crystals are too small. This material was therefore studied by X ray diffraction and the L-phase transition temperature T_c was found to be 193 $\pm$ 3 K. The S-phase above T_c is weak and shows a different ordering from the previous cases (see Fig. 4.5). The 3-δ, η, 0 scan has peaks at η = 0 and 2 in the scan range of -0.25 to +2.25. On the ℓ = 1 layer a peak centered at η = 1 was found in the same scan range. As in the previous cases no peak was found on the second order sheet. This diffraction pattern is consistent with an A-face centered orthorhombic cell as shown in Fig. 4.6. Only one domain of ordered parallel chains is required in this case but the possibility of having two domains with γ angle slightly deviated from 90° cannot be excluded. Since the width (FWHM) of the S-phase peaks is $\sim$ 1.0 a_H^* the uncertainty ε in the relative position of the Hg chains is about $\pm$ 0.5 d_{Hg-Hg}.

4.5 The L-phase

(i) Studies on $Hg_{3-\delta}AsF_6$

Pouget et al. (1978) observed sharp L-phase peaks of $Hg_{3-\delta}AsF_6$ at T << 120 K not only on the plane of the first order diffuse scattering sheet but also on the planes corresponding to the higher order sheets. However, the growth of the peaks was not uniform. When the temperature was just under 120 K only the first order peaks (i.e., peaks on the first order diffuse scattering sheet) were visible indicating that the evolution of the L-phase was initiated by development of a pure sinusoidal fluctuation in the mean atomic density of the chains. This fluctuation had a wavevector whose x-component was Q_1 defined by eq. (2.40). The

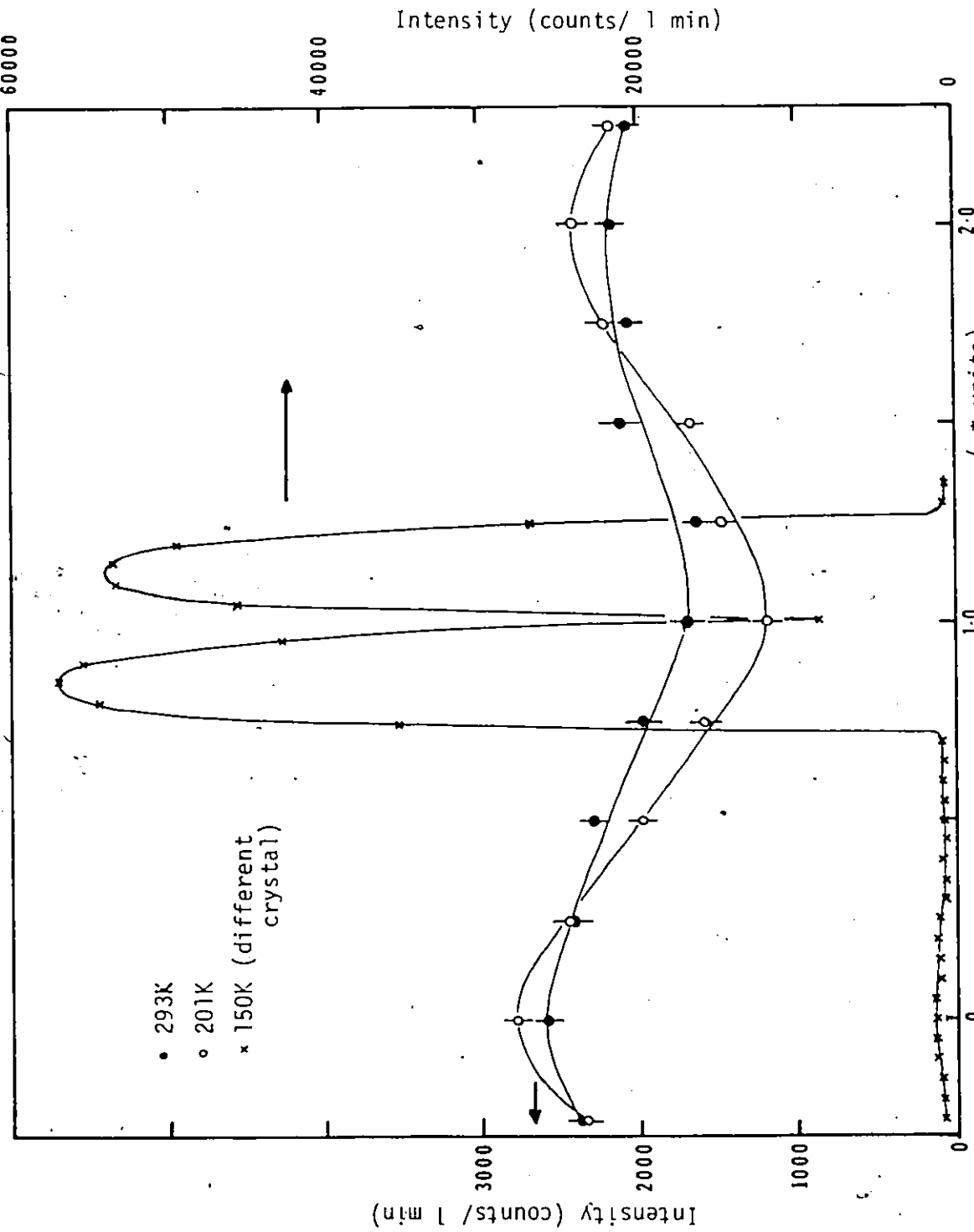

Figure 4.5 The (3-δ,n , 0) scan of $Hg_{3-\delta}TaF_6$. Note that the intensity modulation in S-phase is different from the previous cases.

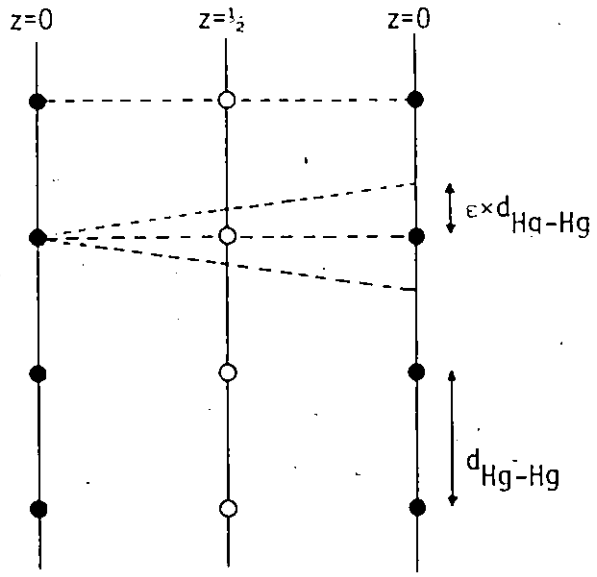

Figure 4.6

Arrangement of the chains in the S-phase of $Hg_{3-\delta}TaF_6$. The chains partially order to form an A-face centered monoclinic lattice.

higher order peaks grew only when fluctuations having wavevectors with the x-components Q_2, Q_3, ... set in one after another at lower temperatures. As $T \to 0$, fully developed peaks could be seen at $n(3-\delta)$, $k \pm n\delta$, ℓ points where $n + k + \ell$ = even integer.

Pouget et al. pointed out that the above diffraction pattern is consistent with the two domains of the crystal predicted by Axe's Theorem if the mutually perpendicular chains couple coherently (see sec. 4.2). In the first domain $n(3-\delta)$, $n(3-\delta)$, ℓ reciprocal lattice points are shared between the two sets of the chains. The situation is depicted in Fig. 4.1 while the corresponding unit cells formed by the Hg atoms are shown in Fig. 4.7. Note that (130) planes of the a-chain Hg cell are parallel to and have the same spacing as (310) planes of the b-chain Hg cell and both are perpendicular to the [110] direction of the host lattice. In order to find out the relative position of the (130) planes of one unit cell with respect to the (310) planes of the other, Pouget et al. measured intensity at the common reciprocal lattice points. The peak at $(3-\delta)$, $(3-\delta)$, 0 was found to be absent while the peak at $(6-2\delta)$, $(6-2\delta)$, 0 was four times stronger than the other reflections with similar 2θ angle. This indicates that the planes of the two unit cells are out of phase for the first reflection but in phase for the second, causing its amplitude to double and intensity to increase by a factor of four. Such arrangement of the planes is shown in Fig. 4.8.

(ii) Studies on $Hg_{3-\delta}SbF_6$ and $Hg_{3-\delta}TaF_6$

The L-phase of $Hg_{3-\delta}SbF_6$ has been studied by using both neutron and X ray diffraction. In the neutron diffraction experiment the

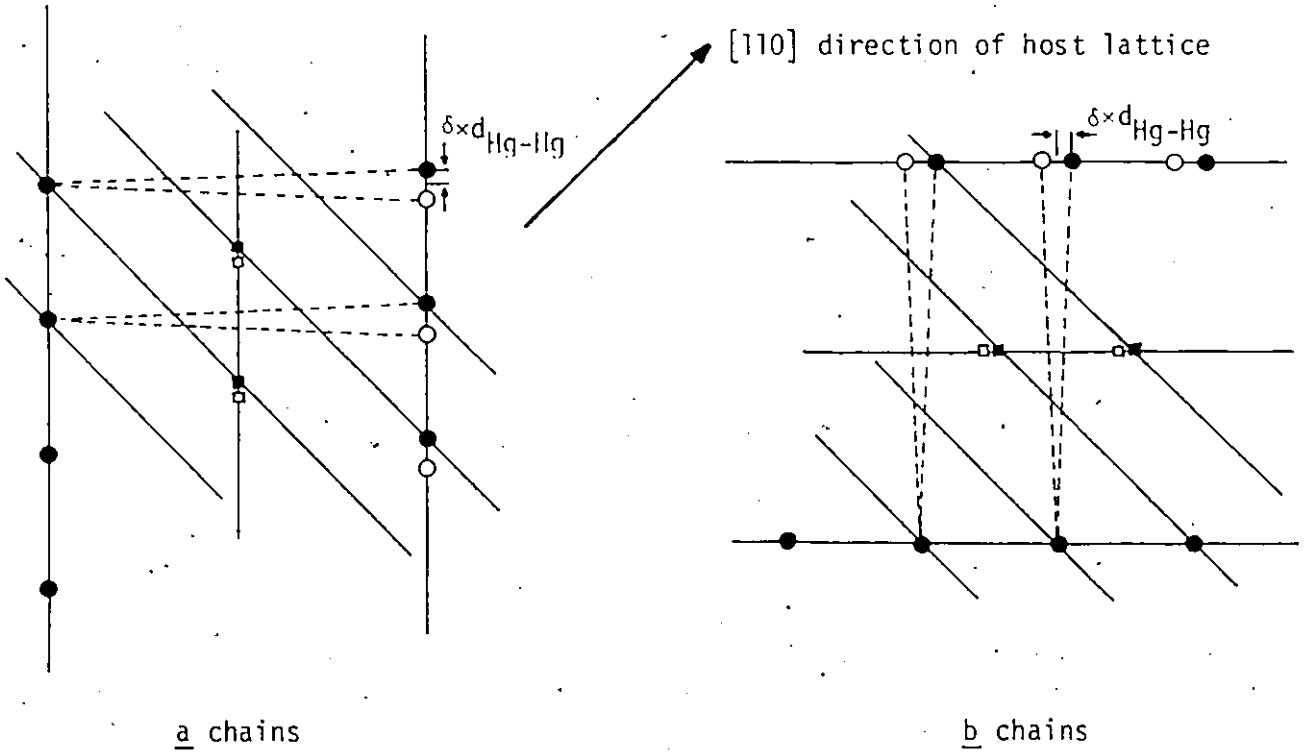

Figure 4.7

Ordered chains in the L-phase. The black atoms represent one domain while the white ones represent the other. Note that both the (310) planes of the a chains (consider only the black atoms) and the (130) planes of the b chains are perpendicular to the host lattice [110] direction, i.e., the two sets of ordered chains are coupled coherently by sharing reciprocal lattice points in that direction.

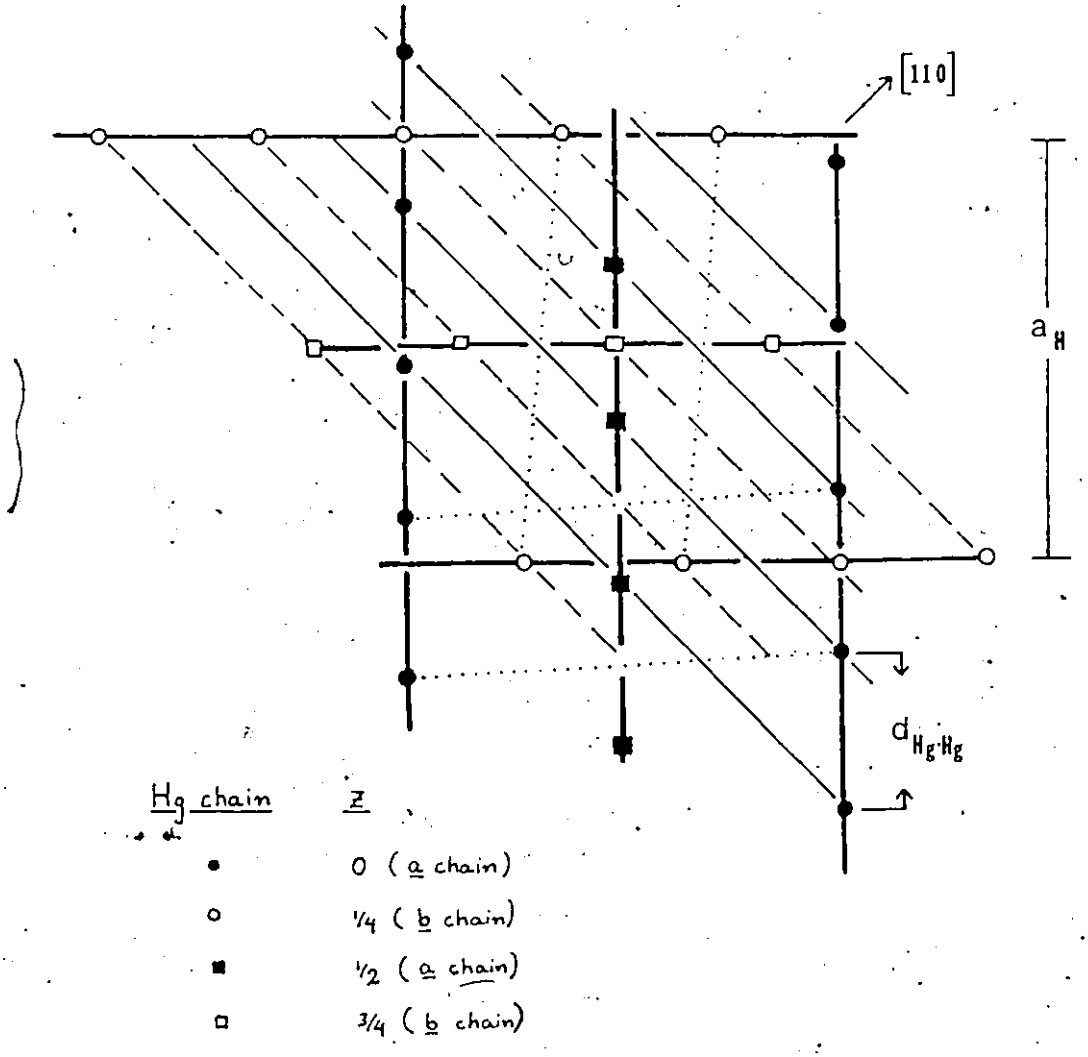

Figure 4.8

Relative position of the (310) Bragg planes of the ordered a chains (light solid lines) with respect to the (130) Bragg planes of the ordered b chains (dashed lines). The monoclinic unit cells defined by the Hg atoms are indicated by the dotted lines.

intensities of the first order peaks and the second order peaks were examined at various temperatures ranging from T_c (186 K) to 10 K. As in the case of $Hg_{3-\delta}AsF_6$, the ordering was initiated by the development of a pure sinusoidal fluctuation with the wavevector Q_1 (the x-component) and only the first order peaks were visible at T close to 186 K. The intensity of $(3-\delta)$, $(1-\delta)$, 0 peak was found always equal to that of $(3-\delta)$, $(1+\delta)$, 0 peak suggesting that the amount of crystal ordered in the L-phase is always equally divided between the two domains.

Fig. 4.4 obtained from an X ray diffraction experiment shows a short scan about the peak $3-\delta$, $1-\delta$, 0 at T = 164 K. The width (FWHM) of the peak is about 0.06 a_H^* or 0.008 $\mathring{A}^{-1}$.† Fig. 4.9 shows a scan across the same peak but in the c_H^* direction and the width is less than 0.10 c_H^*, the size of a step of the scan, or 0.008 $\mathring{A}^{-1}$ indicating that the ordering in the c direction is at least as good as in the a-b plane. Intensities of $(3-\delta)$, $(3-\delta)$, 0 peak and $(6-2\delta)$, $(6-2\delta)$, 0 peak were also measured and, like the case of $Hg_{3-\delta}AsF_6$, the former was found to be absent while the latter was four times stronger than the near-by reflections. The relative arrangement of the a-chain Hg cell and the b-chain Hg cell must be as shown in Fig. 4.8.

L-phase studies of $Hg_{3-\delta}TaF_6$ have been carried out only by X ray diffraction experiment because of the small size of the crystal and the phase could only be studied in the neighbourhood of T_c (193 K).* As in the previous two compounds, only the first order peaks were visible

---

† Resolution of the diffractometer is smaller than a step in the scan which is 0.05 a_H^*.

* The lowest temperature available on the X ray diffractometer is 145 K. See sec. 2.7 for details.

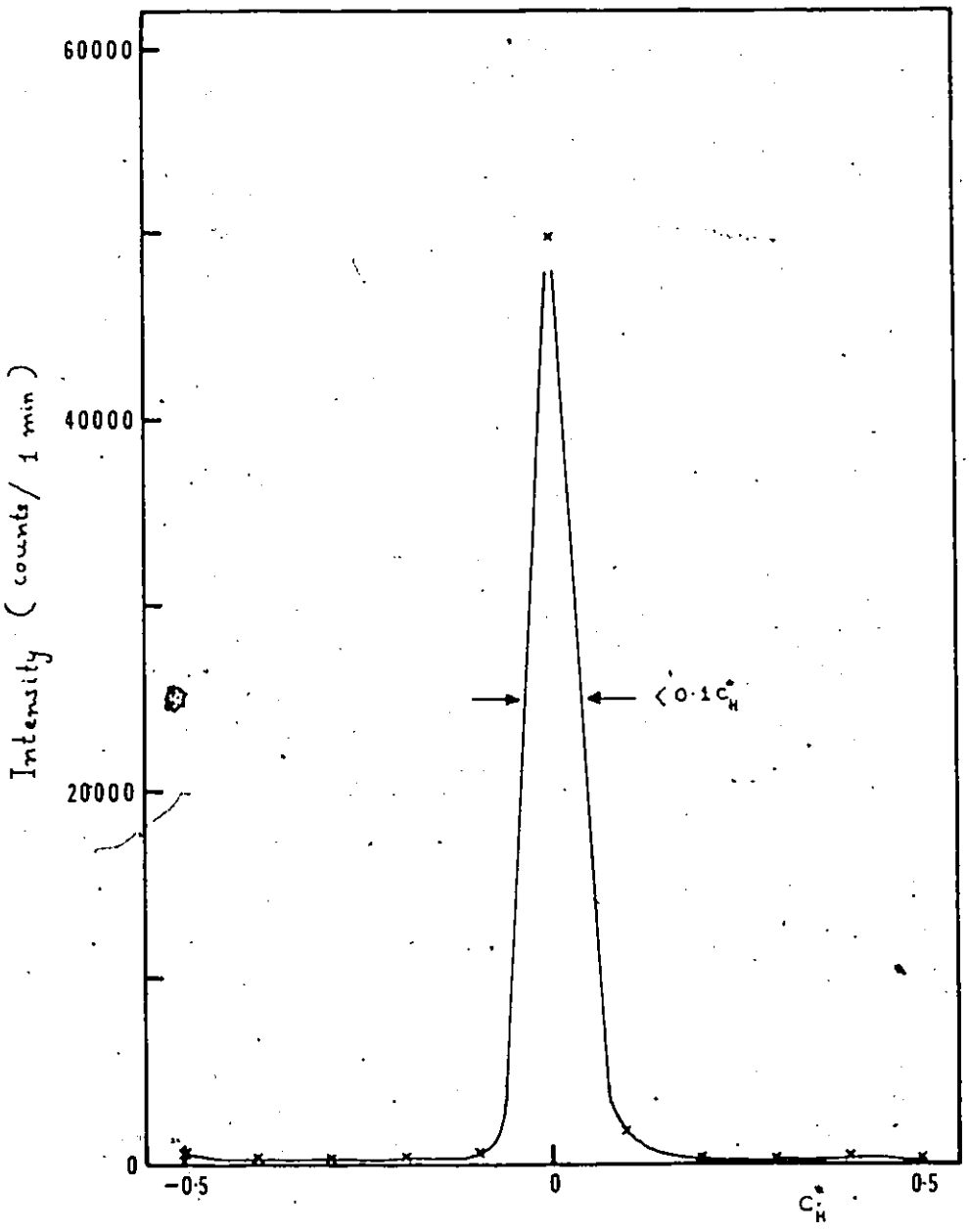

Figure 4.9

Scan across the L-phase peak of $Hg_{3-\delta}SbF_6$ in the c* direction.

at T < 193 K but higher order peaks grew at lower temperatures. The arrangement of the chains must also be identical to the previous cases since an identical diffraction pattern was observed. Fig. 4.5 and 4.10 show scans across the L-phase peaks. The noticeably wide peaks of Fig. 4.5 could be due to the highly anisotropic shape of the crystal which was a flat plate of the dimension 0.2 x 0.2 x 0.01 mm.

4.6 Emery-Axe order parameter theory

Emery and Axe have proposed a mean field theory in order to explain the evolution of the L-phase in the $Hg_{3-\delta}MF_6$ compounds (Emery and Axe, 1978; Axe., 1980). According to the experiments described in the previous section, the phase transition into the L-phase is triggered by the development of a pure sinusoidal wave in the mean atomic density of the chains. The amplitude of this fluctuation, η_1, is employed as the order parameter in the theory.

The mean atomic density of a single chain is denoted by $\langle\rho_x(x)\rangle$ where $\rho_x(x) = \sum_\alpha \delta(x-x_\alpha)$ and the summation is over the whole chain.* The Fourier transform is,

$$\langle\rho_x(Q)\rangle = \int dx \langle\rho_x(x)\rangle e^{iQx} \qquad (4.1)$$

When the chain does not have a long range order $\langle\rho_x(x)\rangle$ is a constant function of x.

$$\therefore \quad \langle\rho_x(Q)\rangle = \delta(Q) \qquad (4.2)$$

In the L-phase, $\langle\rho_x(x)\rangle$ shows fluctuations with amplitudes η_1, η_2, ... and wavevectors Q_1, Q_2, ... In general $\langle\rho_x(Q)\rangle$ is a

---

* In this section all the vectors, both in real space and reciprocal space, are written without an arrow since they are always along the direction of the chain.

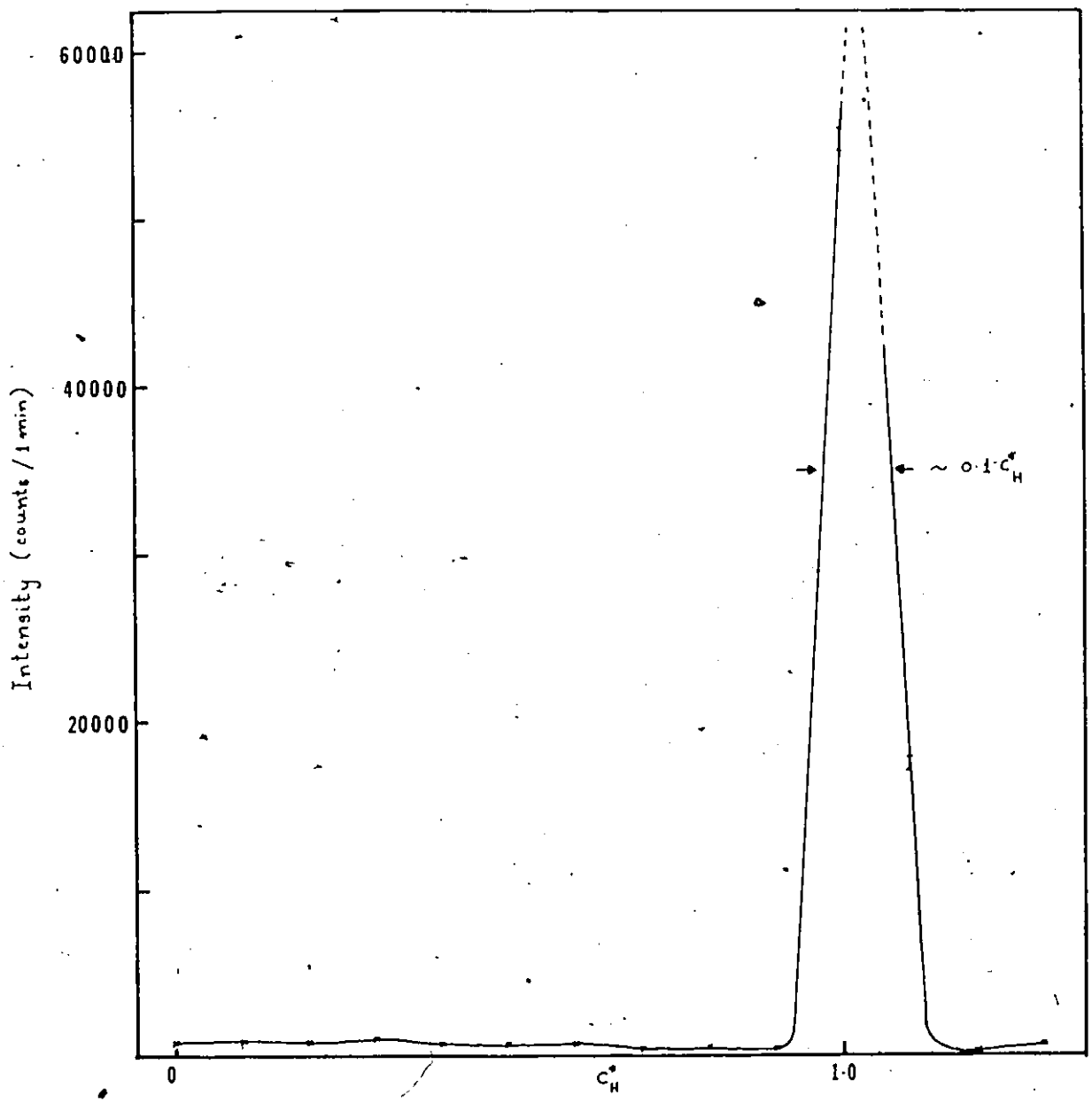

Figure 4.10

Scan across the L-phase peak of $Hg_{3-\delta}TaF_6$ in the c* direction.

complex number but for a suitable choice of origin it can be made real. For the first sinusoidal wave

$$\eta_1 = \langle \rho_x(Q_1) \rangle \tag{4.3}$$

The interaction Hamiltonian for ordering can be constructed as follows. For an isolated chain with harmonic potential between nearest, neighbours, the Hamiltonian is

$$H_o = \sum_\alpha \{ \frac{p_\alpha^2}{2m} + \frac{K}{2}(u_{\alpha+1} - u_\alpha)^2 \} \tag{4.4}$$

where

$$K = mc^2/d_{Hg\text{-}Hg}^2$$

See sec. 2.5 for the definition of other parameters in eq. (4.4). When the chain is ordered with respect to its neighbouring chains the isolated chain Hamiltonian H_o is perturbed by an interaction potential. Emery and Axe assumed that each chain experiences a (commensurate) mean field $\bar{V}(x)$ produced by its neighbouring chains. The perturbation is given by,

$$H' = \int dx \bar{V}(x) \rho_x(x) \tag{4.5}$$

$$= \int dQ \bar{V}(Q) \rho_x(Q)$$

When $T \sim T_c$, the only non-zero Fourier component of $\bar{V}(x)$ is $\bar{V}(Q_1)$. Hence,

$$H'(\eta_1) = \bar{V}(Q_1) \rho_x(Q_1) \tag{4.6}$$

The magnitude of the mean field $\bar{V}(Q_1)$ itself depends on the order parameter η_1 since the field is produced by the similar density fluctuations in the neighbouring chains whose amplitudes are also given

by η_1. Therefore

$$\bar{V}(Q_1) = \eta_1 h(Q_1) \tag{4.7}$$

where the potential h represents the total interaction of the chain in question to its parallel and perpendicular neighbouring chains. It is not necessary to know the details of the potential h, since it can be eliminated in terms of the phase transition temperature T_c.*

The atomic density $\rho_x(Q_m)$ can be expressed as

$$\rho_x(Q_m) = \int dx \rho_x(x) e^{iQ_m x} \qquad (m = 1,2,\ldots) \tag{4.8}$$

$$= \sum_\alpha \cos(Q_m x_\alpha)$$

$$= \sum_\alpha \cos(Q_m u_\alpha) \tag{4.9}$$

By combining eq. (4.4), (4.6), (4.7) and (4.9), the total energy $H = H_0 + H'$ can be obtained.

$$H = \sum_\alpha \{\frac{p_\alpha^2}{2m} + \frac{K}{2}(u_{\alpha+1} - u_\alpha)^2 + \eta_1 h \cos Q_1 u_\alpha\} \tag{4.10}$$

Because of the stiff Hg-Hg bonds, the displacement u_α is a slowly varying function of x. Therefore, $u_{\alpha+1} - u_\alpha$ can be approximated as,

$$u_{\alpha+1} - u_\alpha = \frac{\partial u}{\partial x} \cdot d_{Hg\text{-}Hg} \tag{4.11}$$

---

* Such a relation can be derived by applying the linear response theory to the problem of interaction between the mean field and the chains at above T_c and considering the divergence of fluctuation scattering as $T \to T_c$. See eq. (14b) of Axe, 1980. (Note a misprint in Axe's paper; the sentence after eq. (14b) should read "... setting the denominator of (11) to zero ...").

When eq. (4.11) is substituted into (4.10), the P.E. part of the total Hamiltonian (i.e., the second and the third term of eq. (4.10)) becomes the classical sine-Gordon potential. The following ensemble average is to be calculated by using this potential.

$$\eta_m = \langle \rho_x(Q_m) \rangle = \sum_\alpha \cos(Q_m u_m)$$

$$= \sum_\alpha \int du_1 \ldots du_N \cos(Q_m u_m) e^{-\beta(P.E.)} \qquad (4.12)$$

For a sine-Gordon potential this integral has been solved exactly by Gupta and Sutherland (1976). Emery and Axe followed the same approach and obtained the amplitudes of the first three sinusoidal waves η_1, η_2 and η_3. The three parameters, normalized to 1 at $T \to 0$ K, are shown in Fig. 4.11. Since the parameters η_1, η_2, η_3, ... are the amplitudes of the fluctuations in the mean atomic density of the chains (by definition) the growth of the intensities of the corresponding L-phase peaks is expected to vary as η_n^2 vs. T and this can be tested by an experiment.

4.7 Testing the Emery-Axe order parameter theory

Emery-Axe order parameter theory can be tested by measuring the intensity of various L-phase peaks at different temperatures below T_c. Experiments have been completed on $Hg_{3-\delta}AsF_6$ and $Hg_{3-\delta}SbF_6$ by using neutron diffraction.* A preliminary X ray diffraction experiment has also been carried out on $Hg_{3-\delta}TaF_6$. Each of these experiments will be discussed separately in this section.

---

* A project carried out by Brown and Tun (McMaster University) in collaboration with Axe and Shirane (Brookhaven National Laboratory).

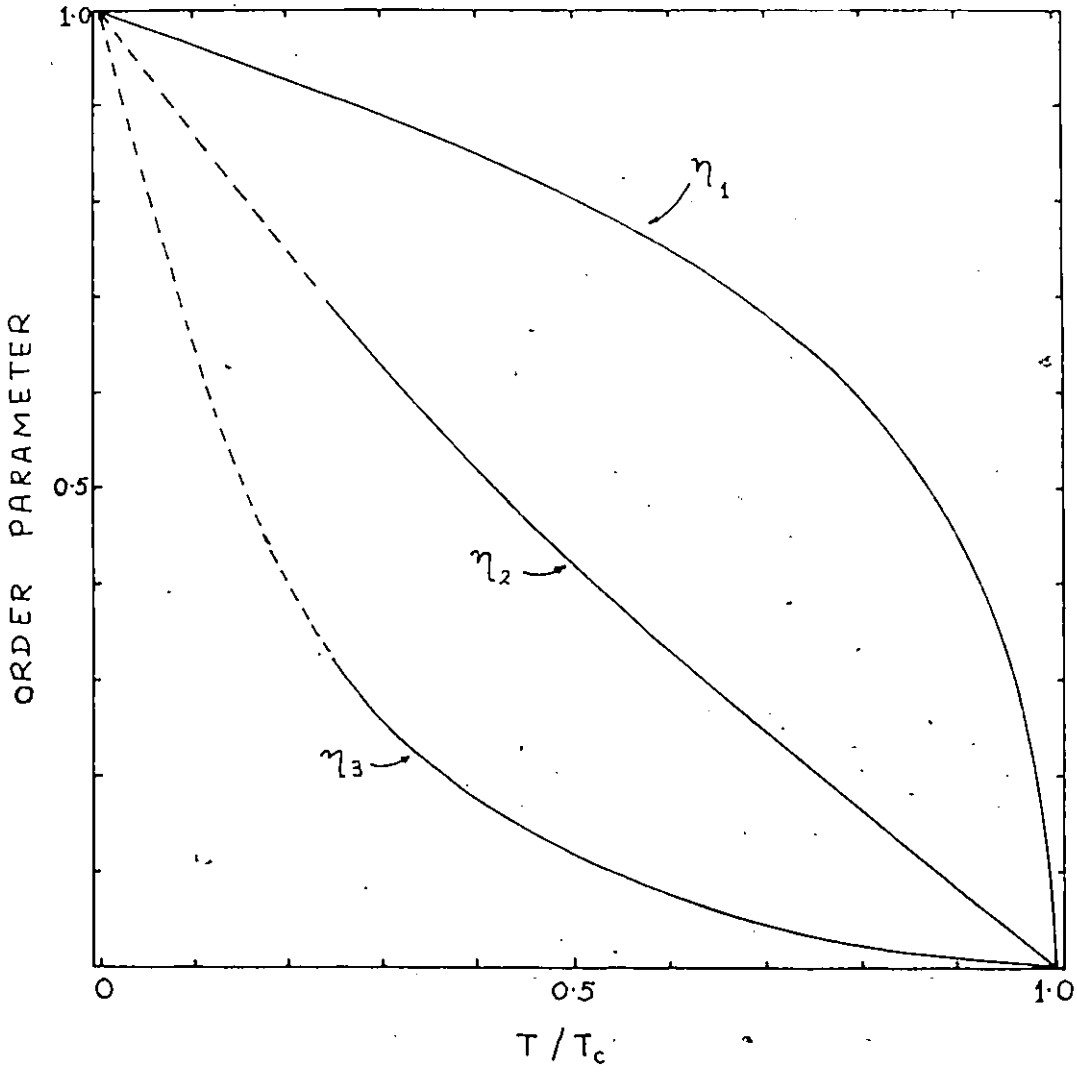

Figure 4.11

The predicted variation of η_1, η_2 and η_3 with temperature. (Taken from Axe, 1980).

(i) Neutron diffraction experiment on $Hg_{3-\delta}AsF_6$

The experiment was carried out by using a triple axis diffractometer at the Brookhaven High-flux Reactor (see sec. 2.7 for details). The crystal, mounted in an aluminium sample holder, was arranged so that the c axis was perpendicular to the plane of the instrument. The approximate dimension of the crystal was 15x12x0.8 mm.

The monochromator and the analyzer of the diffractometer were set to select neutrons with $k = 2\pi/\lambda = 2.670\ \text{Å}^{-1}$. The a* and b* axes were located by centering on the 400 and 040 host lattice reflections at T = 125 K. Intensities of these reflections were maximized by adjusting the arcs of the goniometer. Readjustment of the arcs was not necessary as no sign of crystal movement was seen throughout the experiment. The positions of the L-phase peaks were calculated by using the host lattice unit cell and the previously measured Hg-Hg bond length of 2.670 Å.

The intensities of the $(3-\delta), \pm (1-\delta), 0$ and $(6-2\delta), \mp 2\delta, 0$[†] peaks were measured at 15 different temperatures $\leq$ 125 K. The peaks (especially the second order peaks) were barely visible for two higher temperature measurements (125 K and 120 K) but became clearly visible at lower temperatures. It was therefore possible to monitor and update the centering on the peaks by doing alternate scans in the a* and b* directions. The scan range was always kept large enough so that the background intensity was recorded for at least 3 steps on either side of the peak. Since the hysteresis of the peaks is known to be small ($\sim$ 1.5 K; Pouget (1978)) no attempt was made to measure the intensities in a warming cycle.

---

† Note that $\pm$ pairs belong to different domains.

The background corrected intensity of the (3-δ), (1-δ), 0 and (3-δ), -(1-δ), 0 peaks were added to remove any error which might be caused by the redistribution of domain population as the temperature was lowered.* The sums were then normalized to 1 at the extrapolated temperature T = 0 K. The intensity of (6-2δ), -2δ,0 and (6-2δ), 2δ, 0 peaks were treated similarly.

Fig. 4.12 (a and b) compares the experimental results to the predicted variation η_m^2. The theory clearly predicts a slower growth of the peaks. In fact, the figure shows that the intensities of both first order and second order peaks vary as η rather than η^2.

(ii) Neutron diffraction experiment on $Hg_{3-\delta}SbF_6$

The experimental procedure was similar to the previous experiment but a smaller sample (2x2x0.3 mm) was used. The variations of the first order and the second order peaks with T are shown in Fig. 4.13. Unlike the case of $Hg_{3-\delta}AsF_6$, the agreement between the theory and the experimental results is good.

(iii) X ray diffraction experiment on $Hg_{3-\delta}TaF_6$

The four-circle diffractometer and the cold N_2 gas low temperature apparatus described in sec. 2.7 were used for this experiment and the sample had dimensions of 0.2x0.2x0.01 mm. Calibration of temperature against the stream heater was done before the X ray intensity measurements were made and the uncertainty in temperature for a given heater setting was found to be $\pm$ 3 K. The crystal was centered using 15 host

---

* No evidence of redistribution was observed, however. The two domains were equally developed at all the temperatures.

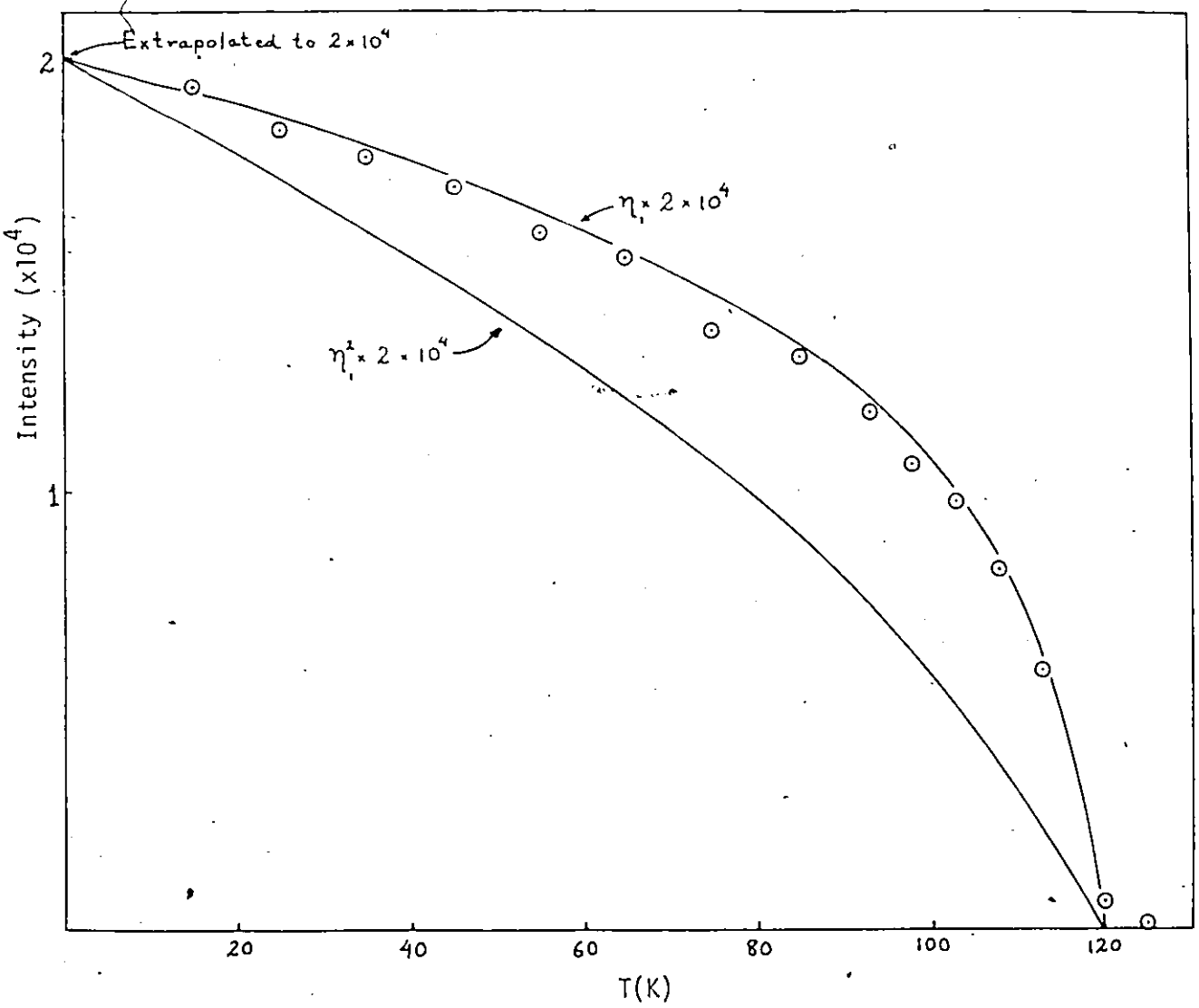

Figure 4.12(a)

Observed variation of the intensity of n=1 L-phase peak with temperature in $Hg_{3-\delta}AsF_6$. Note that the observed variation is closer to η_1 vs. T rather than η_1^2 vs. T.

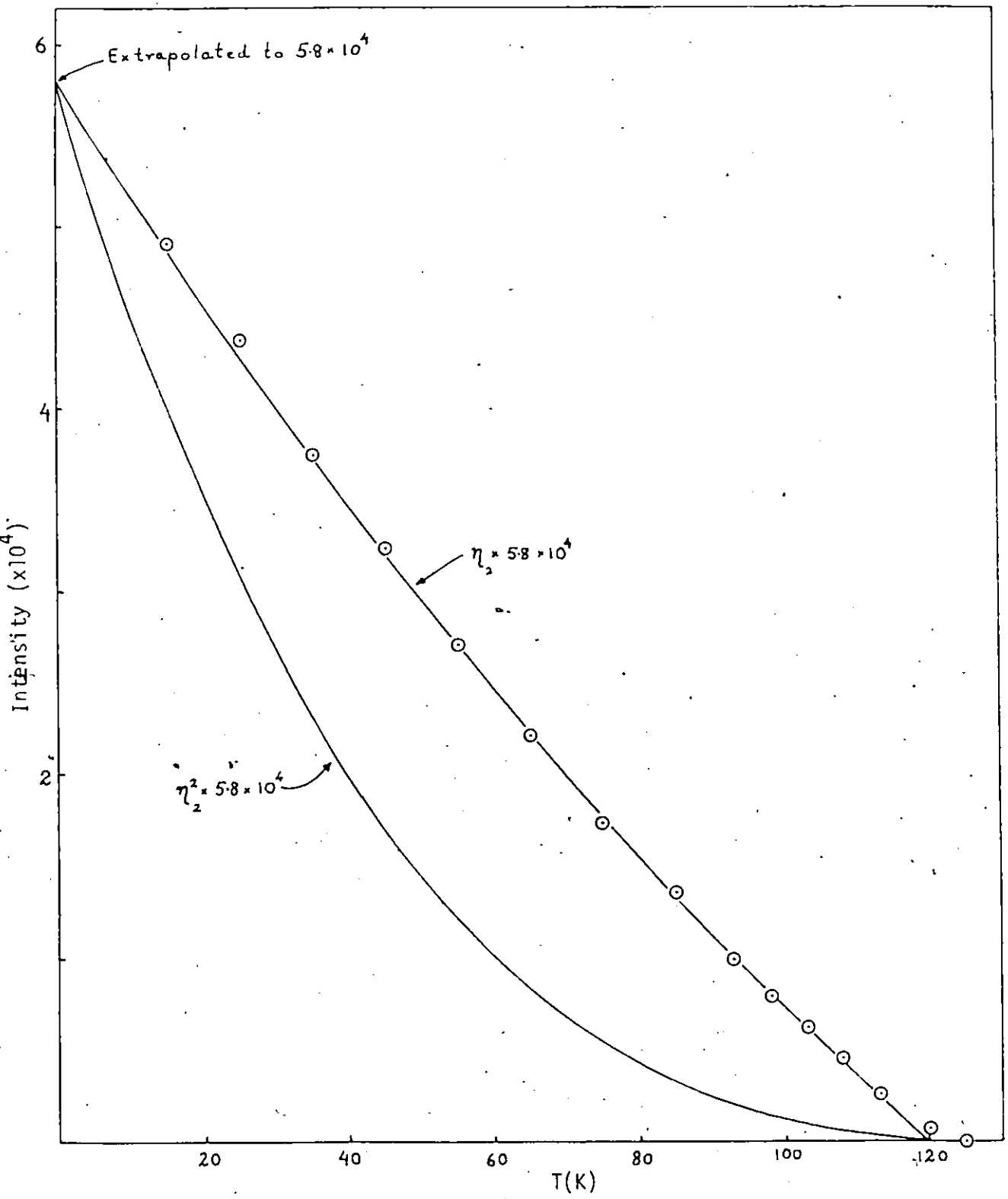

Figure 4.12(b)

Observed variation of the intensity of n=2 L-phase peak with temperature in $Hg_{3-\delta}AsF_6$. Again, the variation is closer to η_2 vs. T. Number of counts plotted on the y-axis for the n=2 peak is higher than that for the n=1 peak because of longer counting time.

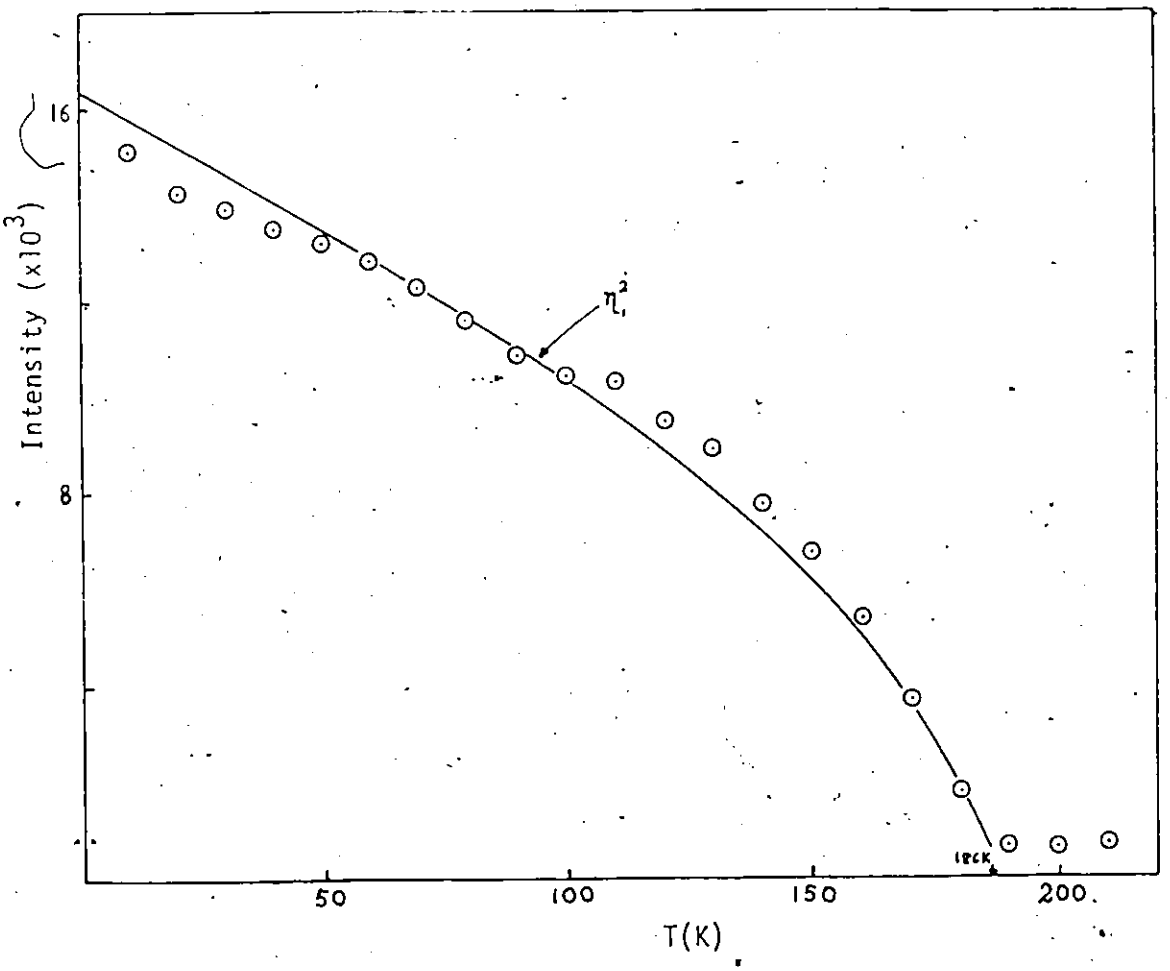

Figure 4.13(a)

Observed variation of the intensity of n=1 L-phase peak with temperature in $Hg_{3-\delta}SbF_6$.

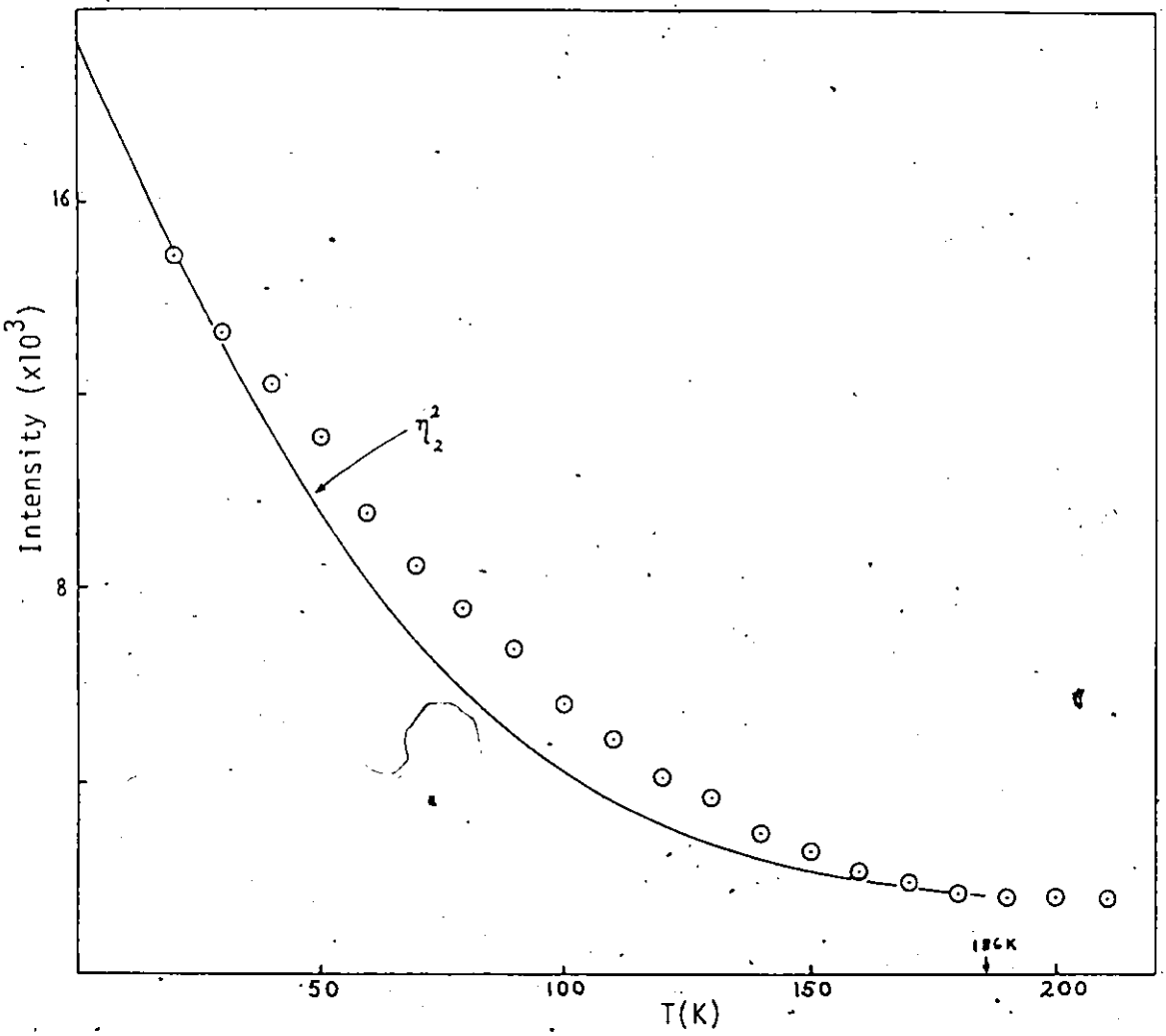

Figure 4.13(b)

Observed variation of the intensity of n=2 L-phase peak in $Hg_{3-\delta}SbF_6$.

lattice reflections and the position of the (3-δ), (1-δ), 0 peak was calculated using the Hg-Hg distance of 2.671 Å. Crystal centering was repeated and the position of the Hg peak recalculated whenever the temperature was changed.

The peak intensity was measured at 5 different temperatures (between 150 K and 182 K) during a warming cycle. The results plotted in Fig. 4.14 show that the variation of intensity with temperature is closer to the variation of η_1 rather than η_1^2.

4.8 Discussion

The chain ordering is weak at room temperature in all $Hg_{3-\delta}MF_6$ compounds indicating that the interchain interactions are very much less than 300 K (300 K is equivalent to 0.026 eV). However, the different S-phases observed in the three materials studied ($Hg_{3-\delta}AsF_6$, $Hg_{3-\delta}SbF_6$ and $Hg_{3-\delta}TaF_6$) suggest that the details of these interactions are not the same. Studying the S-phases provides an insight into the parallel chain interactions.

Fig. 4.15 shows the arrangement of nearest and second nearest neighbour parallel chains in the three compounds studied. Since the third nearest neighbour parallel chains are about 12.6 Å apart, the parallel chain ordering is probably influenced only by the nearest neighbour interaction (v_1) and the second nearest neighbour interaction (v_2). The arrangement of the atoms will be determined by the sign (+ for repulsive, - for attractive) and the relative strength of v_1 and v_2.

For the case of $Hg_{3-\delta}AsF_6$, v_1 and v_2 have been determined by

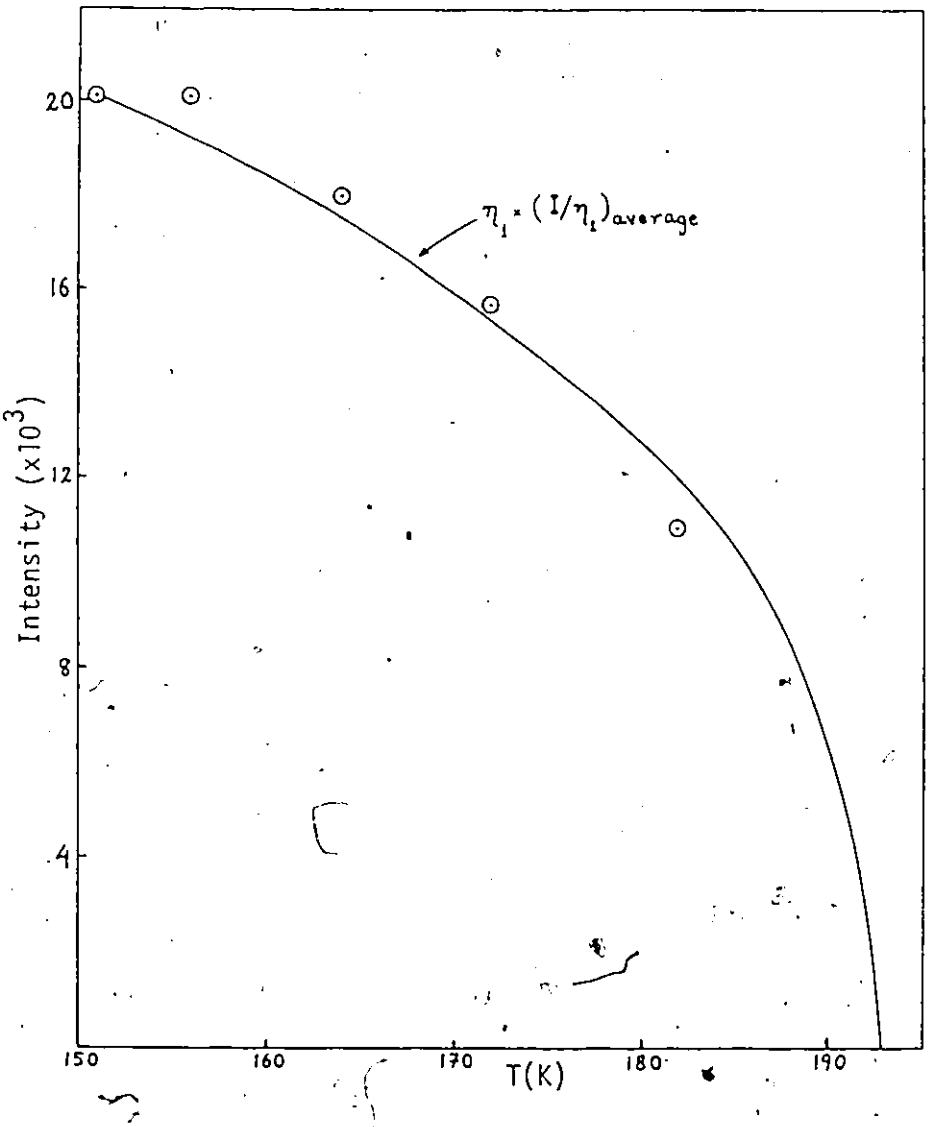

Figure 4.14

Observed variation of the intensity of n=1 L-phase peak in $Hg_{3-\delta}TaF_6$. Also in this case the variation is close to η_1 vs. T.

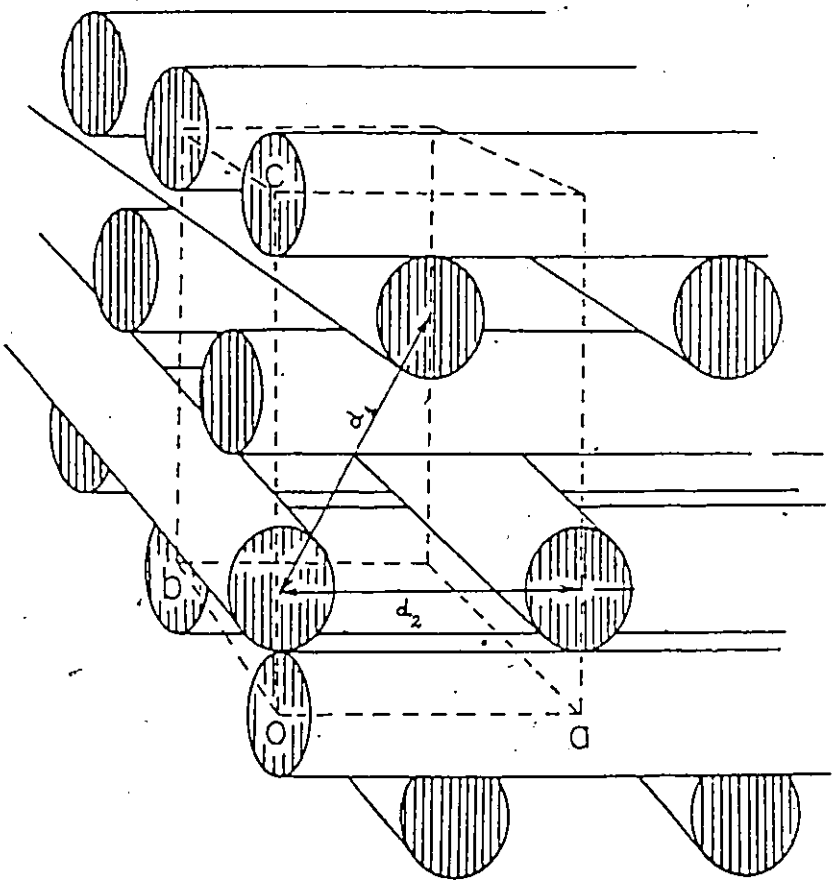

	$Hg_{3-\delta}AsF_6$	$Hg_{3-\delta}SbF_6$	$Hg_{3-\delta}NbF_6$	$Hg_{3-\delta}TaF_6$
d_1	7.253	7.404	7.415	7.435
d_2	7.534	7.711	7.692	7.711

Figure 4.15

Arrangement of the parallel chains and the nearest neighbour distances in $Hg_{3-\delta}MF_6$ compounds. Taken from Brown et al.(1982).

Emery and Axe (1978) using intensity fluctuations observed in the S-phase. The values they obtained are $v_2 = -2v_1 \simeq 0.14$ K. The negative value of v_1 indicates that the interaction is not a Coulomb (bare or screened) interaction. The authors suggested that interactions through the host lattice might be important.

Attractive interchain interactions can be seen also in $Hg_{3-\delta}TaF_6$. Since the Hg atoms partially order to form an A-face centered lattice which minimizes the distance between the Hg atoms from different chains, both v_1 and v_2 must be attractive.

Although the S-phases are different the L-phases of the three materials studied are identical. It is partially because this is the only solution allowed by Axe's Theorem but there are certain features of the L-phase which are not required by the theorem but are seen in all three compounds. For instance, the z-coordinate of the L-phase peaks are not required to be at 0, 1, 2 ... c_H^* but sharp peaks centered at z = 0 are seen in the $\underline{c}^*$ direction scans shown in Fig. 4.9 and 4.10.

The Emery-Axe order parameter theory does not depend on the details of the interchain interactions. It is therefore expected to work in all the compounds but when the theory was tested disagreements were seen in $Hg_{3-\delta}AsF_6$ and $Hg_{3-\delta}TaF_6$ since the intensities of L-phase peaks vary as η_n rather than η_n^2 with temperature. Ignoring the less reliable X ray diffraction experiment on $Hg_{3-\delta}TaF_6$, two explanations can be given for the disagreement observed in the case of $Hg_{3-\delta}AsF_6$.

(i) The perfect agreement between the intensities and η_n rather than η_n^2 suggests that the disagreement is caused by a strong primary extinction (see sec. 2.11). The

large size of $Hg_{3-\delta}AsF_6$ crystal used in the experiment is consistent with this explanation.

(ii) Another explanation is provided by Emery and Axe (1978). It is possible that the disagreement is due to the strong S-phase of $Hg_{3-\delta}AsF_6$ which is not included in the formulation of the order parameter theory. The authors claim that they have worked out a theory (unpublished) in which the competition between the parallel chain ordering (divergence of S-phase) and the perpendicular chain coupling (the observed L-phase) is considered and this theory predicts faster growth of the L-phase peaks and a lower L-phase transition temperature. The low value of T_c observed in $Hg_{3-\delta}AsF_6$ is in agreement with this explanation.

However, none of these arguments can explain the disagreement observed in $Hg_{3-\delta}TaF_6$. The crystal used in this experiment was small so that a serious primary extinction cannot be expected. On the other hand, T_c for this material is high, 193 $\pm$ 3 K, even higher than that of $Hg_{3-\delta}SbF_6$. If the results of the experiment on $Hg_{3-\delta}TaF_6$ are assumed to be reliable then a different explanation is required for the observed disagreements.

CHAPTER V

AN ALTERNATIVE STRUCTURE FOR THE STOICHIOMETRY Hg_3MF_6

5.1 Introduction

When the infinite chain compounds $Hg_{3-\delta}NbF_6$ and $Hg_{3-\delta}TaF_6$ were prepared, it was found that the golden crystals were not the ultimate end-products of the reaction if the liquid SO_2 was not removed from the reaction vessel. Under the liquid, the golden crystals slowly transformed over a few hours into silvery plates which were apparently softer than the golden crystals and looked very much like small pieces of crumpled aluminium foil.

The silvery crystals were isolated and studied by X ray diffraction as described below. They were found to have a similar composition to the golden ones, i.e., Hg_3NbF_6 and Hg_3TaF_6, but with a different structure.

5.2 Structure determination of Hg_3NbF_6.

Crystals of Hg_3NbF_6 were prepard by Dr. K. Morgan at McMaster University. The ultra-dry dry-box was used to select the flattest crystals and seal them in glass capillaries of 0.2 or 0.3 mm diameter. Dimensions of a typical crystal were 0.3x0.2x0.05 mm. Because of the softness of the crystals they could not be firmly wedged inside the capillaries.

The poor quality of the crystals restricted the X ray studies to photographic methods. Precession photographs of the zeroth layer reciprocal plane parallel to the flat face clearly showed hexagonal symmetry but the peaks were deformed into arcs of about 6° (see Fig. 5.1).* The arcs suggested an orientational disorder of the crystal domains in the hexagonal a-b plane of approximately ± 3°. The reflections seen on the photographs can be classified into three groups as follows.

(i) Strong peaks:

These peaks, indicated by dark arcs in Fig. 5.2, are much stronger than other peaks with similar 2θ. They form a prominent reciprocal sublattice corresponding to a hexagonal unit cell with $a = 2.90(1)$ Å.

(ii) Weak peaks:

These barely visible peaks of the photograph are represented by light arcs in Fig. 5.2. They, in combination with the strong peaks, form a reciprocal superlattice corresponding to a hexagonal unit cell with $a = 5.02(1)$ Å. Note that this hexagonal lattice is rotated from the sublattice of the strong peaks by 30°. When the peaks are indexed in terms of the cell of the reciprocal superlattice, the strong peaks have $2h+k = 3n$ (n is an integer). This condition has also been found on the first layer ($\ell=1$) precession photographs. It was observed that the intensity ratio between

---

* One sample showed two hexagonal domains one of which was rotated by 30° from the other.

Figure 5.1

The hk0 precession photograph of Hg_3NbF_6.

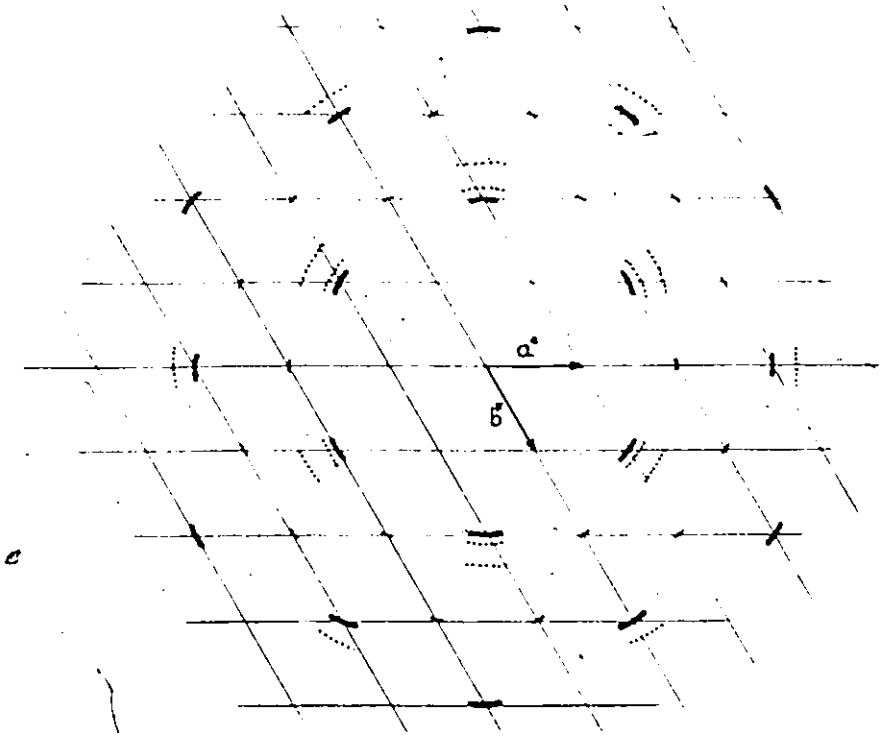

Figure 5.2

Classification of the Bragg reflections seen in the precession photograph of Fig. 5.1 as (i) strong peaks (dark arcs), (ii) weak peaks (light arcs) and (iii) extra peaks (dotted arcs). The first and the second are truly the hk0 reflections and fit into a hexaongal lattice but not the third which are the tails of higher order reflections deformed into large arcs by orientational disorder about axes in the a-b plane.

the sublattice reflections and the superlattice reflections varies from sample to sample. In two out of five samples examined the superlattice reflections were completely absent.

(iii) Extra peaks:

There are some peaks which do not fit either of the lattices of (i) and (ii). They are indicated by dotted arcs in Fig. 5.2 and arise from the large orientational disorder about axes lying in the a-b plane. This disorder causes the tails of the reflections from the nearby higher layers to be visible on the hk0 precession photograph. For instance, Fig. 5.3 depicts the appearance of an hkl reflection in the photograph since the arc spread out by the disorder is large enough to intersect the hk0 plane.

Photographs of the h0ℓ projection showed few reflections for $|\ell| > 1$ except for a complete series of weak 00ℓ reflections corresponding to the c axis length of 7.68(7) Å. Since the radiation absorption was extremely serious in this projection for a thin flat crystal it was expected that only the strongest reflections would be visible. The reflections were deformed into large arcs with a 20° apex indicating that the orientational disorder about axes in the a-b plane is about $\pm$ 10°. The size of the arcs varies from sample to sample since it depends not only on the orientational disorder but also on the extent to which the sample is crumpled.

The observed diffraction pattern is consistent with the model shown in Fig. 5.4 (also see Fig. 5.5). The model consists of layers of

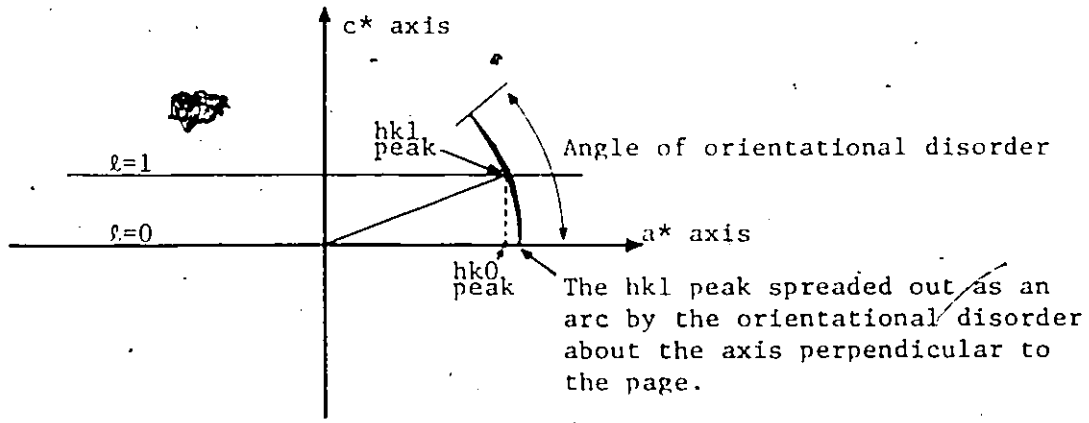

Figure 5.3

An hkl reflection will appear as an extra peak on the hk0 precession photograph if the angle of orientational disorder about the axis perpendicular to the page is larger than $\tan^{-1}(s_{001}/s_{hk0})$ where $s_{hk\ell}$ is the magnitude of the scattering vector $\vec{s}_{hk\ell}$.

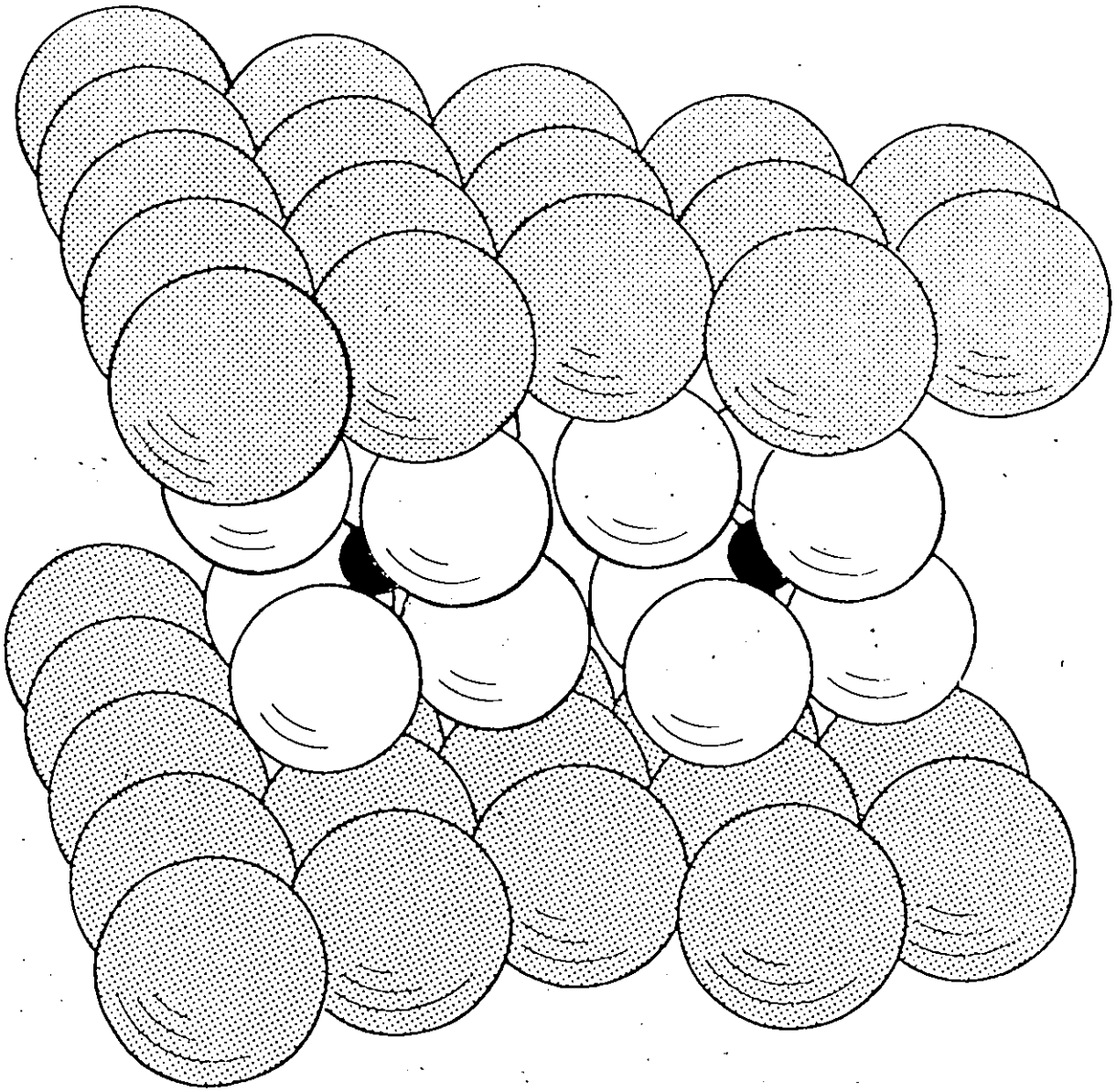

Figure 5.4

Proposed model of Hg_3NbF_6. The Hg, F and Nb are represented by grey, white and black atoms respectively.

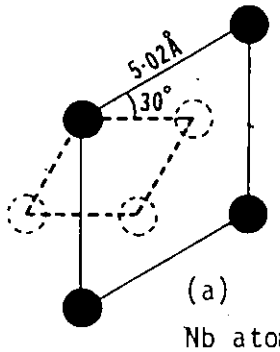

(a)
Nb atoms at z = 0

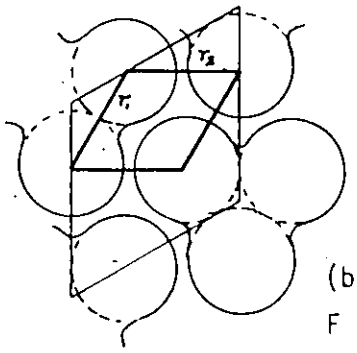

(b)
F atoms at
z = 0.143 (~1/6)

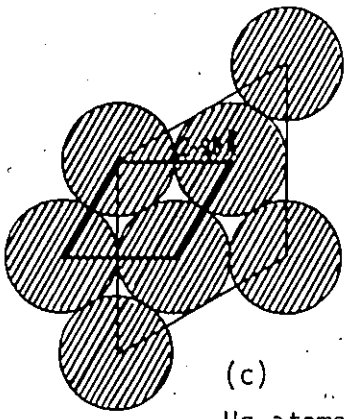

(c)
Hg atoms at z = 1/2

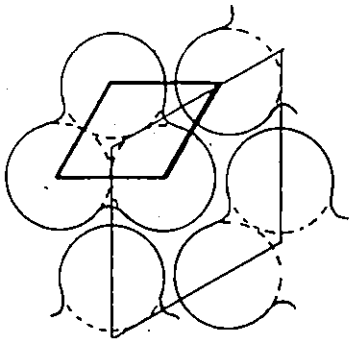

(d)
F atoms at
z = 0.857 or
-0.143 (~-1/6)

Figure 5.5

The proposed model (Fig. 5.4) shown in various atomic layers. Note that the sublattice of Hg in (c) is 30° rotated from the unit cell defined by the Nb atoms in (a). In some samples the Nb atoms may as well occupy the sites shown as ◌.

hexagonally close-packed Hg atoms which are separated by layers of hexagonally close-packed NbF_6 octahedra. The space group of the model is $P\bar{3}1m$ and the hexagonal lattice parameters are $\underline{a}$ = 5.02(1), $\underline{c}$ = 7.68(7) Å. In this model all the atoms except F are located at fixed special positions (see Table 5.1). The position of the F atoms was calculated by assuming a regular octahedron with an Nb-F bond length of 1.90 Å as observed in various NbF_6 ions. For this Nb-F bond length, the distance between the F atom and its neighbouring Hg atoms is about 3.2 Å, a distance comparable to those seen in other Hg compounds. Note that the calculated x coordinate of F is close to 1/3 and could indeed be that value if the NbF_6 ion were slightly larger. In such a case the F atoms, like the Hg atoms, would form an exact hexagonal close-packed layer with an interlayer distance and orientation the same as in the Hg layers (compare Fig. 5.5(b) and (d) to (c)).

Fig. 5.5(c) shows that the intralayer Hg-Hg bond length is $\underline{a}/\sqrt{3} = 5.02/\sqrt{3} = 2.90$ Å and the Hg sublattice is 30° rotated from the unit cell defined by the Nb atoms. Diffraction from the Hg atoms therefore results only in the strong sublattice peaks. Also the F atoms contribute mostly to the sublattice peaks since their intralayer arrangement is almost identical to that of the Hg atoms. Therefore, apart from the small contribution from the F atoms as a result of their not being exactly at 1/3, the weak superlattice reflections arise entirely from the Nb atoms.

This model predicts a high intensity ratio between the sublattice and superlattice peaks, namely $(3f_{Hg} + 6f_F + f_{Nb})^2 : f_{Nb}^2 = 67$ where f_x represents the scattering factor of atom X. Such a large ratio explains the apparent difference in intensities of the strong peaks and the weak

Table 5.1

Proposed model for Hg_3NbF_6

Hg_3NbF_6, M_r = 808.67, trigonal, space group $P\bar{3}1m$,
$z = 1$, $a = 5.02(1)$, $c = 7.68(7)$ Å, $D_x = 8.0(1)$ Mg m^{-3}

Atomic coordinates:

atom	site	x	y	z
Hg(1)	1b	0	0	1/2
Hg(2)	2d	1/3	2/3	1/2
Nb	1a*	0	0	0
F	6k	0.309†	0	0.143†

* In some samples the Nb atom is disordered over the 3 sites 1a and 2c (1/3, 2/3, 0; 2/3, 1/3, 0).

† Calculated assuming an undistorted NbF_6 octahedron with Nb-F = 1.90 Å.

peaks seen in the precession photograph (Fig. 5.1). The absence of superlattice peaks as found in some samples indicates that the Nb atoms randomly occupy different positions in different layers, i.e., the position of the Nb atom in the n^{th} layer is not necessarily 0,0,n but might be $\frac{2}{3},\frac{1}{3},n$ or $\frac{1}{3},\frac{2}{3},n$ (see Fig. 5.5(a)). This occupational disorder is equivalent to having $\frac{1}{3}$ of a Nb atom at each of the positions and since the dimension and the orientation of such a Nb layer are identical to those of the Hg layer diffraction from Nb results only in the sublattice peaks, causing the total absence of the superlattice reflections.

5.3 Structure of Hg_3TaF_6

When the crystals of the $Hg_{3-\delta}TaF_6$ chain compound are prepared and the crystals are left under the SO_2 solution for a few hours they also transform into silver platelets. The hk0 precession photographs of these crystals are essentially identical to those of Hg_3NbF_6 layer compounds suggesting that the materials are isostructural. Because of the extremely poor quality of the crystals no photograph of the h0ℓ projection was taken but the c axis length could be estimated from the position of the hkl extra peaks seen on the hk0 photographs. The lattice parameters thus obtained, a = 5.03(1) and c = 7.4(4) Å, are indistinguishable from those of Hg_3NbF_6. Because of the poor quality of these crystals no further work could be done on them.

5.4 Discussion

The proposed structure for the layer compounds Hg_3MF_6 (M = Nb, Ta) is consistent with the morphology of the soft thin crystals whose metallic luster arises from the sheets of metallically bonded Hg

atoms. Since the location of F atom is close to $\frac{1}{3},0,\frac{1}{6}$ the structure can be approximately described as a cubic close-packed array of Hg and F atoms arranged with hexagonal sheets of Hg atoms separating two similar sheets of F atoms and $\frac{1}{3}$ of the octahedral cavities between the F sheets occupied by the M atoms.

In most compounds Hg shows strong tendency to form straight bonds. For instance, $Hg_3(AsF_6)_2$ and $Hg_4(AsF_6)_2$ consist of essentially straight Hg_3^{2+} and Hg_4^{2+} ions (Cutforth, Davies, Dean, Gillespie, Ireland, Ummat, 1973 and Cutforth et al., 1983). As in the limiting case, the Hg atoms of $Hg_{3-\delta}MF_6$ (M = As, Sb, Nb, Ta) compounds form infinite straight chains (Brown et al., 1974). The Hg_3MF_6 layer compounds are unusual since the Hg atoms are bonded into sheets rather than chains. The Hg-Hg bond length observed in the sheets, 2.90 Å, is larger than that in the chains, 2.671 Å. The formal charge on Hg atoms, however, is very similar in the two cases since it is $+\frac{1}{3}$ for the sheets and $+1/(3-\delta)$ for the chains. The bond length difference can be attributed to the difference in coordination, each Hg atom in the sheets forms six bonds to its nearest Hg neighbours while in the chains these are only two such bonds.

Sheets of Hg atoms have been found in the graphite intercalate. $KHgC_4$ (Lagrange, Makrini, Herold, 1983). The Hg-Hg distance observed in this intercalate is the same as in the Hg_3MF_6 compounds, i.e., 2.90 Å, but each Hg atom in the intercalate has only three Hg neighbours instead of six and a formal charge of zero instead of $+\frac{1}{3}$.

The layer Hg_3MF_6 compounds and the chain $Hg_{3-\delta}MF_6$ compounds may be considered as different structures of essentially the same stoichiometry. The packing is more condensed in the layer compounds as suggested by

the calculated densities. The density of Hg_3MF_6 is 8.0(1) Mg m^{-3} while it is only 6.95(1) Mg m^{-3} for $Hg_{3-\delta}NbF_6$. Such a large density difference and the completely different arrangement of the atoms between the two structures indicate that the transformation of the chain compounds to layer compounds under liquid SO_2 is a reconstructive transition.

Attempts have been made to prepare the layer compounds Hg_3AsF_6 and Hg_3SbF_6 by leaving the corresponding chain compounds under liquid SO_2 for an extended period but no transformation has been observed.

CHAPTER VI

MERCURY IN HIGHER OXIDATION STATES

6.1 Introduction

The structures of two compounds, one with Hg_4^{2+} ion and the other with Hg_3^{2+} ion, which were discovered during attempts to prepare the new infinite chain compounds are reported in this chapter. The formation of the first compound, $Hg_4(Ta_2F_{11})_2$, was observed in the following stoichiometric reaction.

$$3Hg + HgF_2 + 4TaF_5 \xrightarrow{SO_2} Hg_4(Ta_2F_{11})_2$$

The crystals usually grow as small black needles on the surface of liquid Hg.

The second compound, $Hg_3(NbF_5)_2SO_4$, is always formed along with the silvery platelet crystals of Hg_3NbF_6 (layer structure) if the reaction is left undisturbed for an extended period (about two months).

Crystals of these compounds have been isolated and subjected to X ray structure determination as described in the following sections.

6.2 Structure determination of $Hg_4(Ta_2F_{11})_2$

The crystals of $Hg_4(Ta_2F_{11})_2$ prepared by Dr. P.K. Unmat at McMaster University were mounted in glass capillaries of 0.3 mm diameter. Since these crystals do not have well-defined faces an approximately spherical crystal was chosen for X ray studies so that

the measured Bragg intensities could be corrected by using the DIFABS absorption correction described in sec. 2.10. The precession photographs showed symmetry and systematic absences characteristic of the monoclinic space group I2/c or Ic. The non-standard I-setting was chosen in order to make the monoclinic angle β close to 90°.

The initial phase determination was done by using the direct method routines (sec. 2.13) of program SHELX (Sheldrick, 1976). The space group was assumed to be centrosymmetric I2/c. Seven solutions plotted as E-maps were found but only the first solution showed a sensible arrangement of the Hg and Ta atoms. A difference map based on this partial model clearly revealed the F atoms around the Ta atoms and the anion was identified as $(Ta_2F_{11})^{1-}$. Refer to Tables 6.1 and 6.2 for details of the structure determination. The refined structure is illustrated in Fig. 6.1. The final atomic parameters are listed in Table 6.3 while the important bond lengths and angles are given in Table 6.4.

The magnitudes of the observed and calculated structure factors have been tabulated and deposited with McMaster University (Tun, 1984).

6.3 Structure determination of $Hg_3(NbF_5)_2SO_4$

The crystals prepared by Dr. K. Morgan at McMaster University were mounted in sealed glass capillaries of diameter 0.2 mm. The symmetry and systematic absences observed on the precession photographs were consistent with the orthorhombic space group Fdd2. The procedure for structure determination was identical to that of $Hg_4(Ta_2F_{11})_2$ except in the phase determination. Instead of using direct methods

Table 6.1

Common parameters for the structure determination of

$Hg_4(Ta_2F_{11})_2$ and $Hg_3(NbF_5)_2SO_4$

Bragg intensity measurements:

Diffractometer: Nicolet P3

Graphite monochromated MoKα radiation, λ = 0.71069 Å

Lattice constants determined from 15 well-centered reflections

Scan procedure: 2θ-ω scan

Scan angle: 2° + angle between $K\alpha_1$ and $K\alpha_2$ peaks

Background measuring time/scan time = 1

Absorption correction:

Program: DIFABS

Averaging:

Program: AVER

Least-squares refinement:

Program: SHELX

Scattering factors: neutral atoms from International Tables for X ray Crystallography (1974)

Weighting shceme: $w = [\sigma^2(\text{counting}) + gF_o^2]^{-1}$

Table 6.2

Summary of structure determination of $Hg_4(Ta_2F_{11})_2$ and $Hg_3(NbF_5)_2SO_4$

Compound	$Hg_4(Ta_2F_{11})_2$	$Hg_3(NbF_5)_2SO_4$
Spaee group	I2/c (monoclinic; origin on $\bar{1}$ on glide plane c)	Fdd2 (orthorhombic origin on 2)
Lattice parameter a (Å)	18.556(8)	18.068(6)
b	7.528(3)	15.734(5)
c	14.714(8)	9.176(4)
β (deg)	91.72(4)	
Volume ($Å^3$)	2054(2)	2609(2)
Formulae/unit cell	4	8
Calculated density (Mg m^{-3})	6.285(5)	5.467(4)
Reflections used to determine lattice parameters	$24° < 2\theta < 30°$	$18° < 2\theta < 47°$
Variable scan speed (deg min^{-1})	2.0 - 20.0	4.0 - 29.3
Standard reflections	$0\bar{4}0$; 408	10,0,2; 0,10,2
e.s.d. of standard reflections (%)	2.1; 1.5	1.3; 1.2
No. of standard reflection measurements*	62	63
Maximum 2θ	55°	55°
Range of indices	$0 \leq h \leq 25$ $-10 \leq k \leq 10$ $0 \leq \ell \leq 20$	$0 \leq h \leq 23$ $-20 \leq k \leq 20$ $-11 \leq \ell \leq 11$
No. of reflections measured	2394	2974
No. of unique reflections	1248	1515
No. of unobserved reflections measured ($I < 3\sigma_I$)	767	551
Linear absorption coefficient μ (mm^{-1})	52.9	37.9

..... continued

Table 6.2 (continued)

μR value for spherical absorption correction	6.9	4.3
$R^{\dagger}$ of model used to calculate $\|F_{iso}\|$	0.109	0.139
Reflections used to construct Fourier series	1743	2676
Maximum DIFABS absorption correction factor	0.934	1.496
Minimum DIFABS absorption correction factor	0.481	0.702
Internal agreement factor:		
$R^{\$}_{int}$ (before DIFABS)	0.070	0.084
$R^{\$}_{int}$ (after DIFABS)	0.043	0.036
Weighting parameter g (see sec. 2.14)	0.0004	0.00035
k (see sec. 2.14)	0.7791	0.9077
Final R_w (all reflections)	0.049	0.045
Final $R^{\dagger}$ (all reflections)	0.056	0.048
Maximum shift/error in final cycle	0.089	0.071
Averaged shift/error in final cycle	0.022	0.014
Secondary extinction correction g ($x10^5$)	3(1)	3(1)
No. of variables refined	137	92
Residual electron density:**		
maximum ($e\mathring{A}^{-3}$)	+1.2	+3.6
minimum ($e\mathring{A}^{-3}$)	-1.4	-6.1

* No systematic variation in the standard reflections were observed.

† See definition in sec. 2.14.

$ See definition in sec. 2.12.

** See the text for location. If not mentioned the peak does not coincide with any atomic or bonding region.

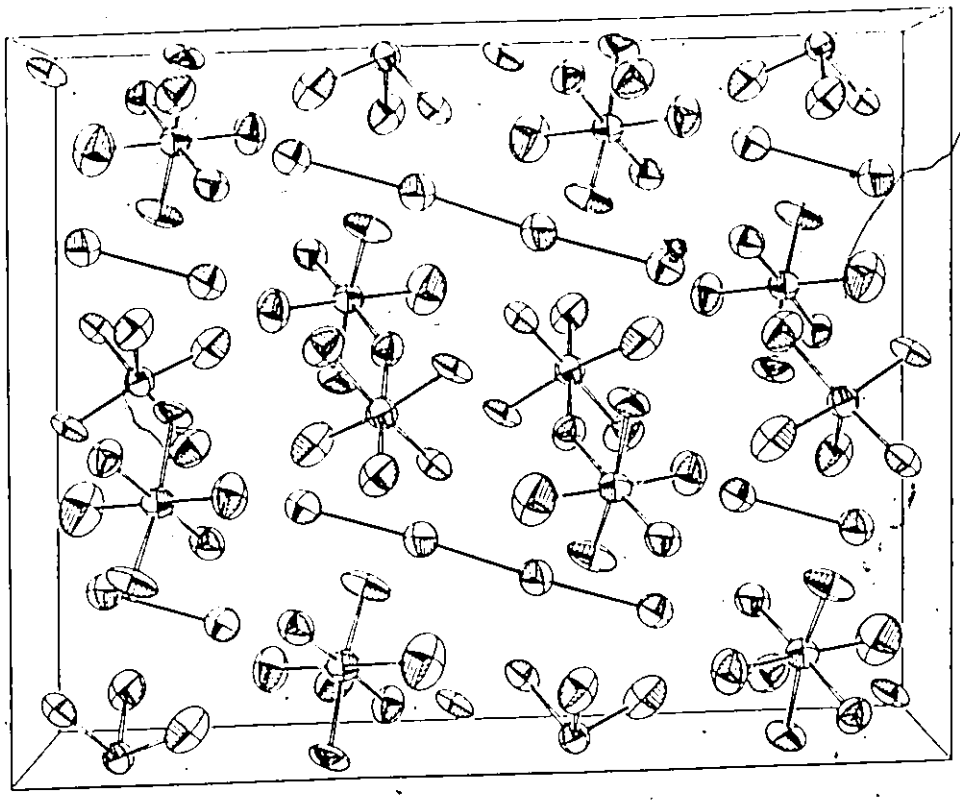

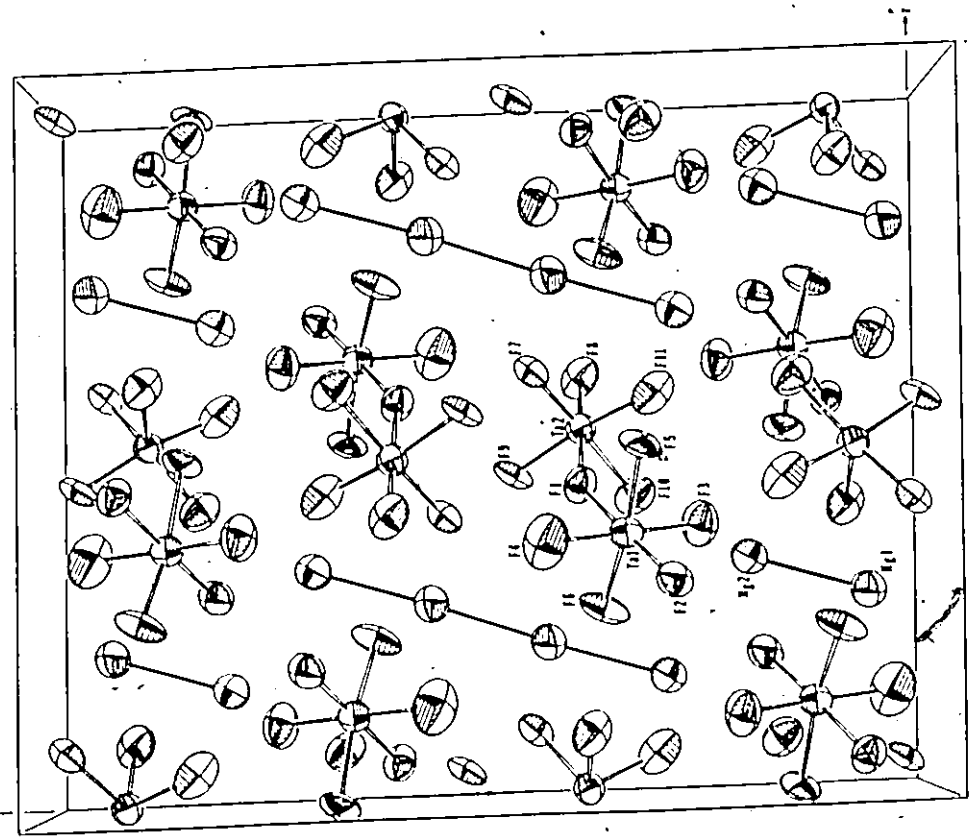

Figure 6.1 Refined model of $Hg_4(Ta_2F_{11})_2$

Table 6.3

Refined atomic parameters of $Hg_4(Ta_2F_{11})_2$ ($\times 10^4$ for positional parameters of Hg and Ta; $\times 10^3$ for positional parameters of F and temperature factors ($Å^2$) of all the atoms)

	x	y	z	U_{11}	U_{22}	U_{33}	U_{12}	U_{13}	U_{23}
Hg(1)	664(1)	2669(2)	2799(1)	63(1)	68(1)	60(1)	-1(1)	5(1)	-2(1)
Hg(2)	2031(1)	2625(2)	3324(1)	58(1)	72(1)	65(1)	-7(1)	4(1)	-2(1)
Ta(1)	3510(1)	7290(1)	3673(1)	48(1)	43(1)	42(1)	0(1)	1(1)	1(1)
Ta(2)	3947(1)	3057(1)	5224(1)	43(1)	43(1)	45(1)	-3(1)	2(1)	1(1)
F(1)	398(1)	522(2)	438(1)	49(11)	59(8)	61(14)	-2(8)	-6(14)	20(9)
F(2)	303(1)	906(2)	302(1)	58(13)	54(8)	53(14)	15(8)	8(16)	2(9)
F(3)	268(1)	591(2)	378(2)	53(14)	70(10)	93(22)	-16(10)	-1(20)	11(12)
F(4)	440(1)	835(3)	358(2)	82(20)	91(13)	127(30)	-23(14)	-12(28)	40(17)
F(5)	337(1)	816(3)	486(1)	75(17)	89(12)	37(14)	30(13)	17(19)	-22(11)
F(6)	374(2)	593(2)	266(2)	111(23)	50(8)	46(15)	11(12)	35(23)	-10(10)
F(7)	451(1)	449(2)	601(1)	54(13)	56(9)	49(14)	-4(9)	18(17)	-2(9)
F(8)	393(1)	114(2)	601(2)	68(15)	67(9)	82(19)	-31(10)	-16(18)	25(11)
F(9)	472(1)	225(2)	461(1)	70(17)	65(9)	41(13)	10(10)	29(18)	-3(10)
F(10)	332(1)	214(2)	426(2)	75(16)	67(9)	72(17)	-13(10)	-15(18)	5(10)
F(11)	315(1)	425(2)	566(2)	81(18)	84(12)	86(21)	0(12)	-27(21)	-8(12)

Table 6.4

Important bond lengths (Å) and angles (deg) in $Hg_4(Ta_2F_{11})_2$.

Values given in brackets are the corresponding values observed in $Hg_4(AsF_6)_2$.

Hg(1) - Hg(2)	2.630(2)	[2.620(2)]	
Hg(1) - Hg(1)	2.593(2)	[2.588(2)]	
Hg(2)...Hg(2)	3.033(2)	[2.985(3)]	
Ta(1) - F(1)	2.05(2)	Ta(2) - F(1)	2.05(2)
Ta(1) - F(2)	1.86(2)	Ta(2) - F(7)	1.88(2)
Ta(1) - F(3)	1.88(2)	Ta(2) - F(8)	1.86(2)
Ta(1) - F(4)	1.84(3)	Ta(2) - F(9)	1.83(2)
Ta(1) - F(5)	1.89(2)	Ta(2) - F(10)	1.94(2)
Ta(1) - F(6)	1.86(2)	Ta(2) - F(11)	1.86(2)
Hg(2) - F(10)	2.74(2)	Hg(1) - F(7)	2.99(2)
Hg(2) - F(11)	2.97(2)	Hg(1) - F(9)	3.23(2)
Hg(2) - F(5)	2.82(2)	Hg(1) - F(6)	3.01(2)
Hg(2) - F(2)	3.18(2)	Hg(1) - F(8)	3.22(2)
Hg(2) - F(3)	2.82(2)		
Hg(2) - Hg(1) - Hg(1)	177.2(1)	[177.3(1)]	
Hg(1) - Hg(2)...Hg(2)	109.7(1)	[124.2(1)]	
Ta(1) - F(1) - Ta(2)	153(1)	F(1) - Ta(2) - F(7)	83.4(7)
F(1) - Ta(1) - F(2)	176.2(7)	F(1) - Ta(2) - F(8)	178.1(7)
F(1) - Ta(1) - F(3)	82.9(8)	F(1) - Ta(2) - F(9)	85.5(8)
F(1) - Ta(1) - F(4)	89.7(9)	F(1) - Ta(2) - F(10)	82.5(7)
F(1) - Ta(1) - F(5)	82.1(8)	F(1) - Ta(2) - F(11)	82.5(8)
F(1) - Ta(1) - F(6)	83.2(8)	F(7) - Ta(2) - F(8)	94.8(8)
F(2) - Ta(1) - F(3)	93.4(8)	F(7) - Ta(2) - F(9)	93.6(9)
F(2) - Ta(1) - F(4)	94(1)	F(7) - Ta(2) - F(10)	165.4(7)
F(2) - Ta(1) - F(5)	98.9(9)	F(7) - Ta(2) - F(11)	86.9(9)
F(2) - Ta(1) - F(6)	95.7(9)	F(8) - Ta(2) - F(9)	94.7(9)
F(3) - Ta(1) - F(4)	171.9(9)	F(8) - Ta(2) - F(10)	99.4(8)
F(3) - Ta(1) - F(5)	88(1)	F(8) - Ta(2) - F(11)	97.4(9)
F(3) - Ta(1) - F(6)	89(1)	F(9) - Ta(2) - F(10)	89(1)
F(4) - Ta(1) - F(5)	94(1)	F(9) - Ta(2) - F(11)	167.8(9)
F(4) - Ta(1) - F(6)	87(1)	F(10) - Ta(2) - F(11)	88(1)
F(5) - Ta(1) - F(6)	165.3(9)	Hg(1) - Hg(2) - F(10)	165.1(5)
Hg(1) - Hg(2) - F(11)	92.1(5)	Hg(1) - Hg(2) - F(5)	90.0(5)
Hg(1) - Hg(2) - F(2)	78.0(4)	Hg(1) - Hg(2) - F(3)	117.3(4)

heavy atoms (Hg) were located by solving a Patterson map (sec. 2.13) which suggested that either three or four heavy atoms separated by ~ 2.56 Å were almost in a straight line. Both Hg_3^{2+} and Hg_4^{2+} ions were tested but only the model with Hg_3^{2+} gave a good agreement between the observed and calculated structure factors. The lighter atoms (Nb, F, S, O) were located using difference syntheses.

Details of the structure determination are summarized in Table 6.1 and 6.2. The difference map calculated at the end of the refinement showed a maximum residual peak of +3.6 $eÅ^{-3}$, 0.9 Å away from the atom Hg2 in the c direction while the minimum peak, -6.1 $Å^{-3}$, was found on the 2-fold axis, 0.9 Å away from the atom Hg1. The resultant structure is illustrated in Fig. 6.2.

The refined atomic parameters and bond lengths and angles are given respectively in Table 6.5 and 6.6. A list of the magnitudes of the observed and calculated structure factors have been deposited with McMaster University (Tun, 1984).

6.4 Discussion

$Hg_4(Ta_2F_{11})_2$ contains essentially the same Hg_4^{2+} ion as $Hg_4(AsF_6)_2$ reported by Cutforth et al. (1983). In both compounds the ions are almost linear (see Table 6.4) and have interionic distances between the terminal atoms of the neighbouring ions (Hg(2) ... Hg(2) about 3.0 Å) which are comparable to the shortest bond lengths observed in the solid Hg, 2.99 Å in α-Hg (Barrett, 1957) and 2.83 Å in β-Hg (Atoji et al. 1959).

The internal geometry of the Hg_3^{2+} ion is not exactly the same in all known compounds. The significant difference occurs in the Hg-Hg-Hg

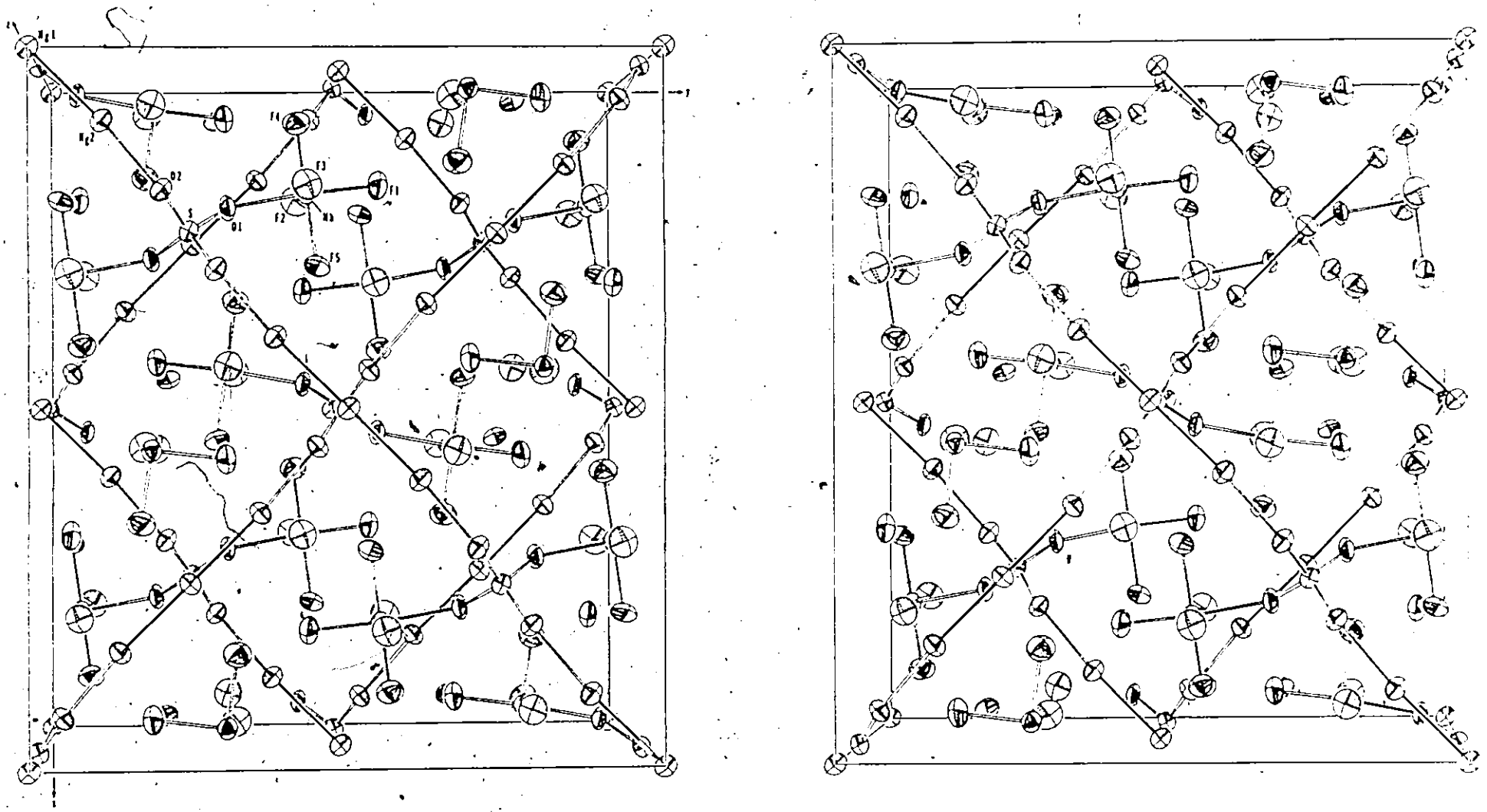

Figure 6.2 Refined model $Hg_3(NbF_5)_2SO_4$

Table 6.5

Refined atomic parameters of $Hg_3(NbF_5)_2SO_4$

($\times 10^4$ for positional parameters and $\mathring{A}^2 \times 10^3$ for temperature factors)

	x	y	z	U_{11}	U_{22}	U_{33}	U_{12}	U_{13}	U_{23}
Hg(1)	0	0	0	32(1)	33(1)	34(1)	-6(1)	0	0
Hg(2)	994(1)	1146(1)	9672(1)	35(1)	33(1)	36(1)	-8(1)	-3(1)	3(1)
Nb	1927(1)	4409(1)	7436(2)	31(1)	26(1)	28(1)	1(1)	-2(1)	3(1)
S	1/4	1/4	8536(7)	30(3)	25(3)	29(3)	-3(2)	0	0
F(1)	1809(7)	5570(7)	7277(18)	58(7)	27(6)	61(9)	-3(5)	-1(8)	6(7)
F(2)	1959(8)	4263(10)	5428(15)	60(9)	63(9)	39(7)	6(7)	4(6)	9(7)
F(3)	1885(8)	4379(9)	9482(16)	63(8)	58(9)	37(7)	3(7)	4(6)	-6(7)
F(4)	911(6)	4250(9)	7352(17)	39(6)	54(8)	57(9)	-2(6)	11(7)	11(7)
F(5)	2961(6)	4567(8)	7532(18)	29(5)	48(7)	71(9)	7(5)	-13(7)	7(7)
O(1)	2139(8)	3118(8)	7551(18)	43(7)	18(6)	49(9)	4(5)	-12(7)	4(6)
O(2)	1954(7)	2073(8)	9441(15)	34(7)	32(7)	33(8)	-9(5)	4(6)	-3(6)

Table 6.6

Important bond lengths (Å) and angles (deg) in $Hg_3(NbF_5)_2SO_4$. Values given in brackets are the corresponding values observed in $Hg_3(AlCl_4)_2$ and $Hg_3(AsF_6)_2$.

Hg(1) - Hg(2) (x2)	2.562(1)	[2.56; 2.552(5)]	
S - O(1) (x2)	1.48(2)	S - O(2) (x2)	1.46(1)
Nb - O(1)	2.07(1)	Nb - F(1)	1.84(1)
Nb - F(2)	1.86(1)	Nb - F(3)	1.88(1)
Nb - F(4)	1.85(1)	Nb - F(5)	1.89(1)
Hg(2) - O(2)	2.28(1)	Hg(2) - F'(5)	2.99(1)
Hg(2) - F(3)	2.81(1)	Hg(2) - F(2)	3.25(1)
Hg(2) - F(5)	2.95(1)	Hg(1) - F(4)	2.96(1)
Hg(2) - F(1)	2.95(2)	Hg(1) - O(2)	3.05(1)
Hg(2) - Hg(1) - Hg(2)	166.5(1)	[174.42(4); 180]	
O(1) - S - O(1)	106(1)	O(2) - S - O(2)	110(1)
O(1) - S - O(2)	110.6(9)		
Nb - O(1) - S	139(2)	Hg(2) - O(2) - S	150(3)
O(1) - Nb - F(1)	175.7(8)	O(1) - Nb - F(2)	85.6(8)
O(1) - Nb - F(3)	86.1(8)	O(1) - Nb - F(4)	93.0(7)
O(1) - Nb - F(5)	86.8(7)	F(1) - Nb - F(2)	92.7(9)
F(1) - Nb - F(3)	95.7(8)	F(1) - Nb - F(4)	91.0(7)
F(1) - Nb - F(5)	89.3(8)	F(2) - Nb - F(3)	171.4(8)
F(2) - Nb - F(4)	88.5(8)	F(2) - Nb - F(5)	91.8(9)
F(3) - Nb - F(4)	89.9(9)	F(3) - Nb - F(5)	89.8(8)
F(4) - Nb - F(5)	179.6(6)		
Hg(1) - Hg(2) - O(2)	174.8(3)	Hg(1) - Hg(2) - F(1)	92.2(3)
Hg(1) - Hg(2) - F(3)	102.8(5)	Hg(1) - Hg(2) - F'(5)	145.0(3)
Hg(1) - Hg(2) - F(5)	105.0(4)	Hg(1) - Hg(2) - F(2)	85.8(4)

angle. The Hg_3^{2+} in $Hg_3(AsF_6)_2$ is the straightest, since the central Hg atom is located on a center of symmetry and the ion is required to be linear. $Hg_3(AlCl_4)_2$ features a slightly bent Hg_3^{2+} ion (Hg-Hg-Hg = 174.42(4), Ellison et al., 1972) while that of $Hg_3(NbF_5)_2SO_4$ is even more bent with an Hg-Hg-Hg angle of 166.5(1). The case of the last compound is unusual also because each Hg_3^{2+} ion is linked to another Hg_3^{2+} ion by the SO_4^{2-} ion residing on a neighbouring two fold axis. The Hg(2)-O bond (2.28 Å) is the shortest bond formed by the terminal Hg(2) atom to the nearby X atoms (X being either O or F).

There is a correlation between the Hg-X bond length and the Hg-Hg-X angle. The correlation can be seen in the environments of all the polyatomic Hg cations as illustrated in the polar diagram of Fig. 6.3 where all the known Hg_4^{2+} and Hg_3^{2+} compounds and two representative Hg_2^{2+} compounds are included. Hg-Cl distances have been reduced by 0.45 Å (Source: Pauling, 1960, pp. 514), the difference between the ionic radii of F and Cl, but no correction has been applied to the Hg-O bonds. The diagram indicates that the bonding between the terminal Hg atom and the X atoms is directional since the Hg-X bonds with large Hg-Hg-X angles (close to 180°) are generally shorter than those with smaller angles.

For comparison, the short Hg...Hg interionic distances observed in both Hg_4^{2+} compounds are also shown on the diagram. Although the ionic radius for Hg is larger than for F, the Hg...Hg distances are comparable to the lengths of those Hg-F bonds that have a similar Hg-Hg-X angle.

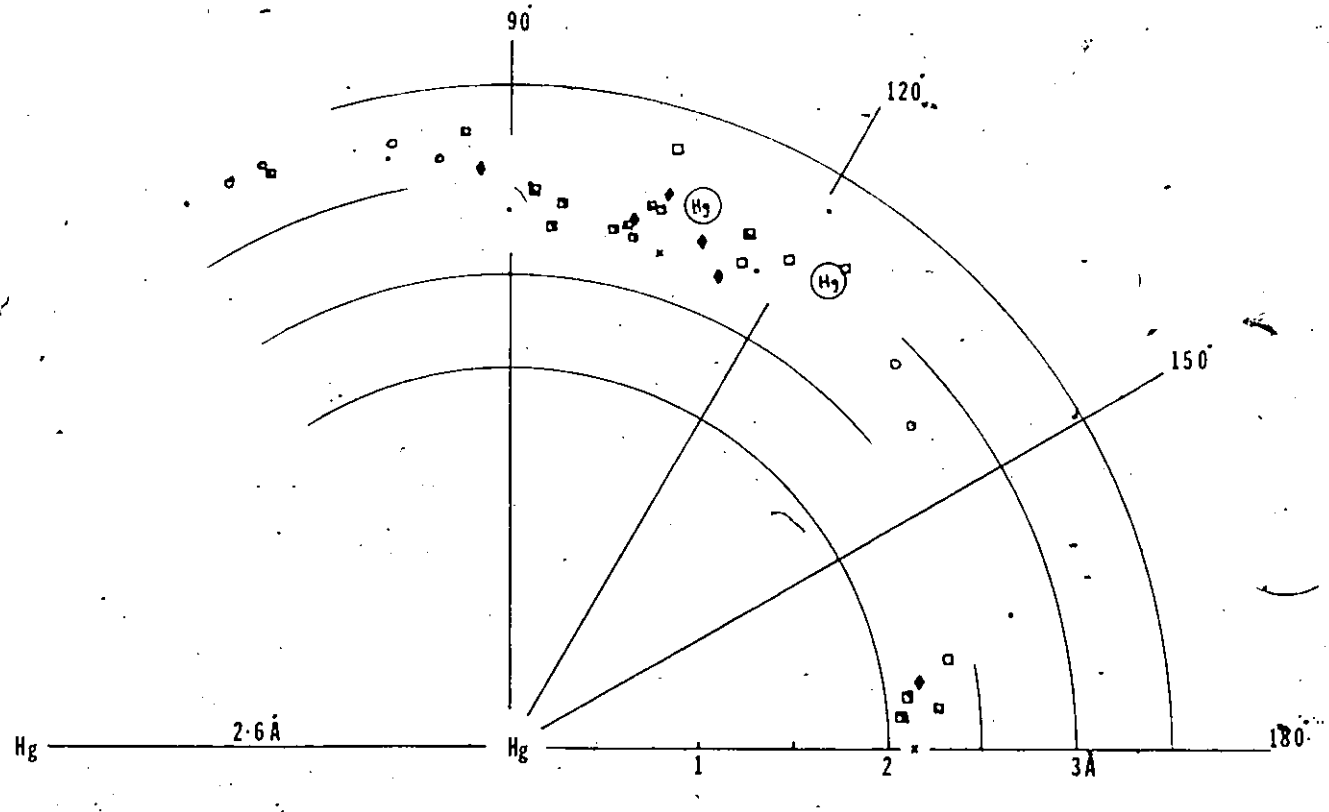

- $Hg_4(AsF_6)_2$ Cutforth et al.(1983)
- $Hg_4(Ta_2F_{11})_2$
- $Hg_3(AlCl_4)_2$ Ellison et al.(1972)
- $Hg_3(AsF_6)_2$ Cutforth,Davies,Dean,Gillespie,Ireland,Ummat(1973)
- $Hg_3(NbF_5)_2SO_4$
- Hg_2F_2 Dorm (1971)
- $Hg_2SiF_6.2H_2O$ Dorm (1971)

Figure 6.3

Correlation between Hg-X bond length (X = O, F, Cl) and Hg-Hg-X angle. The Hg-Cl distances have been reduced by 0.45 Å, the difference between the ionic radii of Cl and F. For comparison the short inter-ionic Hg...Hg distances seen in the Hg_4^{2+} compounds are also shown.

CHAPTER VII

CONCLUSIONS

7.1 Structural analysis on the chain and the layer compounds

It was pointed out in Chapter III that although the known $Hg_{3-\delta}MF_6$ (M = As, Sb, Nb, Ta) compounds are very similar to each other, small but significant differences can be seen by comparing their room temperature structures. Differences occur, for instance, in the tetragonal lattice parameters a and c, the crystallographic composition parameter δ and the undulation of the chains u_o. Among the bond lengths and other interatomic distances, the principle difference occurs in the M-F bond lengths while the other distances, d_{Hg-Hg}, (F-chain) and (chain-chain), remain unchanged from one compound to another (see Table 3.4).

Interrelation between the various parameters and the bond lengths can best be expressed in terms of the following equations which can be derived from Fig. 3.2 and 3.3.

From Fig. 3.2 it can be seen that

$$c = 2[F(1)\text{-chain}] + 2[M\text{-}F(1)] + (\text{chain-chain}) \qquad (7.1)$$

where $$(\text{chain-chain}) = \frac{c}{4} + 2u_o \qquad (7.2)$$

and from Fig. 3.3

$$a = 2\{[F(2)\text{-chain}]^2 - (c/8)^2\}^{\frac{1}{2}} + \sqrt{2}[M\text{-}F(2)] \qquad (7.3)$$

The composition parameter δ is related to the lattice parameter $\underline{a}$ as

$$3-\delta = a/d_{Hg\text{-}Hg} \qquad (7.4)$$

From Table 3.4 the following distances, the same in all the known compounds, are obtained.

$$\begin{aligned} d_{Hg\text{-}Hg} &= 2.67\ \text{Å} \\ F(1)\text{-chain} &= 2.86 \\ F(2)\text{-chain} &= 2.98 \\ \text{chain-chain} &= 3.23 \end{aligned} \qquad (7.5)$$

Substituting these values into eq. (7.1-7.4) gives predictions for $\underline{a}$, $\underline{c}$, u_o and δ for any chain compound once the M-F bond lengths are known. Table 7.1 lists the predicted and, where known, the observed values of these four parameters for the compounds with M = P, As, Sb, Nb, Ta, Bi. The small values of δ and u_o expected in $Hg_{3-\delta}BiF_6$ suggest that it might exist as a stoichiometric compound with almost straight Hg chains.

Similar arguments can be applied to the case of the Hg_3MF_6 layer compounds reported in Chapter V. In this structure the metallically bonded Hg atoms in the hexagonal sheets are located at fixed special positions so that the hexagonal lattice parameter $\underline{a}$ is completely determined by the $d_{Hg\text{-}Hg}$ distance within the sheet. From Fig. 5.5(c),

$$a = \sqrt{3}d_{Hg\text{-}Hg} \qquad (7.6)$$

Table 7.1

Predicted [and observed] parameters for $Hg_{3-\delta}MF_6$ compounds.

For the unknown compounds M-F bond lengths are assumed to be the values of the corresponding known MF_6 ions.

	$Hg_{3-\delta}PF_6$	$Hg_{3-\delta}AsF_6$	$Hg_{3-\delta}SbF_6$	$Hg_{3-\delta}NbF_6$	$Hg_{3-\delta}TaF_6$	$Hg_{3-\delta}BiF_6$
M-F(1) (Å)	1.57	[1.70]	[1.84]	[1.87]	[1.88]	1.98
M-F(2) (Å)	1.61	[1.72]	[1.88]	[1.89]	[1.88]	1.98
a (Å)	7.41	7.53 [7.534(7)]	7.72 [7.711(2)]	7.72 [7.692(1)]	7.70 [7.711(1)]	7.85
c (Å)	12.09	12.35 [12.395(8)]	12.63 [12.641(2)]	12.69 [12.679(2)]	12.71 [12.714(2)]	12.91
u_o (Å)	0.104	0.071 [0.07(1)]	0.036 [0.037(4)]	0.029 [0.026(3)]	0.026 [0.030(3)]	0.009
δ	0.22	0.18 [0.178(6)]	0.11 [0.10(2)]	0.11 [0.119(3)]	0.12 [0.116(4)]	0.06

In both existing compounds d_{Hg-Hg} bond length is found to be 2.90 Å. Since the Hg atoms are in the same oxidation state, it is reasonable to suppose that this bond length does not vary for different MF_6 ions. All compounds which crystallize in the Hg_3MF_6 structure are therefore expected to have the same a axis length, namely $2.90 \times \sqrt{3} = 5.02$ Å. The M atoms located at the hexagonal lattice points would then be separated by 5.02 Å in each layer. This leaves only M-F bond length and F-M-F angles as unknown parameters to determine the exact positions of F atoms.

The ideal structure is the one in which the F atoms form a hexagonal sheet of 2.90 Å spacing without introducing any distortion in the MF_6 ions. As an indicator of how close the F sheet is to this ideal arrangement a parameter ξ can be defined as follows.

$$\xi = \frac{\text{closest F-F distance bonded to different M atoms}}{\text{closest F-F distance bonded to same M atom}}$$

$$= \frac{r_2}{r_1} \qquad (7.7)$$

(The distances r_1 and r_2 are shown in Fig. 5.5(b)).

For the ideal hexagonal arrangement $\xi = 1$.

Table 7.2 lists the values of ξ for Hg_3NbF_6, Hg_3TaF_6 and various hypothetical compounds calculated by assuming typical values of known M-F bond lengths and setting all F-M-F angles = 90°. In the first three entries ξ is larger than the value corresponding to Hg_3NbF_6 and Hg_3TaF_6 which might be the reason why layer structures of $Hg_{3-\delta}AsF_6$ and $Hg_{3-\delta}SbF_6$ have not been observed. The table suggests an upper threshold value of ξ for layer compound formation between 1.12 and 1.17. On the other

Table 7.2

Value of ε calculated for the known and hypothetical Hg_3MF_6 compounds assuming a distortion-free MF_6 ion

Compound	M-F bond length (Å)	ε
Hg_3PF_6	1.60	1.44
Hg_3AsF_6	1.70	1.32
Hg_3SbF_6	1.85	1.17
Hg_3NbF_6	1.90	1.12
Hg_3TaF_6	1.90	1.12
Hg_3BiF_6	1.98	1.05

Ideal M-F bond length = 2.05 Å

hand, the unknown Hg_3BiF_6 might be expected to have a stable layer phase.

7.2 Geometry of polyatomic mercury ions in low oxidation states

The two compounds reported in Chapter VI, $Hg_4(Ta_2F_{11})_2$ and $Hg_3(NbF_5)_2SO_4$, contain Hg in higher oxidation states than the chain and the sheet compounds, i.e., $+\frac{1}{2}$ and $+\frac{2}{3}$ respectively. The former compound shows the tendency of Hg ions to link together into infinite zigzag chains while the latter does not show such a tendency. These observations are in good agreement with the structures of $Hg_4(AsF_6)_2$, $Hg_3(AlCl_4)_2$ and $Hg_3(AsF_6)_2$ (Cutforth et al. (1983); Ellison et al. (1972); Cutforth, Davies, Dean, Gillespie; Ireland, Ummat (1973)). Many compounds containing the Hg_2^{2+} are known, e.g., Hg_2X_2 (X = F, Cl, Br, I). They feature Hg in a higher oxidation state than $+\frac{2}{3}$ and also do not exhibit any tendency to link into infinite chains (Dorm, 1971). On the other end, the elemental solid Hg with an oxidation state of zero crystallizes in two phases with three dimensional Hg linkages.

Table 7.3 lists compounds with Hg in various oxidation states. The table shows that the internal Hg-Hg bonds of the polyatomic ion gets shorter with increasing oxidation state. A systematic trend in the geometry of Hg atoms can also be seen in the table.

The oxidation states of Hg in these compounds given in Table 7.3 can be written in the series

$$\frac{2}{\infty}, \frac{2}{6}, \frac{2}{6-2\delta}, \frac{2}{4}, \frac{2}{3}, \frac{2}{2}, \frac{2}{1}$$

The missing member of the series is Hg_5^{2+} ion. This ion was not observed in the series of reactions between elemental Hg and AsF_5

Table 7.3

The Hg-Hg distances and geometry of Hg observed in various oxidation states.

The distances which may represent significant interactions are given in brackets.

Material	Oxidation State	Hg-Hg distance (Å)	Geometry of Hg
α-solid Hg	0	2.99(x6)	3-dimensional structure
β-solid Hg	0	2.83(x2), 3.16(x8)	
Hg_3MF_6 (M = Nb,Ta)	1/3	2.90(x6)	2-dimensional infinite sheets
$Hg_{3-\delta}MF_6$ (M = As,Sb,Nb,Ta)	> 1/3	2.671(x2)	1-dimensional straight chains
$Hg_4(AsF_6)_2$	1/2	2.588, 2.620(x2), [2.985]	Non-uniform zigzag chains
$Hg_4(Ta_2F_{11})_2$	1/2	2.593, 2.630(x2), [3.033]	
$Hg_3(AlCl_4)_2$	2/3	2.551, 2.562	Terminal Hg atoms covalently bonded to central atom but no short interionic distances
$Hg_3(AsF_6)_2$	2/3	2.552(x2)	
$Hg_3(NbF_5)_2SO_4$	2/3	2.562(x2)	
Hg_2F_2	1	2.507 (Dorm, 1971)	Each Hg atom covalently bonded to nearest Hg atom but Hg-F bonds have partial ionic character
HgF_2	2	-	Isolated ion

under SO_2 and may not be stable with respect to the chain compounds. However if the Hg_5^{2+} ion is ever prepared it is expected to be almost linear with the structure shown in the following diagram

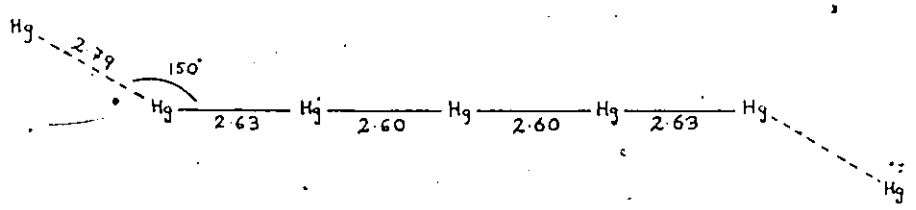

where the Hg-Hg distances predicted are according to the trend seen in Table 7.3.

Another trend seen in Table 7.3 is that the Hg-Hg bonding becomes more and more directional as the oxidation state of the atom increases. In the lowest oxidation state, i.e., zero, Hg forms metallic Hg-Hg bonds in all three directions (α-Hg and β-Hg) but as the oxidation state increases to +1/3 the metallic Hg-Hg bonds occur only in two-dimensional layers while bonding to the atoms outside the layers (i.e., bonding to the six nearest F atoms about 3.2 Å away) becomes that of ionic character. When the oxidation state further increases the dimensionality of the Hg-Hg bonding is reduced to one, leading to the formation of infinite chains of the $Hg_{3-\delta}MF_6$ compounds. In these chains each Hg atom forms two metallic Hg-Hg bonds of equal strength along the chain direction but the interaction in the other directions is ionic. The anisotropy of the Hg-Hg bonding increases as the oxidation state increases to +1/2 (Hg_4^{2+} compounds) for, in this case, the terminal Hg atoms form a strong bond towards the central atom but the interionic

interaction with the terminal atom of the nearby Hg_4^{2+} ion is weak. At this point the continuous path for electronic conduction is broken and the materials, although containing metal atoms, become insulators and loose their metallic luster. The internal bonds of the Hg_4^{2+} ion should more appropriately be called covalent rather than metallic since the electronic charges are localized within each ion as explained in Sec. 1.1. The trend continues for oxidation state of +2/3 (Hg_3^{2+} compounds) where the Hg_3^{2+} ions are well-separated from each other and no short inter-ionic distances can be found. Although the central atom of the Hg_3^{2+} ion still forms Hg-Hg bonds of equal strength in two opposite directions the terminal atoms form only one such bond. As the oxidation state increases to +1 each Hg atom forms only one Hg-Hg bond with its nearest neighbour. The example given in Table 7.3, Hg_2F_2, consists of Hg-Hg bonds of covalent character (2.51 Å) while the other bonds, namely Hg-F bonds, have partial ionic character as suggested by the bond length of 2.14 Å (Dorm, 1971). In the extreme case of oxidation state +2, Hg-Hg bonding does not occur at all. Hg_2F_2 listed in Table 7.3 as an example represents complete electronic transfer from Hg to F and the material is a simple ionic insulator.

APPENDIX I

DETAILS OF ABSORPTION CORRECTION

This appendix provides detailed information on the numerical integration absorption corrections used for some of the structure determinations of $Hg_{3-\delta}MF_6$ compounds reported in Chapter III. The corrections were applied using the program ABSORB, a routine of XRAY76 edited by Stewart (1976). Table A.1 summarizes the input parameters to program ABSORB and wherever five entries separated by semi-colons are given they correspond respectively to the structure determination of the (i) $Hg_{3-\delta}SbF_6$ (sample 1) at 293K, (ii) $Hg_{3-\delta}SbF_6$ (sample 2) at 293K, (iii) $Hg_{3-\delta}SbF_6$ (sample 2) at 173K, (iv) $Hg_{3-\delta}TaF_6$ at 293K and (v) $Hg_{3-\delta}TaF_6$ at 150K.

Table A.1

Input parameters to ABSORB

Linear absorption coefficient μ: 63.9; 63.9, 64.8; 74.9; 76.4 mm^{-1}

Radiation wavelength λ: 0.71069 Å

Number of grid points for integration: 10x10x10

Primary orientation reflection hkℓ: 200; 200; 200; 200; 200
χ: 68.47; 281.38; 279.07; 0.37; 0.11
ϕ: 21.05; 52.50; 49.73; 293.61; 294.22

Secondary orientation reflection hkℓ: 002; 002; 002; 008; 008
χ: 21.05; 11.40; 9.06; 1.50; 0.72
ϕ: 213.80; 48.90; 50.82; 203.58; 204.18

The following tables list the orientation and distances of the crystal faces from an arbitrarily chosen origin inside the crystal. The room temperature and low temperature orientations are slightly different (in tables A.3 and A.4) because of small crystal movements during cooling. Only the room temperature orientations were measured as described in Sec. 3.2. The low temperature orientations were deduced from the difference between the crystal orientation matrices printed by the diffractometer. The distances (d) were adjusted to minimize the internal agreement factor R_{int} between the equivalent reflections of data set II.

Table A.2

Crystal face orientations and distances for $Hg_{3-\delta}SbF_6$ (sample 1)

χ(293K)	ϕ(293K)	d(mm) x 10^3 measured	d(mm) x 10^3 adjusted
217.4	30.1	48±10	45
195.0	153.6	32	34
196.2	242.6	81	81
187.3	271.7	65	63
173.6	213.5	39	37
174.4	95.4	48	48
167.1	332.3	26	27
144.0	210.1	55	52
101.4	58.4	65	58

Table A.3

Crystal face orientations and distances for $Hg_{3-\delta}SbF_6$ (sample 2)

χ(293K)	φ(293K)	χ(173K)	φ(173K)	d(mm) x 10^3 measured	d(mm) x 10^3 adjusted
12.2	51.6	10.1	53.3	45±15	32.3
354.2	57.8	352.0	59.3	52±15	38.7
353.5	288.5	355.3	290.0	97±10	96.8
6.8	229.9	8.9	231.4	65±10	51.6
16.6	228.1	18.6	229.4	65±10	64.5
22.8	226.0	25.0	268.1	90±10	90.3
22.8	140.9	22.0	141.7	81±10	80.6
355.4	157.9	355.2	159.7	68±10	67.7
87.8	251.8	90.0	0.0	97±10	100.0
272.2	71.8	270.0	0.0	65±10	64.5

Table A.4

Crystal face orientations and distances for $Hg_{3-\delta}TaF_6$

χ(293K)	φ(293K)	χ(150K)	φ(150K)	d(mm) x 10^3 measured	d(mm) x 10^3 adjusted
178.4	25.1	179.2	25.7	5±10	5.2
181.6	205.1	180.8	205.7	5	5.2
180.0	115.1	180.2	115.7	97	96.8
180.0	295.1	179.8	295.7	97	96.8
90.0	0.0	90.8	43.3	97	96.8
270.0	0.0	269.2	223.3	97	96.8

REFERENCES

Atoji, M., Schirber, J.E. and Swenson, C.A. (1959), J. Chem. Phys., 31, 1628-1629.

Axe, J.D. (1980), In Ordering in Strongly Fluctuating Condensed Matter Systems, edited by T. Riste, New York: Plenum Press.

Barrett, C.S. (1957), Acta Cryst., 10, 58-60.

Batalla, E., Razavi, F.S. and Datars, W.R. (1982), Phys. Rev. B., 25, 2109-2118.

Brown, I.D., Cutforth, B.D., Davies, C.G., Gillespie, R.J., Ireland, P.R. and Vekris, J.E. (1974), Can. J. Chem., 52, 791-793.

Brown, I.D., Datars, W.R. and Gillespie, R.J. (1982), In Extended Linear Chain Compounds, Vol. III, New York: Plenum Press, 1-41.

Brown, I.D., Gillespie, R.J., Morgan, K.R., Tun, Z. and Ummat, P.K., submitted to Inorg. Chem.

Cutforth, B.D. (1976), unpublished Ph.D. Thesis, McMaster University.

Cutforth, B.D., Datars, W.R., van Schyndel, A. and Gillespie, R.J. (1977), Solid State Comm. 21, 377-379.

Cutforth, B.D., Davies, C.G., Dean, P.A.W., Gillespie, R.J., Ireland, P.R. and Ummat, P.K. (1973), Inorg. Chem. 12, 1343-1347.

Cutforth, B.D., Gillespie, R.J. and Ireland, P.R. (1973), Chem. Comm. 723.

Cutforth, B.D., Gillespie, R.J., Ireland, P., Sawyer, J.F. and Ummat, P.K. (1983), Inorg. Chem. 22, 1344-1347.

Darwin, C.G. (1914), Phil. Mag. 27, 315-333, 675-690.

Datars, W.R., van Schyndel, A., Lass, J.S., Chartier, D. and Gillespie, R.J. (1978), Phys. Rev. Lett., 40, 1184-1187.

Davies, C.G., Dean, P.A.W., Gillespie, R.J. and Ummat, P.K. (1971), Chem. Comm. 782.

Dorm, E. (1971), Chem. Comm. 466-467 and Acta Chemi. Scand. 25, 1655-1662.

Ellison, R.D., Levy, H.A. and Fung. K.W. (1972), Inorg. Chem. 11, 833-836.

Emery, V.J. and Axe, J.D. (1978), Phys. Rev. Lett., 40, 1507-1511.

Gillespie, R.J. and Ummat, P.K. (1971), Chem. Comm. 1168.

Grant, D.F. and Killean, R.C.G. (1969), Acta Cryst. B25, 374-376.

Gupta, N. and Sutherland, B. (1976), Phys. Rev. A., 14, 1790-1801.

Hastings, J.M., Pouget, J.P., Shirane, G., Heeger, A.J., Miro, N.D. and MacDiarmid, A.G. (1977), Phys. Rev. Lett., 3, 1484-1487.

Heilmann, I.U., Axe, J.D., Hastings, J.M., Shirane, G., Heeger, A.J. and MacDiarmid, A.G. (1979), Phys. Rev. B., 20, 751-762.

International Tables for X-ray Crystallography (1959), Vol. II, Birmingham: Kynoch Press.

International Tables for X-ray Cyrstallography (1974), Vol. IV, Birmingham: Kynoch Press.

James, R.W. (1958), The Optical Principles of The Diffraction of X Rays, London: G. Bell and Sons Ltd.

Khan, A.A. (1976), Acta Cryst. A32, 11-16.

Kittel, C. (1976), Introduction to Solid State Physics (fifth edition), New York: John Wiley and Sons, Inc.

Koteles, E.S., Datars, W.R., Cutforth, B.D. and Gillespie, R.J. (1976), Solid State Comm. 20, 1129-1131.

Lagrange, P., El Makrini, M. and Herold, A. (1983), Rev. Chim. Miner. 20, 229-246.

Larson, A.C. (1967), Acta Cryst., 23, 664-665.

Marshall, W. and Lovesey, S.W. (1971), Theory of Thermal Neutron Scattering, Oxford: Clarendon Press.

Ng, H.N. (1978), AVER, McMaster University, Hamilton, Canada.

Patterson, A.L. (1934), Phys. Rev., 46, 372-376.

Pauling, L. (1960), The Nature of the Chemical Bond (third edition), Ithaca, New York: Cornell Univ. Press.

Pouget, J.P., Shirane, G., Hastings, J.M., Heeger, A.J., Miro, N.D. and MacDiarmid, A.G. (1978), Phys. Rev. B, 18, 3645-3656.

Razavi, F.S., Datars, W.R., Chartier, D. and Gillespie, R.J. (1979), Phys. Rev. Lett., 42, 1182-1185.

Reichl, L.E. (1980), A Modern Course in Statistical Physics, Austin: University of Texas Press.

Scholz, G.A., Datars, W.R., Chartier, D. and Gillespie, R.J. (1977), Phys. Rev. B 16, 4209-4214.

Schultz, A.J., Williams, J.M., Miro, N.D., MacDiarmid, A.G. and Heeger, A.J. (1978), Inorg. Chem. 17, 646-649.

Sheldrick, G.M. (1976), SHELX, University of Cambridge, Cambridge, England.

Spal, R., Chen, C.E., Egami, T., Nigrey, P.J. and Heeger, A.J. (1980), Phys. Rev. B 21, 3110-3118.

Stephens, J. (1973), CUDLS, McMaster University, Hamilton, Canada.

Stewart, J.M. (1976), XRAY76, Tech. Rep. TR-446, Computer Science Center, University of Maryland, College Park, Maryland, U.S.A.

Stout, G.H. and Jensen, L.H. (1968), X-ray Structure Determination, New York: The MacMillan Company.

Talbot, E.F. (1979), Unpublished M.Sc. Thesis, University of Toronto.

Torsi, G. and Mamantov, G. (1970), Inorg. Nucl. Lett., 6, 843-846.

Tun, Z. (1984), McMaster University Thesis Tables #1. Available from Thode Library, McMaster University, Hamilton, Canada.

Tun, Z. and Brown, I.D. (1982), Acta Cryst., B38, 2321-2324.

Walker, N. and Stuart, D. (1983a), Acta Cryst., A39, 158-166.

Walker, N. and Stuart, D. (1983b), DIFABS, Chemistry Department, Queen Mary College, England.

Woolfson, M.M. (1963), Direct Methods in Crystallography, Oxford: Clarendon Press.

Woolfson, M.M. (1979), An Introduction to X-Ray Crystallography, Cambridge University Press.

McMASTER UNIVERSITY THESIS

TABLES #1.

This report contains magnitudes of observed and calculated structure factors for refined models described in the Ph.D. Thesis:

STRUCTURES OF SOME MERCURY COMPOUNDS IN LOW OXIDATION STATES

By

Zin Tun, B.Sc.

The Thesis was submitted to the School of Graduate Studies, McMaster University, in October, 1984.

TABLE OF CONTENTS

TABLE 1. OBSERVED AND CALCULATED STRUCTURE FACTORS OF HG3-6S8F6

(UNOBSERVED REFLECTIONS ARE MARKED +)

H	K	L	FO	FC	SIG	H	K	L	FO	FC	SIG	H	K	L	FO	FC	SIG
0	0	4	4774	4837	72	0	6	12	342+	113	72	1	6	1	733	766	29
0	0	8	5743	5946	86	0	7	1	715	688	32	1	6	3	536	606	33
0	0	12	1440	1487	33	0	7	3	1562	1588	27	1	6	5	476	513	41
0	0	16	1441	1442	36	0	7	5	1428	1459	26	1	6	7	440	503	39
0	1	1	2109	2142	31	0	7	7	490	399	40	1	6	9	429+	469	47
0	1	3	4717	4734	66	0	7	9	317+	356	61	1	6	11	330+	378	85
0	1	5	4208	4214	60	0	7	11	755	744	35	1	6	13	332+	262	75
0	1	7	1352	1341	24	0	8	0	1281	1302	36	1	7	2	654	632	32
0	1	9	1094	1066	26	0	8	2	862	817	31	1	7	4	185+	14	87
0	1	11	1953	1966	31	0	8	4	419+	422	50	1	7	6	571	624	32
0	1	13	1395	1432	27	0	8	6	641	654	33	1	7	8	335+	116	67
0	1	15	334+	294	65	0	8	8	917	894	28	1	7	10	347+	356	61
0	2	0	5123	5003	74	0	9	1	471+	402	53	1	8	1	402	350	58
0	2	2	3557	3518	51	0	9	3	721	763	36	1	8	3	327+	292	58
0	2	4	2672	2606	38	0	9	5	661	713	38	1	8	5	278+	252	65
0	2	6	2546	2575	37	0	9	7	326+	232	67	1	8	7	273+	258	71
0	2	8	3052	3043	44	0	10	0	679	711	66	1	8	9	312+	272	72
0	2	10	1440	1459	27	1	1	2	1787	1740	31	1	9	2	354+	328	63
0	2	12	558	489	41	1	1	6	1946	1931	32	1	9	4	232+	3	77
0	2	14	701	689	36	1	1	10	510	528	61	1	9	6	332+	340	57
0	2	16	902	867	33	1	1	14	868	835	42	2	2	0	2157	2211	39
0	3	1	2739	2691	40	1	2	1	1213	1183	20	2	2	4	1227	1193	26
0	3	3	3154	3160	45	1	2	3	584	654	25	2	2	8	1232	1250	32
0	3	5	2946	2924	43	1	2	5	679	705	25	2	2	12	559	601	62
0	3	7	1490	1476	25	1	2	7	848	793	25	2	3	1	1348	1368	22
0	3	9	1188	1126	26	1	2	9	692	617	33	2	3	3	956	1019	21
0	3	11	1517	1515	28	1	2	11	548	544	42	2	3	5	929	960	24
0	3	13	1157	1173	29	1	2	13	484	455	48	2	3	7	874	884	27
0	3	15	335+	247	76	1	2	15	338+	265	75	2	3	9	572	624	41
0	4	0	3911	3837	59	1	3	2	815	841	20	2	3	11	625	532	43
0	4	2	2499	2519	37	1	3	4	172+	6	72	2	3	13	518	453	49
0	4	4	1581	1597	25	1	3	6	1222	1212	24	2	3	15	411+	277	71
0	4	6	1897	1902	29	1	3	8	159+	7	88	2	4	0	1478	1526	26
0	4	8	2367	2334	35	1	3	10	455	415	52	2	4	2	70+	28	91
0	4	10	1144	1166	26	1	3	12	237+	11	89	2	4	4	1010	988	33
0	4	12	427+	282	54	1	3	14	620	663	43	2	4	6	233+	18	79
0	4	14	581	581	45	1	4	1	919	938	20	2	4	8	949	927	28
0	5	1	1115	1130	24	1	4	3	664	623	27	2	4	10	158+	37	97
0	5	3	2694	2742	39	1	4	5	602	563	30	2	4	12	575	542	42
0	5	5	2474	2502	36	1	4	7	690	660	31	2	4	14	248+	45	104
0	5	7	737	691	29	1	4	9	618	587	36	2	5	1	650	602	29
0	5	9	609	602	34	1	4	11	468+	436	48	2	5	3	524	502	32
0	5	11	1198	1183	28	1	4	13	352+	318	66	2	5	5	579	556	33
0	5	13	935	945	33	1	5	2	1079	1074	23	2	5	7	515	513	40
0	6	0	2904	2896	45	1	5	4	279+	11	78	2	5	9	240+	355	77
0	6	2	1581	1523	27	1	5	6	1068	1061	25	2	5	11	376+	341	73
0	6	4	454	494	40	1	5	8	239+	28	75	2	5	13	311+	346	86
0	6	6	1168	1187	24	1	5	10	479+	495	45	2	6	0	771	680	36
0	6	8	1792	1754	29	1	5	12	221+	22	86	2	6	2	80+	21	133
0	6	10	717	734	33	1	5	14	507	504	55	2	6	4	492	496	41

TABLE 1. OBSERVED AND CALCULATED STRUCTURE FACTORS OF HG3-6SBF6

(UNOBSERVED REFLECTIONS ARE MARKED +)

H	K	L	FO	FC	SIG	H	K	L	FO	FC	SIG	H	K	L	FO	FC	SIG
2	6	6	284+	6	72	3	5	12	226+	15	96	4	7	1	459	370	44
2	6	8	510	541	40	3	6	1	319+	362	61	4	7	3	330+	350	59
2	6	10	0+	16	148	3	6	3	43+	271	118	4	7	5	470	345	45
2	6	12	412+	350	58	3	6	5	218+	261	87	4	7	7	418+	315	48
2	7	1	408+	392	42	3	6	7	410	309	48	4	7	9	341+	249	64
2	7	3	330+	365	52	3	6	9	303+	304	67	4	8	0	408+	485	68
2	7	5	471	391	42	3	6	11	182+	262	107	4	8	2	0+	2	145
2	7	7	421	342	52	3	7	2	499	494	37	4	8	4	458+	408	48
2	7	9	316+	250	62	3	7	4	201+	3	82	4	8	6	183+	4	105
2	7	11	345+	240	63	3	7	6	435+	487	51	4	9	1	358+	235	64
2	8	0	594	572	50	3	7	8	302+	14	71	4	9	3	437	234	56
2	8	2	0+	12	143	3	7	10	468+	317	60	5	5	2	629	690	41
2	8	4	434+	461	46	3	8	1	455	409	43	5	5	6	591	622	50
2	8	6	291+	4	69	3	8	3	295+	362	63	5	5	10	455+	401	70
2	8	8	562	416	42	3	8	5	331+	314	61	5	6	1	488	506	37
2	9	1	349+	302	71	3	8	7	314+	299	67	5	6	3	367+	413	48
2	9	3	220+	296	103	3	9	2	410+	426	54	5	6	5	468	388	45
2	9	5	321+	286	66	3	9	4	157+	1	109	5	6	7	451+	378	44
3	3	2	1662	1674	28	4	4	0	1017	1027	37	5	6	9	361+	311	63
3	3	6	1480	1513	32	4	4	4	761	744	38	5	7	2	513	489	39
3	3	10	594	626	56	4	4	8	573	670	52	5	7	4	220+	2	94
3	3	14	564	612	66	4	4	12	263+	471	129	5	7	6	437	428	52
3	4	1	935	943	21	4	5	1	454	472	37	5	7	8	166+	2	107
3	4	3	772	726	24	4	5	3	392+	409	45	5	8	1	260+	239	73
3	4	5	651	666	30	4	5	5	432	411	44	5	8	3	235+	218	84
3	4	7	598	655	36	4	5	7	490	419	38	5	8	5	306+	209	67
3	4	9	638	545	39	4	5	9	335+	329	57	6	6	0	577	574	68
3	4	11	433	398	58	4	5	11	416+	267	65	6	6	4	569	566	54
3	4	13	330+	319	71	4	6	0	599	588	42	6	6	8	471+	397	64
3	5	2	567	571	30	4	6	2	239+	8	69	6	7	1	439	307	53
3	5	4	38+	14	126	4	6	4	416	494	48	6	7	3	311+	246	66
3	5	6	670	660	31	4	6	6	123+	5	106	6	7	5	262+	236	83
3	5	8	193+	9	91	4	6	8	362+	444	54	6	8	0	349+	224	103
3	5	10	222+	379	86	4	6	10	331+	3	79	7	7	2	357+	282	80

TABLE 2. OBSERVED AND CALCULATED STRUCTURE FACTORS OF HG3-6S3F6 AT 293K

(UNOBSERVED REFLECTIONS ARE MARKED +)

H	K	L	FO	FC	SIG	H	K	L	FO	FC	SIG	H	K	L	FO	FC	SIG
0	0	4	4596	4311	259	0	6	12	28+	84	113	1	5	14	458	425	44
0	0	8	5149	5762	290	0	7	1	674	651	46	1	6	1	741	767	46
0	0	12	1350	1297	77	0	7	3	1453	1516	82	1	6	3	557	570	41
0	0	16	1335	1234	76	0	7	5	1361	1386	77	1	6	5	445	493	42
0	1	1	2445	2143	137	0	7	7	333+	360	49	1	6	7	430	503	42
0	1	3	5043	4767	232	0	7	9	376	311	47	1	6	9	441	445	42
0	1	5	4117	4170	231	0	7	11	652	665	44	1	6	11	355+	335	47
0	1	7	1276	1284	73	0	8	0	1266	1266	75	1	6	13	216+	232	61
0	1	9	943	965	55	0	8	2	773	774	49	1	7	2	617	614	41
0	1	11	1733	1824	97	0	8	4	419	407	44	1	7	4	52+	11	99
0	1	13	1255	1258	71	0	8	6	552	604	43	1	7	6	615	609	43
0	1	15	333+	228	39	0	8	8	796	825	50	1	7	8	201+	14	73
0	2	0	5559	5084	311	0	9	1	355+	374	57	1	7	10	239+	327	68
0	2	2	5723	5527	209	0	9	3	708	711	46	1	8	1	326+	350	50
0	2	4	2494	2585	140	0	9	5	676	664	47	1	8	3	334	271	47
0	2	6	2287	2507	128	0	9	7	372+	202	60	1	8	5	237+	237	61
0	2	8	2749	2895	154	0	10	0	710	680	59	1	8	7	355+	252	51
0	2	10	1361	1354	77	1	1	2	1865	1753	104	1	8	9	257+	250	60
0	2	12	454	424	38	1	1	6	1941	1864	110	1	9	2	232+	310	56
0	2	14	581	594	39	1	1	10	556	559	47	1	9	4	197+	3	75
0	2	16	705	741	46	1	1	14	698	719	46	1	9	6	339+	322	50
0	3	1	2747	2655	154	1	2	1	1289	1187	72	2	2	0	2342	2272	131
0	3	3	3072	3116	172	1	2	3	643	649	37	2	2	4	1217	1161	70
0	3	5	2551	2831	143	1	2	5	712	694	45	2	2	8	1238	1215	76
0	3	7	1401	1426	79	1	2	7	794	772	50	2	2	12	533	562	53
0	3	9	1044	1032	61	1	2	9	580	598	45	2	3	1	1477	1364	62
0	3	11	1412	1388	80	1	2	11	493	506	40	2	3	3	1008	1006	56
0	3	13	1052	1011	61	1	2	13	380	394	39	2	3	5	940	939	54
0	3	15	241+	202	54	1	2	15	277+	243	60	2	3	7	853	852	52
0	4	0	3579	3851	201	1	3	2	869	829	49	2	3	9	639	613	46
0	4	2	2355	2499	132	1	3	4	197+	2	71	2	3	11	542	507	44
0	4	4	1630	1583	92	1	3	6	1208	1174	69	2	3	13	419	398	44
0	4	6	1813	1837	102	1	3	8	0+	4	132	2	3	15	165+	247	71
0	4	8	2120	2224	119	1	3	10	403	405	47	2	4	0	1627	1552	92
0	4	10	1015	1058	59	1	3	12	73+	3	100	2	4	2	207+	7	51
0	4	12	235+	249	68	1	3	14	555	569	40	2	4	4	972	913	56
0	4	14	564	483	41	1	4	1	967	937	55	2	4	6	90+	29	99
0	5	1	1127	1090	65	1	4	3	566	587	38	2	4	8	891	905	54
0	5	3	2463	2652	138	1	4	5	572	552	41	2	4	10	97+	33	98
0	5	5	2271	2435	127	1	4	7	669	640	45	2	4	12	574	485	44
0	5	7	655	604	45	1	4	9	487	543	41	2	4	14	47+	30	107
0	5	9	535	560	42	1	4	11	484	405	41	2	5	1	610	571	40
0	5	11	1067	1058	62	1	4	13	288+	293	51	2	5	3	450	471	37
0	5	13	865	842	52	1	4	15	190+	227	73	2	5	5	559	555	40
0	6	0	2564	2861	150	1	5	2	1061	1056	61	2	5	7	514	505	41
0	6	2	1430	1488	81	1	5	4	8+	34	114	2	5	9	317+	304	56
0	6	4	471	479	46	1	5	6	1008	1007	59	2	5	11	272+	296	72
0	6	6	1109	1134	64	1	5	8	0+	55	125	2	5	13	345+	322	51
0	6	8	1561	1652	88	1	5	10	453	492	44	2	6	0	700	730	49
0	6	10	700	671	45	1	5	12	173+	43	83	2	6	2	0+	10	117

TABLE 2. OBSERVED AND CALCULATED STRUCTURE FACTORS OF HG3-δASF6 AT 293K

(UNOBSERVED REFLECTIONS ARE MARKED +)

H	K	L	FO	FC	SIG
2	6	4	407	437	39
2	6	6	11+	18	116
2	6	8	570	527	43
2	6	10	257+	23	70
2	6	12	335+	313	52
2	7	1	421	369	38
2	7	3	352	376	41
2	7	5	402	398	42
2	7	7	259+	317	58
2	7	9	131+	224	63
2	7	11	265+	227	70
2	8	0	605	601	49
2	8	2	91+	11	94
2	8	4	439	410	41
2	8	6	121+	14	91
2	8	8	426	411	47
2	9	1	341+	265	51
2	9	3	329+	295	56
2	9	5	234+	289	61
3	3	2	1713	1644	96
3	3	6	1457	1498	83
3	3	10	606	597	55
3	3	14	585	544	51
3	4	1	982	955	56
3	4	3	704	691	43
3	4	5	537	638	41
3	4	7	634	640	43
3	4	9	504	518	43
3	4	11	343+	377	55
3	4	13	341+	290	53
3	5	2	583	561	40
3	5	4	131+	32	84
3	5	6	532	629	42
3	5	8	205+	37	70
3	5	10	352+	361	53
3	5	12	174+	34	91
3	6	1	319+	364	44
3	6	3	251+	253	50
3	6	5	149+	246	70
3	6	7	378	299	48
3	6	9	3[illegible]0+	284	56
3	6	11	281+	231	63
3	7	2	453	471	39
3	7	4	11+	4	111
3	7	6	486	475	40
3	7	8	42+	13	109
3	7	10	283+	281	59
3	8	1	453	401	43
3	8	3	389+	335	42
3	8	5	345+	292	52
3	8	7	306+	285	51
3	9	2	413	400	44
3	9	4	228+	1	80
4	4	0	1052	1053	65
4	4	4	770	729	49
4	4	8	600	657	49
4	4	12	506	421	59
4	5	1	495	499	39
4	5	3	413	371	38
4	5	5	376	412	38
4	5	7	451	437	40
4	5	9	307+	295	50
4	5	11	190+	229	87
4	6	0	622	594	47
4	6	2	0+	15	115
4	6	4	384	456	39
4	6	6	434+	7	79
4	6	8	441	422	42
4	6	10	44+	4	115
4	7	1	372+	363	42
4	7	3	411	305	45
4	7	5	257+	359	51
4	7	7	318+	302	46
4	7	9	277+	229	65
4	8	0	447	455	53
4	8	2	159+	15	72
4	8	4	350+	376	45
4	8	6	53+	12	107
4	9	1	253+	234	64
4	9	3	373+	209	50
5	5	2	579	690	47
5	5	6	556	589	47
5	5	10	431	395	55
5	6	1	432	477	40
5	6	3	330	388	40
5	6	5	419	385	39
5	6	7	390	369	42
5	6	9	246+	272	60
5	7	2	479	451	40
5	7	4	89+	6	86
5	7	6	390+	394	49
5	7	8	184+	11	82
5	8	1	154+	227	84
5	8	3	11+	191	122
5	8	5	214+	194	68
6	6	0	453	598	69
6	6	4	435	495	50
6	6	8	419	392	65
6	7	1	357	281	68
6	7	3	212+	245	68
6	7	5	338+	236	49
6	8	0	241+	245	85
7	7	2	232+	279	91

TABLE 3. OBSERVED AND CALCULATED STRUCTURE FACTORS OF HG3-6S3F6

(UNOBSERVED REFLECTIONS ARE MARKED +)

H	K	L	FO	FC	SIG	H	K	L	FO	FC	SIG	H	K	L	FO	FC	SIG
0	0	4	4483	4620	494	0	7	1	1125	1039	125	1	6	7	655	689	78
0	0	8	6199	6383	682	0	7	3	2099	2189	231	1	6	9	579	615	71
0	0	12	2212	2103	244	0	7	5	1993	2106	219	1	6	11	515	522	66
0	0	16	2680	2497	295	0	7	7	832	792	95	1	7	2	750	790	85
0	1	1	2435	2076	268	0	7	9	677	683	79	1	7	4	252+	26	67
0	1	3	4940	4506	544	0	7	11	1266	1333	140	1	7	6	882	891	100
0	1	5	4289	4311	472	0	8	0	1971	2026	218	1	7	8	293+	65	82
0	1	7	1517	1560	168	0	8	2	1370	1402	151	1	7	10	412	486	62
0	1	9	1334	1331	147	0	8	4	911	874	103	1	8	1	517	475	67
0	1	11	2494	2574	274	0	8	6	1154	1173	128	1	8	3	444	395	61
0	1	13	1993	2006	219	0	8	8	1412	1517	156	1	8	5	412+	365	62
0	1	15	732	657	85	0	9	1	879	805	101	1	8	7	429	390	69
0	2	0	5229	4742	576	0	9	3	1361	1334	151	1	8	9	418	370	62
0	2	2	3879	3541	427	0	9	5	1235	1283	137	1	9	2	587	478	76
0	2	4	2873	2762	316	1	1	2	1855	1732	205	1	9	4	337+	33	77
0	2	6	3549	2835	291	1	1	6	2243	2053	248	1	9	6	561	538	72
0	2	8	3208	3337	353	1	1	10	678	637	87	2	2	0	2514	2359	288
0	2	10	1943	1940	214	1	1	14	1049	1055	119	2	2	4	1456	1290	162
0	2	12	910	850	103	1	2	1	1374	1207	151	2	2	8	1444	1375	162
0	2	14	1205	1149	134	1	2	3	674	656	79	2	2	12	905	846	107
0	3	1	2962	2771	326	1	2	5	787	739	91	2	3	1	1630	1504	179
0	3	3	2962	3285	326	1	2	7	889	864	103	2	3	3	1112	1058	123
0	3	5	2662	3134	293	1	2	9	706	665	87	2	3	5	1079	1070	119
0	3	7	1717	1889	189	1	2	11	669	633	81	2	3	7	1138	1027	126
0	3	9	1464	1568	161	1	2	13	499	496	67	2	3	9	875	813	100
0	3	11	1973	2038	217	1	2	15	295+	327	68	2	3	11	691	701	82
0	3	13	1663	1637	183	1	3	2	874	846	97	2	3	13	545	585	68
0	3	15	753	684	87	1	3	4	212+	8	66	2	3	15	349+	378	68
0	4	0	3814	4193	420	1	3	6	1379	1337	152	2	4	0	1788	1726	197
0	4	2	2694	2862	296	1	3	8	266+	26	82	2	4	2	190+	39	68
0	4	4	1924	1933	212	1	3	10	446	403	64	2	4	4	1105	1044	122
0	4	6	2089	2383	230	1	3	12	228+	15	127	2	4	6	292+	17	84
0	4	8	2553	2869	281	1	3	14	835	844	94	2	4	8	1134	1091	126
0	4	10	1574	1625	173	1	4	1	1052	1011	116	2	4	10	69+	56	120
0	4	12	694	625	80	1	4	3	625	636	72	2	4	12	727	749	85
0	4	14	1081	1044	120	1	4	5	738	675	85	2	4	14	229+	26	73
0	5	1	1403	1356	156	1	4	7	757	752	87	2	5	1	714	714	81
0	5	3	2943	3207	324	1	4	9	599	656	73	2	5	3	470	486	60
0	5	5	2671	3059	294	1	4	11	531	534	66	2	5	5	669	623	78
0	5	7	953	940	107	1	4	13	425	421	62	2	5	7	637	543	76
0	5	9	992	989	110	1	5	2	1197	1203	132	2	5	9	459+	406	67
0	5	11	1718	1828	189	1	5	4	111+	82	99	2	5	11	398	391	64
0	5	13	1558	1584	172	1	5	6	1296	1291	142	2	5	13	534	484	70
0	6	0	3196	3642	352	1	5	8	136+	94	89	2	6	0	844	908	99
0	6	2	2021	2084	232	1	5	10	580	651	71	2	6	2	231+	34	64
0	6	4	817	809	94	1	5	12	308+	118	76	2	6	4	510	542	65
0	6	6	1587	1736	175	1	5	14	707	723	82	2	6	6	246+	46	78
0	6	8	2249	2527	247	1	6	1	895	916	100	2	6	8	685	674	81
0	6	10	1196	1260	132	1	6	3	664	710	78	2	6	10	213+	23	81
0	6	12	262+	295	69	1	6	5	630	675	76	2	6	12	496	495	66

TABLE 3. OBSERVED AND CALCULATED STRUCTURE FACTORS OF HG3-6SBF6

(UNOBSERVED REFLECTIONS ARE MARKED +)

H	K	L	FO	FC	SIG	H	K	L	FO	FC	SIG	H	K	L	FO	FC	SIG
2	7	1	553	553	68	3	6	3	315+	304	64	4	7	1	557	543	68
2	7	3	469	478	63	3	6	5	359+	327	56	4	7	3	337	416	55
2	7	5	474	494	65	3	6	7	360+	387	58	4	7	5	438	429	62
2	7	7	514	488	66	3	6	9	455	368	62	4	7	7	508	476	65
2	7	9	350+	359	68	3	6	11	439+	325	65	4	7	9	436	380	67
2	7	11	423+	387	65	3	7	2	651	637	77	4	8	0	750	716	89
2	8	0	825	884	97	3	7	4	223+	40	74	4	8	2	281+	10	60
2	8	2	217+	34	88	3	7	6	728	730	83	4	8	4	552	586	68
2	8	4	628	630	75	3	7	8	261+	16	92	4	8	6	276+	2	69
2	8	6	325+	38	86	3	7	10	438	404	64	4	9	1	431	421	61
2	8	8	669	667	80	3	8	1	492	600	64	5	5	2	874	916	99
2	9	1	531	466	71	3	8	3	534	510	70	5	5	6	832	877	100
2	9	3	506	441	67	3	8	5	492	496	63	5	5	10	630	616	85
2	9	5	491	464	67	3	8	7	507	470	66	5	6	1	653	679	75
3	3	2	1909	1798	210	3	9	2	652	659	77	5	6	3	550	546	66
3	3	6	1880	1863	207	3	9	4	163+	19	83	5	6	5	550	570	67
3	3	10	792	796	95	4	4	0	1343	1287	149	5	6	7	503	685	71
3	3	14	960	946	109	4	4	4	891	878	101	5	6	9	480	427	64
3	4	1	1151	1088	127	4	4	8	861	860	99	5	7	2	606	658	72
3	4	3	825	793	92	4	4	12	763	679	93	5	7	4	201+	19	69
3	4	5	806	760	90	4	5	1	635	657	73	5	7	6	652	652	76
3	4	7	833	834	94	4	5	3	407	434	57	5	7	8	143+	5	90
3	4	9	641	665	76	4	5	5	546	541	65	5	8	1	353+	358	60
3	4	11	564	569	72	4	5	7	618	593	73	5	8	3	239+	294	71
3	4	13	514	437	71	4	5	9	471	421	64	5	8	5	274+	325	64
3	5	2	755	637	86	4	5	11	271+	322	78	6	6	0	917	918	108
3	5	4	171+	38	65	4	6	0	825	817	94	6	6	4	728	750	86
3	5	6	803	811	90	4	6	2	148+	2	78	6	6	8	532	678	84
3	5	8	265+	101	71	4	6	4	560	599	67	6	7	1	437	462	63
3	5	10	333+	427	67	4	6	6	265+	14	57	6	7	3	371+	372	57
3	5	12	264+	65	82	4	6	8	587	603	71	6	7	5	362+	392	58
3	6	1	310+	453	68	4	6	10	264+	4	85						

TABLE 4. OBSERVED AND CALCULATED STRUCTURE FACTORS FOR HGE-&NBF6.

(UNOBSERVED REFLECTIONS ARE MARKED +)

H	K	L	FO	FC	SIG
0	0	4	55176	53404	621
0	0	8	56387	55209	650
0	0	12	15095	14842	183
0	0	16	10799	10659	150
0	1	1	24968	24619	275
0	1	3	45518	46174	499
0	1	5	40320	40199	450
0	1	7	15216	14641	173
0	1	9	12984	12257	151
0	1	11	16460	16103	188
0	1	13	11240	11633	136
0	1	15	3353	3186	142
0	2	0	46957	48450	518
0	2	2	35320	35325	388
0	2	4	29106	28642	325
0	2	6	24566	24584	277
0	2	8	25346	25593	285
0	2	10	13227	13295	153
0	2	12	5799	5740	104
0	2	14	5760	5778	109
0	2	16	6015	5944	113
0	3	1	28455	28356	313
0	3	3	27971	28196	308
0	3	5	25134	25573	283
0	3	7	15446	15600	177
0	3	9	11230	11985	134
0	3	11	11931	12267	142
0	3	13	8735	8861	117
0	3	15	2927	2832	162
0	4	0	33197	33510	381
0	4	2	23643	23612	266
0	4	4	17289	17162	195
0	4	6	17365	17415	197
0	4	8	18596	18783	211
0	4	10	9640	9825	121
0	4	12	3505	3690	128
0	4	14	4520	4517	118
0	5	1	11921	11783	139
0	5	3	22986	22954	259
0	5	5	20364	20697	230
0	5	7	6893	7061	103
0	5	9	6155	6332	102
0	5	11	8668	8812	116
0	5	13	6686	6786	110
0	6	0	22852	22850	266
0	6	2	13165	13239	153
0	6	4	5589	5832	103
0	6	6	9816	10048	123
0	6	8	12611	12805	148
0	6	10	5783	5976	107
0	6	12	2271	1541	186
0	7	1	6679	6660	102
0	7	3	11863	11780	141
0	7	5	10849	10678	132
0	7	7	4262	4123	118
0	7	9	3171	3295	143
0	7	11	5072	5006	114
0	8	0	9143	8805	134
0	8	2	6380	6351	104
0	8	4	4157	4159	116
0	8	6	5052	4887	109
0	8	8	5893	5690	108
0	9	1	3173	3398	143
0	9	3	5118	4936	112
0	9	5	4761	4521	116
0	9	7	2274	2023	193
0	10	0	4844	4190	155
1	1	2	14105	13410	156
1	1	6	15329	14607	182
1	1	10	3483	3365	168
1	1	14	5149	5116	145
1	2	1	8941	8650	99
1	2	3	3209	3545	54
1	2	5	4807	4915	87
1	2	7	5989	5806	94
1	2	9	3692	3446	115
1	2	11	3539	3342	122
1	2	13	2931	3135	144
1	2	15	2179	1494	248
1	3	2	4646	4805	60
1	3	4	0+	295	569
1	3	6	8340	8373	106
1	3	8	1134+	309	356
1	3	10	1880	2083	206
1	3	12	867+	200	391
1	3	14	4148	4039	123
1	4	3	6476	6584	91
1	4	5	3624	3678	100
1	4	7	4033	3885	102
1	4	9	4431	4432	103
1	4	11	3447	3328	121
1	4	13	2531	2553	155
1	4	15	1857+	2192	233
1	5	1	1439+	1342	272
1	5	2	7391	7380	101
1	5	4	676+	161	350
1	5	6	6823	6889	101
1	5	8	127+	196	563
1	5	10	2828	3144	147
1	5	12	1349+	206	275
1	5	14	2747	2708	165
1	6	1	4503	5026	107
1	6	3	3309	3768	129
1	6	5	2755	3321	151
1	6	7	2914	3269	141
1	6	9	2817	2721	147
1	6	11	1804+	2050	223
1	6	13	1613+	1468	278
1	7	2	3933	3681	110
1	7	4	1351+	23	265
1	7	6	3579	3593	122
1	7	8	1381+	43	269
1	7	10	2154	1922	201
1	8	1	1871	1831	207
1	8	3	1868	1553	211
1	8	5	1475+	1343	246
1	8	7	1577+	1379	261
1	8	9	1613+	1309	274
1	9	2	2295	1647	193
1	9	4	732+	23	423
1	9	6	1855+	1624	235
2	2	0	17198	18054	198
2	2	4	8915	8400	117
2	2	8	9352	8813	130
2	2	12	3752	3807	167
2	3	1	10945	10793	143
2	3	3	7328	7437	83
2	3	5	7130	6969	99

TABLE 4. OBSERVED AND CALCULATED STRUCTURE FACTORS FOR HG3-SNBF6.

(UNOBSERVED REFLECTIONS ARE MARKED +)

H	K	L	FO	FC	SIG	H	K	L	FO	FC	SIG
2	3	7	6152	6162	100	3	6	9	1653+	1673	228
2	3	9	4109	4216	114	3	6	11	1795+	1418	242
2	3	11	3724	3588	122	3	7	2	2962	2744	136
2	3	13	3138	2818	145	3	7	4	1319+	91	317
2	3	15	1217+	1398	358	3	7	6	2610	2820	155
2	4	0	11037	10959	138	3	7	8	1242+	77	341
2	4	2	699+	63	350	3	7	10	1948+	1554	203
2	4	4	6369	6493	95	3	8	1	2454	2364	162
2	4	6	859+	63	329	3	8	3	2135	2077	203
2	4	8	5960	6103	100	3	8	5	1955+	1754	203
2	4	10	1369+	230	297	3	8	7	1832+	1551	215
2	4	12	3180	3156	137	3	9	2	2502	2227	174
2	4	14	1449+	188	280	3	9	4	1134+	35	350
2	5	1	3849	3661	105	4	4	0	6179	6322	152
2	5	3	2928	2651	125	4	4	4	4819	4735	129
2	5	5	3452	3383	116	4	4	8	4087	4033	151
2	5	7	3188	3233	126	4	4	12	2768	2594	218
2	5	9	2161	1846	195	4	5	1	2862	3002	131
2	5	11	1804+	1839	211	4	5	3	2000	1993	176
2	5	13	2161	2081	195	4	5	5	2640	2361	142
2	6	0	3620	3855	164	4	5	7	2707	2598	144
2	6	2	0+	154	620	4	5	9	1750	1770	245
2	6	4	2038	2610	186	4	5	11	1797+	1362	236
2	6	6	1166+	40	544	4	6	0	3114	3295	180
2	6	8	2845	2986	144	4	6	2	0+	253	611
2	6	10	1533+	150	299	4	6	4	2632	2846	152
2	6	12	2440	1907	178	4	6	6	995+	-170	319
2	7	1	2384	2290	156	4	6	8	2293	2394	177
2	7	3	2461	2061	158	4	6	10	214+	43	572
2	7	5	2178	2140	176	4	7	1	2679	2323	142
2	7	7	1934	1916	195	4	7	3	1494+	1753	232
2	7	9	1736+	1348	231	4	7	5	1948	1725	193
2	7	11	1387+	1317	298	4	7	7	1812+	1806	249
2	8	0	3554	3267	168	4	7	9	1640+	1378	255
2	8	2	477+	80	487	4	8	0	2781	2416	207
2	8	4	2425	2619	166	4	8	2	800+	194	393
2	8	6	0+	11	641	4	8	4	2458	2303	165
2	8	8	2586	2209	166	4	8	6	1318+	124	268
2	9	1	1519+	1637	251	4	9	1	1761+	1293	219
2	9	3	1887+	1531	211	5	5	2	4231	4327	142
2	9	5	1985+	1460	213	5	5	6	3722	3618	158
3	3	2	12570	12479	141	5	5	10	2753	2342	217
3	3	6	11500	11408	147	5	6	1	2392	2907	159
3	3	10	3574	3621	176	5	6	3	2405	2556	158
3	3	14	3745	3342	186	5	6	5	2474	2415	158
3	4	1	6603	6683	97	5	6	7	2115	2171	161
3	4	3	4769	4713	100	5	6	9	1882+	1569	231
3	4	5	4238	4168	107	5	7	2	2487	2653	156
3	4	7	4097	4216	112	5	7	4	632+	54	426
3	4	9	3123	3348	135	5	7	6	2204	2242	193
3	4	11	2552	2609	164	5	7	8	791+	45	407
3	4	13	1884+	1869	220	5	8	1	958+	1123	379
3	5	2	2721	2883	141	5	8	3	1347+	1004	285
3	5	4	417+	214	463	5	8	5	1115+	995	304
3	5	6	3560	3789	120	6	6	0	3153	3637	256
3	5	8	1405+	357	277	6	6	4	2813	2910	201
3	5	10	2016	1979	202	6	6	8	1783+	2259	313
3	5	12	1022+	252	357	6	7	1	1428+	1414	259
3	6	1	966+	1796	338	6	7	3	1217+	1362	297
3	6	3	530+	1322	476	6	7	5	1227+	1293	311
3	6	5	764+	1249	394	6	8	0	1030+	1132	445
3	6	7	978+	1534	362	7	7	2	0+	1296	903

TABLE 5. OBSERVED AND CALCULATED STRUCTURE FACTORS FOR HG3-6TaF6

(UNOBSERVED REFLECTIONS ARE MARKED +)

H	K	L	FO	FC	SIG
0	0	4	38658	40346	708
0	0	8	62960	62160	1148
0	0	12	8705	9198	227
0	0	16	15481	15265	310
0	1	1	16056	15406	291
0	1	3	49113	50656	694
0	1	5	44836	46366	813
0	1	7	8246	8164	222
0	1	9	6548	6414	211
0	1	11	21187	21733	392
0	1	13	15303	15869	291
0	1	15	1488+	603	488
0	2	2	35897	34569	648
0	2	4	18028	17959	329
0	2	6	24063	24713	439
0	2	8	34450	34621	626
0	2	10	14188	13707	285
0	2	12	1282+	476	659
0	2	14	6191	6563	200
0	2	16	10781	10143	227
0	2	0	56994	54894	1030
0	3	3	35710	35571	645
0	3	5	31617	32841	574
0	3	7	9894	9951	203
0	3	9	7087	6885	206
0	3	11	17619	17272	337
0	3	13	13119	12892	269
0	3	15	1505+	446	631
0	3	1	21563	21018	390
0	4	2	24618	24046	447
0	4	4	8812	8826	175
0	4	6	17701	18211	326
0	4	8	26013	26768	475
0	4	10	10246	10499	219
0	4	12	1189+	1177	876
0	4	14	5982	5065	252
0	4	0	43816	43520	799
0	5	3	29807	29851	541
0	5	5	26843	27291	488
0	5	7	3246	2729	217
0	5	9	3156	2889	255
0	5	11	12608	12988	255
0	5	13	10564	10249	241
0	5	1	6730	6450	151
0	6	4	543+	937	760
0	6	6	10688	10869	214
0	6	8	18382	19415	343
0	6	10	6677	6667	192
0	6	12	2771+	2138	447
0	6	0	31843	31988	585
0	6	2	14141	14123	266
0	7	3	16663	17045	310
0	7	5	15476	15869	891
0	7	7	2211+	1266	307
0	7	9	2230+	999	365
0	7	11	8076	8045	208
0	7	1	3345	3293	197
0	8	4	2486+	577	299
0	8	6	5572	5594	186
0	8	8	9920	10193	214
0	8	0	14707	14905	293
0	8	2	7219	7222	178
0	9	5	7620	7747	197
0	9	7	2084+	368	524
0	9	1	1911+	1552	412
0	9	3	8240	8336	200
0	10	0	8040	8009	252
1	1	2	25371	25120	458
1	1	6	25057	25315	483
1	1	10	10628	10708	269
1	1	14	10290	10275	247
1	2	1	17827	17178	321
1	2	3	11177	11796	203
1	2	5	11869	12285	227
1	2	7	12270	12205	258
1	2	9	9331	9198	260
1	2	11	8642	8418	233
1	2	13	7114	6863	206
1	2	15	4656	4196	230
1	3	2	15752	15505	285
1	3	4	793+	280	442
1	3	6	17143	17901	318
1	3	8	530+	213	953
1	3	10	8471	8675	233
1	3	12	1972+	129	623
1	3	14	8752	8624	225
1	4	1	13946	13807	255
1	4	3	10600	10373	200
1	4	5	10051	9939	197
1	4	7	9985	9915	208
1	4	9	8040	8354	203
1	4	11	6815	6719	225
1	4	13	5134	5222	283
1	4	15	3966	3815	315
1	5	2	16058	15965	293
1	5	4	1878+	194	651
1	5	6	14284	14564	271
1	5	8	1307+	193	535
1	5	10	8213	8437	203
1	5	12	1582+	282	653
1	5	14	6672	6443	255
1	6	3	8754	8855	178
1	6	5	7592	7907	175
1	6	7	7004	7483	186
1	6	9	6493	6518	195
1	6	11	5205	5215	230
1	6	13	2703+	3877	439
1	7	4	1508+	52	516
1	7	6	8751	9020	195
1	7	8	1592+	100	590
1	7	10	5664	5775	211
1	8	3	4779	4793	170
1	8	5	4598	4322	200
1	8	7	4035	4218	244
1	8	9	4252	3854	249
1	9	4	931+	24	782
1	9	6	5125	5095	225
1	6	1	10413	10621	197
1	7	2	9468	9758	186
1	8	1	5471	5458	145
1	9	2	4950	5400	175
2	2	0	30062	29237	543
2	2	4	19011	18855	348
2	2	8	17209	17346	357
2	2	12	9320	9334	302
2	3	1	19217	18400	346
2	3	3	14666	14631	263
2	3	5	13528	13795	252

TABLE 5. OBSERVED AND CALCULATED STRUCTURE FACTORS FOR HGI-6TAF6

(UNOBSERVED REFLECTIONS ARE MARKED +)

H	K	L	FO	FC	SIG
2	2	7	11636	12042	230
2	2	9	9383	9227	244
2	2	11	8073	7945	310
2	2	13	6661	6312	269
2	2	15	4068	3930	296
2	4	0	21681	20899	395
2	4	2	961+	237	335
2	4	4	15550	15232	285
2	4	6	1269+	46	447
2	4	8	13100	13232	255
2	4	10	1920+	403	668
2	4	12	8164	8034	266
2	4	14	1606+	343	777
2	5	1	9927	9555	186
2	5	3	8356	8216	164
2	5	5	8694	8767	175
2	5	7	7842	7953	178
2	5	9	5741	5722	214
2	5	11	5128	5230	285
2	5	13	4782	4967	329
2	6	0	11155	11091	219
2	6	2	2+	356	675
2	6	4	8848	8963	178
2	6	6	129+	28	763
2	6	8	8466	8328	200
2	6	10	1387+	201	601
2	6	12	5823	5598	269
2	6	14	6570	6410	145
2	7	3	6068	5985	148
2	7	5	5851	5974	159
2	7	7	5351	5383	186
2	7	9	3730	4063	288
2	7	11	4285	3741	299
2	8	2	1211+	203	390
2	8	4	7103	7061	167
2	8	6	277+	27	777
2	8	8	6224	5942	211
2	9	3	4304	4159	184
2	9	5	4049	4005	219
2	9	7	8405	8276	189
2	9	9	4527	4390	162
2	10	2	22816	22311	412
2	10	4	19666	20004	368
2	10	6	9452	9666	315
2	10	8	8166	7945	337
2	11	1	13493	13107	247
2	11	3	11177	10993	298
2	11	5	9856	9806	192
2	11	7	8971	9302	196
2	11	9	7284	7661	203
2	12	0	6134	6231	304
2	12	2	5981	4699	486
2	12	4	10622	10356	200
2	12	6	1393+	149	343
2	13	1	10345	10410	203
2	13	3	343+	392	749
2	13	5	6735	6753	225
2	13	7	1538+	244	832
2	14	0	6287	6404	142
2	14	2	5411	5572	142
2	14	4	5095	5216	151
2	14	6	4952	5194	181
2	14	8	4771	4919	225
3	3	6	3873	4138	370
3	3	7	8224	8054	167
3	3	7	1139+	132	458
3	3	7	7427	7529	173
3	3	7	351+	61	818
3	3	7	4656	5037	260
3	3	8	5724	5731	151
3	3	8	4845	5143	159
3	3	8	4672	4616	175
3	3	8	4266	4159	217
3	3	9	5798	5858	164
3	3	9	1352+	47	491
4	4	0	153385	149556	296
4	4	4	121860	119444	236
4	4	8	98825	100067	225
4	4	12	7166	6830	442
4	5	1	8098	7823	162
4	5	3	6930	6797	148
4	5	5	7007	6933	156
4	5	7	6688	6515	162
4	5	9	4974	5128	206
4	5	11	3903	4199	346
4	6	0	95700	94995	200
4	6	2	2+	138	686
4	6	4	8089	8121	167
4	6	6	486+	110	631
4	6	8	6925	6933	178
4	6	10	2+	19	1038
4	7	1	5699	5665	145
4	7	3	5351	5255	148
4	7	5	5046	5062	156
4	7	7	4848	4650	181
4	7	9	3683	3723	263
4	8	0	7018	6778	189
4	8	2	1170+	114	483
4	8	4	5999	5994	164
4	8	6	560+	38	689
4	9	1	3582	3497	197
4	9	3	3054	3320	236
5	5	2	108640	104740	217
5	5	6	9089	8976	206
5	5	10	6329	6297	274
5	6	1	6930	6792	153
5	6	5	6210	6203	151
5	6	5	5837	5807	159
5	6	7	5370	5306	173
5	6	9	4219	4214	233
5	7	2	7120	7057	159
5	7	4	1211+	75	866
5	7	6	6123	6070	170
5	7	8	876+	22	666
5	8	3	4065	3657	173
5	8	3	3516	3390	192
5	8	5	3258	3239	227
6	6	0	81420	84490	230
6	6	4	73550	73120	197
6	6	8	62227	57900	236
6	7	1	4065	4164	270
6	7	3	4027	3937	175
6	7	5	3867	3765	192
6	8	0	4101	4118	249
7	7	2	4562	4435	230
8	0	10	4258	3560	428

TABLE 6. OBSERVED AND CALCULATED STRUCTURE FACTORS OF HG3-6TAF6 AT 150K

(UNOBSERVED REFLECTIONS ARE MARKED +)

H	K	L	FO	FC	SIG	H	K	L	FO	FC	SIG	H	K	L	FO	FC	SIG
0	0	4	3550	3327	156	0	6	2	2051	2078	87	1	6	7	1038	1080	46
0	0	8	6884	6503	293	0	7	3	2563	2655	109	1	6	9	834	952	41
0	0	12	1767	1786	76	0	7	5	2451	2584	104	1	6	11	935	848	41
0	0	16	3055	3110	130	0	7	7	552	532	31	1	7	4	134+	13	53
0	1	1	1430	1511	63	0	7	9	554	517	33	1	7	6	1315	1383	57
0	1	3	4523	4474	192	0	7	11	1669	1717	72	1	7	8	39+	7	101
0	1	5	4621	4553	196	0	7	1	757	765	35	1	7	10	[illegible]	896	41
0	1	7	1030	1071	48	0	8	4	550	519	31	1	8	3	740	715	34
0	1	9	1006	1031	46	0	8	6	1258	1256	55	1	8	5	653	675	34
0	1	11	2988	3020	123	0	8	8	1933	2011	83	1	8	7	695	700	76
0	1	13	2413	2504	103	0	8	0	2522	2577	108	1	8	9	[illegible]	654	36
0	1	15	524	487	33	0	8	2	1421	1436	61	1	9	4	158+	6	70
0	2	2	3379	3382	143	0	9	5	1647	1711	71	1	9	6	900	941	42
0	2	4	1988	2048	82	0	9	1	646	616	34	1	6	1	1441	1393	61
0	2	6	2567	2838	113	0	9	3	1705	1741	73	1	7	2	1400	1350	60
0	2	8	3911	3902	166	1	1	2	2493	2440	106	1	8	1	932	860	39
0	2	10	2056	2019	88	1	1	6	2949	2665	127	1	9	2	939	931	42
0	2	12	514	488	36	1	1	10	1241	1282	57	2	2	0	3233	3022	139
0	2	14	1263	1273	55	1	1	14	1386	1440	61	2	2	4	2026	2065	86
0	2	16	1363	1347	80	1	2	1	1880	1750	80	2	2	8	2055	2011	90
0	2	0	5435	4720	139	1	2	3	1089	1180	46	2	2	12	1350	1334	64
0	3	3	3633	3684	154	1	2	5	1235	1301	53	2	3	1	2130	2039	92
0	3	5	3456	3574	147	1	2	7	1470	1358	64	2	3	3	1594	1608	67
0	3	7	1400	1528	60	1	2	9	1082	1039	52	2	3	5	1492	1574	63
0	3	9	1217	1256	53	1	2	11	1029	995	48	2	3	7	1428	1484	61
0	3	11	2597	2513	111	1	2	13	896	875	42	2	3	9	1372	1237	58
0	3	13	2107	2049	90	1	2	15	585	582	35	2	3	11	1249	1116	60
0	3	15	604	594	37	1	3	2	1661	1620	70	2	3	13	939	898	48
0	3	1	2242	2264	95	1	3	4	0+	45	86	2	3	15	570	603	40
0	4	2	2779	2806	118	1	3	6	1916	2002	82	2	4	0	2450	2378	104
0	4	4	1195	1250	51	1	3	8	253+	54	63	2	4	2	22+	29	60
0	4	6	2270	2388	96	1	3	10	1025	950	48	2	4	4	1750	1733	74
0	4	8	3339	3499	142	1	3	12	223+	50	78	2	4	6	170+	14	50
0	4	10	1701	1731	73	1	3	14	1274	1253	56	2	4	8	1594	1662	68
0	4	12	383+	283	47	1	4	1	1672	1555	71	2	4	10	136+	30	133
0	4	14	1247	1158	56	1	4	3	1123	1144	48	2	4	12	1306	1190	60
0	4	0	4837	4668	796	1	4	5	1140	[illegible]	49	2	4	14	317+	29	64
0	5	3	3606	3688	153	1	4	7	1173	1213	51	2	5	1	1235	1154	55
0	5	5	3459	3589	147	1	4	9	986	1016	45	2	5	3	966	915	42
0	5	7	505	580	31	1	4	11	934	899	44	2	5	5	1042	1052	45
0	5	9	701	712	35	1	4	13	807	763	43	2	5	7	1073	1049	45
0	5	11	2210	2272	94	1	5	2	1990	1901	84	2	5	9	713	738	37
0	5	13	2049	2030	88	1	5	4	78+	25	69	2	5	11	591	693	42
0	5	[illegible]	902	909	39	1	5	6	1815	1888	77	2	5	13	825	764	45
0	6	4	292	260	33	1	5	8	151+	36	65	2	6	0	1507	1461	68
0	6	6	1736	1768	74	1	5	10	1134	1185	50	2	6	2	104+	52	46
0	6	8	1939	3141	127	1	5	12	136+	65	94	2	6	4	1148	1137	49
0	6	10	1321	1362	57	1	5	14	1066	1084	50	2	6	6	24+	14	88
0	6	12	243+	106	58	1	6	3	1146	1130	49	2	6	8	1121	1143	49
0	6	0	4279	4232	569	1	6	5	1047	1083	46	2	6	10	157+	6	95

TABLE 6. OBSERVED AND CALCULATED STRUCTURE FACTORS OF HG3-STAF6 AT 150K

(UNOBSERVED REFLECTIONS ARE MARKED +)

H	K	L	FO	FC	SIG	H	K	L	FO	FC	SIG	H	K	L	FO	FC	SIG
2	6	12	876	875	45	3	6	1	930	877	42	4	6	10	37+	2	95
2	7	1	1047	967	45	3	6	3	683	706	31	4	7	1	949	899	41
2	7	3	890	850	39	3	6	5	632	675	30	4	7	3	835	803	37
2	7	5	879	880	39	3	6	7	631	704	32	4	7	5	828	810	37
2	7	7	830	862	39	3	6	9	713	701	37	4	7	7	808	793	37
2	7	9	676	673	37	3	6	11	568	647	46	4	7	9	645	656	35
2	7	11	661	637	41	3	7	2	1229	1196	53	4	8	0	1255	1196	55
2	8	2	110+	52	54	3	7	4	185+	17	45	4	8	2	105+	32	62
2	8	4	1180	1182	51	3	7	6	1206	1250	52	4	8	4	1038	1042	45
2	8	6	263+	22	62	3	7	8	312+	12	49	4	8	6	0+	13	104
2	8	8	1013	1084	47	3	7	10	774	799	41	4	9	1	739	682	34
2	9	3	820	739	37	3	8	1	912	1007	41	4	5	2	1608	1591	69
2	9	5	734	773	36	3	8	3	885	884	40	4	5	6	1398	1420	60
2	8	0	1473	1389	63	3	8	5	770	814	36	4	5	10	1050	1072	51
2	9	1	875	818	39	3	8	7	762	786	37	4	6	1	1111	1087	48
3	3	2	2577	2487	110	3	9	2	1112	1114	48	4	6	3	970	944	42
3	3	6	2375	2538	101	3	9	4	57+	8	84	4	6	5	969	951	42
3	3	10	1369	1293	65	4	4	0	2019	1909	86	4	6	7	909	941	41
3	3	14	1461	1408	68	4	4	4	1519	1473	65	4	6	9	723	743	36
3	4	1	1713	1558	73	4	4	8	1370	1395	60	4	7	2	1131	1141	51
3	4	3	1263	1266	54	4	4	12	1194	1066	66	4	7	4	37+	27	60
3	4	5	1132	1198	49	4	5	1	1137	1067	48	4	7	6	1067	1086	47
3	4	7	1155	1195	50	4	5	3	924	876	40	4	7	8	154+	25	61
3	4	9	1051	1050	47	4	5	5	976	958	42	4	8	1	657	653	31
3	4	11	1029	943	51	4	5	7	928	956	41	4	8	3	573	571	30
3	4	13	844	723	57	4	5	9	710	728	35	4	8	5	570	584	31
3	5	2	1268	1224	54	4	5	11	637	636	42	4	6	0	1488	1426	65
3	5	4	0+	40	87	4	6	0	1485	1393	64	4	6	4	1245	1256	54
3	5	6	1319	1355	56	4	6	2	0+	18	81	4	6	8	1034	1109	48
3	5	8	229+	89	58	4	6	4	1183	1152	51	4	7	1	773	764	35
3	5	10	869	850	43	4	6	6	67+	16	71	4	7	3	688	683	32
3	5	12	162+	82	122	4	6	8	1080	1085	47	4	7	5	678	682	33

TABLE 7 . OBSERVED AND CALCULATED STRUCTURE FACTORS FOR HG4(TA,F11)2.

H	K	L	FO	FC	SIG	H	K	L	FO	FC	SIG	H	K	L	FO	FC	SIG
2	0	0	1107	777	29	2	6	0	634	621	23	11	4	1	1131	1178	29
4	0	0	3939	3963	91	4	6	0	222	148	40	13	4	1	512	483	22
6	0	0	1093	1098	32	6	6	0	555	525	21	15	4	1	876	888	23
8	0	0	1913	1995	46	8	6	0	884	938	23	17	4	1	311	291	26
10	0	0	783	798	28	10	6	0	582	593	20	19	4	1	147	36	46
12	0	0	769	777	28	12	6	0	181	156	38	21	4	1	270	292	22
14	0	0	998	1016	31	14	6	0	1057	1051	26	0	5	1	1170	1129	28
16	0	0	262	348	56	16	6	0	52	38	75	2	5	1	1098	1092	26
18	0	0	280	256	46	18	6	0	341	340	20	4	5	1	1435	1467	33
20	0	0	1381	1269	34	1	7	0	441	370	23	6	5	1	918	911	24
22	0	0	896	857	25	3	7	0	750	718	22	8	5	1	1258	1292	30
24	0	0	650	621	21	5	7	0	676	634	21	10	5	1	635	673	21
1	1	0	922	908	22	7	7	0	953	975	24	12	5	1	140	173	57
3	1	0	656	649	17	9	7	0	282	305	26	14	5	1	355	320	24
5	1	0	1073	1017	26	11	7	0	176	174	41	16	5	1	210	221	36
7	1	0	495	479	24	13	7	0	140	165	40	18	5	1	379	385	20
9	1	0	753	762	22	15	7	0	469	455	18	20	5	1	235	236	26
11	1	0	153	54	63	0	8	0	263	237	28	1	6	1	737	748	23
13	1	0	111	186	69	2	8	0	312	290	25	3	6	1	1376	1367	33
15	1	0	597	582	25	4	8	0	359	322	23	5	6	1	483	490	22
17	1	0	0	67	126	6	8	0	386	377	21	7	6	1	591	631	20
19	1	0	242	243	34	8	8	0	467	454	19	9	6	1	337	357	25
21	1	0	200	145	35	10	8	0	466	461	18	11	6	1	951	949	24
23	1	0	110	94	57	12	8	0	161	35	38	13	6	1	183	174	39
0	2	0	8479	8093	192	1	9	0	92	7	56	15	6	1	763	763	21
2	2	0	554	493	18	3	9	0	374	329	19	17	6	1	124	77	46
4	2	0	2525	2467	58	5	9	0	132	84	43	19	6	1	99	65	53
6	2	0	257	245	28	7	9	0	616	565	18	0	7	1	491	480	22
8	2	0	1642	1635	38	9	9	0	131	88	41	2	7	1	933	892	23
10	2	0	148	135	57	0	1	1	2351	2218	54	4	7	1	425	410	22
12	2	0	403	427	24	2	1	1	114	103	50	6	7	1	219	233	35
14	2	0	1370	1410	33	4	1	1	5172	5118	118	8	7	1	314	317	24
16	2	0	280	300	36	6	1	1	4052	4027	93	10	7	1	248	205	28
18	2	0	113	22	65	8	1	1	5106	5304	117	12	7	1	337	332	21
20	2	0	968	936	24	10	1	1	2083	2160	48	14	7	1	38	82	79
22	2	0	771	763	21	12	1	1	1612	1627	37	16	7	1	293	263	21
1	3	0	362	362	24	14	1	1	1125	1141	29	1	8	1	712	665	20
3	3	0	1023	1045	24	16	1	1	497	531	25	3	8	1	522	494	19
5	3	0	1709	1727	39	18	1	1	215	136	39	5	8	1	378	336	21
7	3	0	1396	1398	32	20	1	1	145	66	55	7	8	1	247	239	27
9	3	0	1416	1394	33	22	1	1	418	392	20	9	8	1	135	165	30
11	3	0	269	216	29	1	2	1	292	187	27	11	8	1	434	510	18
13	3	0	220	212	41	3	2	1	2014	1881	46	13	8	1	150	94	39
15	3	0	912	948	24	5	2	1	248	285	27	0	9	1	245	244	24
17	3	0	73	105	76	7	2	1	613	612	19	2	9	1	655	597	19
19	3	0	456	485	20	9	2	1	741	695	21	4	9	1	147	13	46
21	3	0	168	223	35	11	2	1	1055	1102	26	6	9	1	32	89	57
0	4	0	4683	4607	107	13	2	1	249	229	41	8	9	1	170	101	30
2	4	0	378	359	23	15	2	1	631	654	23	0	0	2	1045	1046	29
4	4	0	914	901	23	17	2	1	234	299	38	2	0	2	314	277	24
6	4	0	175	215	38	19	2	1	172	21	49	4	0	2	1541	1422	37
8	4	0	1307	1401	31	21	2	1	206	240	34	6	0	2	3156	3250	74
10	4	0	349	372	29	23	2	1	212	200	27	8	0	2	136	224	77
12	4	0	245	239	37	0	3	1	3342	3113	76	10	0	2	1294	1354	32
14	4	0	1325	1301	31	2	3	1	1097	1067	26	12	0	2	2097	2193	49
16	4	0	235	179	33	4	3	1	3130	3143	72	14	0	2	3956	4098	94
18	4	0	217	205	32	6	3	1	2712	2757	62	16	0	2	1175	1093	31
20	4	0	481	534	18	8	3	1	3668	3691	84	18	0	2	854	858	27
22	4	0	357	395	18	10	3	1	1651	1729	38	20	0	2	753	780	26
1	5	0	822	781	22	12	3	1	388	418	27	22	0	2	58	44	99
3	5	0	1099	1088	26	14	3	1	860	813	24	1	1	2	752	665	19
5	5	0	1626	1607	37	16	3	1	72	47	79	3	1	2	847	206	21
7	5	0	1175	1229	28	18	3	1	307	317	26	5	1	2	359	236	24
9	5	0	1060	1067	26	20	3	1	117	134	53	7	1	2	218	216	39
11	5	0	277	229	30	22	3	1	394	413	18	[illegible]	1	2	272	242	32
13	5	0	22	164	99	1	4	1	294	260	27	11	1	2	537	537	22
15	5	0	905	876	23	3	4	1	2222	2193	51	13	1	2	314	353	37
17	5	0	203	228	34	5	4	1	360	351	22	15	1	2	435	405	29
19	5	0	531	548	18	7	4	1	1473	1481	34	17	1	2	0	75	123
0	6	0	1344	1889	45	9	4	1	620	606	19	19	1	2	259	246	31

TABLE 7. OBSERVED AND CALCULATED STRUCTURE FACTORS FOR HG4(TA... 1112.

H	K	L	FO	FC	SIG	H	K	L	FO	FC	SIG	H	K	L	FO	FC	SIG	H	K	L	FO	FC	SIG
21	1	2	0	25	11	12	8	2	0	134	96	13	6	3	462	473	29						
23	1	2	176	159	33	1	9	2	344	348	19	15	6	3	444	459	19						
0	2	2	1739	1645	40	3	9	2	118	124	48	17	6	3	303	282	22						
2	2	2	280	225	28	5	9	2	308	298	20	0	7	3	317	295	25						
4	2	2	1108	1052	26	7	9	2	403	387	17	2	7	3	238	247	25						
6	2	2	3177	3121	73	9	9	2	215	231	23	4	7	3	617	641	19						
8	2	2	699	710	20	0	1	3	4559	4580	104	6	7	3	563	565	19						
10	2	2	974	1007	24	2	1	3	5041	5045	115	8	7	3	538	618	19						
12	2	2	1650	1630	38	4	1	3	1240	1236	29	10	7	3	340	326	22						
14	2	2	2883	3005	67	6	1	3	2246	2215	52	12	7	3	755	745	20						
16	2	2	742	729	22	8	1	3	701	748	21	14	7	3	498	501	18						
18	2	2	664	637	21	10	1	3	1146	1173	28	16	7	3	474	479	17						
20	2	2	528	552	20	12	1	3	358	380	26	1	8	3	186	199	41						
22	2	2	94	51	61	14	1	3	1281	1281	31	3	8	3	656	685	19						
1	3	3	928	905	23	16	1	3	585	586	23	5	8	3	590	598	18						
3	3	3	205	53	35	18	1	3	1280	1240	31	7	8	3	644	637	19						
5	3	3	1037	1041	20	20	1	3	181	199	40	9	8	3	372	372	19						
7	3	3	1625	1603	37	22	1	3	1035	1010	25	11	8	3	0	93	97						
9	3	3	672	659	19	1	2	3	676	631	19	13	8	3	76	38	54						
11	3	3	981	1002	25	3	2	3	1914	1851	44	0	9	3	115	69	48						
13	3	3	170	37	54	5	2	3	1450	1361	34	2	9	3	121	152	40						
15	3	3	611	585	21	7	2	3	1700	1714	39	4	9	3	287	315	29						
17	3	3	154	23	55	9	2	3	226	158	32	6	9	3	285	250	19						
19	3	3	620	650	19	11	2	3	268	242	31	8	9	3	399	386	16						
21	3	3	79	46	65	13	2	3	810	815	24	0	0	4	257	54	68						
0	4	4	1629	1578	38	15	2	3	283	319	34	2	0	4	2656	2575	62						
2	4	4	500	512	19	17	2	3	439	491	23	4	0	4	331	295	30						
4	4	4	1551	1051	51	19	2	3	180	184	39	6	0	4	6479	6560	147						
6	4	4	2693	2792	62	21	2	3	149	91	42	8	0	4	364	351	31						
8	4	4	507	488	19	23	2	3	218	226	26	10	0	4	2287	2413	54						
10	4	4	221	157	43	0	3	3	2343	2422	54	12	0	4	1152	1207	30						
12	4	4	772	769	22	2	3	3	3158	3138	72	14	0	4	532	570	33						
14	4	4	1759	1757	41	4	3	3	800	806	21	16	0	4	355	353	39						
16	4	4	263	271	30	6	3	3	1071	1053	26	18	0	4	677	682	27						
18	4	4	293	298	24	8	3	3	84	7	70	20	0	4	642	635	25						
20	4	4	255	219	26	10	3	3	883	908	22	22	0	4	201	56	54						
1	5	5	746	767	21	12	3	3	585	594	22	1	1	4	833	764	23						
3	5	5	249	241	29	14	3	3	1215	1218	29	3	1	4	130	128	49						
5	5	5	926	907	24	16	3	3	602	610	21	5	1	4	980	947	24						
7	5	5	1463	1486	34	18	3	3	764	774	21	7	1	4	193	214	36						
9	5	5	704	679	21	20	3	3	100	155	57	9	1	4	724	740	21						
11	5	5	939	910	24	22	3	3	648	671	18	11	1	4	521	494	21						
13	5	5	174	67	41	1	4	3	704	692	20	13	1	4	513	525	32						
15	5	5	671	659	20	3	4	3	2292	2316	52	15	1	4	323	326	32						
17	5	5	49	28	77	5	4	3	737	721	20	17	1	4	95	47	74						
19	5	5	633	666	19	7	4	3	2276	2306	52	19	1	4	95	177	70						
0	6	6	1625	1667	38	9	4	3	209	171	42	21	1	4	0	68	109						
2	6	6	476	441	23	11	4	3	319	314	29	23	1	4	129	45	42						
4	6	6	710	698	21	13	4	3	812	799	22	0	2	4	234	182	31						
6	6	6	1735	1749	40	15	4	3	397	408	23	2	2	4	1731	1711	40						
8	6	6	490	506	21	17	4	3	474	486	20	4	2	4	929	884	23						
10	6	6	510	510	20	19	4	3	358	367	21	6	2	4	6283	6416	143						
12	6	6	468	500	20	21	4	3	202	209	27	8	2	4	181	82	50						
14	6	6	601	567	19	0	5	3	1361	1401	32	10	2	4	1822	1835	42						
16	6	6	135	9	45	2	5	3	1222	1223	29	12	2	4	898	896	24						
18	6	6	32	32	77	4	5	3	624	601	19	14	2	4	159	178	43						
1	7	7	133	14	56	6	5	3	935	938	24	16	2	4	268	248	33						
3	7	7	253	168	30	8	5	3	691	693	21	18	2	4	610	570	29						
5	7	7	94	9	66	10	5	3	621	600	21	20	2	4	601	598	19						
7	7	7	859	868	22	12	5	3	866	839	23	22	2	4	135	90	35						
9	7	7	84	37	64	14	5	3	802	784	22	1	3	4	1877	1899	43						
11	7	7	628	608	19	16	5	3	678	679	20	3	3	4	1038	1009	25						
13	7	7	176	172	34	18	5	3	250	267	26	5	3	4	1229	1212	29						
15	7	7	350	355	19	20	5	3	106	23	51	7	3	4	1036	1036	25						
0	8	8	954	951	24	1	6	3	157	169	52	9	3	4	988	989	24						
2	8	8	388	381	21	3	6	3	1476	1506	35	11	3	4	1160	1142	28						
4	8	8	440	404	19	5	6	3	635	661	21	13	3	4	854	857	23						
6	8	8	911	925	23	7	6	3	1384	1416	33	15	3	4	662	674	21						
8	8	8	280	287	23	9	6	3	65	161	77	17	3	4	116	70	59						
10	8	8	408	405	18	11	6	3	44	76	84	19	3	4	246	284	39						

TABLE 7. OBSERVED AND CALCULATED STRUCTURE FACTORS FOR HG4(TA2F11)2.

H	K	L	FO	FC	SIG	H	K	L	FO	FC	SIG	H	K	L	FO	FC	SIG
21	3	4	296	313	22	15	2	5	175	207	46	16	0	6	445	416	32
0	4	4	679	692	19	17	2	5	646	613	21	18	0	6	429	439	31
2	4	4	418	398	21	19	2	5	201	182	43	20	0	6	1127	1099	29
4	4	4	756	780	20	21	2	5	364	378	21	22	0	6	298	312	31
6	4	4	3427	3522	78	0	3	5	884	886	22	1	1	6	740	762	23
8	4	4	305	298	30	2	3	5	1637	1629	38	3	1	6	227	54	50
10	4	4	742	709	22	4	3	5	1897	1886	44	5	1	6	1232	1168	29
12	4	4	289	302	29	6	3	5	1444	1459	33	7	1	6	182	130	37
14	4	4	140	113	52	8	3	5	945	889	23	9	1	6	348	332	23
16	4	4	217	146	32	10	3	5	1521	1564	36	11	1	6	337	360	30
18	4	4	304	338	23	12	3	5	1445	1460	34	13	1	6	282	291	34
20	4	4	608	644	18	14	3	5	1330	1327	32	15	1	6	202	200	47
1	5	4	1071	1053	26	16	3	5	432	421	21	17	1	6	206	124	47
3	5	4	804	787	23	18	3	5	596	563	19	19	1	6	0	45	112
5	5	4	468	461	23	20	3	5	292	261	23	21	1	6	133	83	60
7	5	4	758	771	22	1	4	5	865	884	22	0	2	6	2933	2899	65
9	5	4	869	848	23	3	4	5	736	742	20	2	2	6	2130	2229	50
11	5	4	1024	1005	25	5	4	5	919	908	23	4	2	6	559	582	19
13	5	4	898	887	23	7	4	5	227	197	41	6	2	6	448	465	20
15	5	4	621	590	20	9	4	5	882	893	24	8	2	6	277	268	27
17	5	4	156	138	37	11	4	5	156	176	49	10	2	6	1009	1020	26
19	5	4	155	155	34	13	4	5	546	523	21	12	2	6	1942	1952	45
0	6	4	960	984	24	15	4	5	319	297	24	14	2	6	139	20	52
2	6	4	115	127	59	17	4	5	786	767	21	16	2	6	233	265	28
4	6	4	512	516	21	19	4	5	223	198	26	18	2	6	502	479	20
6	6	4	1174	1158	28	0	5	5	676	678	22	20	2	6	1019	965	25
8	6	4	145	34	47	2	5	5	316	251	30	22	2	6	321	320	20
10	6	4	18	80	97	4	5	5	1599	1620	37	1	3	6	2133	2152	50
12	6	4	140	75	43	6	5	5	849	873	23	3	3	6	656	639	19
14	6	4	278	284	26	8	5	5	1120	1122	27	5	3	6	2458	2427	56
16	6	4	345	321	21	10	5	5	783	809	22	7	3	6	706	723	20
18	6	4	176	55	39	12	5	5	475	425	20	9	3	6	757	803	22
1	7	4	354	354	23	14	5	5	724	708	21	11	3	6	746	752	22
3	7	4	590	609	19	16	5	5	164	132	39	13	3	6	381	400	24
5	7	4	125	153	48	18	5	5	162	104	43	15	3	6	435	443	21
7	7	4	370	366	22	1	6	5	649	656	21	17	3	6	355	371	22
9	7	4	466	485	19	3	6	5	221	233	36	19	3	6	148	80	38
11	7	4	573	565	19	5	6	5	555	542	20	21	3	6	311	318	20
13	7	4	612	612	18	7	6	5	288	273	27	0	4	6	1159	1170	28
15	7	4	238	261	25	9	6	5	616	620	20	2	4	6	713	714	20
0	8	4	668	699	19	11	6	5	385	357	22	4	4	6	272	272	27
2	8	4	267	275	25	13	6	5	382	372	22	6	4	6	319	286	30
4	8	4	429	438	18	15	6	5	327	334	22	8	4	6	551	507	22
6	8	4	212	182	29	17	6	5	517	516	17	10	4	6	327	279	27
8	8	4	119	17	48	0	7	5	618	639	19	12	4	6	1585	1567	37
10	8	4	235	277	24	2	7	5	135	153	46	14	4	6	257	239	29
12	8	4	118	96	44	4	7	5	1120	1128	27	16	4	6	177	135	36
1	9	4	160	112	29	6	7	5	303	272	26	18	4	6	349	368	20
3	9	4	295	326	20	8	7	5	995	979	24	20	4	6	428	457	17
5	9	4	103	122	41	10	7	5	258	258	26	1	5	6	1503	1509	36
7	9	4	174	140	28	12	7	5	90	89	56	3	5	6	465	431	23
0	1	5	290	297	36	14	7	5	131	107	38	5	5	6	[illegible]	2054	46
2	1	5	791	821	41	1	8	5	498	545	17	7	5	6	356	350	26
4	1	5	1001	1028	25	3	8	5	162	170	34	9	5	6	[illegible]	698	21
6	1	5	2377	2455	54	5	8	5	191	190	31	11	5	6	[illegible]	374	25
8	1	5	386	417	22	7	8	5	354	377	19	13	5	6	354	330	23
10	1	5	2281	2325	52	9	8	5	142	175	36	15	5	6	227	184	29
12	1	5	2001	2046	47	11	8	5	294	289	20	17	5	6	291	307	22
14	1	5	2337	2330	54	0	9	5	281	326	18	19	5	6	118	20	38
16	1	5	722	722	22	2	9	5	126	116	43	0	6	6	171	112	55
18	1	5	840	839	23	4	9	5	575	596	17	2	6	6	142	151	51
20	1	5	372	373	23	6	9	5	150	61	31	4	6	6	256	305	30
22	1	5	470	476	18	0	0	6	2461	2527	58	6	6	6	548	593	20
1	2	5	613	590	19	2	0	6	1966	2010	46	8	6	6	353	369	23
3	2	5	702	706	19	4	0	6	753	751	24	10	6	6	218	191	33
5	2	5	846	839	22	6	0	6	305	334	31	12	6	6	1098	1086	26
7	2	5	246	298	29	8	0	6	240	254	36	14	6	6	442	402	19
9	2	5	832	846	22	10	0	6	1268	1218	31	16	6	6	239	235	25
11	2	5	0	75	127	12	0	6	2185	2270	52	1	7	6	395	914	23
13	2	5	692	697	23	14	0	6	113	194	89	3	7	6	156	142	43

TABLE 7 . OBSERVED AND CALCULATED STRUCTURE FACTORS FOR HG4(TAF11)2.

H	K	L	FO	FC	SIG	H	K	L	FO	FC	SIG	H	K	L	FO	FC	SIG
5	7	6	1256	1275	30	5	6	7	371	377	23	12	4	8	1228	1234	29
7	7	6	145	26	40	7	6	7	148	135	43	14	4	8	140	137	43
9	7	6	348	365	21	9	6	7	1057	1063	26	16	4	8	307	291	28
11	7	6	47	65	76	11	6	7	331	338	23	18	4	8	390	359	28
13	7	6	280	301	22	13	6	7	852	879	22		5	8	352	878	33
0	8	6	75	131	59	15	6	7	139	121	40	1	5	8	434	375	24
2	8	6	332	310	20	0	7	7	846	886	22	3	5	8	177	253	45
4	8	6	1195	212	30	2	7	7	650	673	20	5	5	8	337	333	27
6	8	6	503	518	18	4	7	7	30	59	86	7	5	8	352	314	22
8	8	6	215	225	26	6	7	7	359	356	21	9	5	8	255	233	22
10	8	6	330	302	19	8	7	7	241	195	26	11	5	8	354	352	22
1	9	6	329	325	17	10	7	7	74	83	57	13	5	8	376	375	25
3	9	6	32	8	70	12	7	7	296	306	21	15	5	8	455	450	24
5	9	6	499	511	26	14	7	7	244	221	23	17	5	8	127	119	52
0	1	7	752	759	24	1	8	7	312	277	22	0	6	8	592	565	20
2	1	7	1963	2033	45	3	8	7	314	274	21	2	6	8	1133	1198	28
4	1	7	6632	4877	106	5	8	7	144	134	37	4	6	8	759	759	17
6	1	7	2134	2085	49	7	8	7	54	37	63	6	6	8	135	194	27
8	1	7	2439	2500	56	9	8	7	422	421	17	10	6	8	451	443	19
10	1	7	1034	1050	26	0	9	7	391	434	16	12	6	8	345	366	17
12	1	7	239	153	41	2	9	7	244	285	22	14	6	8	125	108	29
14	1	7	734	734	22	0	0	8	1460	1518	37	1	7	8	452	466	24
16	1	7	855	836	23	2	0	8	736	763	27	3	7	8	126	31	32
18	1	7	173	50	49	4	0	8	3848	4055	90	5	7	8	279	267	24
20	1	7	539	497	19	6	0	8	343	260	36	7	7	8	133	80	32
22	1	7	53	122	69	8	0	8	702	710	23	9	7	8	229	206	27
1	2	7	553	545	21	10	0	8	195	128	53	11	7	8	144	47	28
3	2	7	653	643	20	12	0	8	2729	2729	65	13	7	8	222	252	24
5	2	7	668	678	20	14	0	8	88	35	92	15	7	8	0	59	18
7	2	7	438	440	21	16	0	8	954	927	27	0	8	8	528	490	18
9	2	7	1057	1100	27	18	0	8	535	520	26	2	8	8	450	456	18
11	2	7	156	114	51	20	0	8	425	427	26	4	8	8	531	603	21
13	2	7	974	985	25	1	1	8	502	525	26	6	8	8	239	149	27
15	2	7	0	49	113	3	1	8	409	421	27	8	1	9	2331	3053	66
17	2	7	315	332	25	5	1	8	32	31	103	0	1	9	351	340	32
19	2	7	219	216	31	7	1	8	542	561	20	2	1	9	613	616	23
21	2	7	162	51	43	9	1	8	0	10	117	4	1	9	266	234	32
0	3	7	667	675	21	11	1	8	151	49	49	6	1	9	1959	2033	46
2	3	7	1761	1842	41	13	1	8	305	244	28	8	1	9	1129	1168	27
4	3	7	3092	3201	71	15	1	8	190	148	40	10	1	9	1226	1193	29
6	3	7	1952	1950	45	17	1	8	185	226	42	12	1	9	411	373	22
8	3	7	1607	1632	38	19	1	8	226	162	30	14	1	9	557	542	20
10	3	7	603	603	21	21	1	8	135	135	42	16	1	9	730	699	20
12	3	7	299	284	27	0	2	8	1291	1348	31	18	1	9	530	554	20
14	3	7	117	44	22	2	2	8	421	389	24	20	1	9	911	945	25
16	3	7	692	679	20	4	2	8	3251	3403	74	1	2	9	1228	1238	30
18	3	7	160	203	36	6	2	8	312	313	26	3	2	9	1057	1103	26
20	3	7	406	412	18	8	2	8	653	664	22	5	2	9	354	380	30
1	4	7	627	636	20	10	2	8	122	72	67	7	2	9	758	745	23
3	4	7	206	218	42	12	2	8	2205	2282	51	9	2	9	263	227	34
5	4	7	603	612	22	14	2	8	0	82	115	11	2	9	317	259	26
7	4	7	187	64	43	16	2	8	806	776	22	13	2	9	233	244	31
9	4	7	1412	1467	33	18	2	8	523	525	19	15	2	9	30	44	56
11	4	7	1442	1454	22	20	2	8	368	385	20	17	2	9	207	168	29
13	4	7	1237	1231	29	1	3	8	1236	1262	29	19	2	9	1994	1969	47
15	4	7	0	107	105	3	3	8	670	656	20	0	3	9	218	197	43
17	4	7	372	354	20	5	3	8	36	89	104	2	3	9	297	258	35
19	4	7	189	229	29	7	3	8	612	659	21	4	3	9	41	44	51
0	5	7	1062	1087	27	9	3	8	0	26	122	6	3	9	1156	1123	28
2	5	7	1089	1113	27	11	3	8	422	420	23	8	3	9	994	979	25
4	5	7	1290	1295	31	13	3	8	316	314	25	10	3	9	816	810	22
6	5	7	877	886	23	15	3	8	531	518	19	12	3	9	457	445	21
8	5	7	459	473	21	17	3	8	526	519	18	14	3	9	440	420	19
10	5	7	283	263	28	19	3	8	405	406	18	16	3	9	301	314	22
12	5	7	405	385	21	0	4	8	397	430	29	18	3	9	398	938	25
14	5	7	166	17	46	2	4	8	280	311	34	1	4	9	1282	1285	31
16	5	7	385	379	19	4	4	8	2070	2102	48	3	4	9	1211	1221	29
18	5	7	366	346	18	6	4	8	737	767	22	5	4	9	677	714	21
1	6	7	422	456	23	8	4	8	251	303	33	7	4	9	611	638	21
3	6	7	153	35	51	10	4	8	313	352	27	11	4	9	231	216	31

H	K	L	FO	FC	SIG	H	K	L	FO	FC	SIG	H	K	L	FO	FC	SIG
13	4	9	294	289	26	17	3	10	261	245	24	2	5	11	1221	1209	29
15	4	9	241	255	27	0	4	10	532	553	24	4	5	11	87	88	89
17	4	9	112	8	47	2	4	10	265	241	35	6	5	11	636	689	20
0	5	9	520	503	22	4	4	10	1662	1693	39	8	5	11	522	537	19
2	5	9	169	126	51	6	4	10	361	354	25	10	5	11	337	285	22
4	5	9	45	430	23	8	4	10	601	567	20	12	5	11	349	368	20
6	5	9	171	109	55	10	4	10	492	506	20	14	5	11	57	3	62
8	5	9	462	489	21	12	4	10	240	247	30	1	6	11	148	141	49
10	5	9	869	894	23	14	4	10	199	187	31	3	6	11	86	76	69
12	5	9	327	347	23	16	4	10	207	213	27	5	6	11	97	99	67
14	5	9	580	554	19	1	5	10	244	255	34	7	6	11	37	67	54
16	5	9	255	242	23	3	5	10	245	265	33	9	6	11	38	21	54
1	6	9	712	698	21	5	5	10	140	71	52	11	6	11	56	95	61
3	6	9	1157	1145	28	7	5	10	923	938	24	0	7	11	210	175	26
5	6	9	885	901	23	9	5	10	207	216	32	2	7	11	645	634	19
7	6	9	606	644	19	11	5	10	1074	1106	26	4	7	11	199	223	30
9	6	9	321	336	22	13	5	10	187	197	34	6	7	11	502	485	19
11	6	9	73	86	61	15	5	10	402	408	18	8	7	11	377	372	19
13	6	9	107	60	44	0	6	10	340	272	25	1	8	11	55	103	96
15	6	9	188	104	28	2	6	10	406	406	22	0	0	12	778	768	38
0	7	9	172	77	42	4	6	10	767	757	21	2	0	12	419	341	46
2	7	9	135	159	43	6	6	10	107	105	56	4	0	12	670	694	31
4	7	9	513	542	19	8	6	10	113	43	47	6	0	12	1331	1343	34
6	7	9	216	171	34	10	6	10	385	363	19	8	0	12	551	598	30
8	7	9	189	13	31	12	6	10	65	109	67	10	0	12	1854	1847	45
10	7	9	532	636	18	1	7	10	151	184	45	12	0	12	0	68	149
12	7	9	134	78	46	3	7	10	83	52	60	14	0	12	161	10	47
1	8	9	466	460	18	5	7	10	195	159	31	16	0	12	256	218	33
3	8	9	576	552	18	7	7	10	446	457	18	18	0	12	597	592	21
5	8	9	352	365	19	9	7	10	175	145	29	1	1	12	377	352	41
7	8	9	346	328	18	0	8	10	38	166	75	3	1	12	654	693	26
0	0	10	535	512	39	2	8	10	357	354	19	5	1	12	62	70	92
2	0	10	1035	1088	30	4	8	10	166	219	31	7	1	12	351	373	28
4	0	10	3177	3358	74	0	1	11	1797	1863	43	9	1	12	165	80	46
6	0	10	1456	1471	37	2	1	11	2356	2457	55	11	1	12	227	147	32
8	0	10	1508	1532	37	4	1	11	1538	1568	37	13	1	12	0	45	102
10	0	10	369	405	33	6	1	11	805	771	24	15	1	12	46	7	74
12	0	10	912	914	26	8	1	11	484	453	24	17	1	12	152	91	36
14	0	10	405	364	28	10	1	11	1556	1594	36	0	2	12	639	631	27
16	0	10	787	[illegible]	24	12	1	11	729	734	20	2	2	12	239	154	48
18	0	10	761	[illegible]	24	14	1	11	715	709	20	4	2	12	394	299	43
20	0	10	215	158	37	16	1	11	592	587	19	6	2	12	1012	969	27
1	1	10	102	24	84	18	1	11	150	162	37	8	2	12	392	335	27
3	1	10	588	596	23	1	2	11	308	194	41	10	2	12	1534	1526	36
5	1	10	202	23	51	3	2	11	170	117	71	12	2	12	150	72	40
7	1	10	518	493	24	5	2	11	396	393	32	14	2	12	109	30	53
9	1	10	268	235	36	7	2	11	182	106	51	16	2	12	116	59	44
11	1	10	347	363	24	9	2	11	199	201	45	1	3	12	474	483	26
13	1	10	209	197	34	11	2	11	136	56	57	3	3	12	1279	1284	31
15	1	10	170	152	37	13	2	11	159	87	44	5	3	12	230	322	34
17	1	10	0	142	105	15	2	11	410	408	20	7	3	12	743	732	22
19	1	10	20	9	50	17	2	11	157	130	41	9	3	12	132	97	39
0	2	10	634	634	28	0	3	11	946	930	27	11	3	12	200	208	32
2	2	10	766	791	26	2	3	11	1750	1725	41	13	3	12	154	168	35
4	2	10	2484	2533	58	4	3	11	779	807	24	15	3	12	115	40	43
6	2	10	1029	1020	27	6	3	11	783	772	23	0	4	12	404	376	27
8	2	10	1033	1055	27	8	3	11	545	564	21	2	4	12	238	313	31
10	2	10	339	355	29	10	3	11	1047	1073	26	4	4	12	122	97	62
12	2	10	686	707	21	12	3	11	602	614	19	6	4	12	542	497	21
14	2	10	343	354	23	14	3	11	384	380	20	8	4	12	0	7	109
16	2	10	597	589	19	16	3	11	446	455	18	10	4	12	975	992	24
18	2	10	729	719	30	1	4	11	432	454	25	12	4	12	241	284	24
1	3	10	306	269	37	3	4	11	152	85	56	14	4	12	39	46	44
3	3	10	431	431	28	5	4	11	332	319	27	1	5	12	434	423	23
5	3	10	167	61	58	7	4	11	85	115	66	3	5	12	1393	1351	31
7	3	10	933	932	24	9	4	11	231	224	30	5	5	12	322	308	25
9	3	10	205	192	35	11	4	11	200	248	34	7	5	12	738	727	20
11	3	10	1067	1113	27	13	4	11	229	211	29	9	5	12	123	47	47
13	3	10	269	246	27	15	4	11	511	522	18	11	5	12	159	162	34
15	3	10	450	436	19	0	5	11	27	148	105	13	5	12	205	154	32

H	K	L	FO	FC	SIG	H	K	L	FO	FC	SIG	H	K	L	FO	FC	SIG
0	6	12	112	211	57	5	1	14	115	15	63	4	5	15	73	47	67
2	6	12	386	394	22	7	1	14	183	131	43	6	5	15	236	199	26
4	6	12	117	92	52	9	1	14	87	36	63	8	5	15	512	512	24
6	6	12	106	143	53	11	1	14	0	61	108	1	6	15	677	655	19
8	6	12	310	267	20	13	1	14	162	134	44	0	0	16	520	496	35
10	6	12	479	499	17	15	1	14	0	11	93	2	0	16	650	671	30
1	7	12	204	205	30	0	2	14	449	437	29	4	0	16	625	613	27
3	7	12	792	793	21	2	2	14	1665	1695	39	6	0	16	375	364	32
5	7	12	221	184	26	4	2	14	532	516	24	8	0	16	0	110	150
7	7	12	380	361	17	6	2	14	73	68	84	10	0	16	378	352	29
0	1	13	144	86	87	8	2	14	372	339	25	12	0	16	550	573	23
2	1	13	848	1922	43	10	2	14	756	740	21	1	1	16	111	123	70
4	1	13	111	164	79	12	2	14	198	218	33	3	1	16	172	78	55
6	1	13	122	1113	28	14	2	14	390	391	17	5	1	16	177	63	43
8	1	13	414	391	24	1	3	14	214	216	48	7	1	16	106	106	53
10	1	13	478	462	22	3	3	14	386	335	27	9	1	16	236	197	29
12	1	13	251	259	27	5	3	14	115	45	60	11	1	16	178	89	32
14	1	13	909	920	23	7	3	14	228	202	34	0	2	16	420	392	28
16	1	13	301	298	20	9	3	14	0	40	111	2	2	16	555	572	23
1	2	13	221	219	53	11	3	14	0	17	104	4	2	16	439	472	23
3	2	13	0	35	136	13	3	14	342	310	19	6	2	16	435	395	23
5	2	13	373	420	30	0	4	14	501	446	23	8	2	16	51	31	79
7	2	13	387	357	27	2	4	14	1048	993	26	10	2	16	369	365	29
9	2	13	503	495	22	4	4	14	636	600	21	1	3	16	190	181	44
11	2	13	359	385	23	6	4	14	142	12	52	3	3	16	253	247	44
13	2	13	309	295	21	8	4	14	175	48	35	5	3	16	211	282	38
15	2	13	210	207	27	10	4	14	457	442	18	7	3	16	178	204	39
0	3	13	369	367	31	12	4	14	79	7	59	9	3	16	439	513	19
2	3	13	1241	1242	31	1	5	14	235	288	32	0	4	16	164	107	47
4	3	13	261	248	36	3	5	14	264	268	28	2	4	16	475	494	21
6	3	13	579	564	22	5	5	14	159	110	43	4	4	16	50	87	79
8	3	13	485	455	22	7	5	14	165	135	38	6	4	16	298	298	24
10	3	13	196	211	36	9	5	14	17	13	83	8	4	16	220	164	26
12	3	13	220	214	27	0	6	14	338	297	22	1	5	16	142	125	45
14	3	13	579	602	18	2	6	14	359	327	21	3	5	16	55	125	71
1	4	13	0	119	122	4	6	14	525	512	18	0	1	17	1377	1393	33
3	4	13	134	90	53	6	6	14	159	152	32	2	1	17	270	320	33
5	4	13	518	502	21	0	1	15	80	86	95	4	1	17	515	543	21
7	4	13	533	506	20	2	1	15	398	406	30	6	1	17	77	62	45
9	4	13	731	723	20	4	1	15	308	284	31	8	1	17	335	382	26
11	4	13	513	556	18	6	1	15	989	957	25	10	1	17	133	12	36
13	4	13	356	353	19	8	1	15	1055	1043	26	1	2	17	252	246	35
0	5	13	607	575	21	10	1	15	656	670	20	3	2	17	0	24	17
2	5	13	652	642	21	12	1	15	339	323	21	5	2	17	196	212	38
4	5	13	447	446	21	14	1	15	0	57	94	7	2	17	148	46	49
6	5	13	200	175	32	1	2	15	537	582	26	9	2	17	56	96	67
8	5	13	385	352	19	3	2	15	230	146	43	0	3	17	1027	994	26
10	5	13	131	106	51	5	2	15	452	476	24	2	3	17	219	146	35
12	5	13	90	64	48	7	2	15	185	171	41	4	3	17	453	447	21
1	6	13	0	42	106	9	2	15	203	214	36	6	3	17	27	79	88
3	6	13	85	52	59	11	2	15	139	124	39	1	4	17	330	276	24
5	6	13	269	245	24	13	2	15	116	95	43	3	4	17	121	21	50
7	6	13	403	401	18	0	3	15	0	88	130	0	0	18	0	144	190
9	6	13	486	484	17	2	3	15	131	174	68	2	0	18	0	121	168
0	7	13	477	475	18	4	3	15	211	157	38	4	0	18	758	722	25
2	7	13	178	178	40	6	3	15	681	674	21	6	0	18	226	165	42
0	1	14	356	423	53	8	3	15	890	857	23	1	1	18	178	110	55
2	0	14	2014	2029	49	10	3	15	393	384	21	3	1	18	167	109	59
4	0	14	506	457	32	12	3	15	318	316	21	5	1	18	0	96	107
6	0	14	0	34	169	1	4	15	943	896	25	7	1	18	117	68	52
8	0	14	532	618	26	3	4	15	188	173	39	0	2	18	76	98	90
10	0	14	771	750	26	5	4	15	766	735	21	2	2	18	124	101	63
12	0	14	406	405	27	7	4	15	220	206	30	4	2	18	655	648	20
14	0	14	430	457	23	9	4	15	285	235	23	1	3	18	310	277	26
1	1	14	204	68	53	0	5	15	314	296	25	3	3	18	339	348	31
3	1	14	53	135	100	2	5	15	131	23	58	0	1	19	235	228	37

TABLE 8 . OBSERVED AND CALCULATED STPUCTURE FACTORS FOR HG3(N3F5)2SO4

H	K	L	FO	FC	SIG	H	K	L	FO	FC	SIG	H	K	L	FO	FC	SIG
1	1	-11	840	823	67	13	7	-9	590	568	64	15	1	-7	638	635	49
3	1	-11	773	730	61	1	9	-9	985	995	60	17	1	-7	446	309	75
5	1	-11	631	697	60	3	9	-9	1234	1153	52	19	1	-7	648	607	54
7	1	-11	967	1002	42	5	9	-9	496	642	92	1	3	-7	857	862	70
9	1	-11	331	164	83	7	9	-9	506	610	84	3	3	-7	2539	2649	57
1	3	-11	842	720	67	9	9	-9	490	477	80	5	3	-7	1317	1340	40
3	3	-11	946	1046	40	11	9	-9	780	815	57	7	3	-7	770	724	44
5	3	-11	540	570	54	1	11	-9	321	457	131	9	3	-7	1300	1358	39
7	3	-11	440	479	73	3	11	-9	569	634	87	11	3	-7	1013	1026	39
1	5	-11	617	604	84	5	11	-9	555	473	86	13	3	-7	315	332	97
3	5	-11	726	536	71	7	11	-9	1278	1275	48	15	3	-7	919	902	42
5	5	-11	421	437	85	1	13	-9	1042	1092	57	17	3	-7	1530	1470	42
7	5	-11	351	281	94	3	13	-9	473	538	97	1	5	-7	1368	1415	52
1	7	-11	836	882	65	0	0	-8	3644	3503	83	3	5	-7	1350	1386	51
3	7	-11	0	150	271	4	0	-8	2185	2202	55	5	5	-7	1652	1687	47
2	0	-10	1524	1572	69	8	0	-8	572	477	68	7	5	-7	721	693	59
6	0	-10	1370	1407	52	12	0	-8	931	944	53	9	5	-7	1928	1950	46
10	0	-10	941	989	55	16	0	-8	1332	1259	49	11	5	-7	1534	1597	43
0	2	-10	161	178	112	2	2	-8	640	713	47	13	5	-7	496	441	71
2	2	-10	1226	1292	39	4	2	-8	1240	1314	37	15	5	-7	840	823	45
4	2	-10	873	933	41	6	2	-8	1447	1572	38	17	5	-7	525	430	65
6	2	-10	927	973	40	8	2	-8	1677	1723	41	1	7	-7	2272	2323	55
[illegible]	[illegible]	-10	1192	1213	39	10	2	-8	1546	1574	40	3	7	-7	558	685	89
[illegible]	[illegible]	-10	213	249	107	12	2	-8	1412	1433	39	5	7	-7	1373	1358	49
[illegible]	2	-10	716	724	46	14	2	-8	627	605	51	7	7	-7	1520	1492	47
2	4	-10	1195	1192	55	16	2	-8	680	598	49	9	7	-7	433	449	81
4	4	-10	896	880	49	0	4	-8	2341	2372	57	11	7	-7	248	108	131
6	4	-10	760	891	49	2	4	-8	695	652	76	13	7	-7	1220	1260	43
8	4	-10	360	350	88	4	4	-8	1948	2020	49	15	7	-7	613	701	61
10	4	-10	1361	1421	41	6	4	-8	623	609	59	17	7	-7	432	228	99
12	4	-10	528	491	60	8	4	-8	1086	1105	41	1	9	-7	1272	1294	53
0	6	-10	1591	1633	53	10	4	-8	294	284	96	3	9	-7	543	332	87
2	6	-10	1325	1304	53	12	4	-8	842	850	45	5	9	-7	1946	1975	50
4	6	-10	558	621	85	14	4	-8	449	428	70	7	9	-7	736	808	60
6	6	-10	618	583	68	16	4	-8	1131	1142	41	9	9	-7	1011	983	50
8	6	-10	525	480	71	2	6	-8	1481	1444	51	11	9	-7	742	704	59
10	6	-10	405	199	118	4	6	-8	1210	1244	52	13	9	-7	775	652	54
2	8	-10	150	161	189	6	6	-8	962	948	53	15	9	-7	1022	1056	46
4	8	-10	443	267	101	8	6	-8	1460	1509	44	1	11	-7	699	611	73
6	8	-10	1320	1504	48	10	6	-8	758	821	55	3	11	-7	1538	1544	49
8	8	-10	437	488	90	12	6	-8	1211	1166	43	5	11	-7	971	868	54
0	10	-10	1002	944	62	14	6	-8	981	873	45	7	11	-7	439	363	99
2	10	-10	925	887	62	16	6	-8	540	517	68	9	11	-7	1443	1420	46
4	10	-10	1209	1043	50	0	8	-8	1508	1445	52	11	11	-7	1151	1123	45
1	1	-9	587	444	90	2	8	-8	835	837	66	13	11	-7	505	393	71
3	1	-9	1145	1235	45	4	8	-8	1414	1400	50	1	13	-7	1321	1279	51
5	1	-9	1551	1672	41	6	8	-8	649	479	70	3	13	-7	758	715	63
7	1	-9	0	121	213	8	8	-8	1656	1555	47	5	13	-7	909	969	56
9	1	-9	1183	1177	38	10	8	-8	398	163	115	7	13	-7	413	445	131
11	1	-9	898	881	41	12	8	-8	987	1053	48	9	13	-7	734	732	56
13	1	-9	285	108	91	14	8	-8	268	159	116	11	13	-7	631	711	62
15	1	-9	987	921	40	2	10	-8	1527	1434	50	1	15	-7	739	595	57
1	3	-9	1952	1962	53	4	10	-8	804	733	62	3	15	-7	522	522	83
3	3	-9	209	358	123	6	10	-8	861	839	56	5	15	-7	516	502	80
5	3	-9	450	546	65	8	10	-8	1161	1050	48	7	15	-7	1307	1339	44
7	3	-9	836	953	43	10	10	-8	821	752	57	2	0	-6	3352	3630	73
9	3	-9	692	677	48	12	10	-8	862	822	53	6	0	-6	2022	2018	43
11	3	-9	874	830	42	0	12	-8	1235	1066	54	10	0	-6	2449	2445	55
13	3	-9	949	948	41	2	12	-8	1066	965	55	14	0	-6	1430	1352	46
15	3	-9	445	505	78	4	12	-8	978	1025	55	18	0	-6	1359	1322	49
1	5	-9	882	839	64	6	12	-8	606	602	71	0	2	-6	342	290	130
3	5	-9	0	249	276	8	12	-8	838	819	55	2	2	-6	3402	3403	69
5	5	-9	1055	1093	49	10	12	-8	307	323	116	4	2	-6	1268	1314	36
7	5	-9	1287	1339	43	2	14	-8	661	642	77	6	2	-6	1408	1402	37
9	5	-9	1002	1094	44	4	14	-8	694	690	66	8	2	-6	2375	2325	50
11	5	-9	735	769	52	6	14	-8	965	942	51	10	2	-6	408	417	65
13	5	-9	522	618	71	1	1	-7	1718	2012	50	12	2	-6	1266	1212	37
1	7	-9	434	338	109	3	1	-7	917	951	41	14	2	-6	939	943	39
3	7	-9	1707	1646	50	5	1	-7	1124	1193	36	16	2	-6	275	211	91
5	7	-9	492	419	90	7	1	-7	2303	2285	49	18	2	-6	1316	1218	39
7	7	-9	879	934	56	9	1	-7	928	890	37	20	2	-6	364	301	81
9	7	-9	657	647	63	11	1	-7	1188	1193	37	2	4	-6	1502	1505	50
11	7	-9	874	805	51	13	1	-7	1703	1633	41	4	4	-6	1324	1324	51

TABLE 8 . OBSERVED AND CALCULATED STRUCTURE FACTORS FOR HG3(NBF5)2SO4

H	K	L	FO	FC	SIG	H	K	L	FO	FC	SIG	H	K	L	FO	FC	SIG
6	4	-6	2920	2905	61	19	3	-5	1253	1222	40	20	2	-4	436	207	72
8	4	-6	887	906	45	21	3	-5	958	867	42	22	2	-4	491	488	67
10	4	-6	1768	1749	43	1	5	-5	1477	1592	49	0	4	-4	2618	2930	57
12	4	-6	1095	1074	40	3	5	-5	513	667	94	2	4	-4	626	802	74
14	4	-6	1791	1741	43	5	5	-5	3126	3219	66	4	4	-4	4161	4293	84
16	4	-6	331	261	94	7	5	-5	3133	3148	65	6	4	-4	1521	1543	41
18	4	-6	758	659	48	9	5	-5	1491	1467	42	8	4	-4	1070	1097	40
0	6	-6	2015	2081	53	11	5	-5	885	832	45	10	4	-4	812	772	45
2	6	-6	2149	2263	53	13	5	-5	1636	1614	42	12	4	-4	735	768	47
4	6	-6	1781	1734	50	15	5	-5	1522	1475	41	14	4	-4	1026	946	39
6	6	-6	1689	1700	48	17	5	-5	279	316	99	16	4	-4	2250	2171	49
8	6	-6	365	440	99	19	5	-5	787	800	48	18	4	-4	534	454	58
10	6	-6	447	272	78	1	7	-5	1891	1882	51	20	4	-4	935	871	43
12	6	-6	843	709	48	3	7	-5	3892	3964	80	2	6	-4	2059	2116	50
14	6	-6	1340	1301	42	5	7	-5	884	811	60	4	6	-4	1538	1703	48
16	6	-6	1118	1153	42	7	7	-5	872	875	58	6	6	-4	1578	1611	46
18	6	-6	980	938	45	9	7	-5	1432	1507	45	8	6	-4	2752	2832	59
2	8	-6	614	865	85	11	7	-5	1495	1545	43	10	6	-4	954	949	47
4	8	-6	645	597	76	13	7	-5	387	366	84	12	6	-4	2416	2414	52
6	8	-6	1747	1708	48	15	7	-5	631	571	58	14	6	-4	1648	1683	42
8	8	-6	976	1005	52	17	7	-5	1580	1518	43	16	6	-4	647	638	54
10	8	-6	2941	2913	63	19	7	-5	545	371	62	18	6	-4	954	936	42
12	8	-6	936	929	49	1	9	-5	2856	2858	63	20	6	-4	389	391	88
14	8	-6	787	779	53	3	9	-5	2224	2226	53	0	8	-4	1934	1959	51
16	8	-6	447	401	83	5	9	-5	620	503	75	2	8	-4	1542	1589	48
18	8	-6	386	193	96	7	9	-5	937	871	54	4	8	-4	1530	1613	48
0	10	-6	2928	2789	65	9	9	-5	1525	1488	45	6	8	-4	723	691	66
2	10	-6	1425	1482	50	11	9	-5	1952	1883	48	8	8	-4	3113	3051	65
4	10	-6	1122	1117	50	13	9	-5	889	893	49	10	8	-4	378	178	102
6	10	-6	1255	1119	47	15	9	-5	572	597	63	12	8	-4	1826	1895	45
8	10	-6	507	463	82	17	9	-5	613	628	59	14	8	-4	500	304	85
10	10	-6	198	123	158	1	11	-5	1160	1179	54	16	8	-4	1076	1163	43
12	10	-6	473	570	83	3	11	-5	698	592	68	18	8	-4	451	499	72
14	10	-6	886	834	49	5	11	-5	1047	1098	50	20	8	-4	910	949	44
16	10	-6	869	849	49	7	11	-5	2681	2567	58	2	10	-4	2443	2416	56
2	12	-6	223	380	150	9	11	-5	813	668	53	4	10	-4	1003	995	54
4	12	-6	1103	1068	51	11	11	-5	448	519	82	6	10	-4	1084	1098	49
6	12	-6	1695	1715	47	13	11	-5	1597	1566	43	8	10	-4	2233	2124	51
8	12	-6	1025	903	47	15	11	-5	439	390	76	10	10	-4	1410	1307	44
10	12	-6	1023	1056	47	17	11	-5	589	594	61	12	10	-4	1589	1608	43
12	12	-6	984	956	46	1	13	-5	1444	1396	50	14	10	-4	774	783	50
14	12	-6	939	851	46	3	13	-5	1429	1460	48	16	10	-4	426	379	93
0	14	-6	1192	1111	53	5	13	-5	1597	1607	46	18	10	-4	1148	1163	41
2	14	-6	1128	1054	52	7	13	-5	547	530	70	0	12	-4	2609	1501	50
4	14	-6	1453	1378	47	9	13	-5	860	811	50	2	12	-4	2059	2019	51
6	14	-6	543	552	72	11	13	-5	838	872	49	4	12	-4	1810	1815	47
8	14	-6	860	840	51	13	13	-5	570	545	62	6	12	-4	531	673	71
10	14	-6	271	204	108	15	13	-5	1138	1132	41	8	12	-4	1052	1002	46
12	14	-6	535	428	68	1	15	-5	327	234	119	10	12	-4	517	458	71
2	16	-6	1377	1224	48	3	15	-5	1349	1289	47	12	12	-4	549	589	57
4	16	-6	645	665	68	5	15	-5	718	700	60	14	12	-4	459	486	71
6	16	-6	541	412	76	7	15	-5	573	596	66	16	12	-4	1037	985	42
8	16	-6	823	796	49	9	15	-5	1309	1269	41	2	14	-4	650	549	68
1	1	-5	1313	1366	34	11	15	-5	1250	1225	41	4	14	-4	1401	1362	46
3	1	-5	2013	2061	43	1	17	-5	1188	995	50	6	14	-4	1870	1826	46
5	1	-5	2967	2888	60	3	17	-5	340	395	116	8	14	-4	824	824	49
7	1	-5	939	928	33	5	17	-5	1180	1181	45	10	14	-4	930	849	45
9	1	-5	3362	3243	68	7	17	-5	647	571	57	12	14	-4	450	540	68
11	1	-5	2805	2731	58	0	0	-4	8791	9007	177	14	14	-4	1048	995	40
13	1	-5	897	876	37	4	0	-4	2869	2742	59	0	16	-4	2360	2163	55
15	1	-5	1335	1335	37	8	0	-4	404	372	72	2	16	-4	1322	1205	47
17	1	-5	1031	968	38	12	0	-4	1500	1426	42	4	16	-4	579	526	70
19	1	-5	968	963	41	16	0	-4	1216	1153	46	6	16	-4	777	841	52
21	1	-5	510	416	66	20	0	-4	2149	2029	53	8	16	-4	36	96	177
1	3	-5	3593	3880	74	2	2	-4	726	632	53	10	16	-4	346	162	83
3	3	-5	1833	1843	46	4	2	-4	3134	3057	63	12	16	-4	621	562	51
5	3	-5	2164	2133	48	6	2	-4	2405	2287	50	2	18	-4	387	324	122
7	3	-5	2253	2249	49	8	2	-4	3086	2929	62	4	18	-4	516	585	65
9	3	-5	1222	1127	37	10	2	-4	2832	2755	58	6	18	-4	750	667	51
11	3	-5	1163	1119	38	12	2	-4	2134	2060	46	8	18	-4	502	375	61
13	3	-5	2036	1961	45	14	2	-4	610	549	47	1	1	-3	4403	4023	88
15	3	-5	1623	1503	40	16	2	-4	1277	1178	37	3	1	-3	507	459	39
17	3	-5	965	803	43	18	2	-4	243	170	116	5	1	-3	614	576	32

TABLE 8 . OBSERVED AND CALCULATED STRUCTURE FACTORS FOR HG3(N9F5)2SO4

H	K	L	FO	FC	SIG	H	K	L	FO	FC	SIG	H	K	L	FO	FC	SIG
7	1	-3	3089	2971	62	9	15	-3	436	515	71	20	10	-2	1342	1428	38
9	1	-3	3119	3030	62	11	15	-3	918	891	42	2	12	-2	561	453	80
11	1	-3	3221	3140	65	13	15	-3	1395	1446	38	4	12	-2	1535	1504	44
13	1	-3	2348	2277	49	1	17	-3	1493	1363	46	6	12	-2	2917	2950	60
15	1	-3	404	244	60	3	17	-3	1007	967	47	8	12	-2	1400	1361	41
17	1	-3	447	490	61	5	17	-3	299	208	101	10	12	-2	837	861	44
19	1	-3	1299	1243	38	7	17	-3	307	159	94	12	12	-2	671	704	51
21	1	-3	1323	1231	39	9	17	-3	1072	1107	39	14	12	-2	1395	1434	39
1	3	-3	752	878	63	11	17	-3	1139	1183	38	16	12	-2	978	1001	39
3	3	-3	4380	4483	88	1	19	-3	1022	936	49	18	12	-2	496	460	59
5	3	-3	3179	3032	64	3	19	-3	1163	1156	45	0	14	-2	1338	1154	47
7	3	-3	2704	2523	55	5	19	-3	350	200	89	2	14	-2	1728	1697	46
9	3	-3	1710	1662	39	2	0	-2	6507	6072	130	4	14	-2	2412	2464	53
11	3	-3	806	802	39	6	0	-2	2487	2443	51	6	14	-2	333	372	97
13	3	-3	1255	1255	36	10	0	-2	3727	3750	76	8	14	-2	795	794	47
15	3	-3	1857	1822	42	14	0	-2	1077	1109	43	10	14	-2	336	309	73
17	3	-3	2247	2151	49	18	0	-2	2033	1997	50	12	14	-2	561	455	54
19	3	-3	322	421	86	22	0	-2	977	979	54	14	14	-2	311	368	83
21	3	-3	437	258	67	0	2	-2	1008	999	47	16	14	-2	939	1018	33
1	5	-3	1395	1530	45	2	2	-2	5670	5663	113	2	16	-2	2040	1896	49
3	5	-3	2516	2581	55	4	2	-2	2490	2268	51	4	16	-2	718	774	54
5	5	-3	4254	4146	86	6	2	-2	2064	1933	43	6	16	-2	538	490	62
7	5	-3	2233	2264	49	8	2	-2	4137	3918	82	8	16	-2	1034	1078	40
9	5	-3	1791	1769	43	10	2	-2	453	430	48	10	16	-2	613	729	50
11	5	-3	1561	1561	41	12	2	-2	2003	1961	43	12	16	-2	1133	1151	37
13	5	-3	1486	1497	40	14	2	-2	1225	1199	35	14	16	-2	385	473	64
15	5	-3	1875	1866	44	16	2	-2	318	401	76	0	18	-2	1351	1291	45
17	5	-3	791	767	45	18	2	-2	1755	1727	41	2	18	-2	641	628	62
19	5	-3	587	607	55	20	2	-2	681	546	46	4	18	-2	539	614	56
21	5	-3	458	343	65	22	2	-2	1348	1275	39	6	18	-2	253	103	120
1	7	-3	3751	3927	77	2	4	-2	1981	1966	48	8	18	-2	1436	1465	59
3	7	-3	2939	3039	62	4	4	-2	1027	980	46	10	18	-2	323	312	75
5	7	-3	1292	1273	47	6	4	-2	5202	5129	104	2	20	-2	705	662	55
7	7	-3	2173	2124	50	8	4	-2	1254	1193	36	1	1	-1	3137	3004	64
9	7	-3	1409	1424	43	10	4	-2	2024	1999	44	3	1	-1	1022	883	26
11	7	-3	793	786	52	12	4	-2	1487	1435	38	5	1	-1	2194	2137	44
13	7	-3	1592	1658	41	14	4	-2	2918	2960	60	7	1	-1	2920	2737	56
15	7	-3	494	546	66	16	4	-2	143	198	137	9	1	-1	4136	4101	82
17	7	-3	786	778	46	18	4	-2	704	735	45	11	1	-1	3574	3592	71
19	7	-3	1084	1120	41	20	4	-2	493	517	59	13	1	-1	2206	2190	46
21	7	-3	1027	1040	40	22	4	-2	336	333	81	15	1	-1	792	753	35
1	9	-3	3097	3137	66	0	6	-2	1924	2115	47	17	1	-1	755	740	33
3	9	-3	1027	980	51	2	6	-2	3161	3173	65	19	1	-1	1498	1495	33
5	9	-3	1868	1900	49	4	6	-2	3076	3086	64	21	1	-1	841	819	40
7	9	-3	848	815	56	6	6	-2	2800	2795	59	23	1	-1	228	432	104
9	9	-3	2410	2318	54	8	6	-2	805	799	49	1	3	-1	3078	2953	62
11	9	-3	1994	1968	47	10	6	-2	122	199	166	3	3	-1	4413	4512	83
13	9	-3	676	672	54	12	6	-2	1270	1304	40	5	3	-1	3245	3077	65
15	9	-3	862	866	45	14	6	-2	2006	2053	45	7	3	-1	2959	2795	63
17	9	-3	337	234	95	16	6	-2	1756	1811	42	9	3	-1	2297	2223	49
19	9	-3	1153	1187	40	18	6	-2	1340	1386	39	11	3	-1	1245	1327	34
1	11	-3	985	986	57	20	6	-2	558	540	54	13	3	-1	1898	1843	43
3	11	-3	2012	2090	50	22	6	-2	675	584	48	15	3	-1	1913	1914	42
5	11	-3	1279	1325	46	2	8	-2	1516	1582	45	17	3	-1	1744	1746	40
7	11	-3	1670	1664	45	4	8	-2	1029	1006	48	19	3	-1	828	835	39
9	11	-3	2039	2009	48	6	8	-2	1391	1324	45	21	3	-1	516	635	49
11	11	-3	1595	1625	43	8	8	-2	1605	1550	44	23	3	-1	796	735	43
13	11	-3	1175	1223	41	10	8	-2	4685	4805	94	1	5	-1	2335	2441	52
15	11	-3	477	473	67	12	8	-2	1223	1335	41	3	5	-1	1974	1955	47
17	11	-3	1012	963	40	14	8	-2	794	750	45	5	5	-1	4529	4523	90
1	13	-3	697	675	70	16	8	-2	551	500	56	7	5	-1	3137	3343	65
3	13	-3	1477	1491	45	18	8	-2	384	351	71	9	5	-1	434	532	59
5	13	-3	2136	2162	50	20	8	-2	177	223	118	11	5	-1	750	741	43
7	13	-3	926	956	47	0	10	-2	5046	5042	101	13	5	-1	1712	1768	42
9	13	-3	820	793	50	2	10	-2	1932	1960	48	15	5	-1	1933	2022	47
11	13	-3	764	688	49	4	10	-2	987	954	51	17	5	-1	674	714	45
13	13	-3	746	738	47	6	10	-2	1675	1695	45	19	5	-1	849	858	79
15	13	-3	1532	1519	40	8	10	-2	703	697	60	21	5	-1	147	333	133
17	13	-3	931	958	40	10	10	-2	172	232	161	1	7	-1	3625	3737	74
1	15	-3	630	664	67	12	10	-2	967	973	42	3	7	-1	4573	4706	93
3	15	-3	815	765	55	14	10	-2	1123	1163	40	5	7	-1	1244	1234	43
5	15	-3	1095	1154	45	16	10	-2	867	906	42	7	7	-1	1563	1683	43
7	15	-3	1783	1832	44	18	10	-2	1024	1038	39	9	7	-1	1311	1365	43

TABLE 8 . OBSERVED AND CALCULATED STRUCTURE FACTORS FOR HG3(NBF5)2SO4

H	K	L	FO	FC	SIG	H	K	L	FO	FC	SIG	H	K	L	FO	FC	SIG
11	7	-1	1155	1255	40	6	4	0	2298	2421	48	2	20	0	732	713	48
13	7	-1	1059	1096	39	8	4	0	970	960	34	4	20	0	834	865	42
15	7	-1	459	347	72	10	4	0	1186	1229	33	1	1	1	2942	2942	60
17	7	-1	1286	1378	38	12	4	0	568	495	45	3	1	1	671	517	27
19	7	-1	641	743	48	14	4	0	1416	1365	36	5	1	1	2053	2036	41
21	7	-1	1011	1116	38	16	4	0	2975	3193	61	7	1	1	2715	2740	54
1	9	-1	3866	3977	79	18	4	0	625	637	44	9	1	1	3836	4015	77
3	9	-1	1754	1787	45	20	4	0	392	406	62	11	1	1	3657	3820	73
5	9	-1	1264	1318	44	22	4	0	452	387	57	13	1	1	2035	2122	43
7	9	-1	315	190	126	2	6	0	3403	3533	69	15	1	1	708	735	37
9	9	-1	2074	2118	48	4	6	0	1426	1513	41	17	1	1	732	846	36
11	9	-1	2421	2519	52	6	6	0	2781	2772	58	19	1	1	1227	1308	35
13	9	-1	468	437	64	8	6	0	3348	3666	68	21	1	1	956	954	36
15	9	-1	372	531	74	10	6	0	500	592	59	23	1	1	372	360	67
17	9	-1	293	323	86	12	6	0	2886	3179	59	1	3	1	2815	2709	58
19	9	-1	929	1058	39	14	6	0	2491	2696	52	3	3	1	4230	4468	86
21	9	-1	930	1060	88	16	6	0	509	572	55	5	3	1	3134	3092	63
1	11	-1	1157	1141	48	18	6	0	1191	1260	36	7	3	1	3033	2934	61
3	11	-1	1571	1612	45	20	6	0	431	471	61	9	3	1	1950	2003	42
5	11	-1	1270	1339	43	22	6	0	558	532	49	11	3	1	1075	1085	32
7	11	-1	2439	2444	53	0	8	0	2136	2167	49	13	3	1	1670	1791	38
9	11	-1	1615	1526	42	2	8	0	1688	1805	43	15	3	1	1858	1938	41
11	11	-1	1346	1423	40	4	8	0	764	758	52	17	3	1	1779	1831	40
13	11	-1	1487	1523	39	6	8	0	1030	1029	44	19	3	1	654	689	42
15	11	-1	504	466	57	8	8	0	4807	4826	96	21	3	1	655	632	43
17	11	-1	1063	1112	37	10	8	0	329	209	95	23	3	1	743	716	40
19	11	-1	617	693	47	12	8	0	2684	2982	56	1	5	1	2638	2742	57
1	13	-1	613	473	95	14	8	0	376	417	71	3	5	1	1731	1851	44
3	13	-1	1645	1674	44	16	8	0	967	1015	37	5	5	1	4339	4457	88
5	13	-1	2143	2297	49	18	8	0	442	489	57	7	5	1	3107	3347	63
7	13	-1	906	929	44	20	8	0	1199	1372	36	9	5	1	658	708	45
9	13	-1	1044	1102	40	2	10	0	3618	3753	74	11	5	1	858	909	38
11	13	-1	866	915	42	4	10	0	658	447	58	13	5	1	1724	1825	40
13	13	-1	572	707	52	6	10	0	489	555	72	15	5	1	1739	1886	41
15	13	-1	1564	1603	39	8	10	0	2941	2871	61	17	5	1	503	505	52
17	13	-1	1076	1083	36	10	10	0	2068	2067	47	19	5	1	934	978	36
1	15	-1	686	695	63	12	10	0	2087	2164	46	21	5	1	394	408	61
3	15	-1	933	921	46	14	10	0	416	436	65	1	7	1	3634	3725	74
5	15	-1	898	886	44	16	10	0	146	290	133	3	7	1	4655	4715	93
7	15	-1	1457	1564	40	18	10	0	1610	1705	39	5	7	1	1065	1089	43
9	15	-1	950	1003	39	20	10	0	513	559	51	7	7	1	1514	1556	40
11	15	-1	1115	1193	37	0	12	0	912	905	55	9	7	1	1457	1518	39
13	15	-1	1459	1507	37	2	12	0	2708	2717	58	11	7	1	917	964	41
15	15	-1	572	515	46	4	12	0	2721	2861	58	13	7	1	943	1067	38
1	17	-1	1414	1269	43	6	12	0	90	390	175	15	7	1	231	225	110
3	17	-1	973	957	45	8	12	0	1549	1562	41	17	7	1	1174	1320	36
5	17	-1	978	986	44	10	12	0	487	465	62	19	7	1	686	842	43
7	17	-1	266	269	92	12	12	0	614	711	50	21	7	1	929	1039	37
9	17	-1	1077	1126	37	14	12	0	212	274	103	1	9	1	3743	3824	76
11	17	-1	863	928	37	16	12	0	1477	1518	38	3	9	1	1839	1930	45
1	19	-1	1085	1064	45	18	12	0	692	722	41	5	9	1	1532	1613	42
3	19	-1	1081	1025	42	2	14	0	381	424	97	7	9	1	512	322	68
5	19	-1	283	318	112	4	14	0	1755	1739	44	9	9	1	2135	2160	43
7	19	-1	602	562	43	6	14	0	2700	2840	57	11	9	1	2140	2242	43
4	0	0	437	488	66	8	14	0	908	878	46	13	9	1	449	556	53
8	0	0	376	473	54	10	14	0	211	150	116	15	9	1	639	679	44
12	0	0	2062	2160	45	12	14	0	434	422	61	17	9	1	440	323	74
16	0	0	440	457	70	14	14	0	1381	1502	37	19	9	1	1027	1147	36
20	0	0	2925	2974	63	16	14	0	381	326	60	21	9	1	849	913	38
2	2	0	1743	1633	39	0	16	0	3355	3125	72	1	11	1	1303	1343	45
4	2	0	4920	4709	98	2	16	0	1534	1460	43	3	11	1	1460	1539	43
6	2	0	3751	3675	75	4	16	0	584	543	60	5	11	1	1120	1195	42
8	2	0	3213	3283	64	6	16	0	938	999	41	7	11	1	2312	2368	51
10	2	0	3998	4319	79	8	16	0	323	284	79	9	11	1	1709	1642	42
12	2	0	1853	1979	40	10	16	0	237	206	97	11	11	1	1358	1406	38
14	2	0	767	832	35	12	16	0	907	951	37	13	11	1	1527	1601	39
16	2	0	1513	1574	36	14	16	0	708	761	39	15	11	1	403	339	66
18	2	0	627	537	42	2	18	0	666	733	53	17	11	1	917	959	38
20	2	0	370	269	63	4	18	0	831	808	45	19	11	1	814	847	38
22	2	0	672	778	46	6	18	0	205	291	128	1	13	1	618	293	69
0	4	0	1492	1535	41	8	18	0	420	353	62	3	13	1	1543	1629	43
2	4	0	1066	950	45	10	18	0	1992	2109	44	5	13	1	2094	2246	47
4	4	0	5569	6743	131	0	20	0	776	663	52	7	13	1	617	710	53

TABLE 8 . OBSERVED AND CALCULATED STRUCTURE FACTORS FOR HG3(NPES)2SO4

H	K	L	FO	FC	SIG	H	K	L	FO	FC	SIG	H	K	L	FO	FC	SIG
9	13	1	1125	1175	38	20	8	2	379	243	66	15	5	3	1879	1815	43
11	13	1	987	973	37	0	10	2	5106	5131	101	17	5	3	813	778	41
13	13	1	721	646	41	2	10	2	1908	1893	46	19	5	3	673	662	46
15	13	1	1575	1635	39	4	10	2	886	924	48	21	5	3	230	355	100
17	13	1	1019	1052	35	6	10	2	1724	1730	43	1	7	3	3929	3937	79
1	15	1	602	502	68	8	10	2	836	858	47	3	7	3	3130	3153	65
3	15	1	903	882	45	10	10	2	429	217	90	5	7	3	1333	1326	41
5	15	1	990	1048	41	12	10	2	1053	1072	39	7	7	3	2020	1995	46
7	15	1	1522	1556	39	14	10	2	1245	1191	38	9	7	3	1297	1267	40
9	15	1	915	913	38	16	10	2	779	840	42	11	7	3	812	831	45
11	15	1	1131	1197	36	18	10	2	976	1031	38	13	7	3	1418	1473	39
13	15	1	1477	1462	37	20	10	2	1425	1465	38	15	7	3	509	575	59
15	15	1	592	599	44	2	12	2	637	573	63	17	7	3	838	866	42
1	17	1	1430	1363	43	4	12	2	1480	1549	42	19	7	3	1060	997	38
3	17	1	887	905	45	6	12	2	2913	3040	61	21	7	3	1072	1101	37
5	17	1	929	896	40	8	12	2	1340	1356	39	1	9	3	3245	3186	67
7	17	1	41	110	177	10	12	2	818	757	42	3	9	3	825	857	47
9	17	1	1028	1064	36	12	12	2	618	526	48	5	9	3	1784	1766	44
11	17	1	992	1029	35	14	12	2	1451	1490	38	7	9	3	734	645	52
1	19	1	1106	1048	42	16	12	2	966	1012	37	9	9	3	2371	2256	51
3	19	1	1044	999	41	18	12	2	449	484	58	11	9	3	2144	2104	48
5	19	1	345	350	90	0	14	2	1196	1156	45	13	9	3	454	473	65
7	19	1	505	637	54	2	14	2	1806	1746	45	15	9	3	781	829	44
2	0	2	6559	6205	131	4	14	2	2430	2542	53	17	9	3	297	198	103
6	0	2	2500	2459	52	6	14	2	219	226	111	19	9	3	1057	1071	38
10	0	2	3626	3694	72	8	14	2	791	805	42	1	11	3	876	873	53
14	0	2	938	1024	45	10	14	2	507	336	53	3	11	3	1924	1965	46
18	0	2	2056	2053	49	12	14	2	624	538	47	5	11	3	1350	1382	41
22	0	2	1045	1024	48	14	14	2	347	237	74	7	11	3	1833	1741	44
0	2	2	1573	1524	41	16	14	2	1016	1043	35	9	11	3	1933	1837	45
2	2	2	5629	5700	112	2	16	2	1972	1934	46	11	11	3	1656	1619	41
4	2	2	2498	2365	51	4	16	2	724	712	48	13	11	3	1183	1233	38
6	2	2	1978	1910	41	6	16	2	583	569	51	15	11	3	525	507	58
8	2	2	4056	3928	81	8	16	2	1052	1085	36	17	11	3	1017	1035	38
10	2	2	421	436	49	10	16	2	775	784	39	1	13	3	555	488	69
12	2	2	1993	2002	43	12	16	2	1126	1181	34	3	13	3	1449	1449	42
14	2	2	1193	1173	34	14	16	2	453	487	51	5	13	3	2077	2159	47
16	2	2	613	595	44	0	18	2	1415	1296	42	7	13	3	978	924	41
18	2	2	1751	1713	40	2	18	2	595	649	59	9	13	3	879	891	41
20	2	2	620	643	46	4	18	2	603	595	51	11	13	3	840	781	41
22	2	2	1334	1302	37	6	18	2	0	19	204	13	13	3	836	780	39
2	4	2	2047	2003	47	8	18	2	1440	1529	37	15	13	3	1541	1499	39
4	4	2	1118	998	40	10	18	2	402	310	55	17	13	3	975	974	37
6	4	2	5043	5198	100	2	20	2	754	684	46	1	15	3	735	666	54
8	4	2	1164	1165	35	1	1	3	3987	3803	80	3	15	3	653	654	55
10	4	2	1934	1990	42	3	1	3	629	549	34	5	15	3	946	995	41
12	4	2	1470	1502	37	5	1	3	824	777	29	7	15	3	1813	1820	42
14	4	2	2949	3027	60	7	1	3	3087	2995	62	9	15	3	578	605	49
16	4	2	136	184	128	9	1	3	3104	3068	62	11	15	3	953	915	36
18	4	2	784	779	39	11	1	3	3052	2993	61	13	15	3	1438	1478	37
20	4	2	410	503	65	13	1	3	2395	2315	50	1	17	3	1401	1276	42
22	4	2	358	340	75	15	1	3	364	266	62	3	17	3	977	1004	42
0	6	2	1982	2017	46	17	1	3	437	491	57	5	17	3	454	421	66
2	6	2	3170	3112	65	19	1	3	1401	1330	37	7	17	3	353	153	68
4	6	2	3031	3166	63	21	1	3	1118	1077	36	9	17	3	1119	1108	35
6	6	2	2853	2823	59	1	3	3	1102	1034	44	11	17	3	1023	1052	34
8	6	2	982	1016	40	3	3	3	4373	4417	87	1	19	3	974	944	43
10	6	2	229	179	118	5	3	3	3023	2967	61	3	19	3	1143	1168	39
12	6	2	1311	1378	38	7	3	3	2581	2469	53	5	19	3	0	145	205
14	6	2	1986	2073	45	9	3	3	2001	1915	43	0	0	4	9016	9157	183
16	6	2	1793	1869	42	11	3	3	909	943	36	4	0	4	2850	2729	59
18	6	2	1385	1412	37	13	3	3	1371	1297	36	8	0	4	423	388	69
20	6	2	535	517	49	15	3	3	1803	1796	41	12	0	4	1408	1339	42
22	6	2	587	521	48	17	3	3	2152	2033	46	16	0	4	1040	978	46
2	8	2	1616	1657	43	19	3	3	568	510	50	20	0	4	2211	2083	53
4	8	2	1003	1063	44	21	3	3	198	317	118	2	2	4	737	749	41
6	8	2	1246	1150	41	1	5	3	1612	1604	42	4	2	4	3283	3240	66
8	8	2	1614	1560	42	3	5	3	2548	2545	54	6	2	4	2355	2277	49
10	8	2	4840	4920	97	5	5	3	4138	4043	83	8	2	4	2967	2794	60
12	8	2	1262	1298	39	7	5	3	2242	2293	48	10	2	4	2836	2807	59
14	8	2	729	770	45	9	5	3	1496	1496	39	12	2	4	1918	1857	42
16	8	2	521	506	55	11	5	3	1342	1376	38	14	2	4	757	712	40
18	8	2	396	444	63	13	5	3	1481	1483	39	16	2	4	1326	1242	36

TABLE 8 . OBSERVED AND CALCULATED STRUCTURE FACTORS FOR HG3(NBF5)2SO4

H	K	L	FO	FC	SIG	H	K	L	FO	FC	SIG	H	K	L	FO	FC	SIG
18	2	4	373	244	85	5	1	5	2978	2841	60	3	17	5	404	360	72
20	2	4	335	196	75	7	1	5	1077	1043	33	5	17	5	1040	1132	38
22	2	4	491	493	57	9	1	5	3355	3235	68	7	17	5	530	457	50
0	4	4	2893	2955	61	11	1	5	3064	2972	62	2	0	6	3855	3691	79
2	4	4	639	541	56	13	1	5	994	933	36	6	0	6	2385	2309	53
4	4	4	4375	4300	87	15	1	5	1406	1331	37	10	0	6	2033	1953	49
6	4	4	1520	1571	38	17	1	5	1071	1009	37	14	0	6	1352	1287	45
8	4	4	1304	1258	37	19	1	5	916	879	39	18	0	6	1417	1326	46
10	4	4	773	793	43	21	1	5	621	562	49	0	2	6	536	376	79
12	4	4	925	891	39	1	3	5	3684	3707	75	2	2	6	3528	3551	71
14	4	4	1003	980	38	3	3	5	1974	1945	44	4	2	6	1236	1278	36
16	4	4	2267	2162	49	5	3	5	2288	2274	49	6	2	6	1219	1202	35
18	4	4	469	494	62	7	3	5	2288	2247	49	8	2	6	2355	2228	49
20	4	4	905	885	40	9	3	5	1225	1169	36	10	2	6	492	429	55
2	6	4	2115	2108	48	11	3	5	1127	1104	37	12	2	6	1111	1138	36
4	6	4	1502	1455	41	13	3	5	1873	1840	43	14	2	6	874	813	38
6	6	4	1626	1606	42	15	3	5	1704	1616	41	16	2	6	439	347	60
8	6	4	2885	2904	60	17	3	5	931	943	39	18	2	6	1252	1198	38
10	6	4	1269	1236	39	19	3	5	1155	1073	37	20	2	6	193	284	111
12	6	4	2536	2541	54	21	3	5	861	872	41	2	4	6	1456	1472	42
14	6	4	1656	1708	41	1	5	5	1971	1963	47	4	4	6	922	925	42
16	6	4	593	548	52	3	5	5	809	747	49	6	4	6	2816	2792	53
18	6	4	920	901	41	5	5	5	3182	3185	65	8	4	6	944	934	40
20	6	4	490	414	57	7	5	5	3239	3205	66	10	4	6	1859	1843	43
0	8	4	1521	1473	45	9	5	5	1264	1213	38	12	4	6	1239	1211	37
2	8	4	1533	1533	43	11	5	5	589	575	55	14	4	6	1739	1684	42
4	8	4	1750	1746	44	13	5	5	1745	1707	42	16	4	6	0	155	210
6	8	4	758	747	51	15	5	5	1434	1369	39	18	4	6	637	646	46
8	8	4	3199	3054	66	17	5	5	344	182	76	0	6	6	1876	1834	47
10	8	4	233	173	127	19	5	5	947	933	40	2	6	6	2030	2094	49
12	8	4	1967	1948	45	1	7	5	2018	1987	48	4	6	6	1628	1639	43
14	8	4	246	337	106	3	7	5	4122	4080	83	6	6	6	1834	1819	45
16	8	4	1319	1313	39	5	7	5	626	593	60	8	6	6	731	696	47
18	8	4	427	466	68	7	7	5	741	695	52	10	6	6	458	240	70
20	8	4	892	892	40	9	7	5	1546	1559	41	12	6	6	739	703	45
2	10	4	2484	2444	55	11	7	5	1331	1314	39	14	6	6	1453	1379	39
4	10	4	777	772	52	13	7	5	336	192	82	16	6	6	1137	1139	39
6	10	4	1354	1338	41	15	7	5	463	456	63	18	6	6	923	974	41
8	10	4	2303	2204	50	17	7	5	1529	1491	40	2	8	6	539	482	73
10	10	4	1193	1144	40	19	7	5	642	476	49	4	8	6	757	682	50
12	10	4	1726	1683	42	1	9	5	2890	2844	61	6	8	6	1578	1548	42
14	10	4	831	740	42	3	9	5	2311	2307	51	8	8	6	938	1014	42
16	10	4	307	297	106	5	9	5	537	602	66	10	8	6	3157	3013	65
18	10	4	1249	1201	38	7	9	5	1001	936	43	12	8	6	958	885	42
0	12	4	1722	1627	46	9	9	5	1605	1546	41	14	8	6	878	877	42
2	12	4	2165	2115	49	11	9	5	1804	1712	43	16	8	6	432	410	62
4	12	4	1875	1826	45	13	9	5	972	939	41	16	8	6	150	27	140
6	12	4	591	476	54	15	9	5	631	535	51	0	10	6	2910	2829	62
8	12	4	1033	962	39	17	9	5	579	593	54	2	10	6	1320	1314	42
10	12	4	283	424	89	1	11	5	1322	1243	44	4	10	6	1093	1097	41
12	12	4	564	570	52	3	11	5	615	525	57	6	10	6	1235	1225	40
14	12	4	267	334	104	5	11	5	1012	1024	41	8	10	6	359	211	79
16	12	4	1094	1001	37	7	11	5	2627	2532	56	10	10	6	130	65	131
2	14	4	727	703	53	9	11	5	879	820	42	12	10	6	551	542	56
4	14	4	1488	1442	41	11	11	5	593	571	53	14	10	6	949	912	41
6	14	4	1818	1837	43	13	11	5	1667	1629	41	16	10	6	738	732	43
8	14	4	791	760	42	15	11	5	389	319	72	2	12	6	432	422	81
10	14	4	812	782	41	17	11	5	655	525	48	4	12	6	1223	1197	40
12	14	4	470	394	58	1	13	5	1240	1185	43	6	12	6	1719	1704	42
14	14	4	982	963	37	3	13	5	1467	1450	41	8	12	6	877	862	41
0	16	4	2435	2213	53	5	13	5	1639	1637	41	10	12	6	1042	1010	38
2	16	4	1255	1203	41	7	13	5	510	401	64	12	12	6	750	748	44
4	16	4	563	543	56	9	13	5	953	959	39	14	12	6	845	809	41
6	16	4	769	851	43	11	13	5	993	960	39	0	14	6	1341	1284	43
8	16	4	364	311	69	13	13	5	454	525	61	2	14	6	1136	1161	41
10	16	4	123	172	127	15	13	5	1283	1229	37	4	14	6	1343	1342	39
12	16	4	597	551	44	1	15	5	300	173	122	6	14	6	469	418	60
2	18	4	332	351	76	3	15	5	1172	1135	40	8	14	6	877	755	39
4	18	4	644	612	50	5	15	5	867	846	42	10	14	6	412	254	62
6	18	4	494	566	55	7	15	5	650	701	46	12	14	6	148	367	129
8	18	4	293	333	113	9	15	5	1196	1224	36	2	16	6	1245	1198	40
1	1	5	1464	1372	36	11	15	5	1257	1253	36	4	16	6	542	585	49
3	1	5	1731	1687	38	1	17	5	1105	1094	42	6	16	6	600	560	48

TABLE 8 . OBSERVED AND CALCULATED STRUCTURE FACTORS FOR HG3(NBF5)2SO4

H	K	L	FO	FC	SIG	H	K	L	FO	FC	SIG	H	K	L	FO	FC	SIG
8	16	6	772	801	40	16	0	8	1144	1104	49	5	5	9	1078	1050	38
1	1	7	1918	1897	43	2	2	8	673	688	45	7	5	9	1382	1379	38
3	1	7	940	889	35	4	2	8	1464	1463	38	9	5	9	930	973	39
5	1	7	1230	1222	35	6	2	8	1500	1462	38	11	5	9	670	672	48
7	1	7	2485	2395	52	8	2	8	1620	1643	39	13	5	9	648	680	49
9	1	7	1041	976	36	10	2	8	1540	1545	39	1	7	9	424	363	74
11	1	7	1217	1167	36	12	2	8	1333	1295	37	3	7	9	1733	1795	43
13	1	7	1856	1806	42	14	2	8	624	596	49	5	7	9	281	265	86
15	1	7	689	617	44	16	2	8	675	657	45	7	7	9	919	926	41
17	1	7	328	283	77	0	4	8	2123	2288	50	9	7	9	710	658	46
19	1	7	657	704	48	2	4	8	386	529	79	11	7	9	714	645	46
1	3	7	724	711	53	4	4	8	1980	2023	45	13	7	9	581	519	52
3	3	7	2676	2725	56	6	4	8	648	653	47	1	9	9	962	967	42
5	3	7	1262	1316	37	8	4	8	1071	1068	38	3	9	9	1207	1244	39
7	3	7	570	633	50	10	4	8	465	307	75	5	9	9	571	651	53
9	3	7	1611	1596	39	12	4	8	843	816	40	7	9	9	711	679	47
11	3	7	1137	1117	37	14	4	8	489	471	60	9	9	9	459	459	64
13	3	7	373	218	73	16	4	8	1189	1142	38	11	9	9	730	764	45
15	3	7	996	942	38	2	6	8	1311	1349	42	1	11	9	277	470	98
17	3	7	1573	1460	40	4	6	8	998	1052	40	3	11	9	536	607	55
1	5	7	1531	1554	43	6	6	8	891	899	42	5	11	9	344	398	75
3	5	7	1411	1432	41	8	6	8	1605	1583	41	7	11	9	1243	1310	37
5	5	7	1767	1732	43	10	6	8	889	904	42	1	13	9	882	937	44
7	5	7	817	800	43	12	6	8	1367	1311	39	3	13	9	342	518	73
9	5	7	1827	1834	43	14	6	8	916	881	41	2	0	10	1577	1631	47
11	5	7	1538	1536	40	16	6	8	626	642	49	6	0	10	1480	1548	45
13	5	7	426	451	72	0	8	8	1175	1189	44	10	0	10	749	729	54
15	5	7	858	791	43	2	8	8	786	831	50	0	2	10	425	360	58
17	5	7	544	478	57	4	8	8	1358	1370	40	2	2	10	1362	1442	37
1	7	7	2314	2463	52	6	8	8	383	466	75	4	2	10	854	941	39
3	7	7	779	784	49	8	8	8	1578	1529	41	6	2	10	827	847	39
5	7	7	1477	1416	41	10	8	8	167	95	135	8	2	10	1164	1187	37
7	7	7	1531	1440	41	12	8	8	1198	1070	38	10	2	10	226	264	100
9	7	7	314	356	87	14	8	8	0	177	213	12	2	10	710	721	43
11	7	7	93	84	165	2	10	8	1446	1407	41	2	4	10	1030	1170	38
13	7	7	1120	1166	40	4	10	8	710	692	49	4	4	10	725	817	43
15	7	7	835	737	42	6	10	8	879	925	41	6	4	10	854	825	39
17	7	7	152	208	141	8	10	8	1158	1165	38	8	4	10	447	437	58
1	9	7	1358	1404	42	10	10	8	668	595	48	10	4	10	1363	1418	38
3	9	7	320	227	93	12	10	8	916	893	40	0	6	10	1338	1508	41
5	9	7	1970	1990	46	0	12	8	1012	1078	45	2	6	10	1089	1187	40
7	9	7	840	754	43	2	12	8	1062	1077	41	4	6	10	523	652	55
9	9	7	1038	993	40	4	12	8	1013	1011	39	6	6	10	720	721	44
11	9	7	879	857	43	6	12	8	519	471	58	8	6	10	535	620	51
13	9	7	629	553	50	8	12	8	705	753	44	10	6	10	99	171	148
15	9	7	1140	1064	39	10	12	8	328	307	80	2	8	10	361	383	73
1	11	7	475	568	75	2	14	8	636	645	53	4	8	10	280	313	99
3	11	7	1530	1523	41	4	14	8	779	797	42	6	8	10	1357	1392	38
5	11	7	964	969	40	6	14	8	864	946	39	8	8	10	575	487	48
7	11	7	464	436	61	1	1	9	226	264	114	0	10	10	974	1046	42
9	11	7	1404	1355	39	3	1	9	973	1031	36	2	10	10	653	776	51
11	11	7	1165	1170	38	5	1	9	1769	1753	41	4	10	10	930	1022	37
13	11	7	577	456	53	7	1	9	215	212	99	1	1	11	639	688	46
1	13	7	1092	1104	42	9	1	9	1230	1168	36	3	1	11	610	746	46
3	13	7	711	743	49	11	1	9	1046	1026	37	5	1	11	551	562	49
5	13	7	896	969	41	13	1	9	350	202	83	7	1	11	928	1050	37
7	13	7	435	428	62	15	1	9	935	997	39	9	1	11	341	208	75
9	13	7	850	866	40	1	3	9	1734	1928	42	1	3	11	441	574	57
11	13	7	822	803	39	3	3	9	390	405	75	3	3	11	940	1076	36
1	15	7	713	619	51	5	3	9	581	597	49	5	3	11	533	535	71
3	15	7	371	385	94	7	3	9	826	857	39	7	3	11	433	517	57
5	15	7	344	422	77	9	3	9	853	835	40	1	5	11	722	781	46
7	15	7	1354	1404	37	11	3	9	933	923	39	3	5	11	474	430	54
0	0	8	3222	3662	72	13	3	9	848	863	41	5	5	11	266	467	91
4	0	8	2145	2123	50	15	3	9	535	584	52	7	5	11	64	271	163
8	0	8	465	361	75	1	5	9	1077	1152	43	1	7	11	923	942	43
12	0	8	836	868	53	3	5	9	262	163	94	3	7	11	285	269	80